AN INVESTIGATION INTO THE STRESS-PERMEABILITY RELATIONSHIP OF COALS AND FLOW PATTERNS AROUND WORKING LONGWALL FACES

BY

S. Durucan, B.Sc., M.Sc.

Thesis submitted to the University of Nottingham for the degree of Doctor of Philosophy

October 1981

CONTENTS

LIST OF FIGURES

LIST OF TABLES

LIST OF PLATES

LIST OF SYMBOLS

Å	Angstrom
ϕ, ϕ_e	Porosity, effective porosity
V	Volume
V_b	Bulk volume
V_s	Volume of solids in a porous body
V_v	Total void space in a porous body
$(V_v)_e$	Effective pore volume
ρ	Density
M	Mass, molecular weight of a gas
P, P_s	Gas pressure, saturation adsorption pressure
V_m	Maximum volume of gas adsorbable
b'	Adsorption coefficient
V_w, V_d	Volumes of methane adsorbed in wet and dry coal
C_o, C_1, C_2	Constants
X_o	Coal oxygen content
Q	Volume flow rate of a fluid
r	Radius of a capillary tube
μ	Viscosity of a fluid
ΔP	Pressure difference across a porous medium
L	Length
Q_1, Q_2	Volume flow rate at the upstream and downstream ends of a porous medium
P_1, P_2	Gas pressure at upstream and downstream ends of a porous medium
$\bar{P}$	Mean gas pressure across a porous medium
R	Gas constant

T	Absolute temperature
γ	Adzumi constant
K'	Constant dependent upon the properties of the particular fluid and of the particular porous medium
A	Cross-sectional area
K	Specific permeability
K_d	Permeability calculated using Darcy's law
$\bar{R}$	Average pore radius
K_v, K_m	Viscous permeability and molecular permeability
K_L	Liquid permeability
λ	Mean free path of gas
b	Klinkenberg constant
K_I	Coefficient of gas conveyance
S	Constant for a particular gas
$\sigma, \sigma_1, \sigma_3$	Stress, maximum and minimum principal stresses
τ	Shear stress
c	Cohesion
Φ	Internal friction angle
ε	Strain
E	Young's modulus of elasticity
ν	Poisson's ratio
K_{frac}	Fracture permeability of a coal specimen
C_x	Compressibility of coal
C	Compressibility factor
a, b	Constants
α	Stress dependent variable for coal permeability
K_{σ_3}	Permeability at Radial Stress σ_3
K_{σ_B}	Permeability constant dependent upon the fracture system of each coal specimen.

ABSTRACT

This research aimed to establish a physical relationship between applied stress and permeabilities of different coals. Seven different coals, ranging from medium volatile to high volatile bituminous, were tested for stress-permeability relationship under simulated subsurface stress conditions.

Prior to the experimental investigations, the stress conditions around a working longwall face were considered in order to achieve an accurate simulation of the stresses experienced underground.

Laboratory stress-permeability experiments were carried out by passing nitrogen gas through a triaxially stressed cylindrical coal specimen. A slightly modified conventional triaxial testing apparatus was used for this purpose.

The stress conditions employed simulated the stresses created in the front abutment zone, the crushing zone, the stress relief zone and the recompaction zone of a working longwall face. A number of specimens of the seven different coals were tested under such stress conditions and stress-permeability curves were obtained for each specimen. The effect of moisture and the direction of gas flow in relation to the direction of bedding planes and major fracture lines were also considered in laboratory investigations.

A relationship between the stress-permeability behaviour and the rank of coals used was established. Combining the general pattern of stress-permeability behaviour obtained in this research together with the stress conditions created around a working longwall face a model was produced which presents the stress-permeability profiles of coal seams in the vicinity of the workings. From these profiles it was possible to suggest the flow patterns of gas around working longwall faces.

INTRODUCTION

INTRODUCTION

From the earliest days of underground mining the emission of methane has been a matter of concern. With modern mining methods allowing higher outputs, faster rates of face advance and mining operations extending to greater depths, the problems of methane emission are becoming increasingly more serious.

Methane is fairly inert. However it burns in air. It is this chemical reaction which makes the existence of methane in coal mines a problem for the mining engineer. A methane flame will propogate spontaneously if the methane concentration is between 5 and 15 percent and at a level about the middle of this range, the air/methane mixture reaches its maximum explosibility. Thus, planning of the mine environmental conditions must ensure that high concentrations of methane do not occur in the workings.

Methane was formed together with the coal material during the long term process of coalification. During the early stages of the process much of the methane produced was lost. However, methane remains adsorbed in the extant coal seams in a state of stable equilibrium pressure which can be considerably in excess of atmospheric pressure. It is not until the strata is fractured by mining that this equilibrium is disturbed and the gas migrates into the workings.

Investigations have shown that gas emission in the region of a working longwall face emanates from three main sources:

(i) the actual seam being worked,

(ii) the waste area behind the face,

(iii) the source beds of carbonaceous material above and below the mine workings.

The methane being emitted from the seam being worked is termed the 'coal front gas'; the gas migrating from the source beds is termed the 'strata gas'.

The release of gas from the seam being worked and the source beds above and below, and its subsequent migration towards the mine airways, is dependent upon the permeability (i.e. the ability of the porous media to allow fluids to flow through it) of the coal seams and of the surrounding strata.

Research has shown that permeability of strata around a working longwall face is effected by the stress disturbances created by the extraction of the coal seam.

Thus, any approach to the problem of methane emission must be based upon an understanding of the stress disturbances and their effects on permeability of coal seams and the strata around working longwall faces.

This research aims to further understanding in this area by providing empirical evidence of stress-permeability behaviour of coals. From this data 'stress-permeability' profiles for coal seams around working longwall faces were produced.

CHAPTER ONE

REVIEW OF CURRENT KNOWLEDGE ON COAL PERMEABILITY

CHAPTER ONE

REVIEW OF CURRENT KNOWLEDGE ON COAL PERMEABILITY

1.1 Introduction

Although there has been a great deal of research carried out on the subject of gas and liquid permeabilities of porous media, very little of this research dealt specifically with permeability of coal. In the main part researchers concentrated on fluid transport characteristics of petroleum reservoir rocks; several text books have been written on this latter area (1), (2), (3).*

Graham (4), (5) was the first research worker to study various properties of coal in relation to methane. He published his first findings on coal permeability in 1916 and 1919. These were followed by a more comprehensive study of the adsorption of methane and some other gases in coal (6). Graham's work appears to have stimulated interest in research in the subject of coal permeability and methane adsorption. In 1932 Audibert published his paper, 'A Hypothesis of Methane Emission' (7). Later, Briggs

---

*Numbers in brackets refer to references at the end of the thesis.

and Sinha (8) studied the changes in permeability with desorption of methane and published their findings in 1933.

These initial works focussed attention on the importance of the subject and a number of studies have been carried out since. In recent years research has emphasised the significance of the effect of stress on permeability of coal. Laboratory investigations have been carried out on this subject and it was found that permeability of coal decreased drastically with increasing stress.

Work in the field of permeability of rock, and more specifically, coal, will be reviewed in this chapter.

1.2 Review of Work on Coal Permeability

The first laboratory investigation into the permeability of coal was conducted by Graham (4). Thin slabs of coal, about 3 mm in thickness and 25 cm^2 in area, were sawn off from a large lump of coal. Flow rates of air, carbon dioxide, methane and hydrogen were measured through these thin slabs of coal. After completing his experiments, Graham stated that:

> "..contrary to what is usually supposed, solid coal is extremely airtight, and lets very little air or gas through, even with a driving pressure of a whole atmosphere."

Later in 1919, Graham published his second set of results on permeability of coal to methane (5). He observed

that the rate of gas flow through the specimen depended on the difference in partial pressure of the methane on the two sides of the slab. Therefore, he suggested that the rate of loss of methane from a lump of coal exposed to the air would not depend on the total external pressure, but upon the partial pressure of the methane in the atmosphere and the pressure of the gas in the coal. An average permeability value of $K_d = 10^{-21}$ m^2 was reported by Graham.

A long period of time elapsed in which no other researchers pursued the subject of coal permeability to gas. However, in the last two decades the importance of the subject was recognised and research was resumed. In 1959, Sevenster (9) conducted permeability measurements on 1 mm thick, 26 mm diameter coal discs using methane, oxygen, water vapour and several other gases. Gas flow through the specimen was considered to be by Knudsen diffusion and permeabilities in the order of $K_d = 10^{-24}$ m^2 were reported. Sevenster suggested that molecular permeability was inversely proportional to the square root of the gas molecular weight.

Huang and Shelton (10) were the first to suggest a relationship between the permeability of coal to gas and coal rank. Coal specimens from ten different coal seams were tested for air permeability and results ranging between $K_d = 10^{-12}$ m^2 and $K_d = 10^{-17}$ m^2 were reported. Permeability of coal was found to increase with decrease in volatile matter up to a critical point

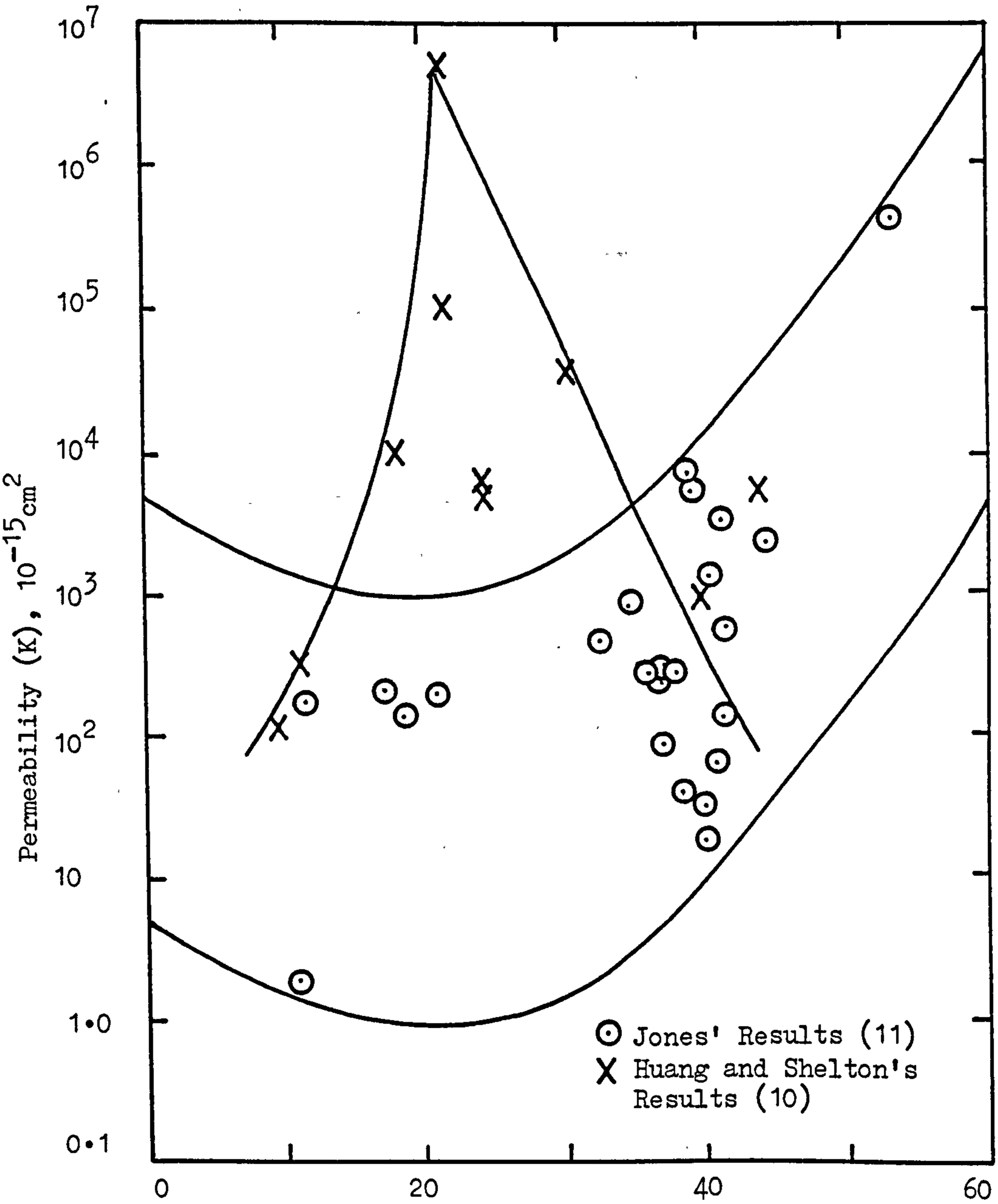

FIGURE (1.2.1) Comparison of Permeability Results Obtained by Jones and Huang and Shelton.

and then decreases as the volatile matter decreased further. In 1969, Jones (11) carried out laboratory measurements on helium permeabilities of 21 different British Coals. His results suggested a relationship between coal permeability and rank which was opposite to that reported by Huang and Shelton in 1962. Results of these two workers are compared in Figure (1.2.1).

Karn et al. (12) and Thimons and Kissel (13) investigated the diffusion of methane through coal employing similar laboratory techniques to those of Sevenster. Thimons and Kissel have shown that water vapour reduces the permeability of coal by a factor of 3 to 25. Karn et al. measured permeability of coal both along and across the bedding planes and observed that permeability along the bedding planes was 2 - 3 times higher.

In situ permeability values for coal have been obtained from borehole pressure measurements. Results of in situ measurements published by Wolstenholme (14) and Kissel (15) have shown that coal has much higher permeability values in situ. Table (1.2.1) compares the experimental and field data reported on coal permeability.

1.3 The Effect of Stress on Permeability of Coal

The effect of overburden pressure on permeability of rocks was first considered by petroleum engineers. Large discrepancies were observed between conventional laboratory

TABLE (1.2.1) Experimental and Field Data on Coal Permeability

SOURCE	K_d (m^2)	METHOD
Graham (5)	10^{-21}	Laboratory
Sevenster (9)	10^{-24}	Laboratory
Huang and Shelton (10)	$10^{-12} - 10^{-17}$	Laboratory
Jones (11)	$10^{-17} - 10^{-21}$	Laboratory
Karn et al. (12)	10^{-24}	Laboratory
Thimons and Kissel (13)	$10^{-18} - 10^{-20}$	Laboratory
Wolstenholme (14)	10^{-15}	In situ
Kissel (15)	$10^{-13} - 10^{-16}$	In situ

measurements on cores at atmospheric pressure and those obtained from the field data.

The earliest inquiry into the effects of stress on permeability of rocks was made by Fatt and Davis (16) in 1952. This was followed by many other research studies, mainly in the field of Petroleum Reservoir Engineering. In 1965, two separate papers were published describing the effects of stress on permeability of coal, the authors were Patching (17) and Gunther (18). These early studies, which were conducted under hydrostatic stress conditions, were later extended into the investigation of stress-permeability behaviour of coal and coal measures under simulated subsurface stress conditions (non-uniform stress).

1.3.1 Permeability under Uniform Stress

Fatt and Davis (16) studied the effect of overburden pressure on the permeabilities of eight different sandstones. Clean, dry core plugs, 25·40 mm in diameter and 76.20 mm long, were mounted in a copper foil jacket or moulded in Lucite jackets. The jacketed core was then placed in a high pressure hydraulic bomb, in which hydraulic pressure as high as 103·40 MN/m^2 could be applied to the specimen. Flow lines from the core were brought out of the bomb through special fittings in the bomb head and connected to a laboratory type gas permeameter. Nitrogen gas was used as the flowing media. Measurements have shown that the specific permeability of sandstone decreased with increase in hydraulic pressure. Most of the decrease was found to take

place over the range of zero to 20•70 MN/m^2 overburden pressure. At this pressure level, the permeability of the eight sandstone cores tested ranged from 59% to 89% of the permeability at zero pressure. Figure (1.3.1) shows some of the results obtained by Fatt and Davis.

Employing the same laboratory techniques, Fatt (19) and McLatchie et al. (20) observed similar effects of hydrostatic stress on permeability of reservoir sandstones. Investigations by the latter workers have shown that the percentage reduction in permeability generally increased as the initial permeability decreased.

As an integral part of a programme of investigations into the problem of sudden outbursts of coal and gas, Patching (17) studied the effects of confining pressure on coal. The coal specimens were cast in cylindrical flexible epoxy resin mounts, fitted with cap pieces, which were connected to high pressure tubing, and enclosed in neoprene sleeves. The enclosed specimens were then placed in a steel shell where hydraulic oil pressure could be raised as high as 20•70 MN/m^2. Dry nitrogen or carbon dioxide was used as the flowing media in most of the experiments. Confining pressure was found to have a marked effect on the permeability of all samples. As shown in Figure (1.3.2), the permeability of most coal specimens was reduced by more than three orders of magnitude (10^{-14} m^2 to 10^{-18} m^2) as the confining pressure was increased to 20•70 MN/m^2. Patching has also examined the hysterisis and time-dependent changes in permeability as the

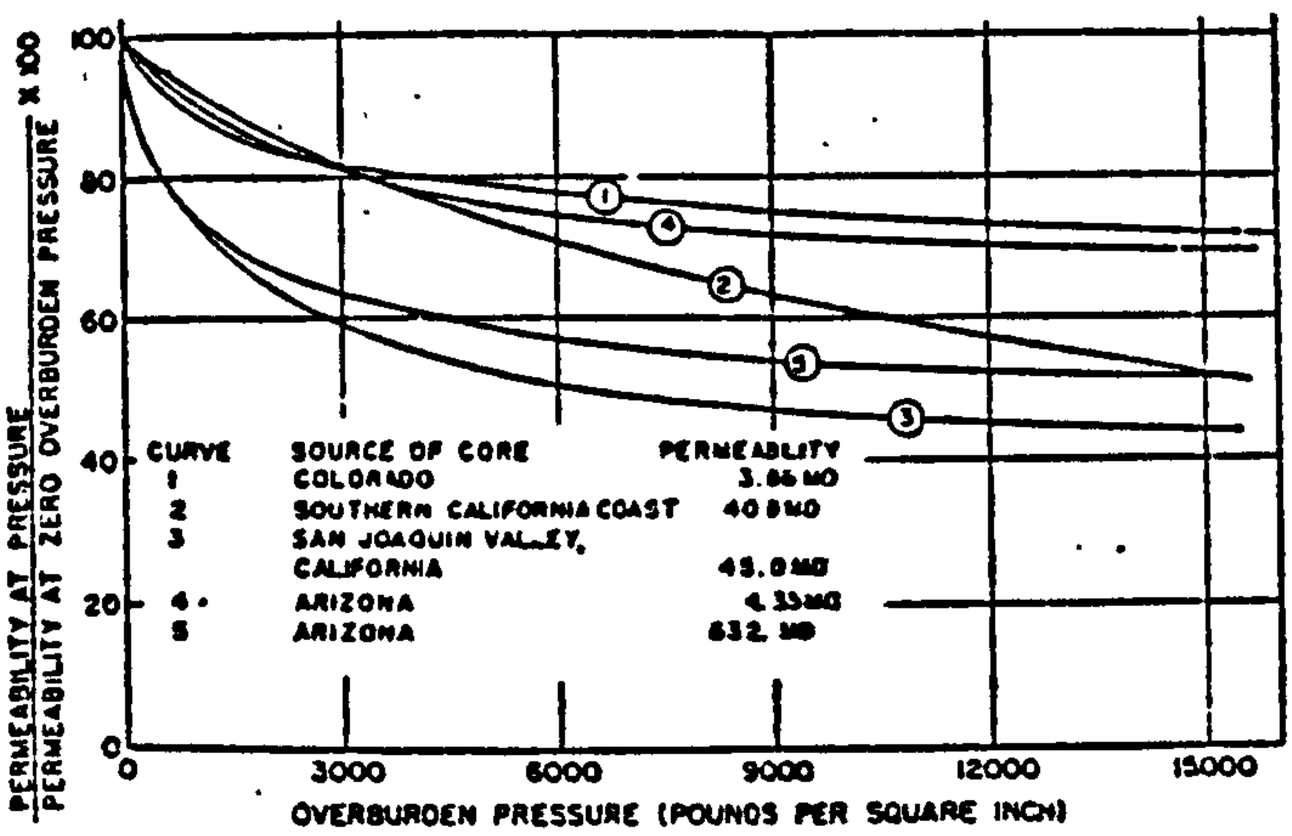

FIGURE (1.3.1) Change in Permeability with Overburden Pressure (After Fatt and Davis (16)).

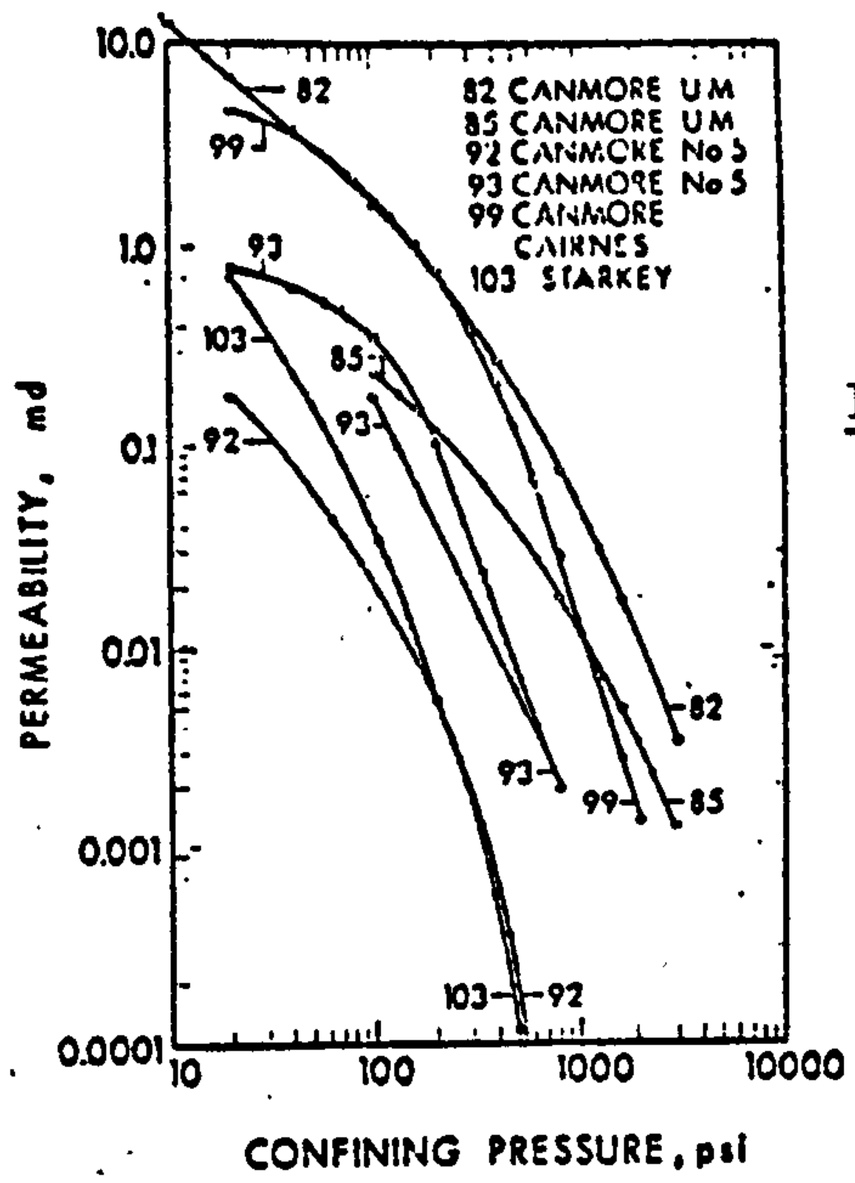

FIGURE (1.3.2) Change in Permeability with Confining Pressure (After Patching (17)).

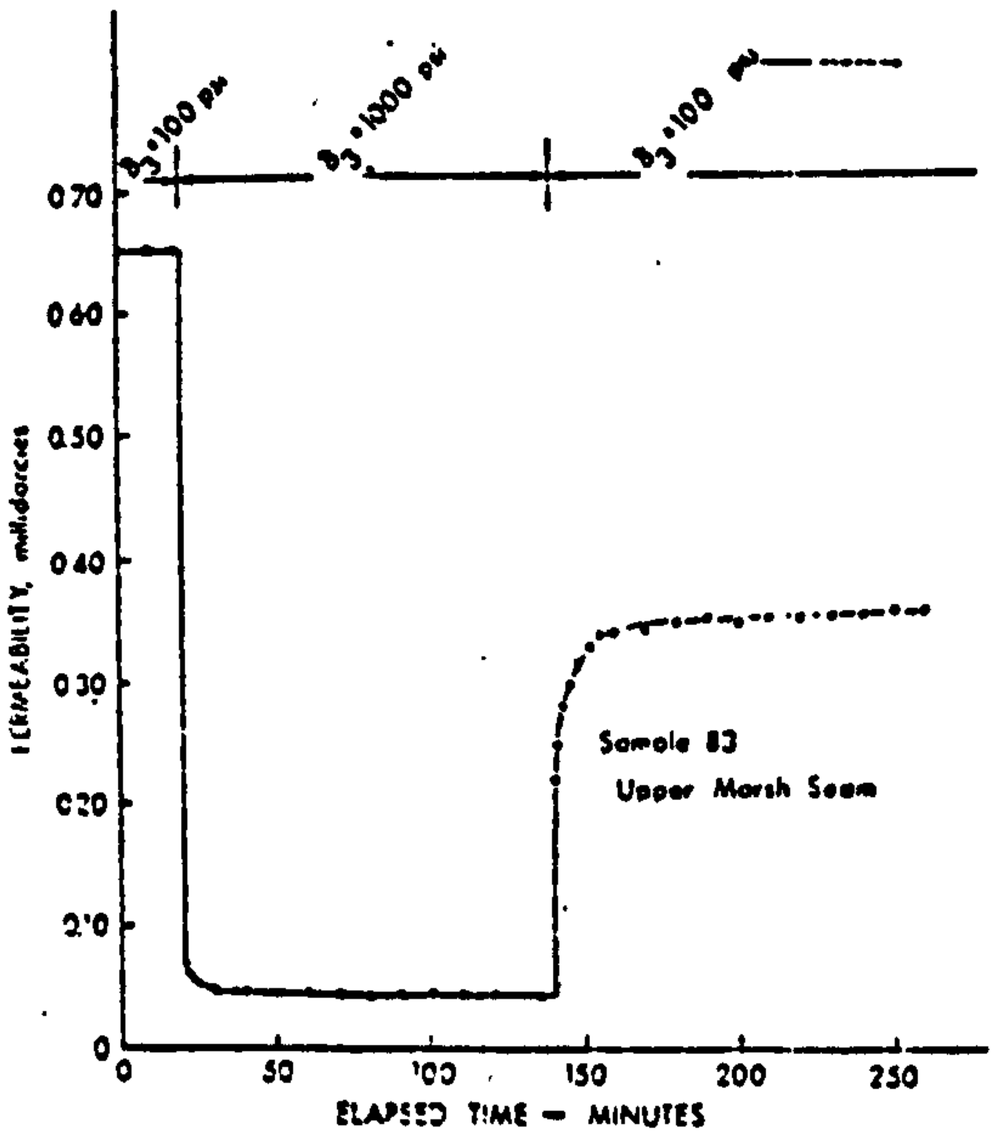

FIGURE (1.3.3) Time Dependent Changes in Permeability of Coal (After Patching (17)).

specimen was loaded and unloaded. A specimen was loaded from 0•69 MN/m^2 to 6•90 MN/m^2 confining pressure and then after some time was unloaded to 0•69 MN/m^2 again. As shown in Figure (1.3.3), permeability continued to decrease for some time after the pressure was applied; when the pressure was removed permeability recovered partially and continued to increase with time. From his findings Patching concluded that the permeability of coal was to some extent dependent on its stress history.

As a part of a wider investigation into the relationship between coal and the gas contained in it, Gunther (18) measured the permeability of coal specimens under hydrostatic pressures of up to 80•00 MN/m^2. Permeability of the specimens was observed to decrease from about 10^{-15} m^2 to 10^{-19} m^2 at 60•00 MN/m^2. These results confirmed the findings of Patching.

In 1974, Dabbous et al. (21) conducted a series of loading/unloading experiments on coal specimens from two different seams. The effect of stress history on permeability of coal was marked by a continuous decrease in permeability of each specimen after consecutive loading/unloading cycles. It was also noticed that the magnitude of the effect of increasing overburden pressure was not the same for coals of different origin.

1.3.2 Permeability under Non-Uniform Stress

An alternative experimental appraoch to the investigation of the effects of stress on permeability of rocks has been based upon the use of triaxial stress conditions. It was felt that such stress conditions would more accurately simulate the stresses experienced underground.

Mordecai (22), (23) was the first to consider the effects of triaxial stressing on permeability of carboniferous rocks within the perspective of mining. A number of British coal measures were tested for stress-permeability relationship where nitrogen was used as the flowing media. At sufficiently high deviator stresses ($\sigma_D = \sigma_1 - \sigma_3$), a steady increase in the permeability of specimens was observed. This was explained by the opening up of flow channels as the fracturing was initiated. Figure (1.3.4) shows a set of experimental results by Mordecai.

Pomeroy and Robinson (24) conducted a series of water permeability measurements on cubes of coal under uniaxial or biaxial confinement. Permeability of coal was found to be increasing at very high uniaxial stresses. On the other hand, permeability always decreased under biaxial confinement.

Somerton et al. (25) investigated the effects of triaxial stressing on gas permeabilities of three bituminous coals. Permeabilities of coal specimens were found to be strongly stress

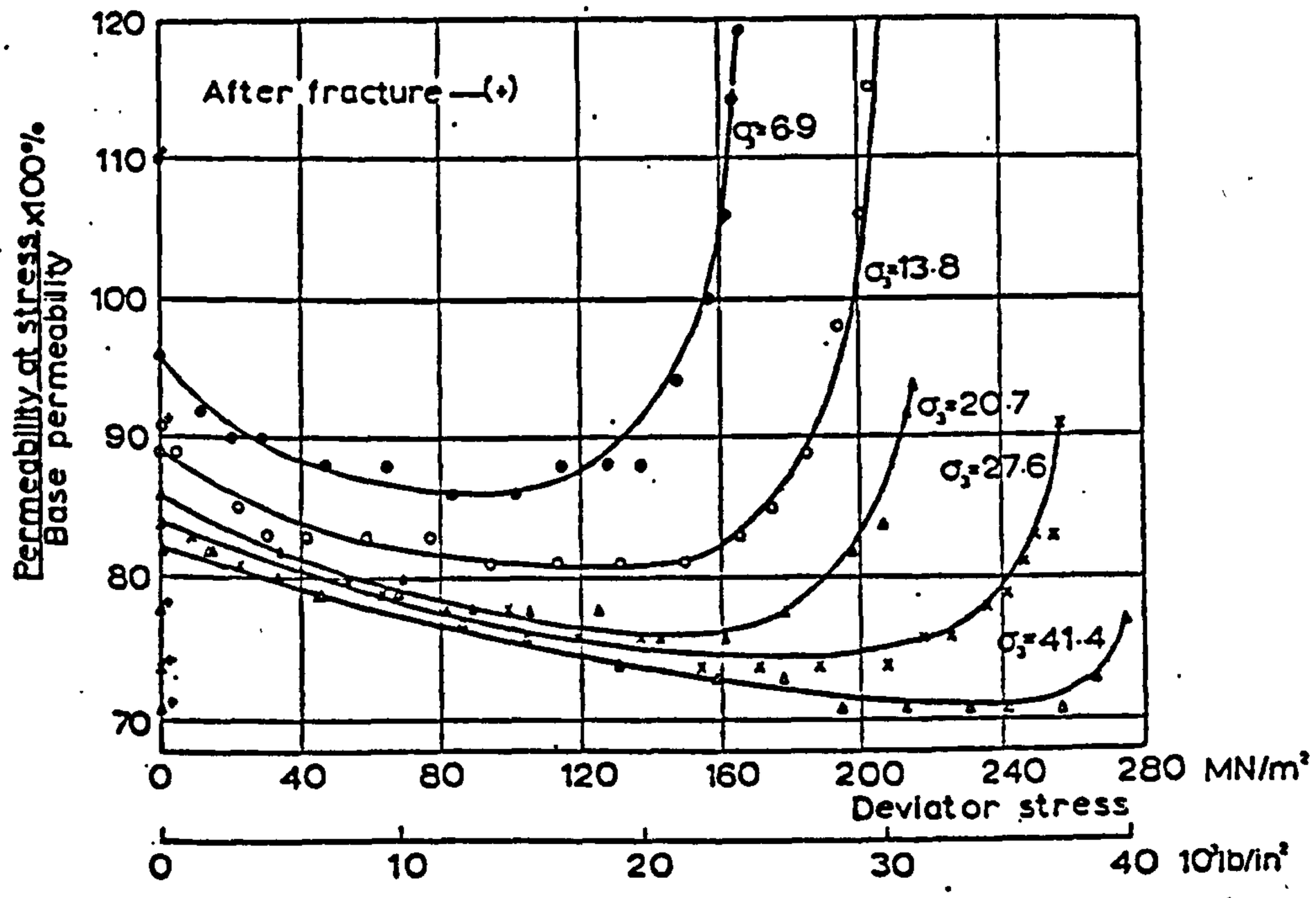

FIGURE (1.3.4) Stress-Permeability Curves for Darley Dale Specimens at Various Confining Pressures (After Mordecai (22)).

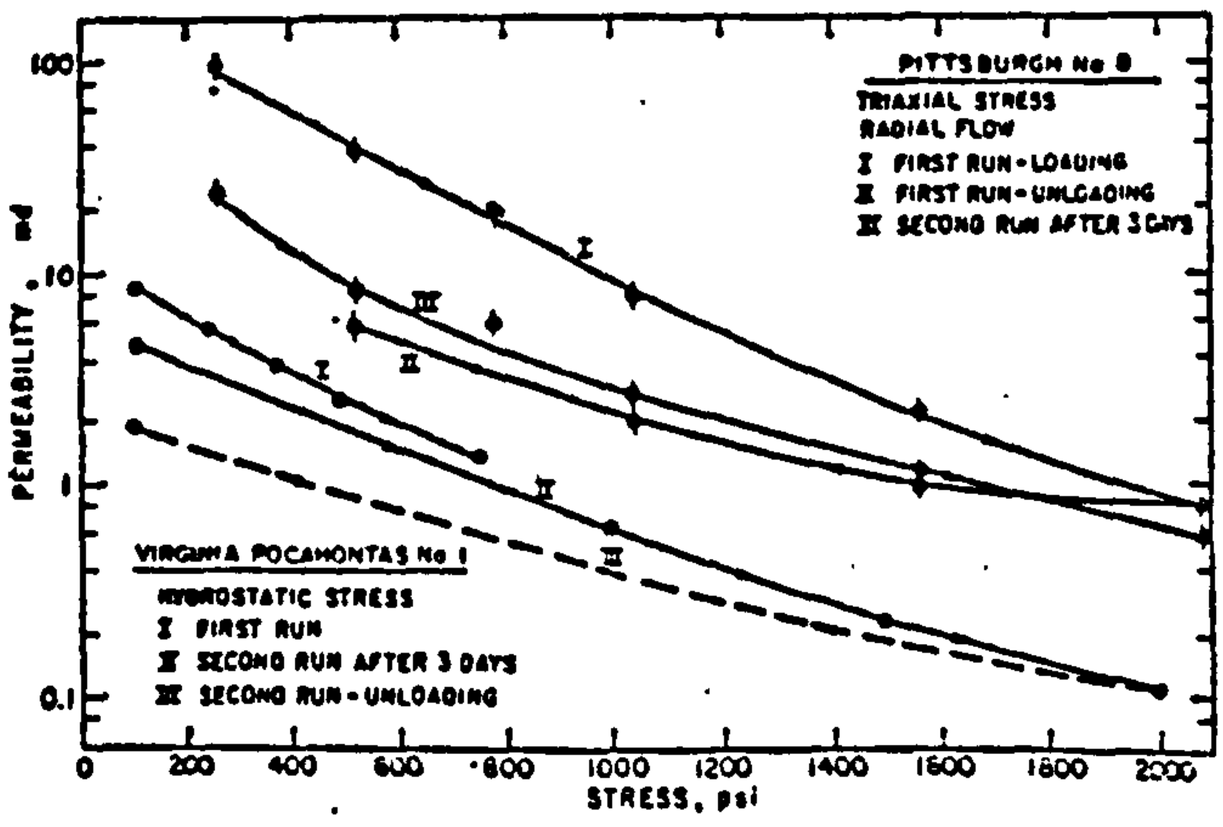

FIGURE (1.3.5) Effect of Repeated Loading on Pittsburgh and Virginia Pocahontas Coal (After Somerton et al. (25)).

dependent. At equivalent stress levels, low permeability coals have shown higher rates of decrease in permeability as compared to high permeability coals. Permeability of coal was also found to be stress-history dependent. Figure (1.3.5) shows some of the results reported by the above authors.

The latest research into the effects of stress on permeability of coal was carried out by Gawuga (26) in 1979. The effects of applied stress and gas pressure on permeability of Blackshale coal were studied. Fracturing of the coal specimens was initiated at very high deviator stresses and similar results to those of Mordecai were obtained. Figure (1.3.6) shows one of Gawuga's stress-permeability curves for a coal specimen tested to failure.

Although it was recognised that permeability of coal was a controlling factor in the flow of methane around working longwall faces comparatively little research has been conducted on the subject, as can be seen from the preceeding review of literature. A number of questions remain unanswered concerning the permeability of coal seams at particular regions around working longwall faces.

It was considered that further studies were required and it was recognised that in order to make a useful contribution coal permeability measurements should be carried out under stress conditions which aimed at simulating the actual conditions created underground by mining operations. In order to achieve

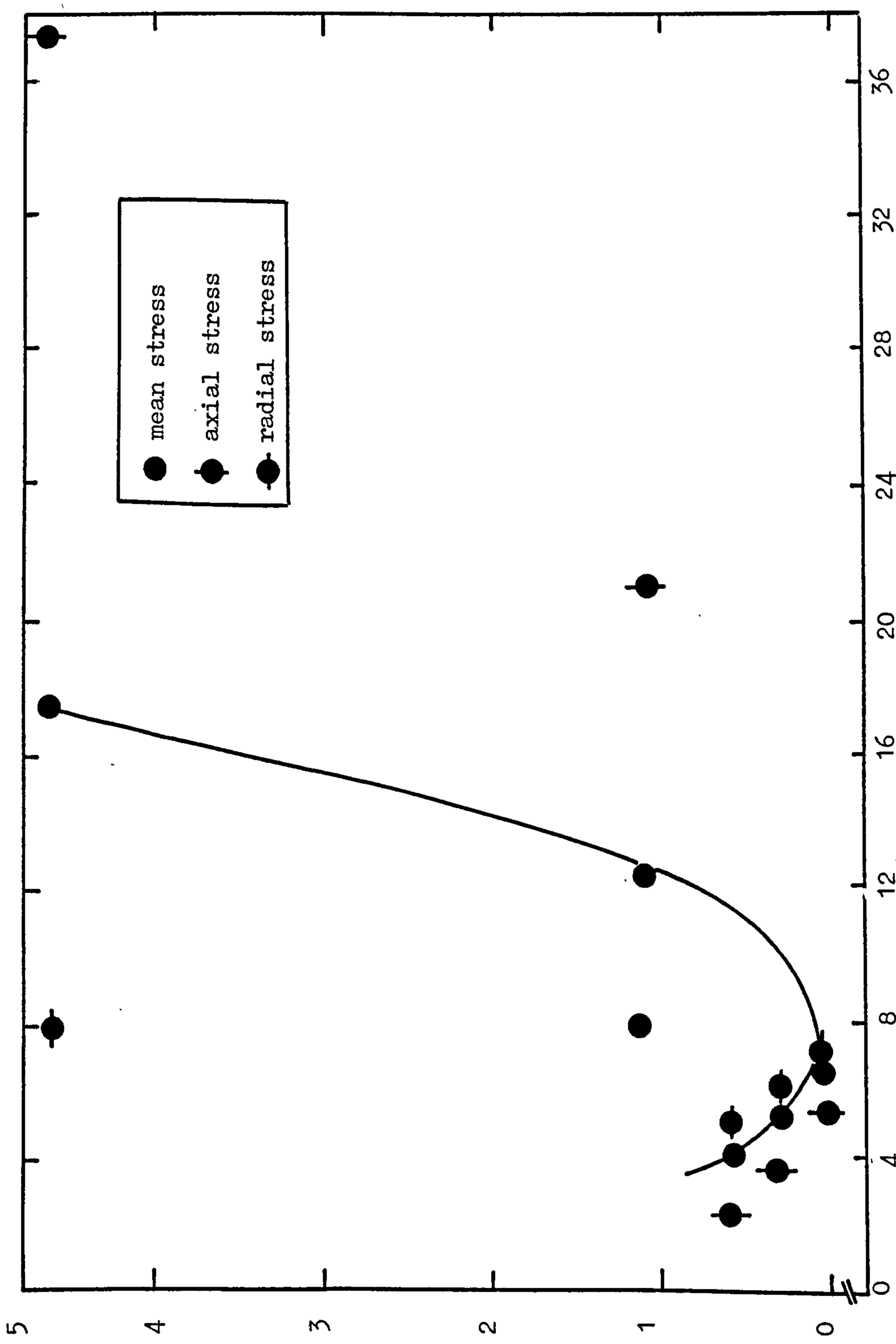

FIGURE (1.3.6) Variation of Permeability with Applied Stress for a Specimen Tested to Failure (After Gawuga (26)).

this an understanding of the stress disturbances in the strata around working longwall faces is required.

McPherson (27) produced a hypothetical profile of coal permeability in the strata above and below an advancing longwall coal face, as shown in Figure (1.3.7). This profile was based upon Mordecai's work on stress-permeability relationship of coal measures and upon the qualitative evidence from the theories of rock mechanics (stresses around longwall faces). He suggested that the permeability of a coal seam would decrease in the stressed zone ahead of the face despite the fact that microfracturing would occur in this zone. The effect of microfracturing would be to cause partial sealing of the interconnections between the pores within the coal. This would occasion a further decrease in permeability which is already very low.

Behind the face, where the rock is relaxed, there will be an increase in permeability by orders of magnitude due to the opening of the microfractures and relaxation of normal cleavage and planes of weakness between beds. This induced permeability provides the paths along which gas can flow. As the cover load is established the permeability decreases to a value which is greater than that of the virgin rock. The increase is due to the existence of new fractures in the rock.

This hypothetical profile required verification by experimental research. It was considered that an investigation

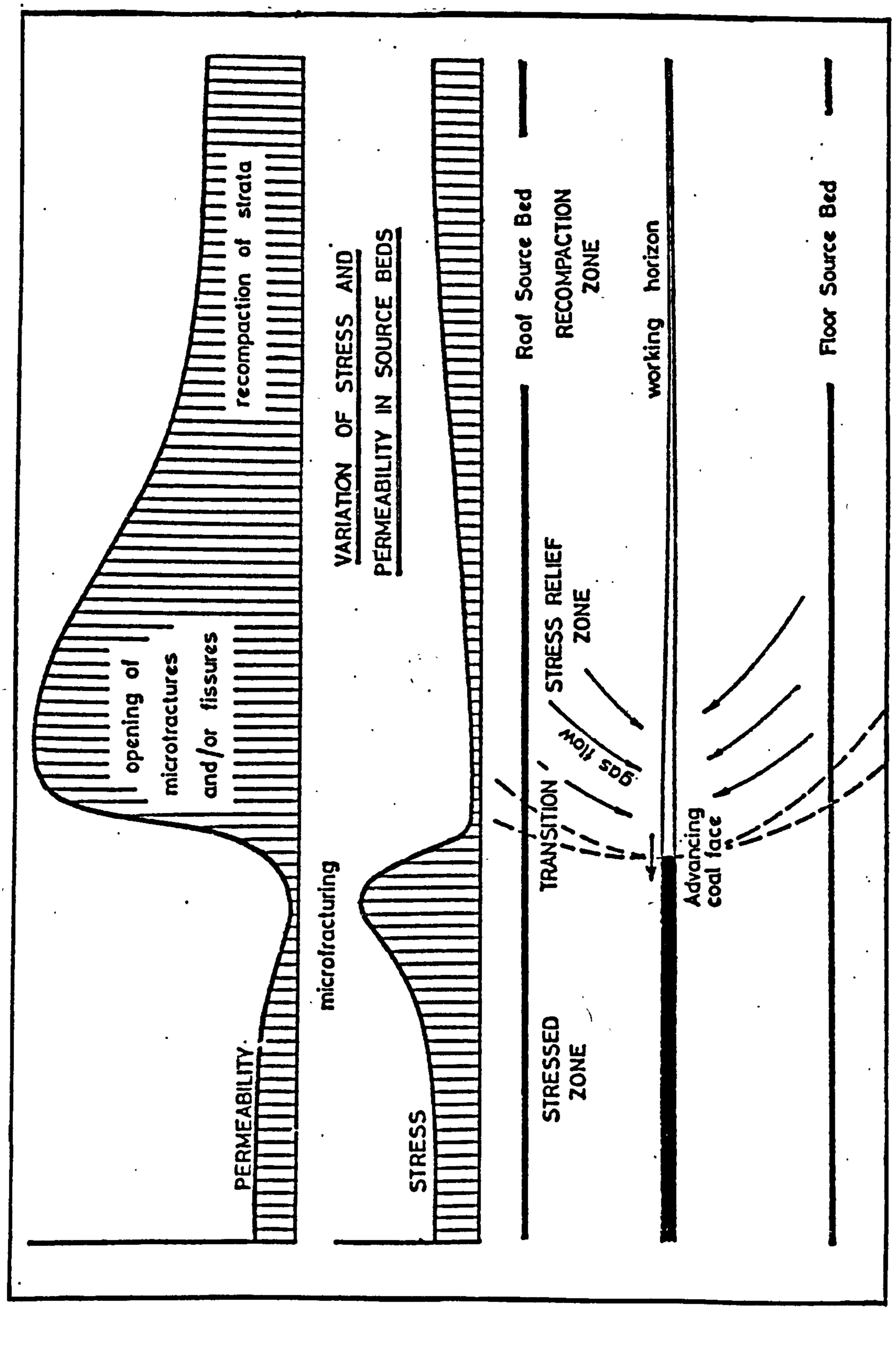

FIGURE (1.3.7) The Variations of Stress and Permeability in Strata Above and Below an Advancing Longwall Coal Face (After McPherson (27)).

of stress-permeability behaviour of coals under actual stress conditions experienced underground would prove whether McPherson's hypotheses were valid. However, it was recognised that the inherent differences in permeability of coal in the virgin state, which is dependent upon both the structural characteristics and stress-history of each individual coal seam, would be significant in the stress-permeability behaviour of coal. Thus, the rank of coal needs to be considered as a factor effecting the permeability of coal under stress. No acknowledgement of rank as a factor determining the stress-permeability behaviour of coal appears in literature.

The objectives of this research were to achieve:

(i) a simulation of the stress conditions around working longwall faces in the laboratory,

(ii) an understanding of the stress-permeability behaviour of different coals under such conditions.

Thus, a physical relationship between the applied stress and permeability of different coals could be established which would be applicable to mining operations.

CHAPTER TWO

STRUCTURAL PROPERTIES OF COAL

CHAPTER TWO

STRUCTURAL PROPERTIES OF COAL

2.1 Introduction

It is believed that the structural properties of coal such as: porosity, pore size distribution, internal surface area, gas and moisture adsorption characteristics, would effect permeability of coal to gas. In this chapter models of coal structure will be reviewed. Laboratory measurements of porosity will be discussed and the findings on porosity, pore size distribution and internal surface areas of coals will be presented. Adsorption theory and the effect of moisture on gas capacities of coals will be considered.

2.2 Models of Coal Structure

Based upon the measurements of the heats of wetting of coals by methanol, Bangham et al. (28) proposed a structural model for coal. It was assumed that coal was made up of spherical shaped building units of equal size. These units were called 'micelles' and it was suggested that their size was determined by molecular aggregation process occuring in an aqueous medium (peat stage). The decrease in porosity with increase in rank of coal was explained as being the result of compaction during the coalification process. Figure (2.2.1) illustrates the progressive

compaction of the spheres with increasing rank as suggested by Bangham et al.

This model was highly simplified and was found to be inapplicable when high porosities of semi-anthracites and anthracites were considered.

Using the X-ray diffraction method of examinig coal structure, Blayden et al. (29) suggested that coal consisted of a structure of flat aromatic lamellae having no particular orientation relative to each other (turbostratic packing). The average dimensions and degree of ordering of these lamellae was found to increase with increase in rank of coal.

Improving on Blayden's studies Brown and Hirsch (30) investigated the complete picture of coal structure using X-ray diffraction curves with a wide scattering range. Their investigations have shown that for coals of approximately 85 percent carbon content, about 60 percent of the lamellae occur singly, 28 percent in groups of two and the remainder in groups consisting of a larger number of units. With increasing carbon content the order improved; the proportion of single layers is reduced and the fraction in larger groups increased. As a result of these investigations three types of coal structure were distinguished:

(i) An open structure, for low rank coals (less than 85 percent carbon). The lamellae were connected by cross links and the orientation was random. Pore diameters extended

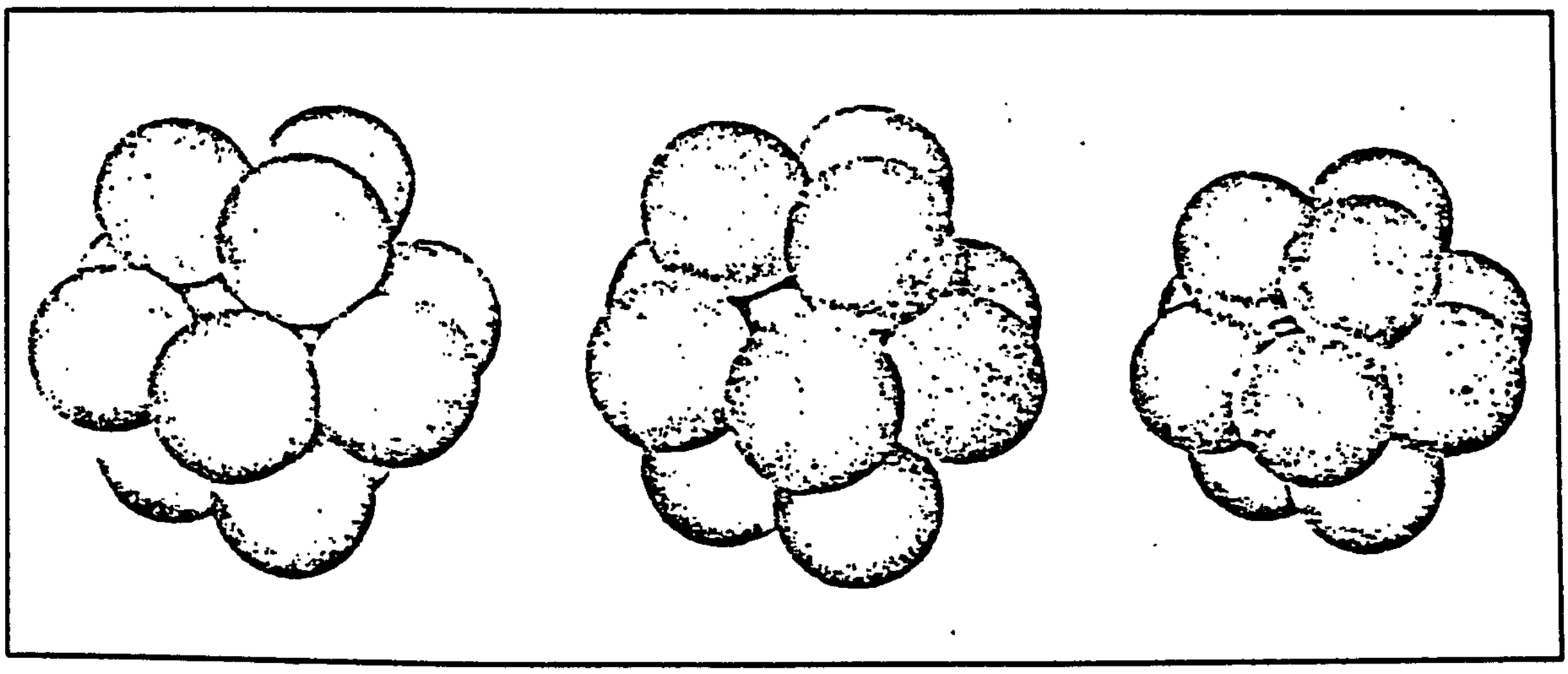

FIGURE (2.2.1) Progressive Compaction of Close-Packed Spheres with Increasing Rank (After Bangham et al. (28)).

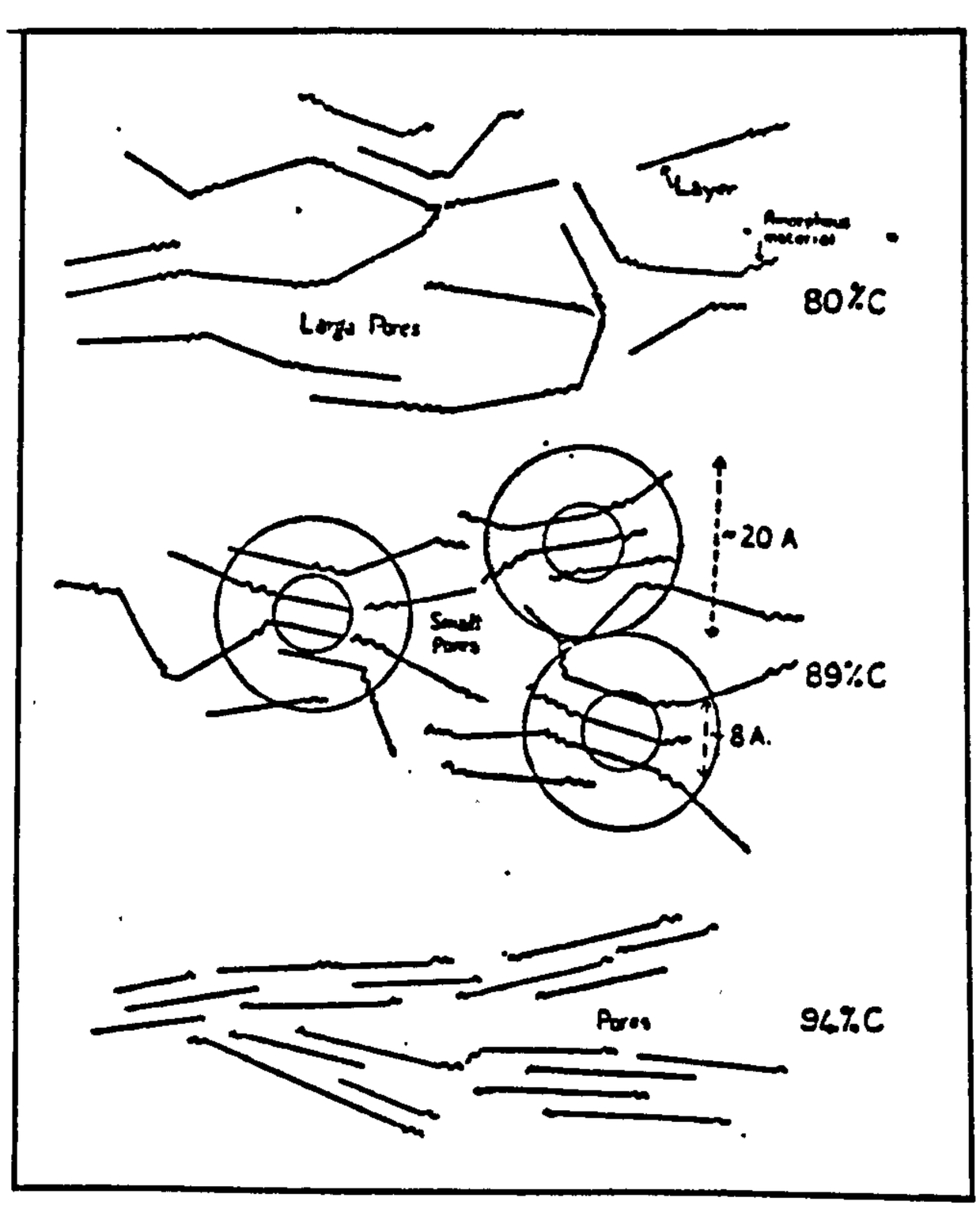

FIGURE (2.2.2) Schematic Diagram of the Packing of Coal Molecules at Various Stages During the Process of Coalification (After Brown and Hirsch (30)).

from a few angstroms to values greater than 5000 Å. The coal was highly porous.

(ii) A liquid-like structure for bituminous coals (85 - 91 percent carbon). Some lamellae orientation was observed and crystallites were formed from two or more lamellae. Pore diameters were found to be approximately 10 Å and the coal had very low porosity.

(iii) An anthracitic structure for high rank coals (more than 94 percent carbon). Local parallel packing of the lamellae is improved and large graphitic layers are formed. This gave rise to the disappearance of the cross-links and the porosity increased due to the parallel packing of the neighbouring lamellae. Average pore diameter was found to be 16 Å.

Figure (2.2.2) shows a schematic diagram of the packing of coal molecules at various stages during the process of coalification, as suggested by Brown and Hirsch.

2.3 Porosity and Porous Materials

A solid body containing holes or voids, which are either connected or non-connected, and are dispersed in either a regular or random manner relatively frequently throughout the solid, is defined as a 'porous material'. These holes or voids may vary in size; extremely small voids are termed 'molecular interstices', very large ones are termed 'caverns', intermediate sized void spaces are termed 'pores'.

Porosity (ϕ) is generally defined as the ratio of volume of the total void space (V_v) to the bulk volume (V_b) of a porous medium:

$$\phi = \frac{V_v}{V_b}$$

then $$\phi = \frac{V_b - V_s}{V_b} = 1 - \frac{V_s}{V_b}$$

Where V_s is the volume of solids within V_b. Usually the porosity, a dimensionless quantity, is expressed in percentages.

The above definition, referring to the total void space is termed the 'total porosity' and is of practical interest in terms of gas holding capacity for coal. However, from the standpoint of flow through porous media, only interconnected pores are of interest. Hence the concept of effective porosity ϕ_e, defined as the ratio of the interconnected (or effective) pore volume $(V_v)_e$, to the bulk volume (V_b) is introduced:

$$\phi_e = \frac{(V_v)_e}{V_b}$$

Effective porosity is a static property; it is an indication of permeability, but not a measure of it.

2.3.1 Laboratory Measurements of Porosity and Pore Size Distribution of Coal

The pore structure of coal is usually studied by density measurements, gas expansion method and mercury porosimetry. The common principle that applies to all these techniques is that the coal structure is penetrated by liquids or gases having very small molecular dimensions, near negligible adsorptive properties and minimal interaction forces between them and coal.

2.3.1.1 Density Method

If the density ρ_s of the material making up the porous medium is known, then the bulk density ρ_b of the latter is related to the porosity as follows:

$$\phi = 1 - \frac{\rho_b}{\rho_s}$$

since

$$M = V_s \rho_s = V_b \rho_b$$

where M is the mass of the sample and V_s and V_b are volume of the grain material and the bulk volume of the porous medium, respectively. The bulk density is determined by weighing the sample and measuring the bulk volume by a volumetric displacement technique. The density of the material of which the porous medium is composed is usually determined by measuring the change in weight of the porous medium after being soaked by a displacement fluid.

Several gases and liquids such as helium, mercury and water have been used as the displacement fluid. Depending on the molecular dimensions and the magnitude of the interaction forces between them and the coal surface, molecules may penetrate totally or partly into the coal material. The porosity of coal determined by this method is therefore a function of the penetrating fluid. Owing to its small molecular size, and negligible adsorptive properties, helium is considered to give the most accurate results.

Employing this technique, King and Wilkins (31) determined the porosity of large numbers of British coals. They found that the porosity decreases with increasing rank up to 89 percent carbon or 20 percent volatile matter (d.a.f.) and then increases again in the anthracite range. This relationship is shown in Figure (2.3.1). Measuring the helium densities of several American coals, a similar relationship was obtained by Gan et al. (32), Figure (2.3.2).

2.3.1.2 Gas Expansion Method

The basic principle of the gas expansion method is direct measurement of the volume of gas contained in the pore space. A specimen of known bulk volume is placed in a container of known volume under certain gas pressure. The container is then connected to an evacuated container of known volume and the change in gas pressure is observed. The pore volume is computed by using the Boyle-Mariotte gas law. This method gives relatively accurate effective porosities and leaves the specimen in an

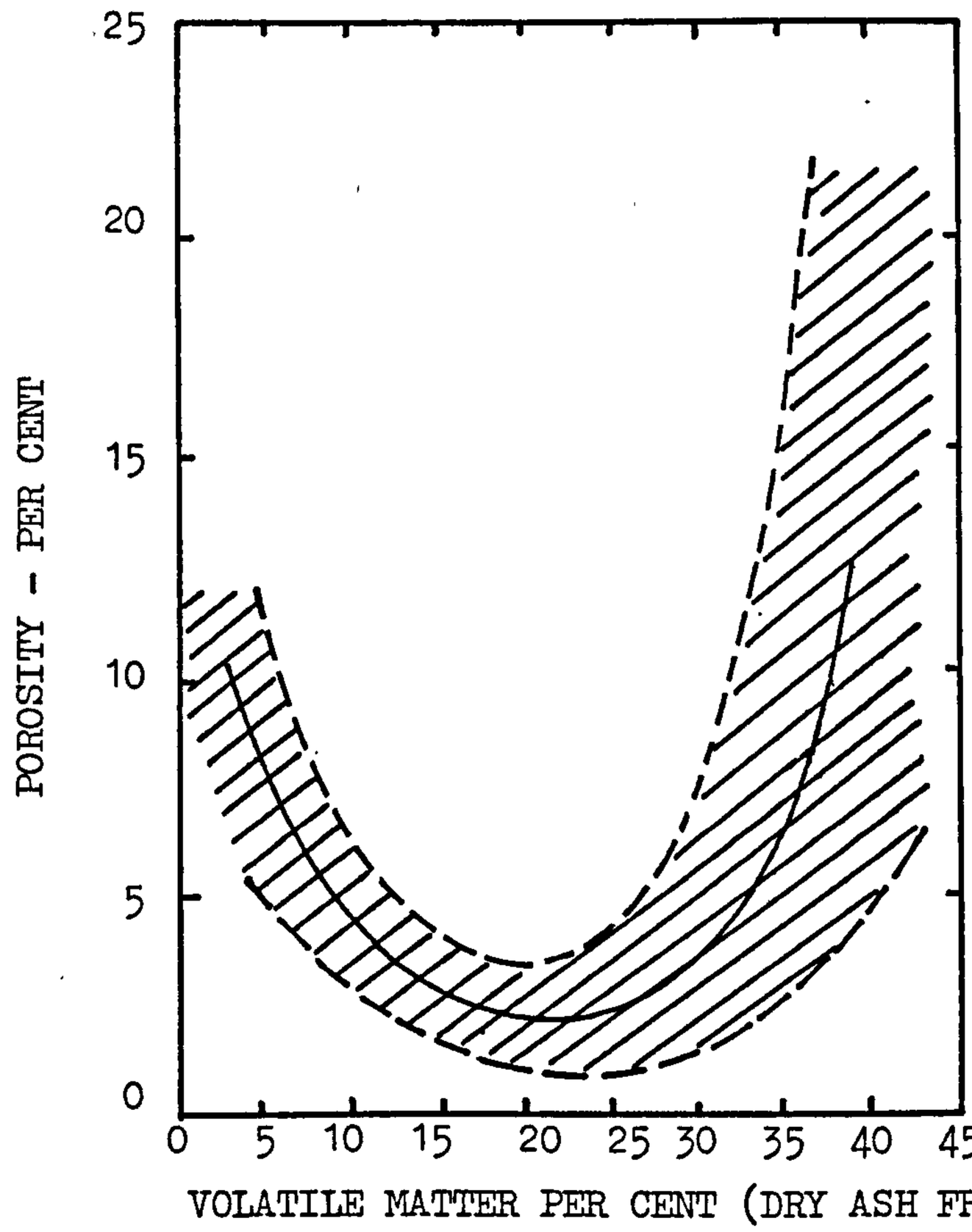

FIGURE (2.3.1) Variation of Coal Porosity with Volatile Matter (After King and Wilkins (31)).

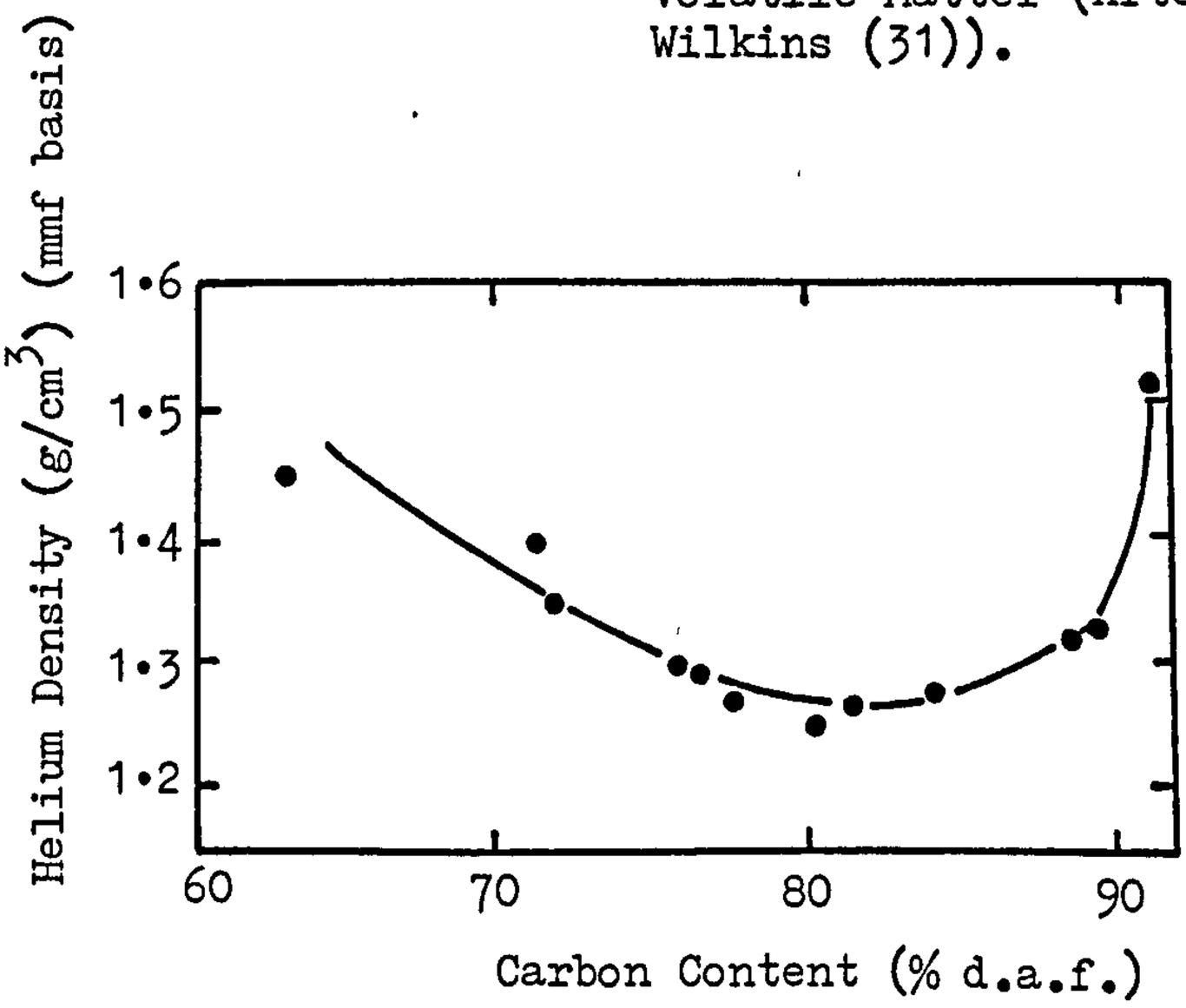

FIGURE (2.3.2) Variation of Helium Density of Coals with Carbon Content (After Gan et al. (32)).

undisturbed state so that other tests can be performed immediately afterwards.

Effective porosities of some of the test specimens used in this research were determined employing an instrument which was developed using the above principle. Measurement of effective porosity using the gas expansion method will be discussed in more detail later in Chapter Six.

2.3.1.3 Mercury Porosimetry

Due to surface tension and its non-wetting properties, mercury does not penetrate into small pores in coal at atmospheric pressure. Thus, the bulk volume of a coal specimen can be measured by displacement of mercury from a container of known volume. As the applied pressure is increased, mercury will penetrate progressively into smaller openings in the coal structure. The pressure, P, required for forcing the mercury into a pore of radius r, is given by the equation:

$$r = -\frac{2\sigma}{P}\cos\theta$$

where

σ is the surface tension of mercury,

θ is the contact angle.

Using the above technique, Zwietering and van Krevelen (33) and Toda and Toyoda (34) measured the porosity of coal in the

pressure range 1 - 1000 atm. Both researchers agreed that the apparent increase of pore volume at very high pressures resulted solely from the compressibility of coal substance. As shown in Figure (2.3.3), the intercept at the ordinate was taken to represent the true pore volume in the range of radius 75000 - 75 Å. Zwietering and van Krevelen produced a pore size distribution curve from mercury penetration data and concluded that coal contains two distinct pore systems; macropores of diameter greater than 75 Å which are accessible to mercury, and micropores of diameter smaller than 75 Å which are only accessible to helium.

Gan et al. (32) studied the porosity of various American coals using mercury porosimetry, helium and mercury displacement and gas adsorption methods. Total pore volumes in the diameter range 12 - 29600 Å were measured and three pore systems were suggested:

(i) macropores (300 - 29600 Å),

(ii) transitional pores (12 - 300 Å),

(iii) micropores (4 - 12 Å).

It was found that in the lower rank coals (carbon content less than 75 percent), porosity was primarily due to the presence of macropores; in coals having a carbon content in the range 76 - 84 percent, about 80 percent of the total pore volume was due to micro and transitional pores; in the coals of higher rank microporosity was predominant. Their results are reproduced in Table (2.3.1).

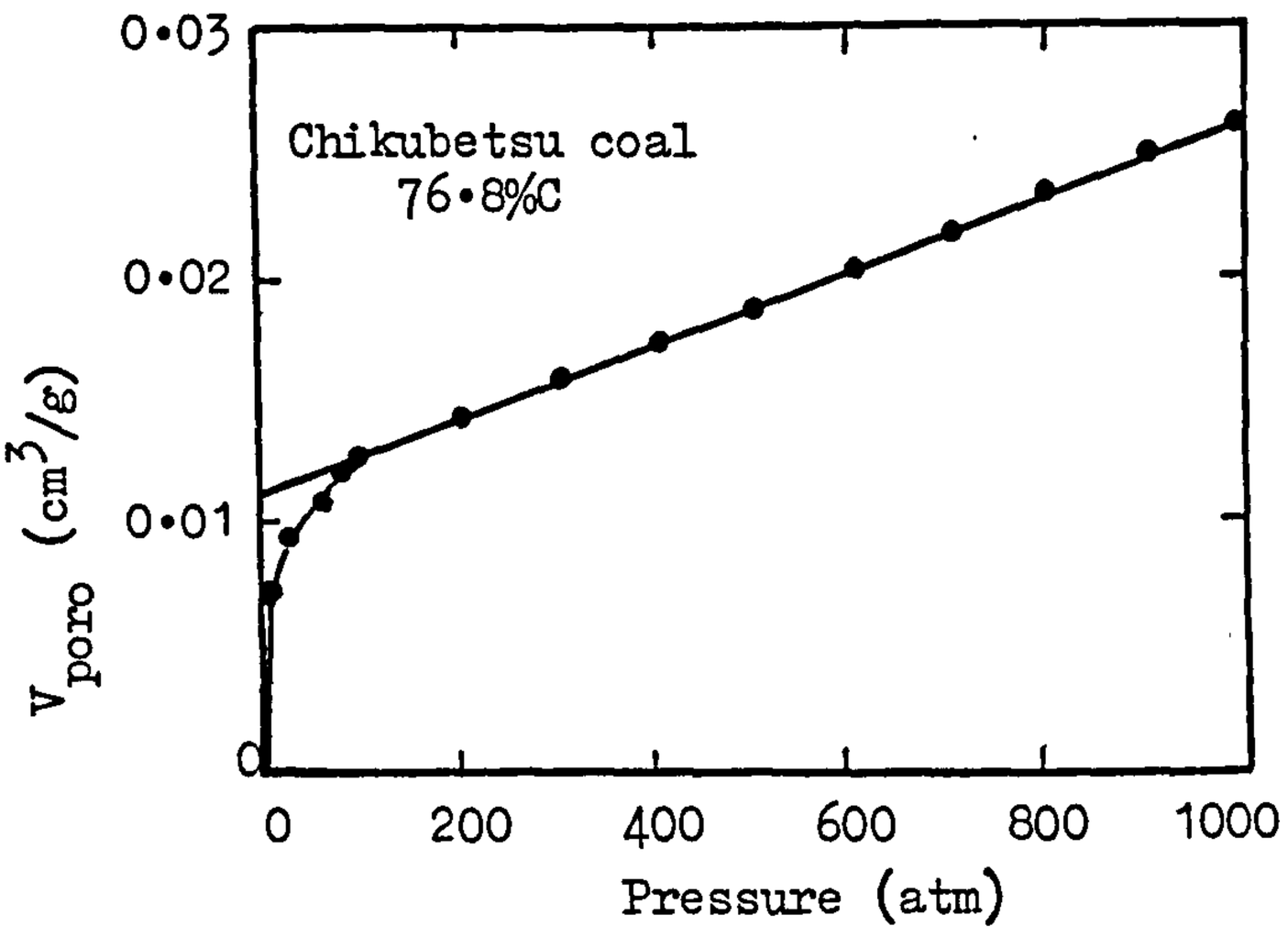

FIGURE (2.3.3) Mercury Porosimetry Results (After Toda and Toyoda (34)).

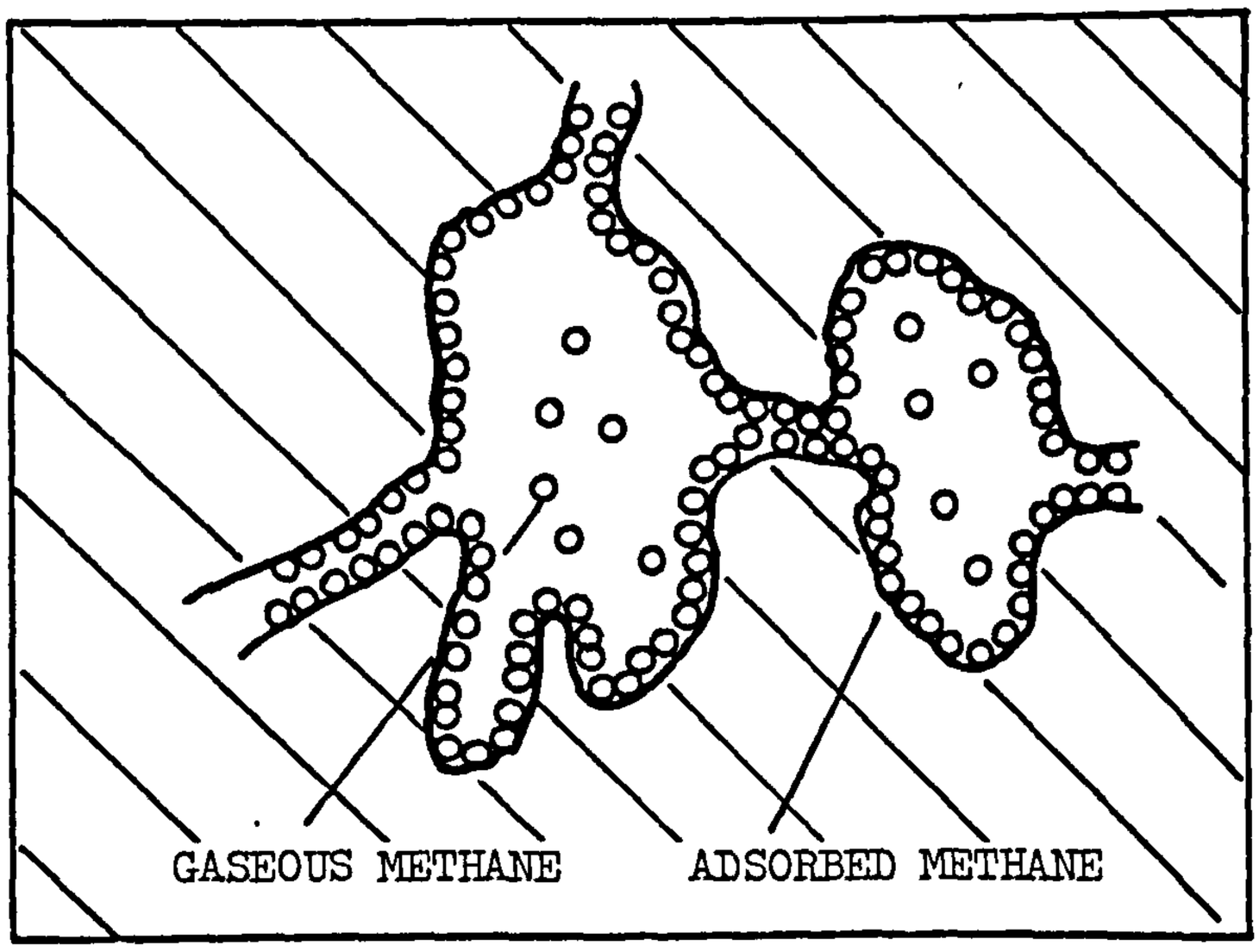

FIGURE (2.4.1) Pictorial Representation of Methane Molecules Inside a Coal Pore.

TABLE (2.3.1) Gross Pore Distribution in Coals (After Gan et al. (32))

SAMPLE	RANK	MICROPORES V_3 (%)	TRANSITIONAL PORES V_2 (%)	MACROPORES V_1 (%)
PSOC - 80	Anthracite	75•0	13•1	11•9
PSOC - 127	LV Bit.	73•0	nil	27•0
PSOC - 135	MV Bit.	61•9	nil	38•1
PSOC - 4	HVA Bit.	48•5	nil	51•5
PSOC - 105A	HVB Bit	29•9	45•1	25•0
Rand	HVC Bit.	47•0	32•5	20•5
PSOC - 26	HVC Bit.	41•8	38•6	19•6
POC - 197	HVB Bit.	66•7	12•4	20•9
PSOC - 190	HVC Bit.	30•2	52•6	17•2
PSOC - 141	Lignite	19•3	3•5	77•2
PSOC - 87	Lignite	40•9	nil	59•1
PSOC - 89	Lignite	12•3	nil	87•7

Micropores are said to account for about 95 percent of the total internal coal surface (13). Internal surface areas ranging from 20 to 200 m^2/gm were reported for British coals by Griffith and Hirst (35). Since virtually all of the methane in coal is physically adsorbed under pressure on this internal surface, most of the methane will be stored in the micropores.

2.4 The Relationship between Coal and its Gas Content

2.4.1 Sorption Theory

When a gas or vapour is brought into contact with an evacuated solid, a part of it is taken up and retained by the material. This process is known as sorption and the opposite process, i.e. the giving up of gas or vapour by a solid, is termed desorption. The molecules either enter the inside of the solid structure in which case the process is called absorption, or, they remain on the surface, the process being termed adsorption. The solid is referred to as adsorbent and the gas or vapour as the adsorbate. If strong chemical bonds exist between the adsorbent and the adsorbate molecules the term chemical adsorption is applied. On the other hand, if the molecules are held only by weak physical forces (e.g. electrostatic forces, or van der Waal's forces), the process is termed physical adsorption. Physical adsorption is reversible; the desorption process generally exhibits similar behaviour to that of adsorption but in an opposite direction. As mentioned before, methane is retained in the internal structure of the coal primarily by the mechanism of physical adsorption. Figure (2.4.1) shows a pictorial representation of methane molecules inside a coal pore.

2.4.2 Adsorption Isotherms

Isotherms are drawn in order to show the constant temperature relationship of pressure to volume. A number of relationships have been proposed to express the adsorptive properties of materials. The two most important mathematical relationships which describe the adsorption isotherms are that of Langmuir (36) and that of Brunauer, Emmet and Teller (known collectively as BET) (37).

Langmuir considered the collisions between gaseous and solid molecules to be inelastic, and suggested that adsorption occurred during the time elapsed when the gas remained in contact with the solid before returning to the gas phase. Assuming that any molecule from the gas phase striking an already adsorbed molecule would rebound elastically, he was able to derive an equation describing the mono-molecular layer adsorption of gases as:

$$V = \frac{V_m b'P}{1+b'P}$$

where

V is the volume of gas adsorbed,

P is the gas pressure,

V_m is the maximum volume of gas adsorbable

b' is the adsorption coefficient.

In order to account for the multi-layer adsorption of gases, Brunauer, Emmet and Teller extended Langmuir's equation to the form:

$$V = \frac{V_m c P}{(P_s - P)\left[1 + (c - 1)\left(\frac{P}{P_s}\right)\right]}$$

where

P_s is the saturation adsorption pressure,

c is a constant.

Jolly (38) determined methane adsorption isotherms for a number of British coals at gas pressures up to 1400 atm. Figures (2.4.2) and (2.4.3) show examples of mono-molecular and multi-molecular layer adsorption isotherms obtained by Jolly.

2.5 Effect of Moisture on Methane Capacity

As with many other properties of coals, moisture content has a considerable effect on its gas capacity. Moisture content is mainly related to the oxygen content of coals. Strong interaction between the polar water molecules and the surfaces of oxygen complexes hold water in pore spaces in an adsorbed state. As the coalification proceeded towards higher ranks, oxygen was lost in the form of carbon dioxide or water resulting in decreased water adsorption capacity.

Joubert et al. (39), (40), studied the adsorption of methane on moist coal and have shown that the methane capacity of coals decrease with increasing moisture up to a certain 'critical' value of moisture content that was characteristic of each coal. Moisture in excess of this critical value was found to have no

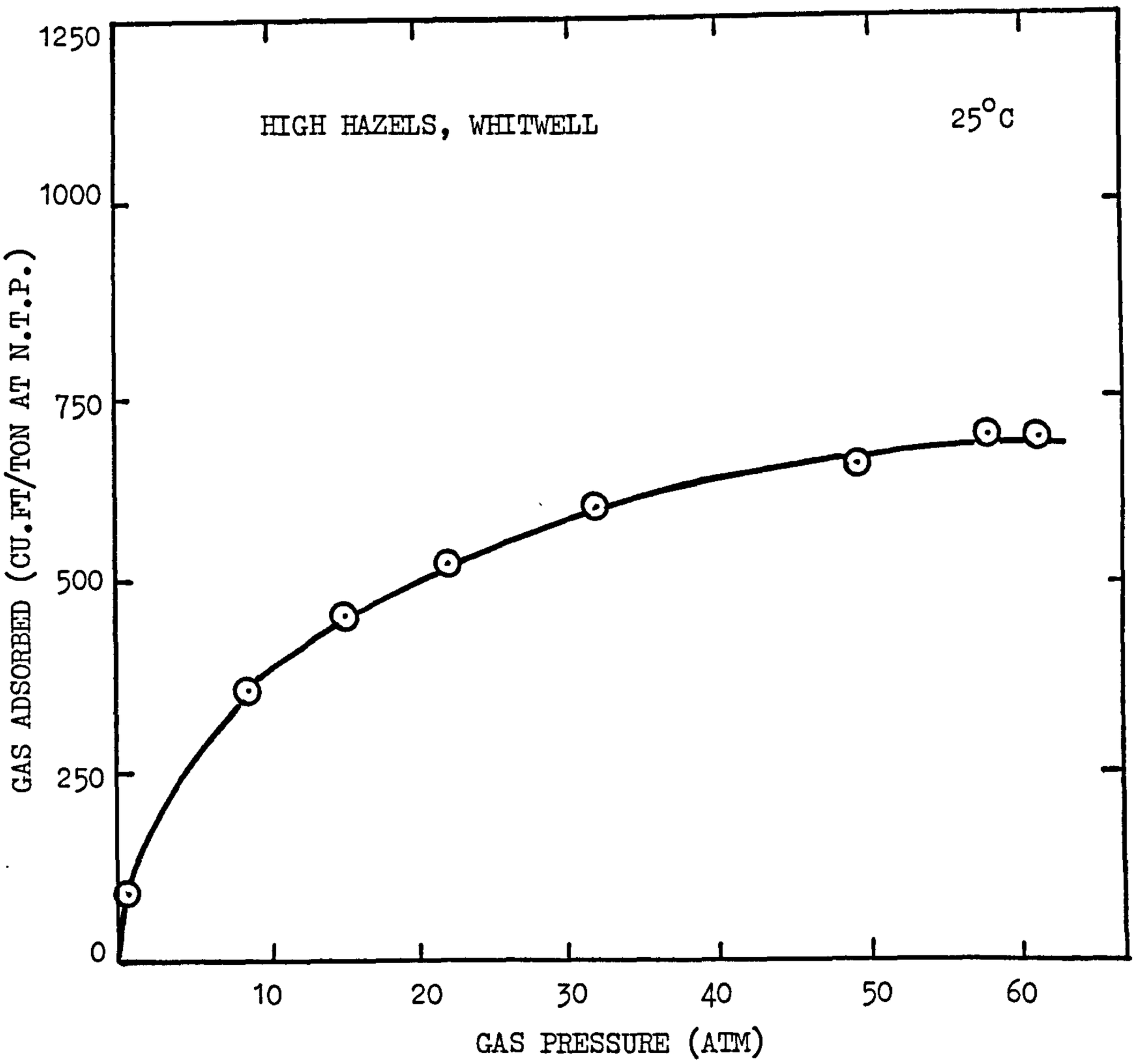

FIGURE (2.4.2) An Example of Mono-Molecular Layer Adsorption Isotherm (After Jolly (38)).

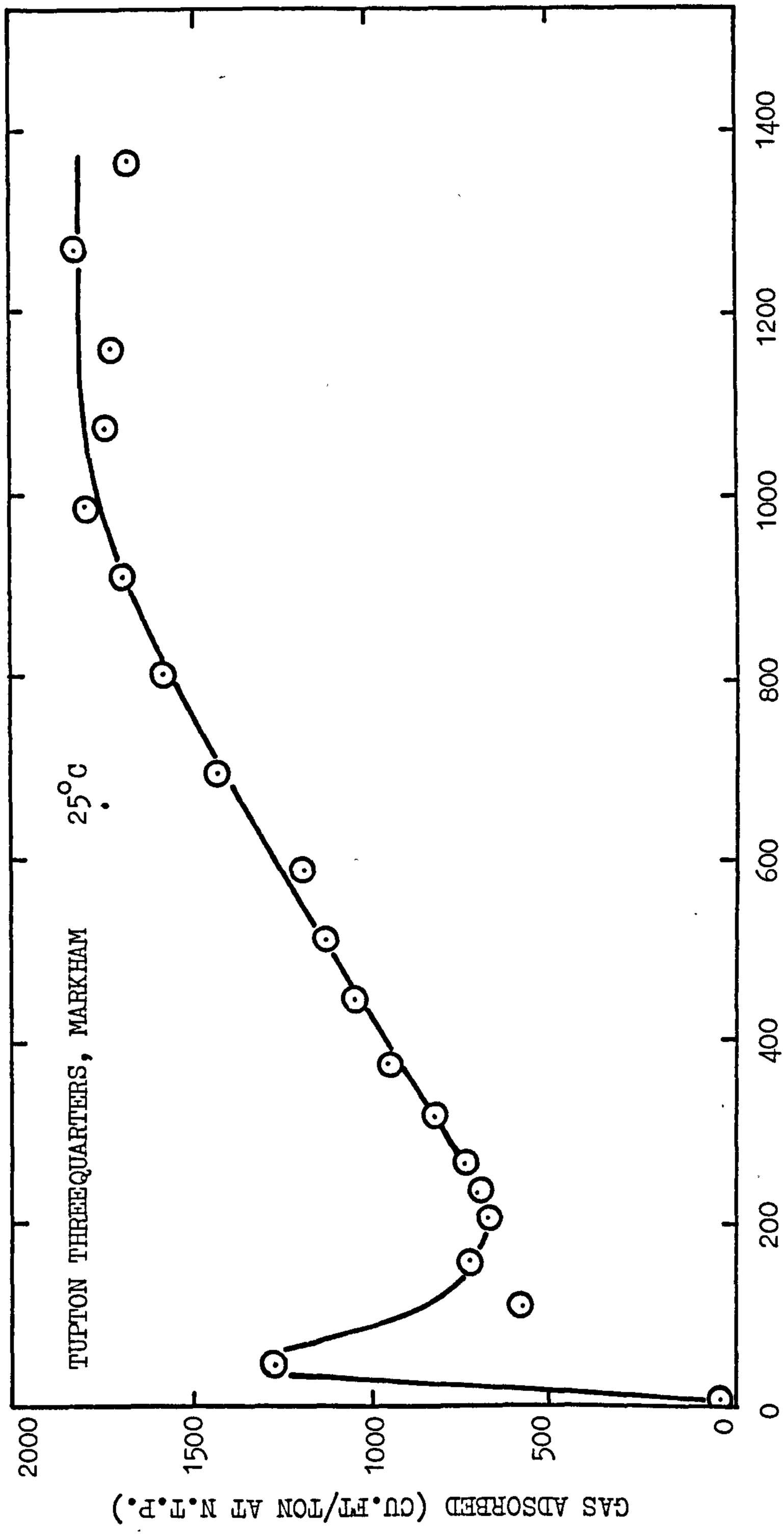

FIGURE (2.4.3) An Example of Multi-Molecular Adsorption Isotherm (After Jolly (38)).

further effect, Figure (2.5.1).

For the values of moisture content m at or below the critical value m_c (wt %) Ettinger (41), (42), developed an empirical formula to express the reduction in methane capacity as:

$$\frac{V_w}{V_d} = \frac{1}{(1 + C_o m)} \qquad (m \leqslant m_c) \quad \ldots\ldots\ldots \quad 2.5.1$$

where V_w and V_d are the volumes of methane adsorbed in moist and dry coal, respectively; and C_o has the value 0·31.

The above equation was verified by Joubert et al. (40) having used $C_o = 0{\cdot}314$ at 1 atm pressure. The constant C_o was found to depend on the gas pressure applied. They related the maximum reduction in methane sorption at or above the critical moisture value to the oxygen content and suggested the following equation:

$$\left(1 - \frac{V_w}{V_d}\right)_{max} = C_1 X_o + C_2 \qquad (m \geqslant m_c) \quad \ldots\ldots\ldots \quad 2.5.2$$

where X_o is the coal oxygen content in weight percent (m.f.b.) and C_1 and C_2 are constants. At 10 atm gas pressure values of C_1 and C_2 were found to be 0·0558 and 0·0837 respectively. As shown in Figure (2.5.2), maximum reduction in methane capacity of coal increases with increasing coal oxygen content. Combining equations

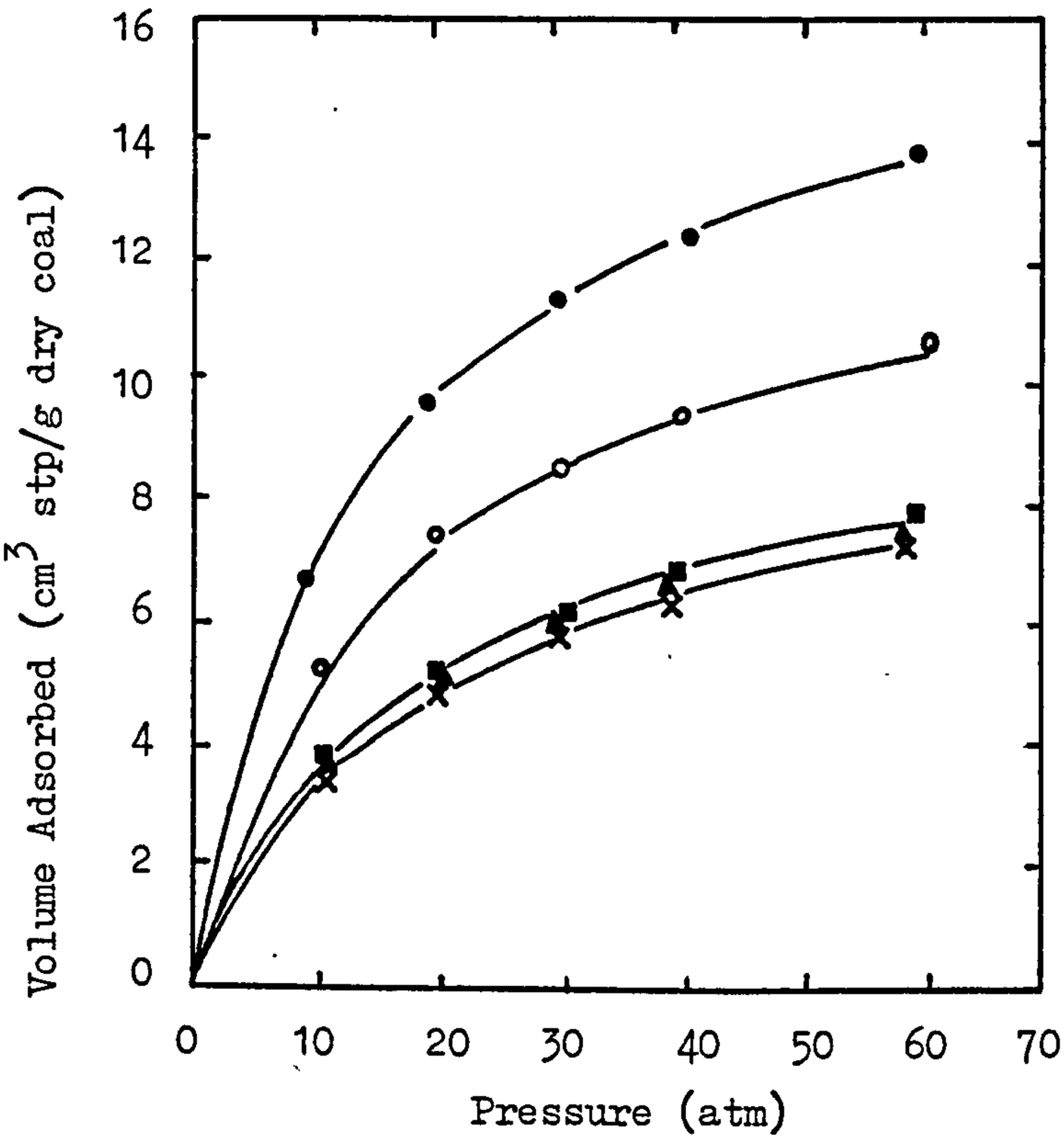

FIGURE (2.5.1) Methane Adsorption Isotherms for Coal at 30°C. Moisture Content:● zero, ○ 1·29%, ■ 3·14%, × 4·74%, ▲ 8·50% (After Joubert et al. (39)).

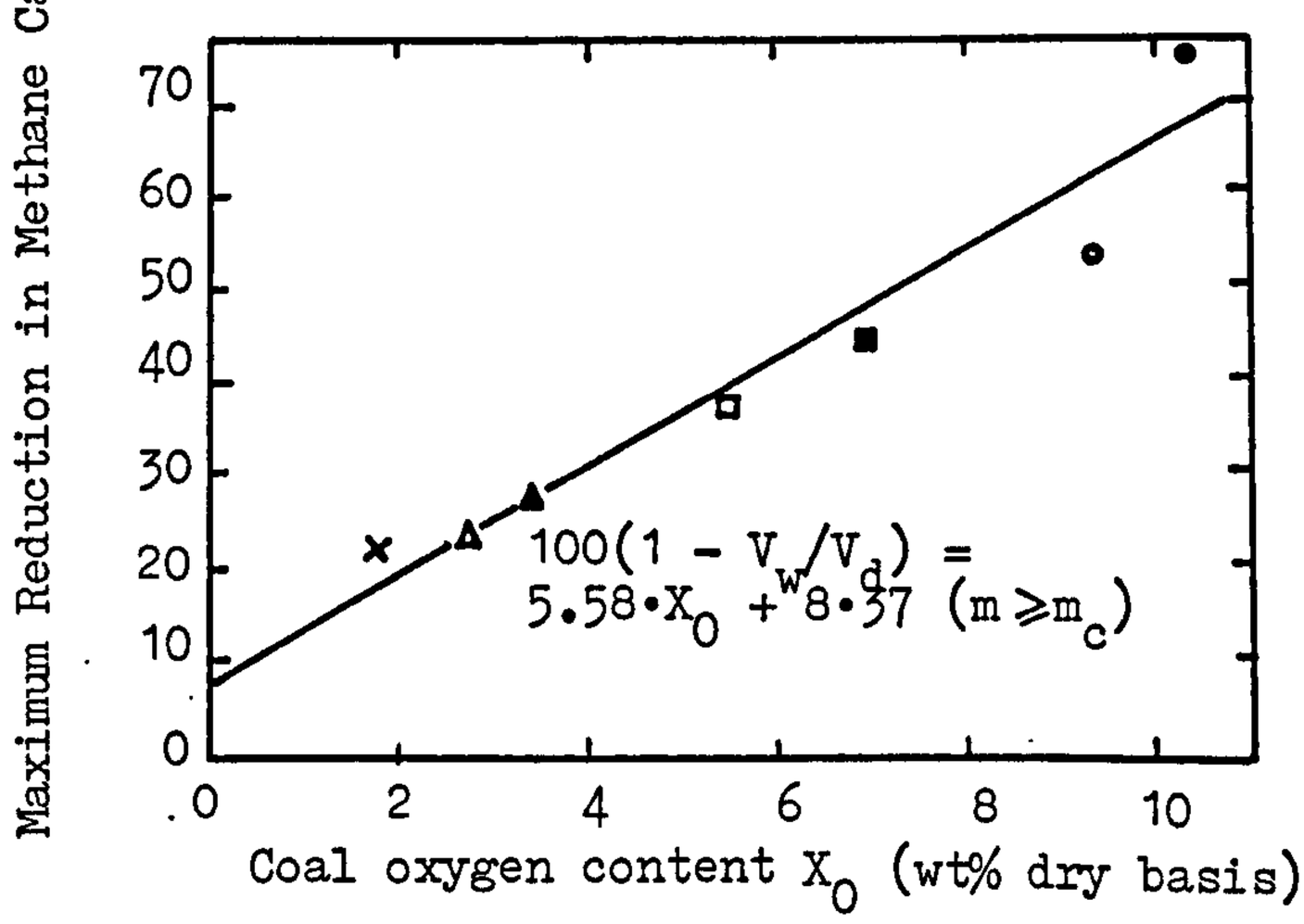

FIGURE (2.5.2) Maximum Reduction in Methane Sorption Versus Coal Oxygen Content at Values of Moisture Content Above the Critical Values; 10 atm, 30°C (After Joubert et al. (39)).

2.5.1 and 2.5.2, one can estimate the critical value of moisture content, m_c, from the equation:

$$m_c = \frac{C_1 X_o + C_2}{C_o(1 - C_1 X_o - C_2)} \qquad \ldots\ldots\ldots \quad 2.5.3$$

It is believed that moisture content, limiting the adsorption of methane, would also limit the flow of methane through coal. It is not known if there is a critical moisture value for each coal, where the effect of moisture on coal permeability reaches its ultimate value. This question was considered during the course of this research; the effect of moisture on permeability of coal under stress was examined.

CHAPTER THREE

THEORIES OF STEADY-STATE FLOW OF FLUIDS THROUGH POROUS MEDIA

CHAPTER THREE

THEORIES OF STEADY-STATE FLOW OF FLUIDS THROUGH POROUS MEDIA

3.1 Introduction

Understanding the nature of gas flow in single capillaries has contributed a great deal towards the solution of problems concerning the more complex permeation process through porous media. A porous medium is often considered as a bundle of straight parallel capillaries and the equations for capillary flow are used as the starting point for many of the equations for flow in porous media.

In this chapter, the theories of fluid flow in single capillaries are reviewed prior to discussion of the theories of fluid flow in porous media. Darcy's fundamental law governing the flow of fluids through porous media is introduced and semi-empirical Adzumi and Klinkenberg methods, which consider the molecular effects of gas flow through porous media, are examined.

3.2 Flow in Capillaries

The types of flow that have been found to occur in capillary systems are:

(i) Poisseuille viscous flow.

(ii) Molecular streaming.

(iii) Turbulent flow.

(iv) Molecular effusion.

(v) Orifice flow.

Molecular effusion occurs in infinitely short capillaries at low gas pressures where the mean free path of the flowing molecules is large compared to the diameter of the capillary. At high pressures, molecular effusion is transformed into orifice flow provided that the capillary is smooth and short enough to act as a nozzle (43), (44). Although these types of flow are considered to occur through fibrous material, such as textiles and paper, they are of very little importance in dealing with 'normal' porous systems and, therefore, will not be discussed in detail here.

3.2.1 Poisseuille Viscous Flow - Poisseuille's Law

The viscosity of a fluid is a measure of internal friction associated with laminar flow. Laminar flow is characterised by a fixed set of streamlines where a fluid element, which at one point is traversing the same path as another, must

follow the path of this element throughout its course.

An 'ideal' viscous fluid flowing over a solid surface adheres to that surface. At the surface of the solid the fluid velocity is zero. If a capillary is held fixed, a force opposing the fluid motion is imposed on the fluid by the capillary surface and a velocity gradient between the centre of the capillary and the capillary surface is created.

The first investigation into fluid flow through capillary tubes was conducted by Poisseuille in 1846 (45). The volume flow rate of fluids through a capillary tube is given by the equation (45), (3):

$$Q = -\frac{\pi r^4}{8\mu}\frac{dP}{dx} \qquad \ldots\ldots\ldots \quad 3.2.1$$

or

$$Q = \frac{\pi r^4}{8\mu}\frac{\Delta P}{L}$$

where

Q	volume flow rate,
r	radius of the capillary tube,
μ	viscosity of the flowing fluid,
ΔP	pressure difference across the tube,
L	length of the capillary tube.

Equation 3.2.1 is valid for non-compressible fluids, where the volume flow rate is constant along the length of the capillary tube. In the case of compressible fluids, the volume flow rate varies from one cross-section of the tube to another along its length. The changes are proportional to the pressure of the gas and the mass flow rate along the tube remains constant.

If Q_2 is the volume flow rate at the downstream end of the capillary tube, where the pressure and density of the gas are P_2 and ρ_2, and Q is the flow rate given by the equation 3.2.1 at any cross-section where the gas pressure and density are P and ρ respectively, one can write:

$$Q_2\rho_2 = Q\rho = -\frac{\pi r^4}{8\mu}\frac{dP}{dx}\rho \qquad \ldots\ldots\ldots \quad 3.2.2$$

Applying the general gas law and assuming isothermal flow, the density of gas at different cross sections can be written as a function of pressure ($\rho = CP$). Hence, equation 3.2.2 can be rewritten in the form:

$$Q_2P_2\,dx = -\frac{\pi r^4}{8\mu}\,P\,dP$$

bearing in mind that μ is independent of P and integrating,

$$Q_2P_2\int_0^L dx = -\frac{\pi r^4}{8\mu}\int_{P_1}^{P_2} P\,dP$$

The flow rate at the downstream end of the capillary tube can be expressed as:

$$Q_2 = -\frac{\pi r^4}{8\mu}\,\frac{P_2^2 - P_1^2}{2P_2L}$$

or

$$Q_2 = \frac{\pi r^4}{8\mu}\,\frac{P_1 + P_2}{2}\,\frac{P_1 - P_2}{P_2L}$$

Inserting $\bar{P}$, the mean pressure across the capillary for $\frac{P_1 + P_2}{2}$ and ΔP, pressure gradient for $P_1 - P_2$ Poisseuille's equation for compressible fluids takes the form:

$$Q_2 = \frac{\pi r^4}{8\mu}\,\frac{\Delta P}{L}\,\frac{\bar{P}}{P_2} \qquad \cdots\cdots\cdots \quad 3\cdot2\cdot3$$

3.2.2 Molecular Streaming - Knudsen's Law

Experimental work has shown that Poisseuille's Law failed to be valid for flow in very narrow tubes, where the mean free path of the flowing molecules becomes comparable to the diameter of the tube. The failure consists in the fact that, instead of the velocity of flow being zero at the capillary walls (as assumption made in deducing Poisseuille's Law (45)), it has a value greater than zero, thus, the gas appears to 'slip' past the wall. The amount of gas coming out from a tube therefore

appears to be greater than the diameter of the tube would warrant.

The 'slip' phenomenon in capillary tubes was first observed experimentally by Kundt and Warburg in 1875 (3). Warburg suggested a 'slip correction' to Poisseuille's formula by adding a constant term to the latter. This meant that under a zero pressure differential there is a finite 'slip flow' through a capillary and for other pressure differentials calculated flow is corrected by this finite value.

From experimental investigations Knudsen (46) put forward yet another equation for the total volume of gas flow Q_2 (measured at pressure P_2) through a capillary tube of radius r and length L. His equation takes the form:

$$Q_2 = \frac{4}{3}\sqrt{\frac{2\pi RT}{M}}\ \frac{r^3}{L}\ \frac{\Delta P}{P_2} \qquad \ldots\ldots\ldots \quad 3.2.4$$

where

R is the gas constant,

T is the absolute temperature of gas,

M is the molecular weight of the gas.

It was established experimentally that Knudsen's equation described the flow correctly if the mean free path of the flowing molecules was very large compared with the radius r of the capillary tube. Poisseuille's equation had to be used if the mean free path was very small.

For intermediate cases, the two conditions were combined by Adzumi (47) and the following equation was suggested:

$$Q_2 = \frac{\pi r^4}{8\mu} \frac{\Delta P}{L} \frac{\bar{P}}{P_2} + \gamma \frac{4}{3} \sqrt{\frac{2\pi RT}{M}} \frac{r^3}{L} \frac{\Delta P}{P_2}$$

Here, γ is a dimensionless proportionality factor which is suggested to have a value of about 0·90 for single gases and 0·66 for gaseous mixtures. It is assumed that γ will be constant for any flow phenomenon; it is called 'Adzumi constant'.

3.2.3 Turbulent Flow

For sufficiently high flow rates, laminar type of flow breaks down so that Poisseuille's Law is no longer valid. For any one system, it is suggested that a 'transition point' exists below which steady flow is stable. Above the transition point the steady flow is more likely to become unsteady forming eddies upon the slightest disturbance and the flow is termed 'turbulent'.

It has been shown by Reynolds that circular straight tubes are dynamically similar, as far as the Poisseuille equation is concerned, if the Reynolds Number (Re) is the same:

$$Re = \frac{2\rho r v}{\mu}$$

where v is the average flow velocity in the tube.

Turbulance will occur in any straight circular tube if a certain Reynolds Number is reached. The transition from laminar to turbulent flow has been found to occur in the neighbourhood of Re = 2200 for straight capillaries (3).

3.3 Flow in Porous Media

3.3.1 Darcy's Law

The fundamental theory of laminar flow through homogenous porous media is based on the experiment originally performed by Henry Darcy in 1856 (48). Darcy conducted a series of experiments on the flow of water through filter sands. By varying the different quantities involved, he arrived at the following relationship:

$$Q = -K'A \frac{h_2 - h_1}{L} \qquad \ldots\ldots\ldots \quad 3.3.1$$

where

Q is the total volume of fluid flowing through the filter sand in unit time,

A is the cross-sectional area of the filter sand,

$h_2 - h_1$ is the difference in head of the fluid across the filter sand with length L,

K' is a constant depending on the properties of the fluid and of the porous medium.

This relationship is known as Darcy's Law, a more detailed discussion of Darcy's work is given by Hubbert (49).

For the one dimensional case of non-compressible fluid flow through a porous medium, equation 3.3.1 takes the form (50):

$$Q = -K'A \frac{dP}{dx}$$

or

$$Q = K'A \frac{\Delta P}{L} \qquad \ldots\ldots\ldots \quad 3.3.2$$

where $\frac{dP}{dx}$ is the pressure gradient.

Proceeding as before (Section 3.2.1) Darcy's Law can be further extended to cover the steady state isothermal flow of compressible fluids through porous media, i.e.

$$Q_2 = K'A \frac{\Delta P}{L} \frac{\bar{P}}{P_2} \qquad \ldots\ldots\ldots \quad 3.3.3$$

3.3.2 The Concept of Permeability

Darcy's Law, in its original form, was found to be rather restricted in its application. Constant K', which was often termed 'permeability-constant', is obviously indicative of the permeability of a certain medium to a particular fluid and it is desirable to separate the effect of the porous medium from that of the fluid.

In an attempt to increase the applicability of Darcy's Law, Nutting (51) suggested the following relationship:

$$K' = \frac{K}{\mu}$$

where

μ is the viscosity of the fluid,

K is the 'specific permeability' of the porous medium.

As stated by Scheidegger (3), this relationship was not generally accepted until it was popularised by Wyckoff et al. Unless otherwise stated all future reference to permeability in this thesis will be taken to mean 'specific permeability' and the symbol 'K_d' will be used to denote permeability calculated by using Darcy's equation.

Substituting $\frac{K_d}{\mu}$ for K', Darcy's equation for steady-state non-compressible fluid flow through porous media takes the form:

$$Q = \frac{K_d A}{\mu} \frac{\Delta P}{L} \qquad \ldots\ldots\ldots \quad 3.3.4$$

and for compressible fluids it can be written as:

$$Q_2 = \frac{K_d A}{\mu} \frac{\Delta P}{L} \frac{\bar{P}}{P_2} \qquad \ldots\ldots\ldots \quad 3.3.5$$

where Q_2 is the volume flow rate measured at the downstream end at pressure P_2.

3.3.3 Slip Flow in Porous Media

It was first observed by Fancher et al. (52) and later by several other researchers that air permeabilities were higher than liquid permeabilities in the same porous medium as calculated from Darcy's Law. It was suggested that the breakdown of Darcy's Law for gases occurs if the pore diameters become comparable with, or less than, the molecular mean free path of the flowing gas.

The two basic approaches by Adzumi (47) and Klinkenberg (53) both used the theory of molecular slip in order to explain the anomalies observed in gas flow through porous media. Adzumi's approach was mainly theoretical whereas Klinkenberg based his theory mainly on experimental investigations.

3.3.3.1 Semi-Empirical Adzumi Theory

Adzumi (47) was the first to use the theory of molecular slip in order to provide an explanation of the anomalies observed in gas flow measurements through porous media. He constructed a theoretical model, in which a porous medium was represented by a bundle of parallel capillaries, each of which is made up of a number of short capillaries of different diameters. Using Knudsen's Law of slip flow through single capillary, Adzumi was able to derive an equation for the flow of a gas through the porous medium. The equation may be written as follows:

$$Q_2 = \frac{\pi \Delta P}{8\mu} E \frac{\bar{P}}{P_2} + \gamma \frac{4}{3} \sqrt{\frac{2\pi RT}{M}} F \frac{\Delta P}{P_2} \quad \ldots\ldots\ldots \quad 3.3.6$$

where γ is the Adzumi constant (γ= 0·9, see Section 3.2.2); $E = n\bar{R}^4/L$; and $F = n\bar{R}^3/L$; with n = number of pores in the cross-sectional area of the porous medium; $\bar{R}$ = average radius of the pores; L = thickness of the porous medium.

Equation 3.3.6 given here is known as the Adzumi equation for slip flow of gases through porous media. Obviously, it is impossible to calculate constants E and F from their separate components for an actual porous medium; therefore they have to be obtained experimentally.

Rose (54) modified Adzumi's equation in order to represent porous media by incorporating cross-sectional area A and length L of the sample. All the constants in the first term of equation 3.3.6 were thought to refer to the physical structure of the porous medium; these constants were collected to give the relationship:

$$K_v = \frac{\pi \bar{R}^4}{8} \frac{1}{A} \quad \ldots\ldots\ldots \quad 3.3.7$$

where K_v was termed as the viscous permeability.

Later, Jones (11) extended this work further to cover the second term of the equation. Gathering together the constants which would refer to the geometry of the porous structure he arrived at the following expression:

$$K_m = \gamma \frac{4}{3}\sqrt{2\pi}\ \bar{R}^3\ \frac{1}{A} \qquad \ldots\ldots\ldots\ 3.3.8$$

where K_m was termed as the molecular permeability. Substituting K_v and K_m in Adzumi's equation one obtains:

$$Q_2 = \frac{A}{L}\ \frac{\Delta P}{P_2}\left(\frac{K_v}{\mu}\bar{P} + K_m\sqrt{\frac{RT}{M}}\right) \qquad \ldots\ldots\ldots\ 3.3.9$$

rewriting equation 3.3.9 as

$$\frac{Q_2P_2}{\Delta P} = \left(\frac{K_vA}{\mu L}\right)\bar{P} + \frac{A}{L}K_m\sqrt{\frac{RT}{M}} \qquad \ldots\ldots\ldots\ 3.3.10$$

a plot of $\frac{Q_2P_2}{\Delta P}$ against $\bar{P}$ will yield a straight line of gradient $K_v\frac{A}{\mu L}$ and intercept $K_m\frac{A}{L}\sqrt{\frac{RT}{M}}$, thus the values of K_v and K_m can be calculated from experimental observations.

3.3.3.2 Semi-Empirical Klinkenberg Theory

A number of years after Adzumi, Klinkenberg (53) also used the theory of slip to explain the observed gas flow anomalies,

apparently without knowing about Adzumi's work. From his experimental work, Klinkenberg found that the permeability of a porous medium remained fairly constant for any type of liquid used. However, when gases were employed the permeability changed with the pressure applied and the gas used.

In his experiments, Klinkenberg used Jena glass as the porous medium and measured its permeability for air, hydrogen, carbon dioxide, nitrogen and iso-octane (liquid) at various pressure differences. As shown in Figure (3.3.1), as the mean gas pressure increased, permeability decreased and approached the liquid permeability. At low gas pressures, permeability for different gases was found to differ widely, the difference lessening gradually as the pressure increased.

In order to explain these discrepancies, Klinkenberg used the theory of molecular slip. He constructed a capillaric model where a porous medium was assumed to be represented by an assemblage of short, fine capillaries of the same average diameter and length which were oriented at random throughout the material. By applying Kundt and Warburg's slip theory to each capillary, Klinkenberg was able to apply a correction to Darcy's equation for gas flow in porous media. Klinkenberg's equation may be stated as:

$$Q_2 = \frac{\pi \bar{R}^4}{8} \eta \frac{1}{\mu} A \left(1 + \frac{4c\lambda}{\bar{R}}\right) \frac{\Delta P}{L} \frac{\bar{P}}{P_2} \quad \ldots\ldots\ldots \quad 3.3.11$$

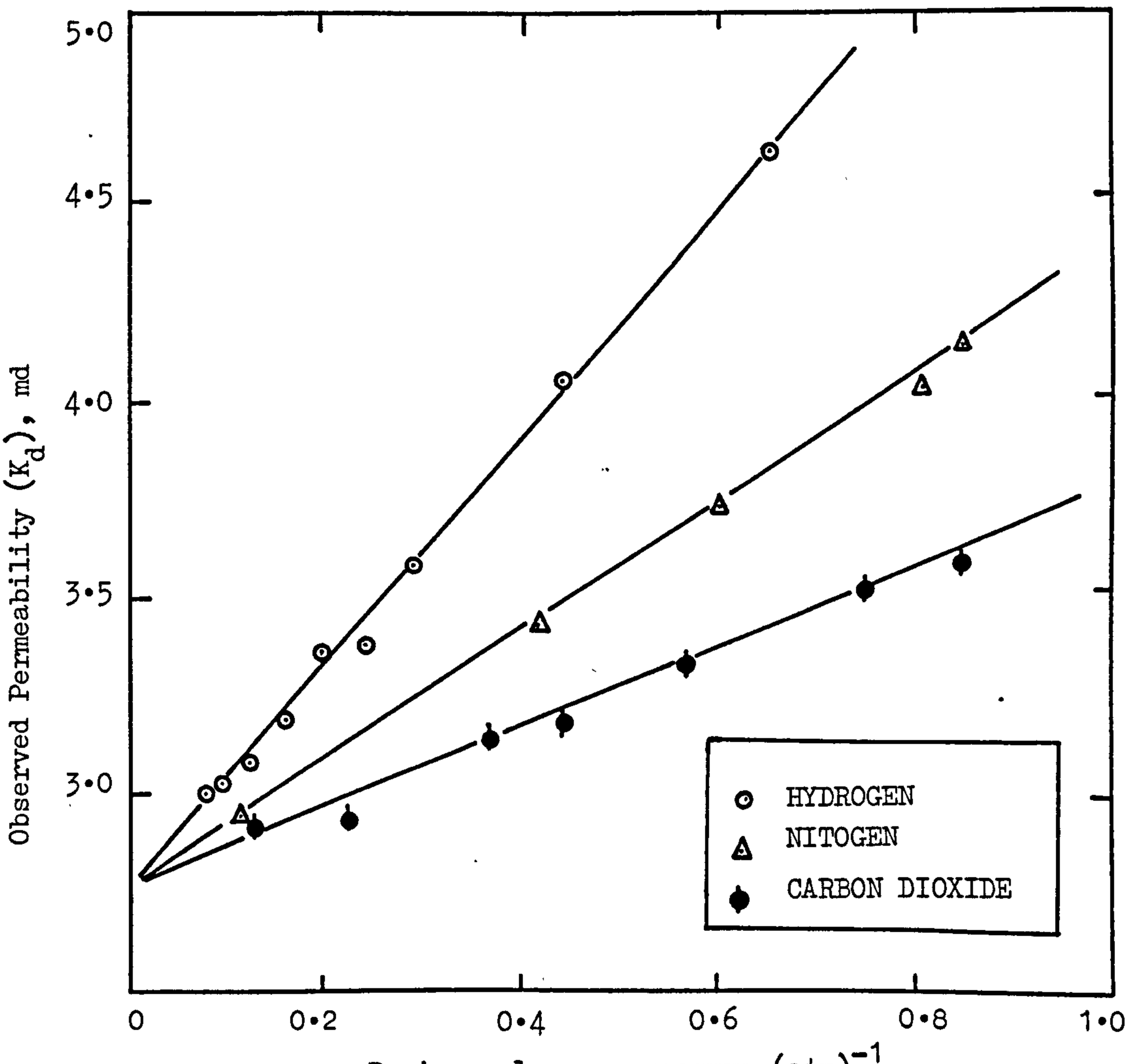

FIGURE (3.3.1) Permeability Constant of Core Sample 'L' to Hydrogen, Nitrogen and Carbon Dioxide at Different Pressures (After Klinkenberg (53)).

where

$\bar{R}$ is the average radius of capillary (a quantity associated with a given porous material),

η is a dimensionless coefficient for a given porous material which refers to the average area and length of the capillaries,

λ is the mean free path of the gas used,

c is a proportionality constant found to be nearly unity.

Gas flow rate Q_2 in equation 3.3.11 and in Darcy's equation for gas flow in porous media,

$$Q_2 = \frac{K_d}{\mu} A \frac{\Delta P}{L} \frac{\bar{P}}{P_2}$$

should yield the same quantity for a given specimen and given experimental conditions, thus the specific permeability K_d in Darcy's equation takes the form:

$$K_d = \left[\frac{\pi \bar{R}^4}{8} \eta \right] \left(1 + \frac{4c\lambda}{\bar{R}} \right) \qquad \ldots\ldots\ldots 3.3.12$$

The quantity in the square brackets in equation 3.3.12 is a constant which depends on the geometric structure of the porous medium concerned. This was recognised by Klinkenberg as being the liquid permeability K_L of the porous medium.

As the mean free path λ is inversely proportional to the mean pressure $\bar{P}$, Klinkenberg could write the following relationship:

$$\frac{b}{\bar{P}} = \frac{4c\lambda}{\bar{R}} \qquad \ldots\ldots\ldots \quad 3.3.13$$

where b is Klinkenberg's constant which is different for each material depending on the structure of the pore system.

Substituting the liquid permeability K_L for $(\pi\bar{R}^4\eta/8)$ and using relationship 3.3.13 we get:

$$K_d = K_L \left(1 + \frac{b}{\bar{P}} \right)$$

or

$$K_d = K_L + K_L\, b\, \frac{1}{\bar{P}} \qquad \ldots\ldots\ldots \quad 3.3.14$$

When K_d is plotted against the reciprocal mean pressure $1/\bar{P}$, it should yield a straight line with intercept equal to K_L and gradient $K_L b$. Apparent permeability K_d can be obtained by solving equation 3.3.5 where all the other variables are experimentally determined. Hence, Klinkenberg constant b and liquid permeability K_L can be determined by using the same experimental data. When Klinkenberg's correction is applied, equation 3.3.5 takes the form:

$$Q_2 = \frac{K_L}{\mu} \left(1 + \frac{b}{\bar{P}} \right) A \frac{\Delta P}{L} \frac{\bar{P}}{P_2} \qquad \ldots\ldots\ldots \quad 3.3.15$$

Rose (54) compared the two semi-empirical equations by Adzumi and Klinkenberg and concluded that they were identical. The apparent difference between the two equations is that Adzumi investigated the flow at low mean pressures where the mean free path becomes greater than the pore dimensions so that the flow is in the form of molecular streaming, whereas Klinkenberg considered the region where mean free path is becoming so small that the gas assumes the flow characteristics of a fluid.

Sowier (55) re-examined Klinkenberg's results on flow of different gases through porous media and concluded that a single intercept of the apparent permeability function with respect to the reciprocal mean pressure was no longer existing for different gases. He suggested that the liquid permeability, often used as viscous permeability, was different for each individual gas so that:

$$K_d = K_I \left(1 + \frac{S}{\bar{P}} \right)$$

where

K_I is the coefficient of gas conveyance which changes for different gases,

S is a constant that varies with temperature.

Figure (3.2.2) shows one of Klinkenberg's experimental results re-plotted by Sowier.

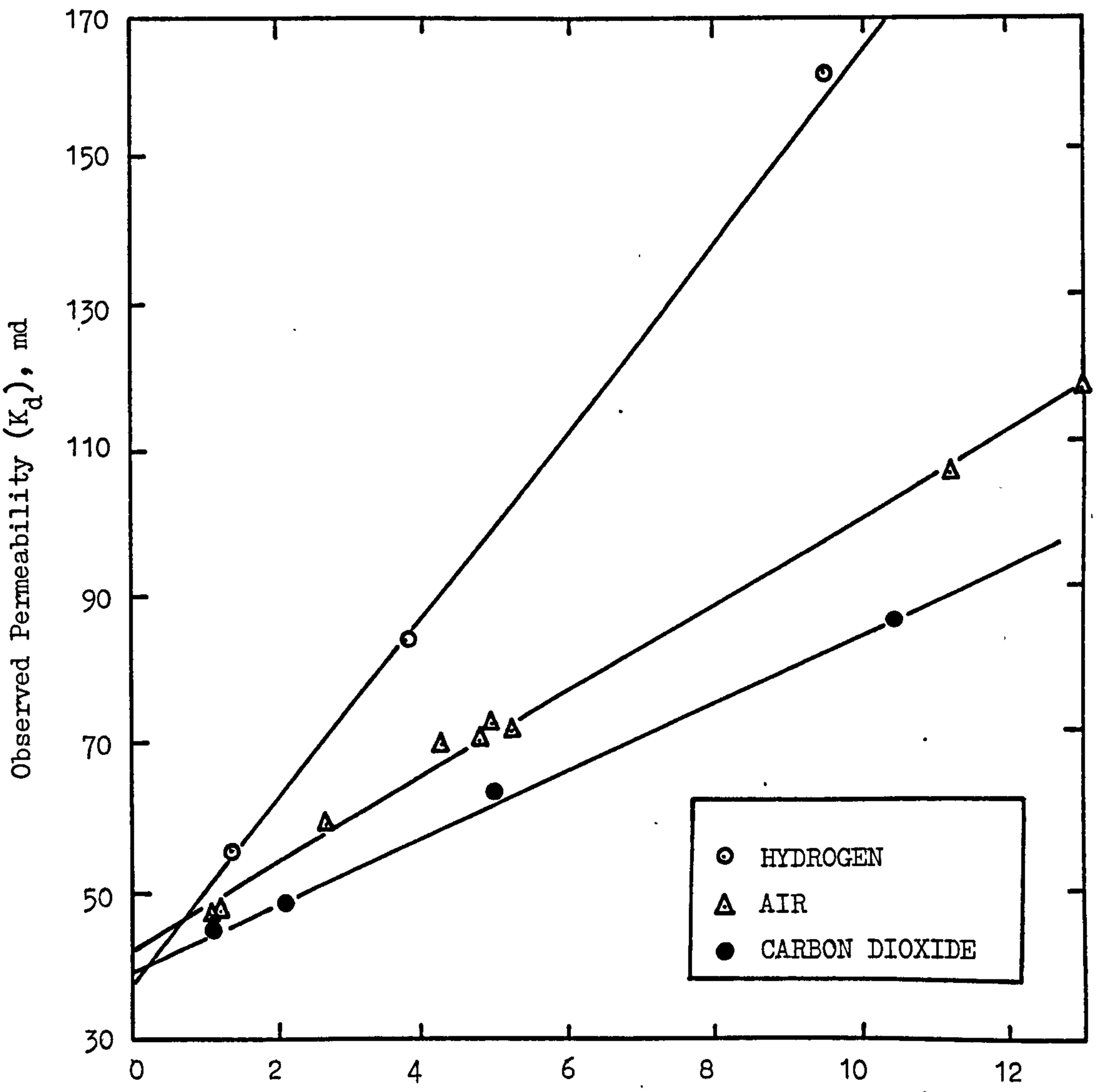

FIGURE (3.2.2) Replot of Klinkenberg's Experimental Data (After Sowier (55)).

Both Adzumi and Klinkenberg approaches are widely used in treating gas flow measurements through porous media, the latter being more commonly used in the petroleum industry.

CHAPTER FOUR

STRATA MECHANICS AND STRENGTH OF COAL SEAMS IN RELATION TO THE CHANGING STRESSES AROUND LONGWALL FACES

CHAPTER FOUR

STRATA MECHANICS AND STRENGTH OF COAL SEAMS IN RELATION TO THE CHANGING STRESSES AROUND LONGWALL FACES

4.1. Introduction

The main purpose of this research is to establish a physical relationship between applied stress and the permeability of some coals. The type of stress conditions studied were related to those encountered under normal mining conditions. It was found necessary to achieve an understanding of stress fields around working longwall faces and of the mechanism of strength and fracturing of coals before the experimental procedure was designed.

Although the actual state of stresses in the vicinity of a longwall face is not exactly known, it is generally agreed that the coal material is triaxially compressed in the abutment zone beyond the face. Stresses become more complex at the face and at the roof behind the face where the strata is relaxed.

Evans and Pomeroy (56) have suggested that the strength and the behaviour of coal under stress is related to its rank. This implied that the rank and structural properties of individual coal seams would effect the permeability induced by changes in stress conditions.

A method of understanding the stresses underground and a model to simulate subsurface stress conditions in the laboratory will be discussed in this chapter.

4.2. Strata Mechanics

Longwall mining of the stratified deposits is the most commonly used underground method of working coal seams in Europe. It has been used in a variety of geological conditions and proved to be the most reliable and economic method allowing high mechanisation and efficiency in production. A longwall coalface is an extraction of either the whole or part, of the coal seam by means of a travelling working front. Although there are exceptions, 50 to 300 m wide longwall faces travelling 800 to 1000 m during their life are the most common practice in the European Coalfields.

4.2.1. Causes and Zones of Longwall Strata Pressure Abutments

Before mining is started, coal seams are loaded by the weight of the overburden where the stresses are uniformly distributed. As the coal is extracted, the roof over the waste area, which is not supported, tends to be deflected as a cantilever and will eventually be caved. As a result of these disturbances, stress conditions in the longwall panel will be readjusted until a new equilibrium is achieved.

This new state of stress is expressed in the form of high pressure zones in the solid ground surrounding the extracted region. These high pressure areas, called 'pressure abutment' zones, have

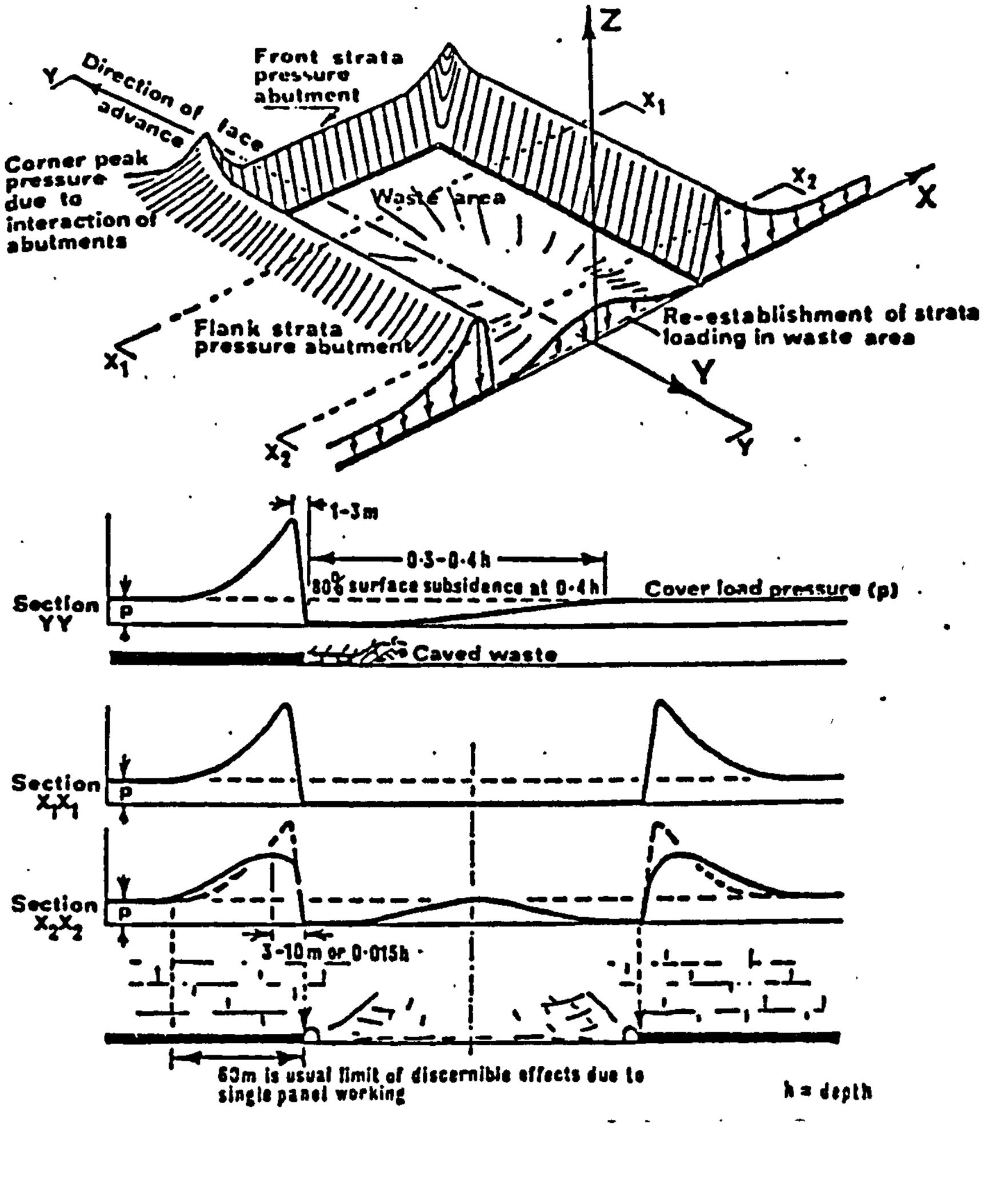

FIGURE (4.2.1) Strata Pressure Redistribution in the Plane of the Seam Around a Longwall Face (After Whittaker (57)).

been the subject of many studies in the field of Rock Mechanics which have attempted to formulate their shape, extent and magnitude. It is widely agreed that the redistribution of the strata pressures take the form illustrated by Figure (4.2.1.). Although the exact location, width and magnitude of the stresses in the abutment zones are not known, a detailed knowledge about these factors is essential in determining the crucial changes induced in permeability of the strata by the forward movement of the face.

Peng (58) reported experimental data and suggested that the effect of front abutment pressure could be discerned 150 metres in advance of the face. However, the increase in magnitude of the stresses at this location was very small. As shown in Figure (4.2.2) stresses increased slightly at a distance between 60 and 40 m from the face, increased rapidly when the face was between 20 and 15 m away, and reached a peak abutment pressure at 1 to 5 m ahead of the face. Metcalf (60) analysed the data from several collieries and concluded that the width of the front abutment did not relate to the depth, but increased with the seam thickness, Figure (4.2.3). Whittaker (57) has suggested that, in general the magnitude of the peak abutment pressure would be 4 to 5 times the cover load.

Referring to Whittaker's model, at the face area, where the roof was totally destressed the vertical pressure would be reduced to much less than the cover load. Toward the waste, pressure gradually built up on the caved waste due to recompaction and reached the cover load at a distance between 3/10 and 4/10 of the overburden thickness behind the faceline (YY section of Figure 4.2.1).

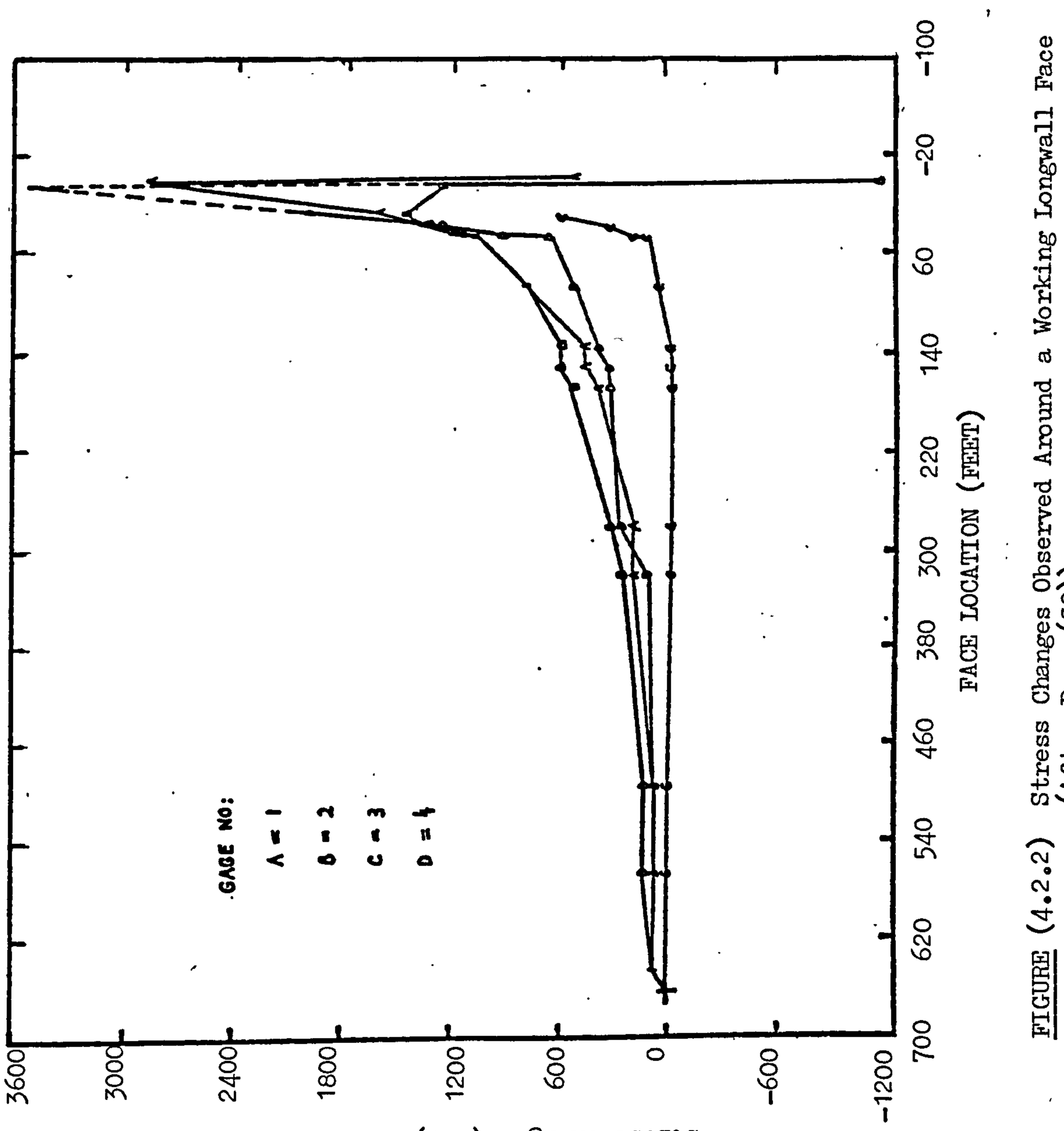

FIGURE (4.2.2) Stress Changes Observed Around a Working Longwall Face (After Peng (59)).

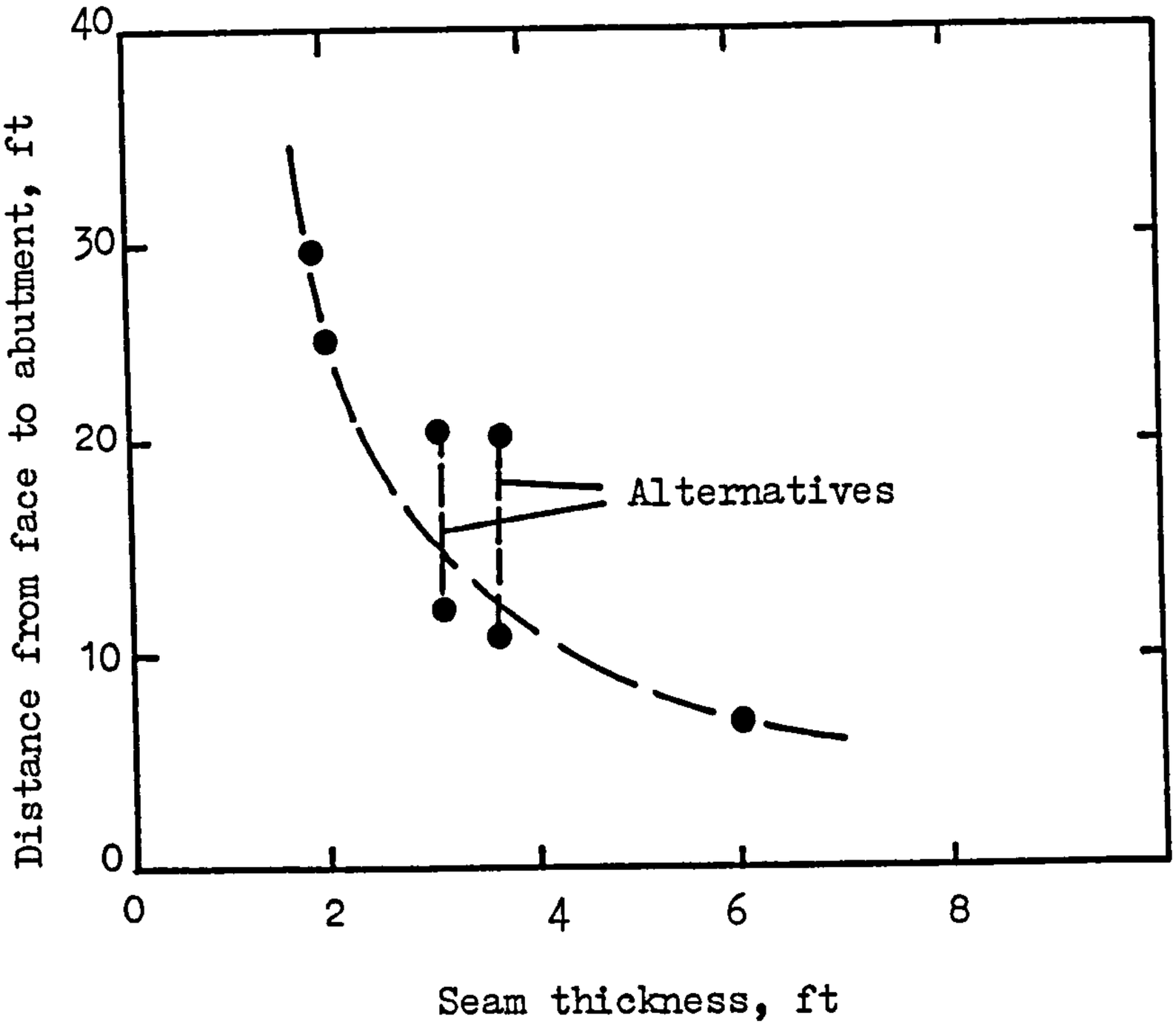

FIGURE (4.2.3) Relation of Abutment Position to Seam Thickness (After Metcalf (60)).

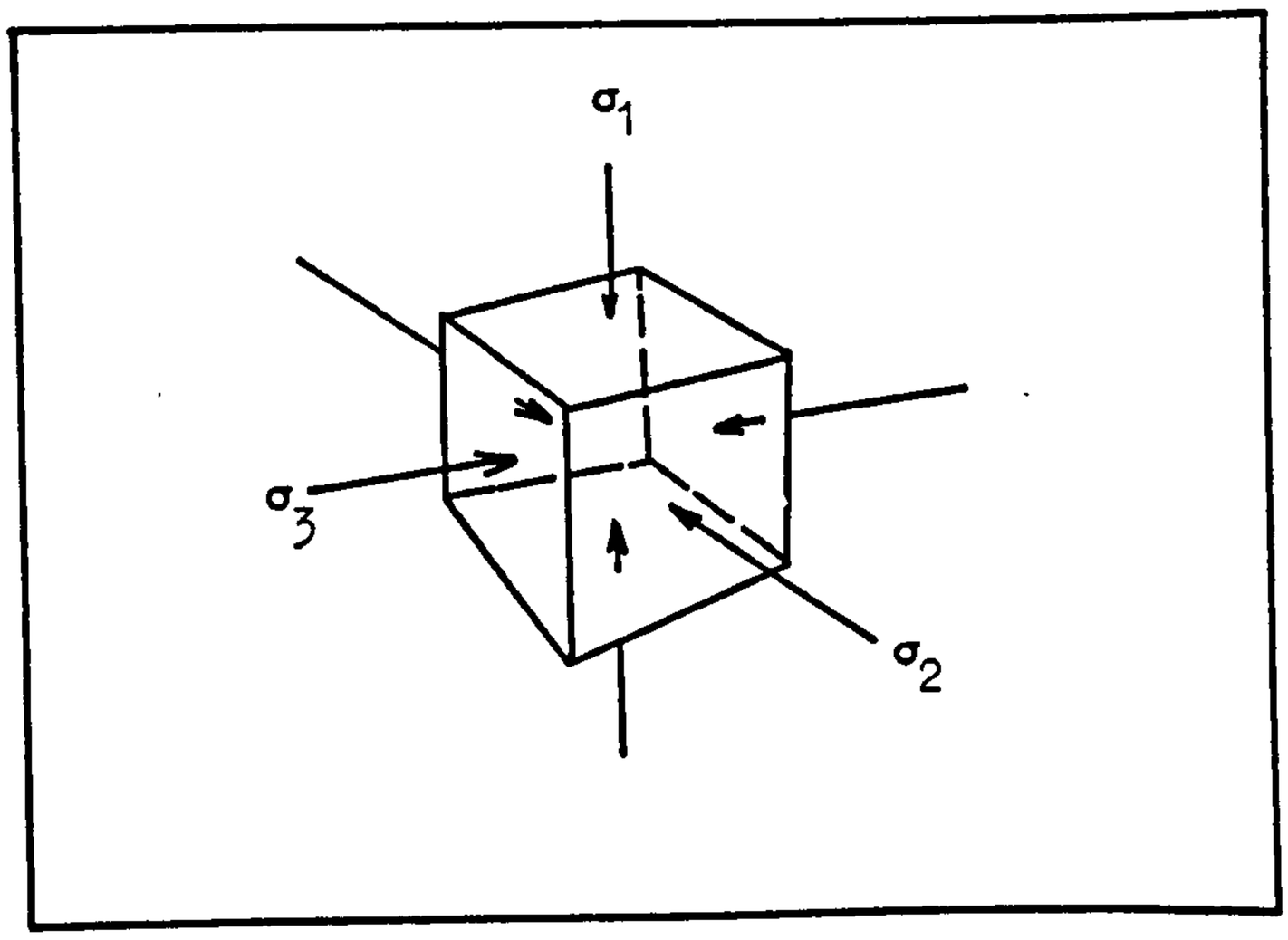

FIGURE (4.2.5) Princial Stresses on an Elementary Volume.

4.2.2 The Finite Element Method of Determining Stresses Around Longwall Faces

The choice of stress state and stress levels for simulating the subsurface stress conditions in the laboratory was the most important factor determining the applicability of the stress-permeability research in practice. It was considered that the state of stresses in the front abutment zone was triaxial compression. However, stresses assumed a much more complex form in the face area. Understanding this complex phenomena was the key factor in creating ideal simulation conditions and in explaining the changes occuring in the permeabilities of coal seams.

A method of two-dimensional stress analysis around longwall faces using the finite element method has been devised by Rock Mechanics Research Workers in the Department of Mining Engineering, University of Nottingham (61), (62). This technique, with some practical considerations to accomodate the dynamic effects of face advance, was adopted to determine the ideal stress conditions for laboratory stress simulations throughout this research.

The finite element method was based on dividing the body considered into a number of smaller bodies (elements) which were joined together at their vertices, called nodal points. Each of these elements was then analysed independently by breaking the continuum into a system of elements. Figure (4.2.4) shows a finite element grid used for both isotropic and anisotropic solutions. The theory, solution and programming of the above technique was discussed at length by Hazine (61).

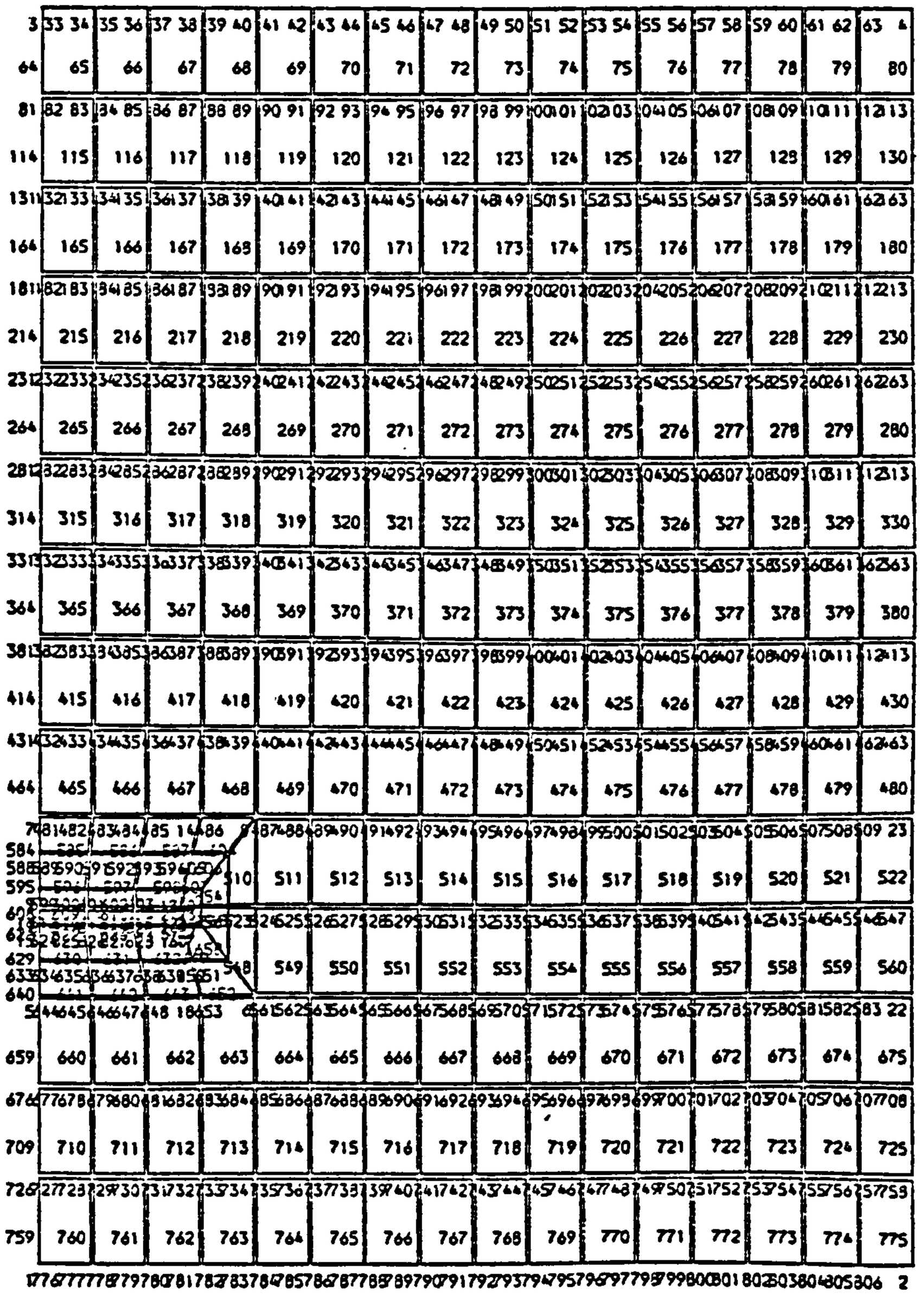

FIGURE (4.2.4) Finite Element Grid Used for Isotropic and Anisotropic Solutions (After Hazine (62)).

4.2.2.1 Principal Stresses and Shear Stress

The stresses on an element of material situated underground may be resolved into three principal stresses. These stresses are at right angles to each other so that each of the principal stresses may be visualised as bearing on two opposite sides of a cube as shown in Figure (4.2.5).

When the three principal stresses are not equal then shear stresses (τ) are induced as a function of the difference between two principal stresses on the same plane. Convention has it that, the largest principal stress (σ_1) and the smallest principal stress (σ_3) are known as the Maximum and Minimum principal stresses respectively.

4.2.2.2 Maximum and Minimum Principal Stress Distributions Around Longwall Faces Determined by the Finite Element Method

The maximum (σ_1) and minimum (σ_3) principal stresses around 300 m, 500 m and 700 m deep longwall faces were determined using the finite element method. The face was assumed to be 160 m wide in a 2 m thick horizontal coal seam. The idea was to determine the magnitudes of the stresses in the front abutment zone, face area and the waste side on both the roof and floor levels of the worked seam. The extent of stress effect into the strata above and below the face level was also observed.

Figures (4.2.6), (4.2.7), (4.2.8) and Tables (4.2.1), (4.2.2), (4.2.3) show the magnitudes of the maximum and minimum

TABLE (4.2.1) Theoretical Values for Maximum and Minimum Principal Stresses Along the Roof of a 300 m Deep Longwall Face.

DISTANCE FROM THE FACE LINE (m)	MAXIMUM PRINCIPAL STRESS σ_1 (MN/m^2)	MINIMUM PRINCIPAL STRESS σ_3 (MN/m^2)
80	0•04	5•24
67	**−0•01	5:16
54	−0•29	5:18
40	0•28	4:92
27	−1•03	6•79
15	0•12	2:71
0	−46•20	−13:80
*−10	−12•70	0:53
−18	−11•70	−6:18
−25	−10•60	−5:15
−35	−9•48	−4•57
−40	−9•30	−3•89
−55	−8•55	−3:51
−70	−8•11	−3•02
−85	−7•83	−2:72
−100	−7•67	−2:51
−115	−7•54	−2:40
−130	−7•43	−2:28
−145	−7•36	−2:22
−160	−7•29	−2•15
−175	−7:27	−2•15
−190	−7•19	−2•06

* Negative sign indicates distance ahead of the face.

** Compressive Stress is indicated by negative sign whereas tensile stress is positive.

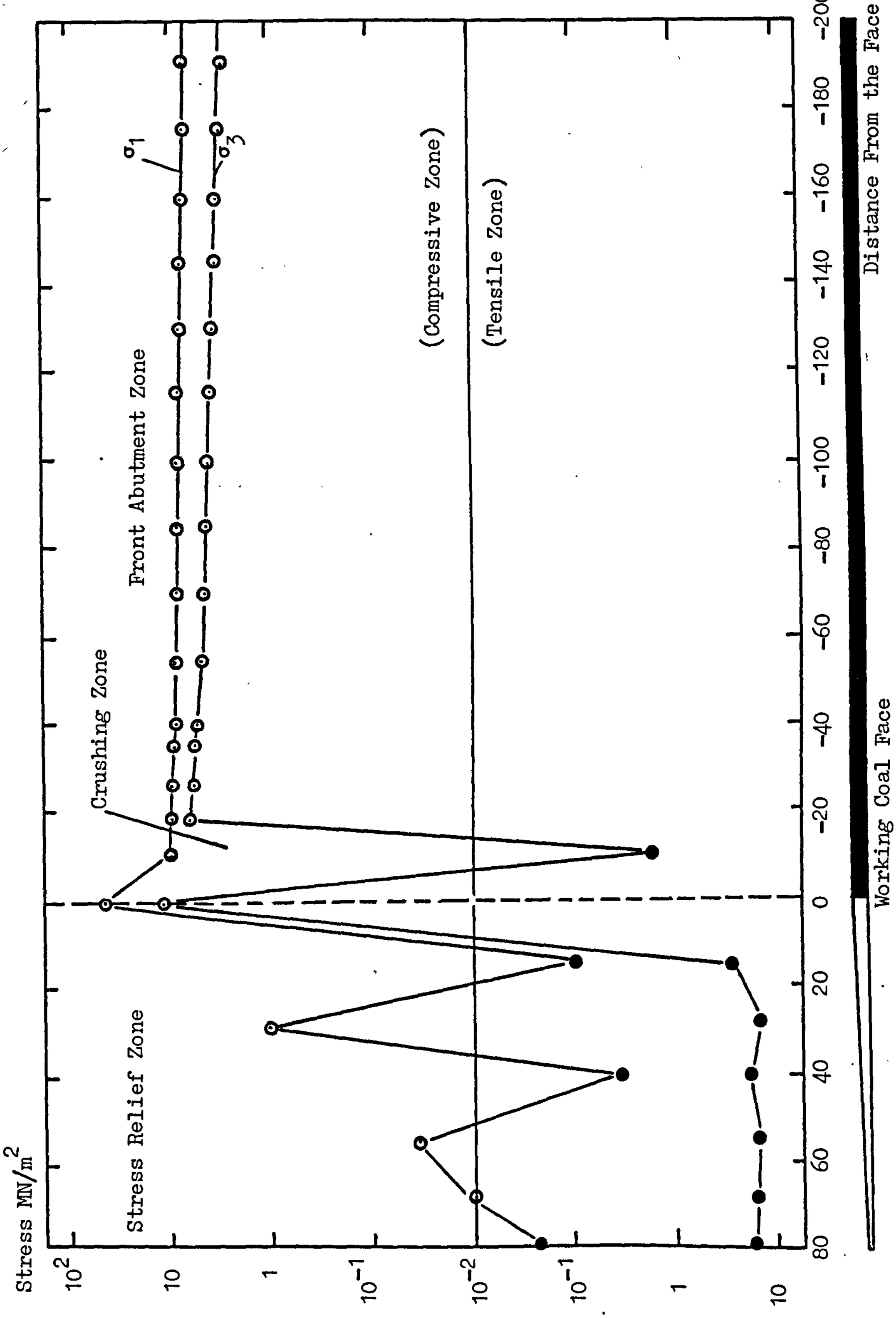

FIGURE (4.2.6) Maximum and Minimum Principal Stresses Along the Roof of a 300m Deep Longwall Face.

TABLE (4.2.2) Theoretical Values for Maximum and Minimum Principal Stresses Along the Roof of a 500 m Deep Longwall Face.

DISTANCE FROM THE FACE LINE (m)	MAXIMUM PRINCIPAL STRESS σ_1 (MN/m^2)	MINIMUM PRINCIPAL STRESS σ_3 (MN/m^2)
80	0•06	8:06
67	-0•01	7:59
54	-0•43	8:00
40	0•45	7:63
27	-1•67	10:70
15	0•21	4:29
0	-74•00	-22:20
-10	-20:40	0:74
-18	-18:90	-10:10
-25	-17•00	-8:43
-35	-15:90	-7:51
-40	-15:10	-6:56
-55	-13•90	-5:80
-70	-13:20	-5:01
-85	-12•80	-4:52
-100	-12:60	-4:16
-115	-12:40	-3:79
-130	-12:30	-3:78
-145	-12•20	-3:66
-160	-12•10	-3:54
-175	-12•10	-3:47
-190	-12•10	-3•39

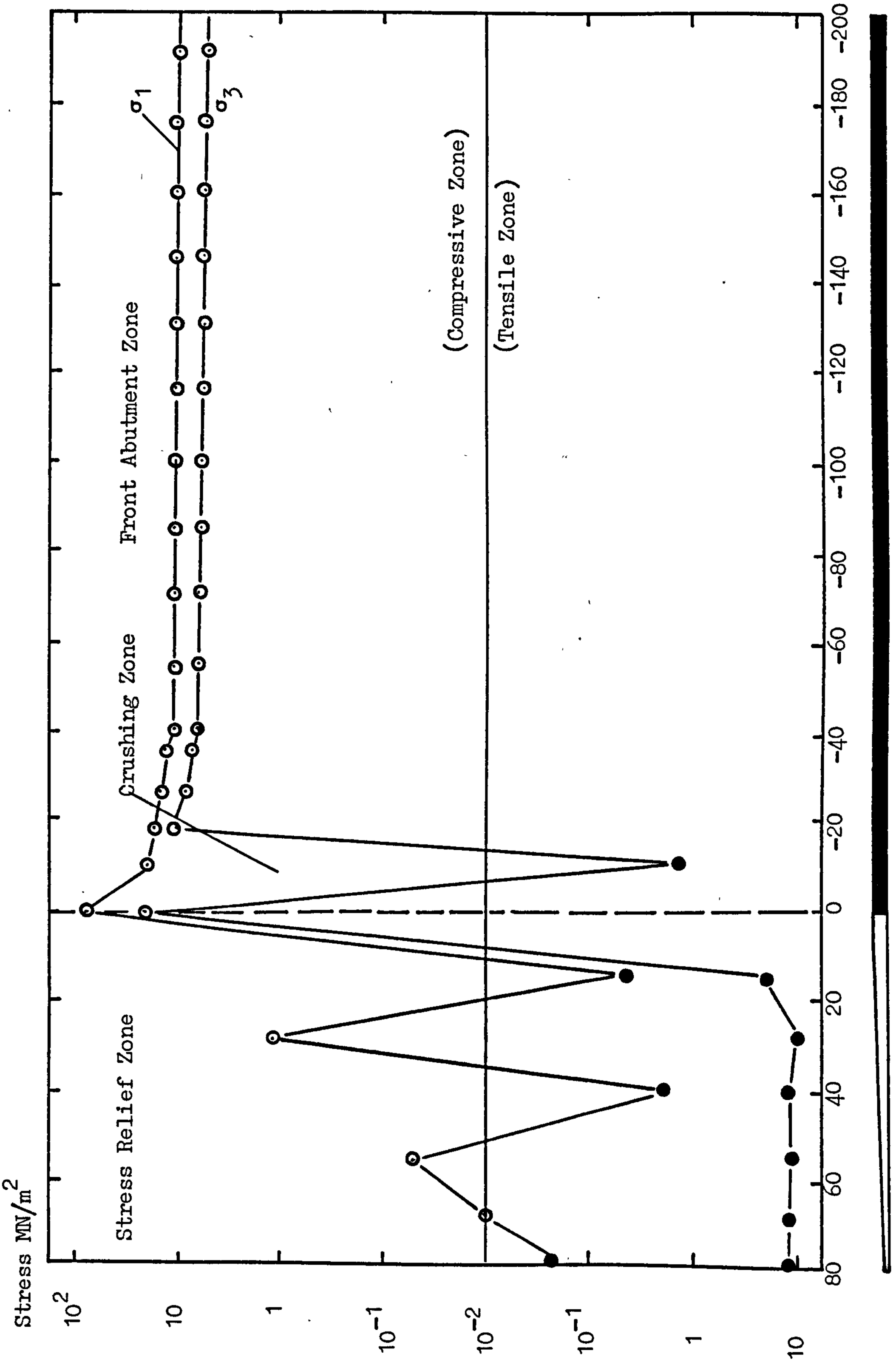

FIGURE (4.2.7) Maximum and Minimum Principal Stresses Along the Roof of a 500m Deep Longwall Face.

TABLE (4.2.3) Theoretical Values for Maximum and Minimum Principal Stresses Along the Roof of a 700 m Deep Longwall Face.

DISTANCE FROM THE FACE LINE (m)	MAXIMUM PRINCIPAL STRESS σ_1 (MN/m^2)	MINIMUM PRINCIPAL STRESS σ_3 (MN/m^2)
80	0•01	11•10
67	-0•10	10•90
54	-0•60	11•00
40	0•62	10•50
27	-2•31	14•80
15	0•29	5•93
0	-102•00	-30•70
-10	-28•30	1•02
-18	-26•20	-14•00
-25	-23•60	-11•70
-35	-22•00	-10•40
-40	-20•80	-9•02
-55	-18•90	-7•65
-70	-17•90	-6•41
-85	-17•40	-5•80
-100	-17•20	-5•33
-115	-17•00	-5•12
-130	-16•80	-4•87
-145	-16•80	-4•74
-160	-16•70	-4•60
-175	-16•70	-4•52
-190	-16•60	-4•44

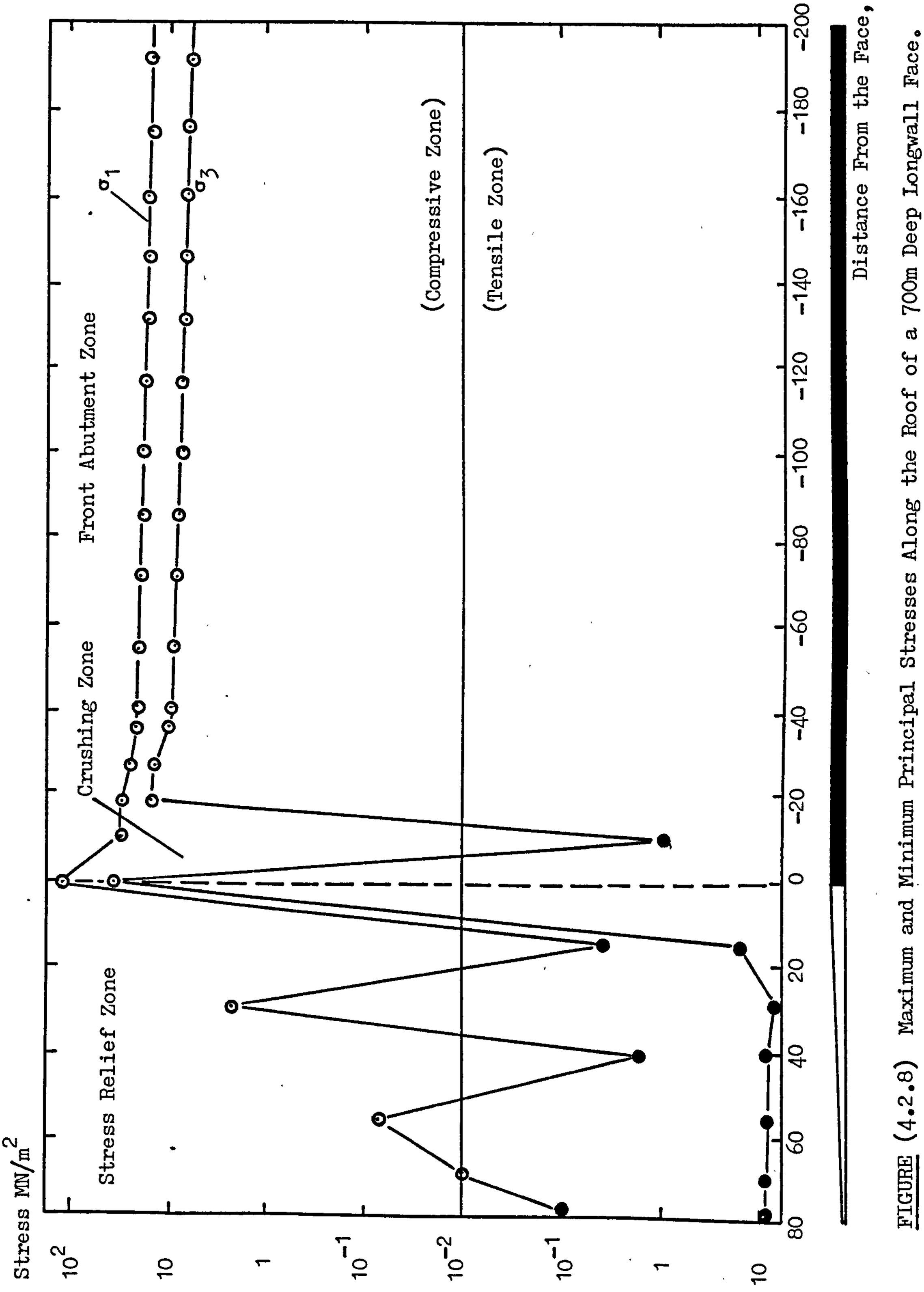

FIGURE (4.2.8) Maximum and Minimum Principal Stresses Along the Roof of a 700m Deep Longwall Face.

principal stresses along the roofs of longwall faces 300 m, 500 m and 700 m deep respectively. Coal seams were loaded triaxially by the weight of the overburden beyond the abutment zone. As the depth of the seam increased the magnitudes of σ_1 and σ_3 became larger consistent with the overburden thickness. Although the magnitude of the increase was quite small, the effect of increasing abutment pressures can be noticed as far as 200 m ahead of the face. Thereafter, both σ_1 and σ_3 continued to increase along the front abutment zone towards the face, the effect being highly compressive at a point 20 m in front of the face.

The most dramatic effect of redistributing the strata pressures around a longwall face was seen between the face and the front abutment zone. Here, it was found that σ_3 suddenly decreased in magnitude and as σ_1 continued to increase and reached its peak compressive value at or a few metres in front of the face, σ_3 became highly tensile causing fracturing and crushing of the coal seam. This zone, which is believed to be of major importance in our attempt to understand the permeability changes occuring in both the worked and adjacent coal seams, will be referred to as 'the crushing zone'.

Complexity of the principal stresses behind the face in the 'stress relief zone' can be seen in Figures (4.2.6), (4.2.7) and (4.2.8) as σ_3 stayed tensile and σ_1 acted either compressive or tensile at different points. It is believed that the principal stresses will take the form of triaxial compression as the cover load is established on the caved area behind the face. This area will be termed 'the recompaction zone'.

As will be discussed later in Chapter 6 the maximum and minimum principal stress combinations in the above defined pressure zones are taken as the basic stress combinations throughout this research. Similar stress combinations were used in simulating the subsurface stress conditions in the laboratory experiments to establish stress-permeability relationships for different coals.

Stress profiles at horizons above and below the seam worked were found to be similar to that of the stresses on the worked seam demonstrated above. The significance of these profiles will be discussed in Chapter 9 in relation to the permeabilities of adjacent coal seams and the flow of strata gas around working longwall faces.

4.3. The Strength and Fracturing of Coal

In the preceding sections, the behaviour of stresses around a working longwall face has been discussed. Stress systems likely to be experienced around a working face can be summarised as:

(i) triaxial compression in the coal seam and

$$|\sigma_1| > |\sigma_2| = |\sigma_3|$$

(ii) a complex stress system at the face in which two of the stresses are compressive and the third is tensile.

$$\sigma_3 > 0 > \sigma_1 \geqslant \sigma_2$$

Coal seams will behave differently under the above stress conditions and the structural changes occuring during these stages will dictate their permeability to gas flow.

4.3.1 Strength of Coal

Even where it is relatively 'homogenous' in the chemical or petrological sense, the physical structure of coal is very complex. The bedding planes are a characteristic feature, recognised to be planes of weakness. Other planes of weakness are 'cleats' and 'cross cleats' intersecting at right angles to each other and often occuring perpendicular to the bedding planes. The strength of coal is sensitive to the direction of application of stress relative to these weaknesses.

Evans and Pomeroy (56) conducted some triaxial compressive strength measurements on British Coals. Figure (4.3.1) shows a typical set of stress-strain curves for specimens of Deep Duffryn, Five Feet coal under different confining pressures. The curves can be interpreted in three phases:

(i) An initial non-linear portion caused by elastic deformation of the basic coal material and the closing of the gross cracks in coal.

(ii) A range of elastic linearity.

(iii) A final non-linear portion which is attributed to pre-rupture cracking and plastic flow.

Percentage strain attributed to the closure of cracks was found to be independent of the confining pressure and the magnitude of closure for anthracite and low-rank coals was greater than for medium rank coals.

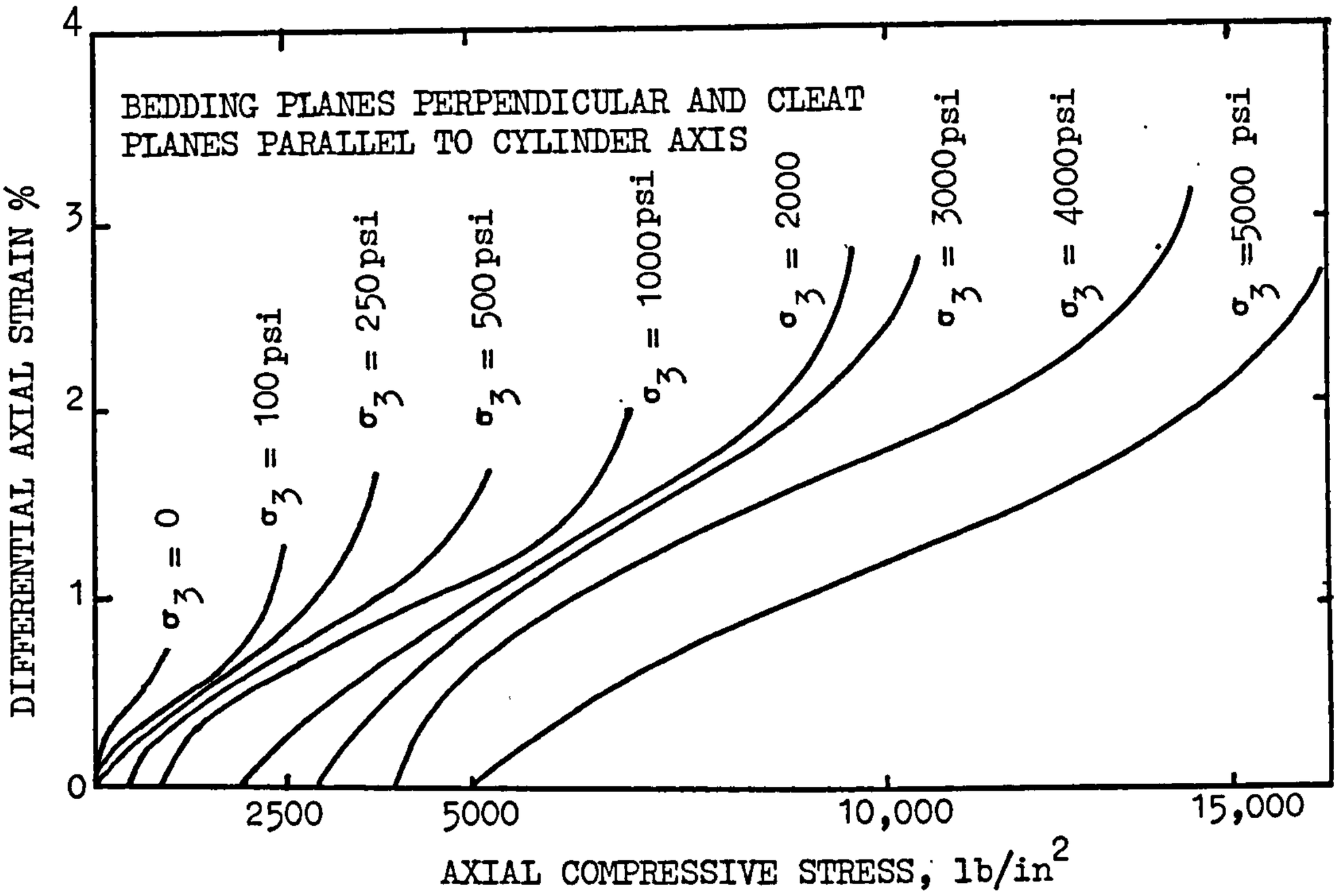

FIGURE (4.3.1) Stress-Strain Curves for Deep Duffryn Coal (After Evans and Pomeroy (56)).

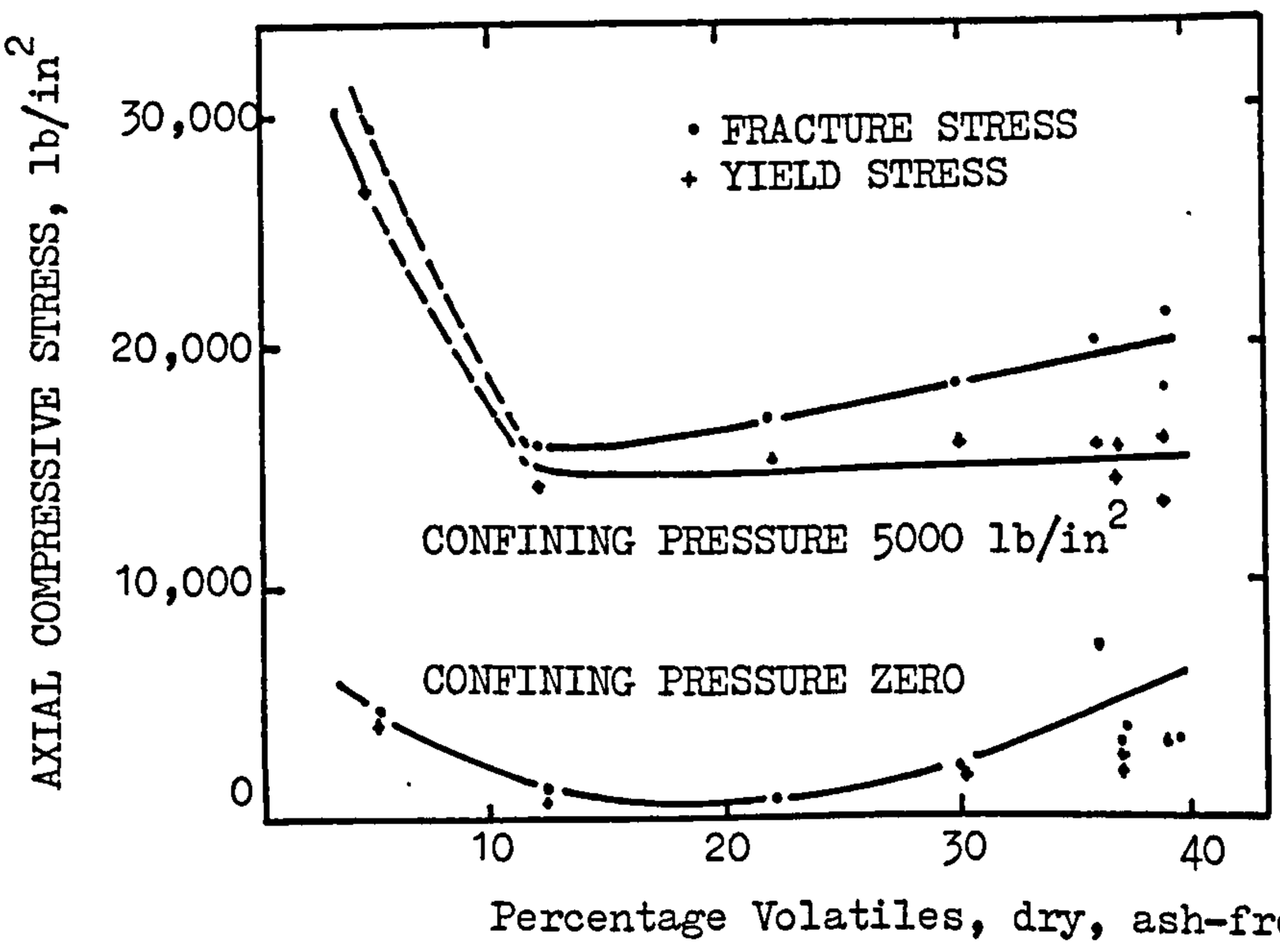

FIGURE (4.3.3) Variation of Axial Compressive Yield and Fracture Stress with Coal Rank (After Evans and Pomeroy (56)).

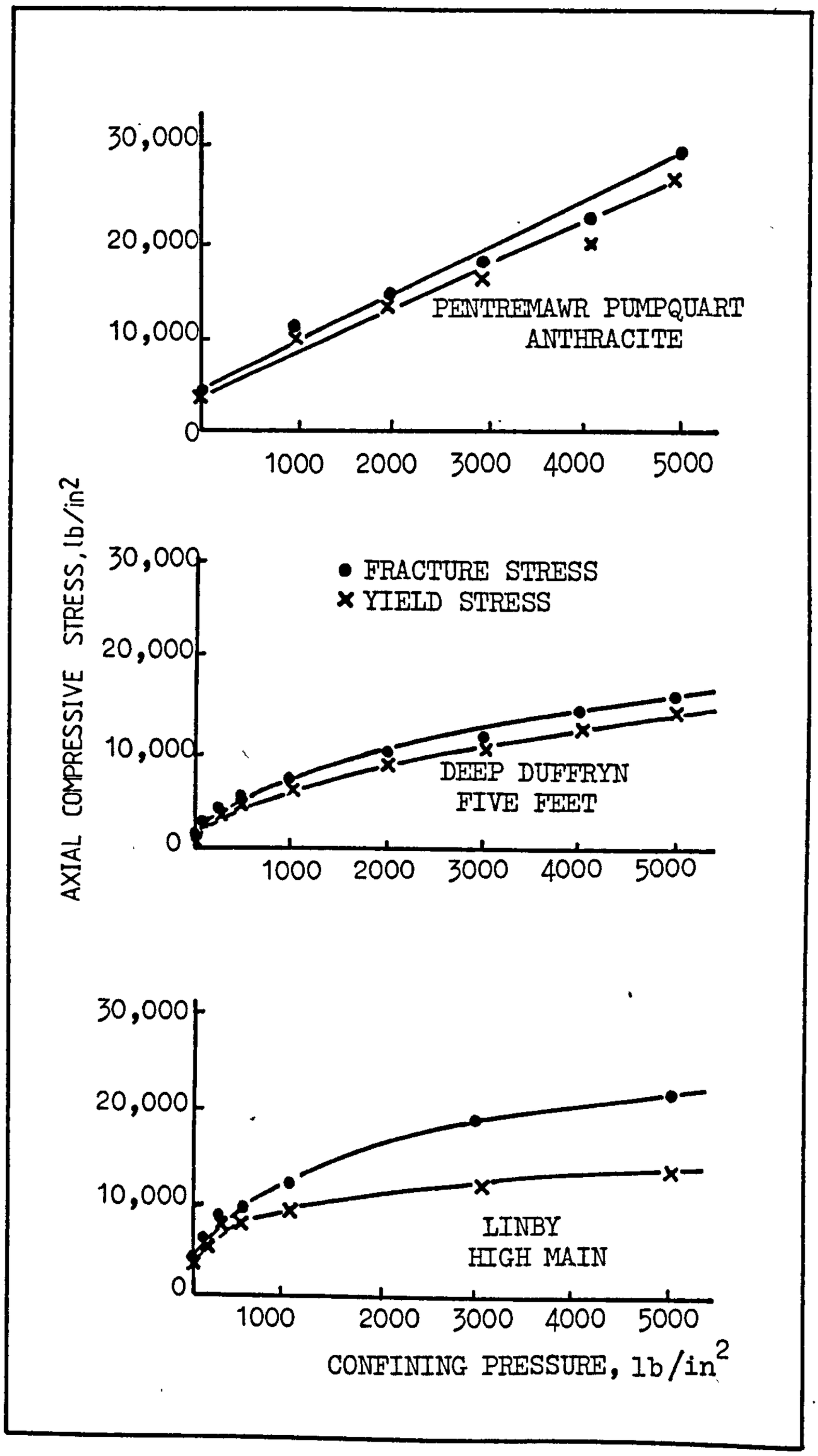

FIGURE (4.3.2) Variation of Axial Compressive Yield and Fracture Stress with Confining Pressure (After Evans and Pomeroy (56)).

Both the yield and fracture stresses were observed to be increasing with confining pressure for all coals, the manner of increase varied from one coal to another as shown in Figure (4.3.2). Comparing the fracture stresses of different rank coals, a U shaped relationship was obtained. At zero confining pressure, both the high and low-rank coals showed higher fracture stresses as compared to that of medium-rank coals. However, excluding anthracite this was indistinguishable at very high confining pressures, Figure (4.3.3).

4.3.2 Fracturing of Coal

Fracturing and failure of coal can be studied under two different stress conditions:

(i) Triaxial compression or induced shear failure.

(ii) Uniaxial compression or induced tensile failure.

Both the above conditions can be considered in relation to the stress conditions in the front abutment zone and at the face of a working coal seam respectively.

4.3.2.1 Induced Shear Failure of Coal

Induced shear failure under triaxial compression occurs when the maximum principal stress becomes excessively high (63). The basic elements of strength of a material which fails in shear when subjected to excessive compressive stress are:

(i) Cohesion (c), or the resistance to shearing stress when no normal stress exists on the shear plane.

(ii) Internal friction, or the resistance due to friction of grain on grain, plus the resistance due to interlocking of grains. Internal friction is designated as $\tan\Phi$ and Φ is called the angle of internal friction.

Referring to Figure (4.3.4) which represents an element, ABC, along any plane making an angle β with the direction of the maximum principal stress, σ_1, the maximum and minimum stresses can be resolved into a normal stress σ_N acting at right angles to plane AB, and a shearing stress, τ, acting parallel to plane AB.

Taking the area of plane AB as unity and

F_1 = total force acting on plane AC

F_3 = total force acting on plane CB

F_N = total force acting normal to AB

then the normal forces acting on the element ABC are

$$F_1 = \sigma_1 \sin\beta$$

$$F_3 = \sigma_3 \cos\beta$$

and $$F_N = F_1 \sin\beta + F_3 \cos\beta$$

Substitution for F_1 and F_3 gives:

$$F_N = \sigma_N = \sigma_1 \sin^2\beta + \sigma_3 \cos^2\beta$$

$$= \cos^2\beta\,(\sigma_3 - \sigma_1) + \sigma_1$$

$$= \frac{\cos 2\beta + 1}{2}\,(\sigma_3 - \sigma_1) + \sigma_1$$

$$\sigma_N = \frac{\sigma_1 + \sigma_3}{2} - \frac{\sigma_1 - \sigma_3}{2}\cos 2\beta \qquad \ldots\ldots\ldots \quad 4.3.1$$

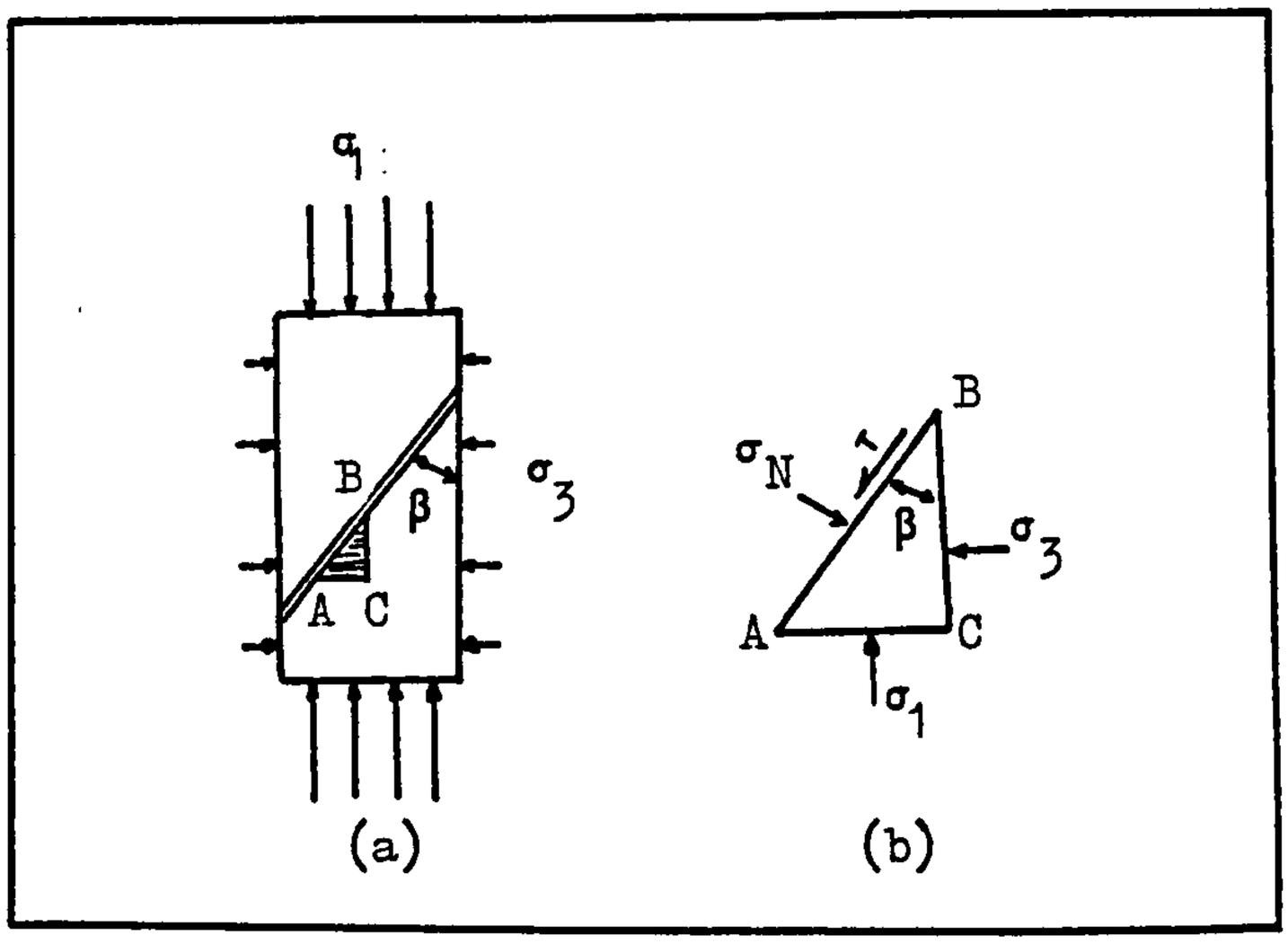

FIGURE (4.3.4) (a) Element Subjected to Maximum and Minimum Principal Stresses,
(b) Forces Acting on an Element
(After Woodruff (63)).

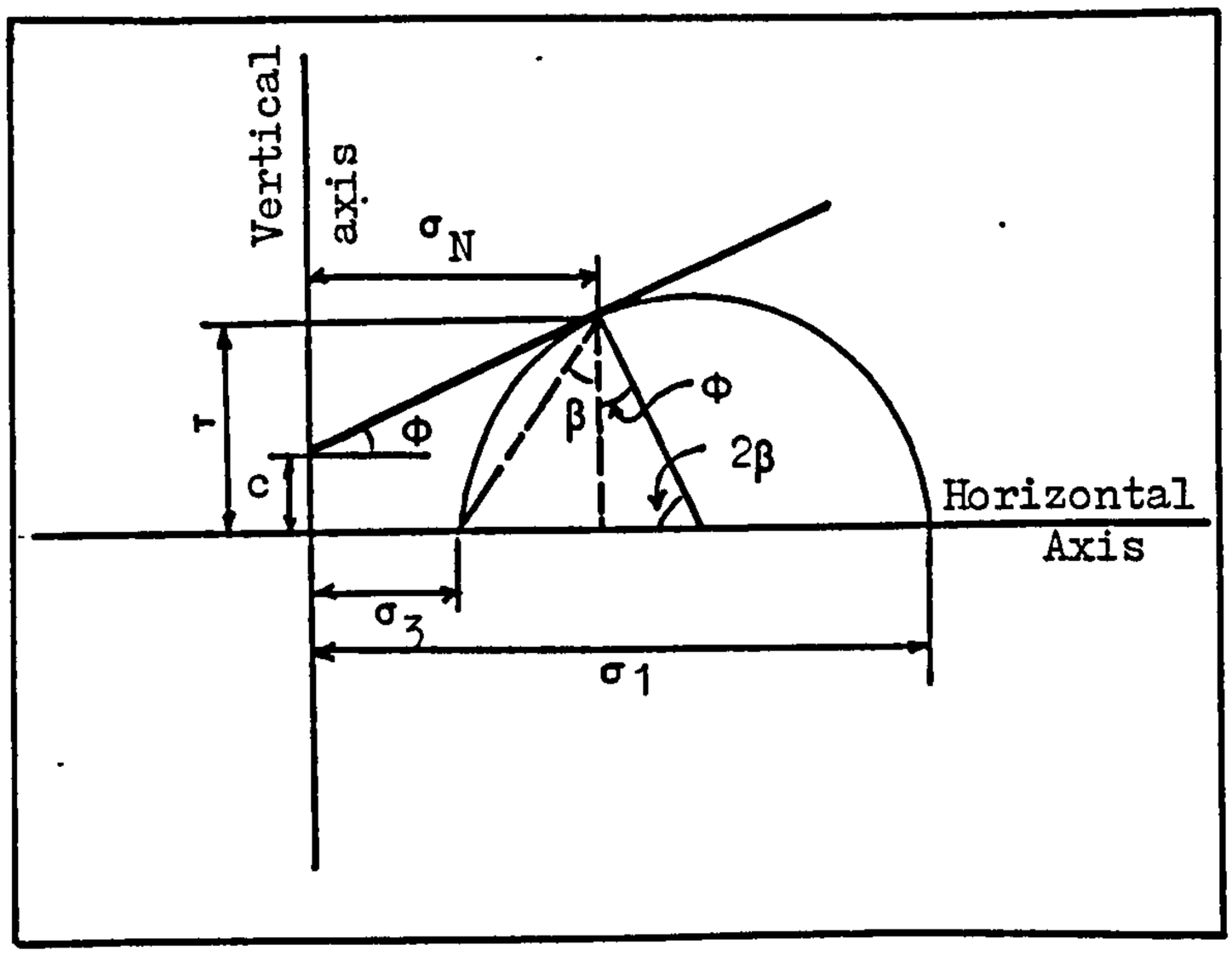

FIGURE (4.3.5) Mohr's Stress Circle
(After Woodruff (63)).

Likewise the tangential force (F_t) can be resolved into two forces:

$$F_t = F_1 \cos\beta - F_3 \sin\beta$$

since the area of AB is unity:

$$F_t = \tau = \sigma_1 \cos\beta \sin\beta - \sigma_3 \cos\beta \sin\beta$$

$$\tau = \frac{\sigma_1 - \sigma_3}{2} \sin 2\beta \qquad \ldots\ldots\ldots \quad 4.3.2$$

Shear stress is maximum when $\sin 2\beta = 1$ or when $\beta = 45^\circ$. Thus planes inclined at 45° to the direction of maximum principal stress, σ_1, sustain maximum shear stress.

However, shear failure takes place along planes of maximum 'effective shear stress' rather than along planes of maximum stress (63). On any plane on which there is a shear stress, τ, there is also a normal stress acting at right angles to the plane. This normal stress, σ_N, on potential shear planes induces a resisting force proportional to $\sigma_N \tan\Phi$. According to Mohr, of all planes having the same normal component of stress, failure will take place along the plane having the greatest shear stress. Thus the inclination of the plane along which shear failure occurs is determined by the coefficient of internal friction for the material.

It is generally agreed that the magnitude of resistance to failure, s, on failure plane is given by Coulomb's friction law:

$$s = c + \sigma_N \tan\Phi \qquad \ldots\ldots\ldots \quad 4.3.3$$

where s is total unit shearing resistance, c is cohesion per unit area and $\sigma_N \tan\Phi$ is the frictional resistance to shearing.

Combining the equations (4.3.1), (4.3.2) and (4.3.3) we get the stress conditions at failure:

$$\frac{\sigma_1 - \sigma_3}{2} \sin 2\beta = c + \tan\Phi \left[\frac{\sigma_1 + \sigma_3}{2} - \frac{\sigma_1 - \sigma_3}{2} \cos 2\beta \right]$$

Referring to Mohr's circle, Figure (4.3.5), at failure $2\beta = 90^\circ - \Phi$ so the above equation becomes,

$$\frac{\sigma_1 - \sigma_3}{2} \cos\Phi = c + \tan\Phi \left[\frac{\sigma_1 + \sigma_3}{2} - \frac{\sigma_1 - \sigma_3}{2} \sin\Phi \right]$$

then

$$\sigma_1 = 2c \frac{\cos\Phi}{1 - \sin\Phi} + \sigma_3 \frac{1 + \sin\Phi}{1 - \sin\Phi}$$

When $\sigma_3 = 0$, σ_1 is the uniaxial compressive strength of the material and representing this by σ_{ult},

$$\sigma_{ult} = 2c \frac{\cos\Phi}{1 - \sin\Phi}$$

so the maximum principal stress σ_1 at failure can be written as:

$$\sigma_1 = \sigma_{ult} + \frac{1 + \sin\Phi}{1 - \sin\Phi} \sigma_3 \qquad \text{..... 4.3.4}$$

Substituting the experimental average uniaxial compressive strength, σ_{ult} values for different rank coals and the average internal friction angle ($\Phi = 40^{\circ}$) reported by Evans and Pomeroy (56) together with the largest σ_3 values obtained from the finite element analysis of stresses at the front abutment zones of 300 m, 500 m, and 700 m deep working coal seams, similar values of fracture stresses (σ_1) to that of Evans and Pomeroy were obtained, Figure (4.3.2). Table (4.3.1) shows the comparison of theoretical fracture stresses and the average fracture stresses reported by Evans and Pomeroy.

Examining Table (4.3.1) it can be seen that the fracture stresses obtained were far higher in magnitude than the maximum principal stresses experienced to a depth of 1000 m in practice. Therefore it seemed unlikely that coal would fracture and fail in the abutment zone beyond the face.

TABLE (4.3.1) Comparison of Theoretical and Experimental Fracture Stresses for Different Rank Coals

σ_{ult} MN/m^2 (Rank)	σ_3 = 6·00 MN/m^2		σ_3 = 10·00 MN/m^2		σ_3 = 14·00 MN/m^2	
	σ_1 THEORETICAL* MN/m^2	σ_1 EXPERIMENTAL** MN/m^2	σ_1 THEORETICAL MN/m^2	σ_1 EXPERIMENTAL MN/m^2	σ_1 THEORETICAL MN/m^2	σ_1 EXPERIMENTAL MN/m^2
15·00 (Medium)	42·50	63·00	60·80	66·00	79·00	73·00
35·00 (Anthracite)	62·50	80·00	80·80	86·00	99·10	100·00
45·00 (Low)	72·50	80·00	90·80	86·00	109·10	100·00

* Determined as in Equation (4.3.4)
** Reported by Evans and Pomeroy (56)

4.3.2.2 Induced Tensile Failure of Coal

Griffith (64) was the first to show that the presence of cracks in a medium would serve to generate tensile stresses even when a uniform compressive stress was exerted at the boundaries of a sample. For example, a crack orientated parallel to a uniaxial compressive stress is subjected to a tensile stress at its extremities which acts at right angles to the applied stress.

Coal has three prominent systems of cracks which are along the bedding planes and the two cleat planes perpendicular to the bedding. When subject to an uniaxial compressive stress, it is likely that one of these systems, parallel to the applied stress, will suffer induced tensile stresses and breakage can be associated with the propogation of these cracks.

Experimental practice has shown that induced tensile failure of coal can be established by the uniaxial compression of regular or irregular shaped coal samples (56). As shown in Figure (4.3.6) the tensile stress induced on a disc specimen subjected to compressive loading is given by the equation:

$$\sigma_t = \frac{2Q_d}{\pi D} \qquad \cdots\cdots\cdots \quad 4.3.5$$

where σ_t is the induced tensile stress

Q_d is the load per unit length at right angles to the plane of the disc

D is the diameter of the disc.

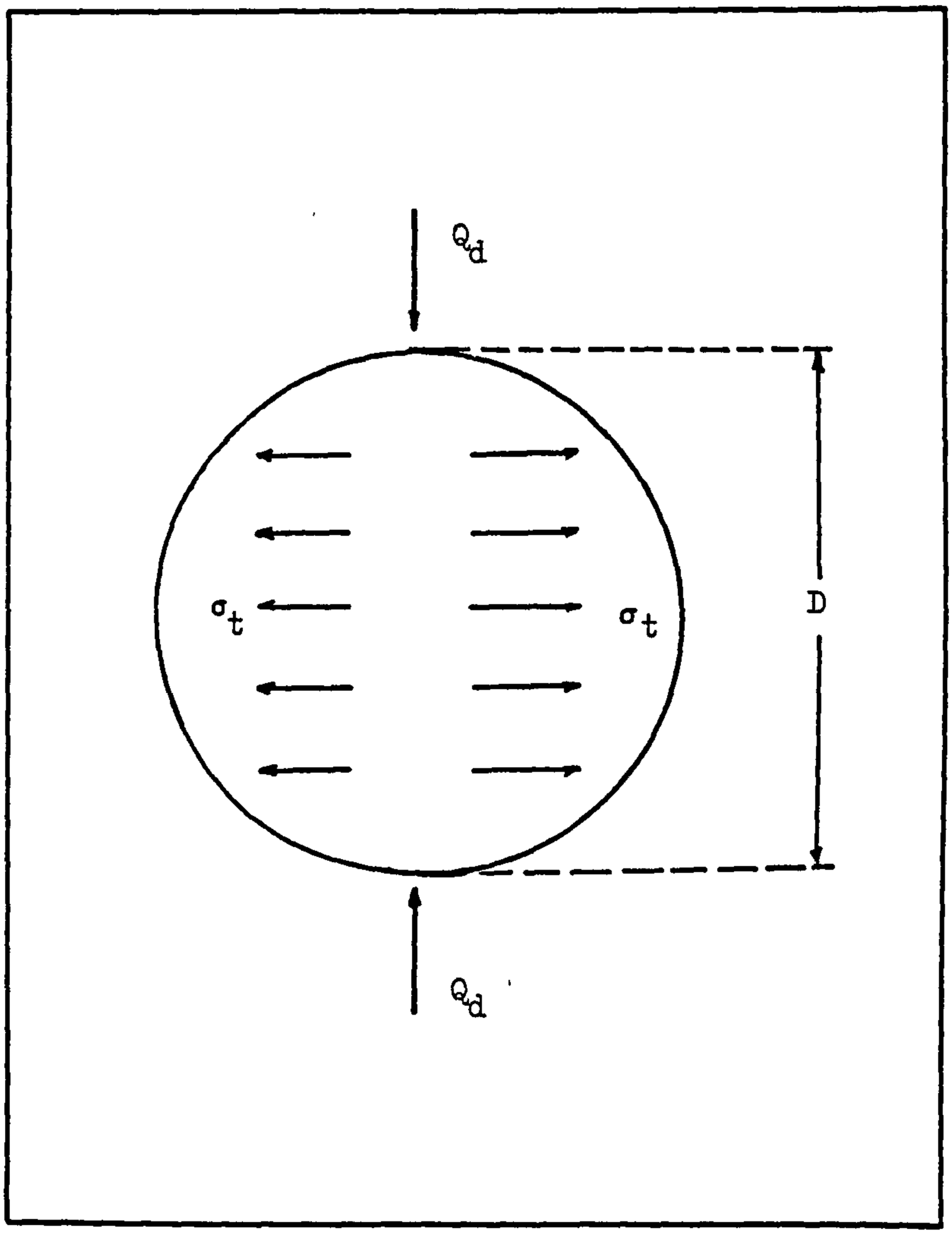

FIGURE (4.3.6) Tensile Stresses in a Disc Subjected to Compressive Loading.

The above observations can be applied to the stress conditions at the face. As the coal seam is extracted, existing high vertical stresses induce tensile stresses in the horizontal plane of the newly exposed coal face (see Figures (4.2.6), (4.2.7) and (4.2.8). Therefore, coal is expected to fracture and fail in the area between the face and the front abutment zone.

4.4 Conclusion

Studies on the maximum and minimum principal stress distributions around working longwall faces have shown that the most important structural changes in coal seams are expected to happen in the front abutment zone and in the crushing zone. It was therefore decided that the stress-permeability experiments in the laboratory should be conducted under the following order and stress conditions:

(i) Triaxial compression with both the maximum and minimum principal stresses increasing proportionately to simulate that of the front abutment zone.

(ii) Induced tensile fracturing of the sample by a sudden release of the minimum principal stress where the maximum principal stress is at its peak value; this is similar to the stresses at the face.

(iii) Triaxial compression of the fractured coal as in (i) to simulate the fracture permeability of coal in the recompaction zone.

As the elastic properties and the mechanical strengths of different coals have been shown to vary by significant amounts, stress-permeability relationships for different rank coals were expected to show different characteristics under the above stress conditions. It was therefore planned to test a wide variety of coals for the stress-permeability relationship and to determine the mechanical properties of the individual coals.

CHAPTER FIVE

TEST SPECIMEN PREPARATION AND APPARATUS FOR STRESS-PERMEABILITY MEASUREMENTS

CHAPTER FIVE

TEST SPECIMEN PREPARATION AND APPARATUS FOR STRESS-PERMEABILITY MEASUREMENTS

5.1 Introduction

As concluded in the previous chapter, the ideal simulation of the subsurface stress conditions could be reached by the triaxial stressing of coal specimens. With certain alterations to allow simultaneous gas flow measurements, a cylindrical core specimen stressed in a conventional triaxial cell provided the required conditions for such laboratory simulations.

The accuracy of the stress-permeability measurements depended mainly on the methods of preparing and storing the test specimens as well as on the success in measuring very low flow rates of gas through coal specimens under high stresses.

This chapter discusses the methods of coal specimen preparation and the equipment used in stress-permeability measurements.

5.2 Preparation of Test Specimens

5.2.1 Choice of Coal Specimens

Owing to its friable nature, coal was found to be a most difficult material from which to obtain reasonably sized core specimens. Although there has been a great deal of success in

developing coal drilling techniques in the Department of Mining Engineering, University of Nottingham, the need to recover intact cores from a lump of coal was one of the main factors which influenced the choice of coals to be worked.

As discussed in the previous chapter, different rank coals show significant changes in their elastic properties and this would obviously effect their permeability when stressed. In order to demonstrate the effect of different structural characteristics of coals on their permeability under stress, it was decided to include a wide range of coals from different coalfields.

Coal lumps, about one foot cube in size, were obtained from different rank coal seams in both underground and opencast sites. It was ensured that these lumps were free from visible fractures or impurities which affected the percentage core recovery. In order to avoid any damage to the coal lumps, they were cored as soon as they arrived at the workshop.

Two medium volatile bituminous coals from highly gassy coal seams in Turkey were also included in this research for comparision.

5.2.2 Preparation of Coal Lumps for Coring

Previous experience in coring coal has shown that drilling parallel to the bedding planes produced a higher percentage of core recovery. On the other hand, the majority of gas flow underground

is expected to take place along the bedding planes of coal seams unless they are totally fractured. Except for those used for determining the directional effect of gas flow on permeability, most of the test specimens were cored parallel to the bedding planes.

Immediately after the coal lumps arrived at the workshop, they were carefully aligned in the desired coring direction and cast in concrete blocks. By this technique, the damage to the coal lump during the coring process was minimised and the percentage core recovery was improved. Plate (5.1) shows a successfully cored lump employing the above technique.

5.2.3 The Coring Machine

The test specimens used in stress-permeability measurements were cored with 38.0 mm diamond impregnated or diamond surface set core bits mounted in a Kitchen and Wade radial drilling machine specially modified for this purpose.

The drilling head traversed along a horizontal arm which rotated on a cylindrical sleeve around a central vertical column. The vertical position of the arm on the sleeve was altered by a 1.12 kW motor and allowed easy positioning of the drill bit on the coal lump. In order to improve the percentage intact core recovery, the machine was equipped with a pneumatic cylinder generating a constant load of about 570 kgf at 2000 rpm. The machine had an infinitely variable speed range of 0 to 2250 rpm. Vibration was minimized by careful maintenance and replacement of worn out parts.

5.2.4 Test Specimen Size

The triaxial cell used in stress-permeability experiments was designed to take specimens 76.0 mm long and 38.0 mm in diameter. 38.0 mm cylindrical core samples were drilled from each coal lump and these were used for both the stress-permeability measurements under triaxial compression and the uniaxial compressive strength measurements of coal.

Most of the core samples obtained from each lump were marked at 76.0 mm length sections, wrapped with P.V.C. tapes, handsawn and machined to its final size in a lathe. This proved to be the most effective technique to prevent the coal from disintegrating; it also provided the smooth surfaces required.

Using the same technique, the remaining cores were trimmed to 38.0 mm long, uniaxial compressive strength specimens having a diameter to length ratio of one as universally adopted for this purpose.

5.2.5 Evacuation and Storage of Test Specimens

Before testing the coal specimens for permeability, the gases which were adsorbed on the internal surfaces of the pores had to be removed. These gases were mainly, methane, ethane, propane, butane and water vapour; their presence in coal may partially block the micropores thus reducing the gas permeability.

After machining down to the required size, the test specimens were placed in a dessicator and evacuated at absolute pressures of between 10^{-2} and 10^{-3} torr. In order to avoid any deterioration of the internal structure of coal at high temperatures, the evacuation process was carried out at room temperature as suggested by Palvelev (65). Recent research in the Department of Mining Engineering, University of Nottingham, has shown that the evacuation time for coal is a function of permeability (66). The first few hours of evacuation have shown the most significant pressure drop in adsorbed gas pressure for all coals. As shown in Figure (5.2.1), the same levels of maximum pressure drop for highly permeable medium volatile bituminous coals and low permeability high volatile bituminous coals were reached in 22 and 96 hours respectively. In the light of the evidence discussed above, an evacuation time of 96 hours was thought to be sufficient and was adopted throughout this research.

After the evacuation was completed, the dessicator was charged with 1 Atm. pressure nitrogen which was used as the flowing media in stress-permeability measurements. This was thought to prevent any recontamination of coal when in contact with air. Test specimens were then removed from the dessicator and immediately wrapped in 'cling film' for storing until use.

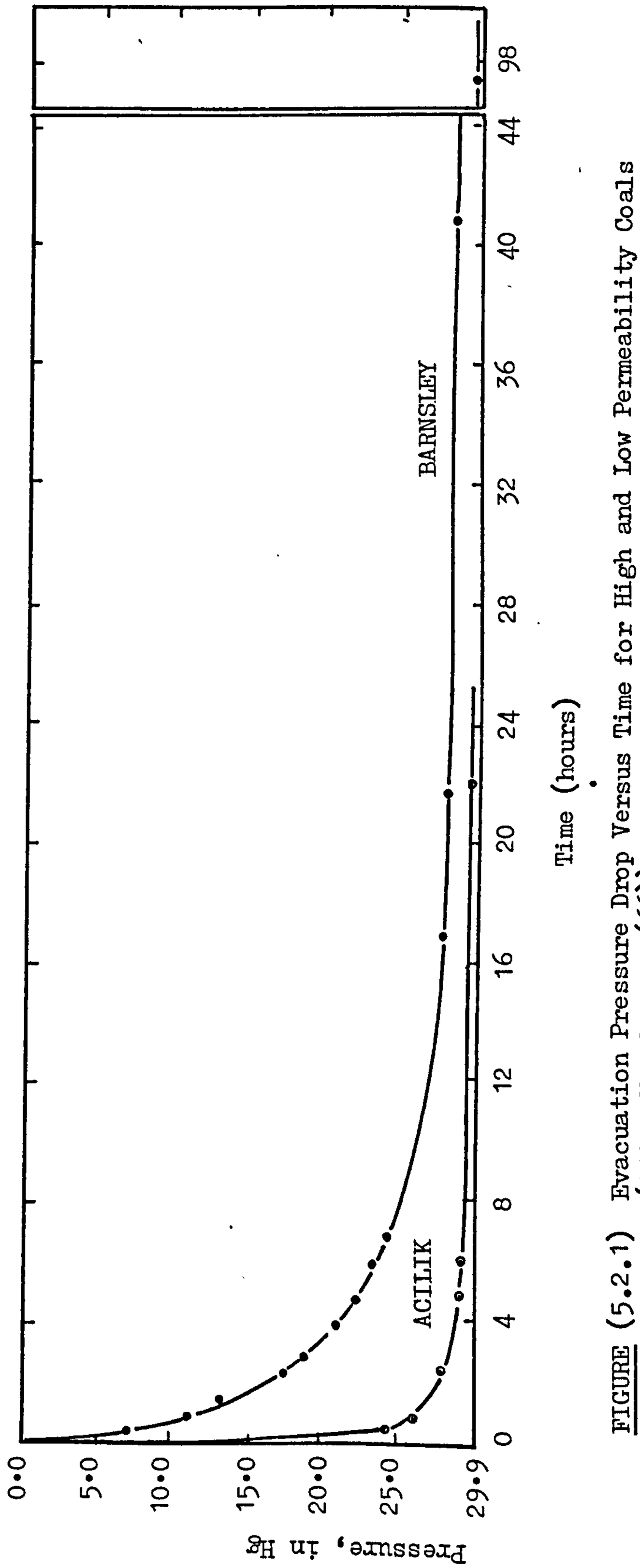

FIGURE (5.2.1) Evacuation Pressure Drop Versus Time for High and Low Permeability Coals (After Yerebasmaz (66)).

PLATE (5.1) A Coal Lump Cored After Being Cast in Concrete.

PLATE (5.3) The Coal Specimen and the Component Parts of the Triaxial Cell.

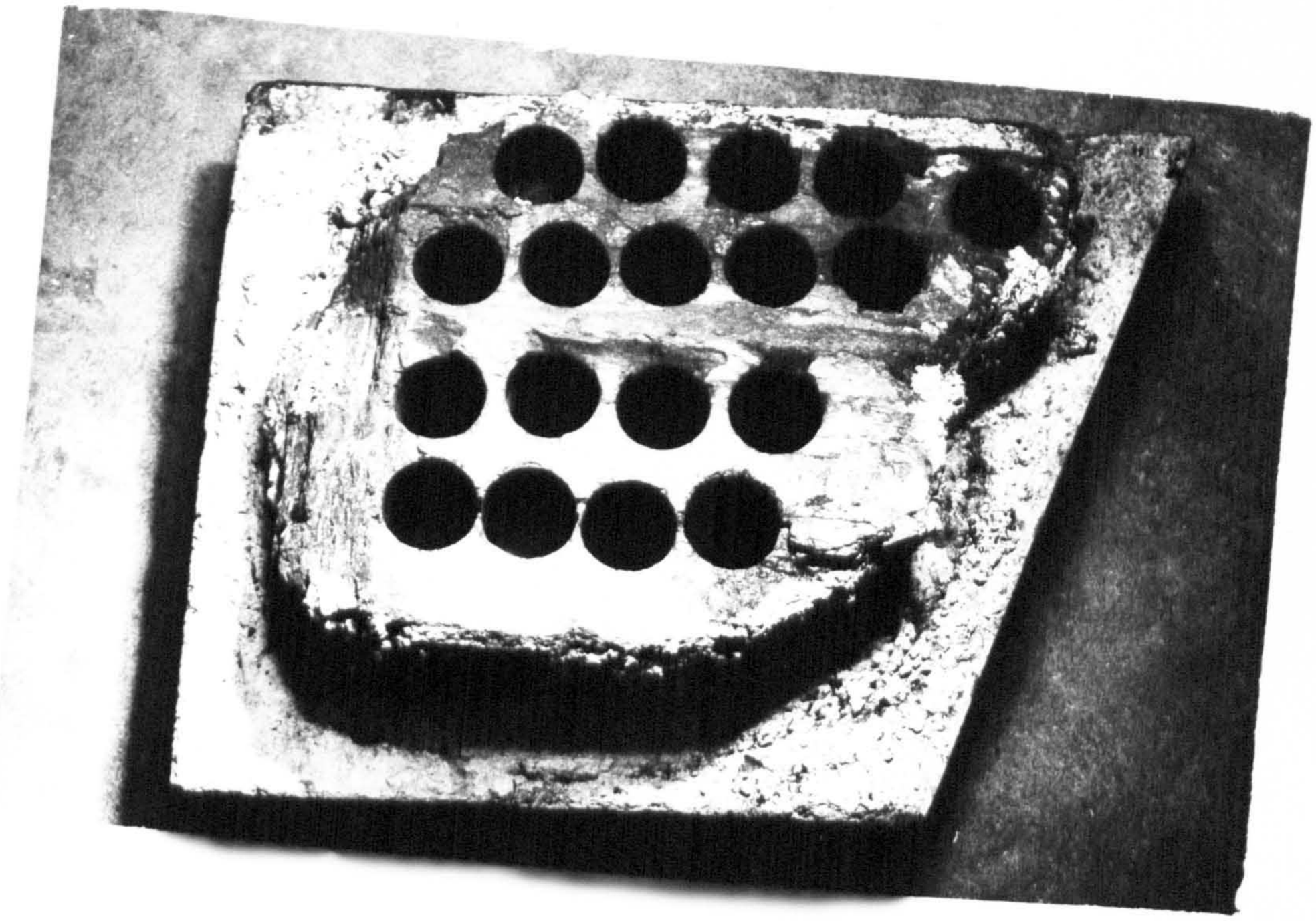

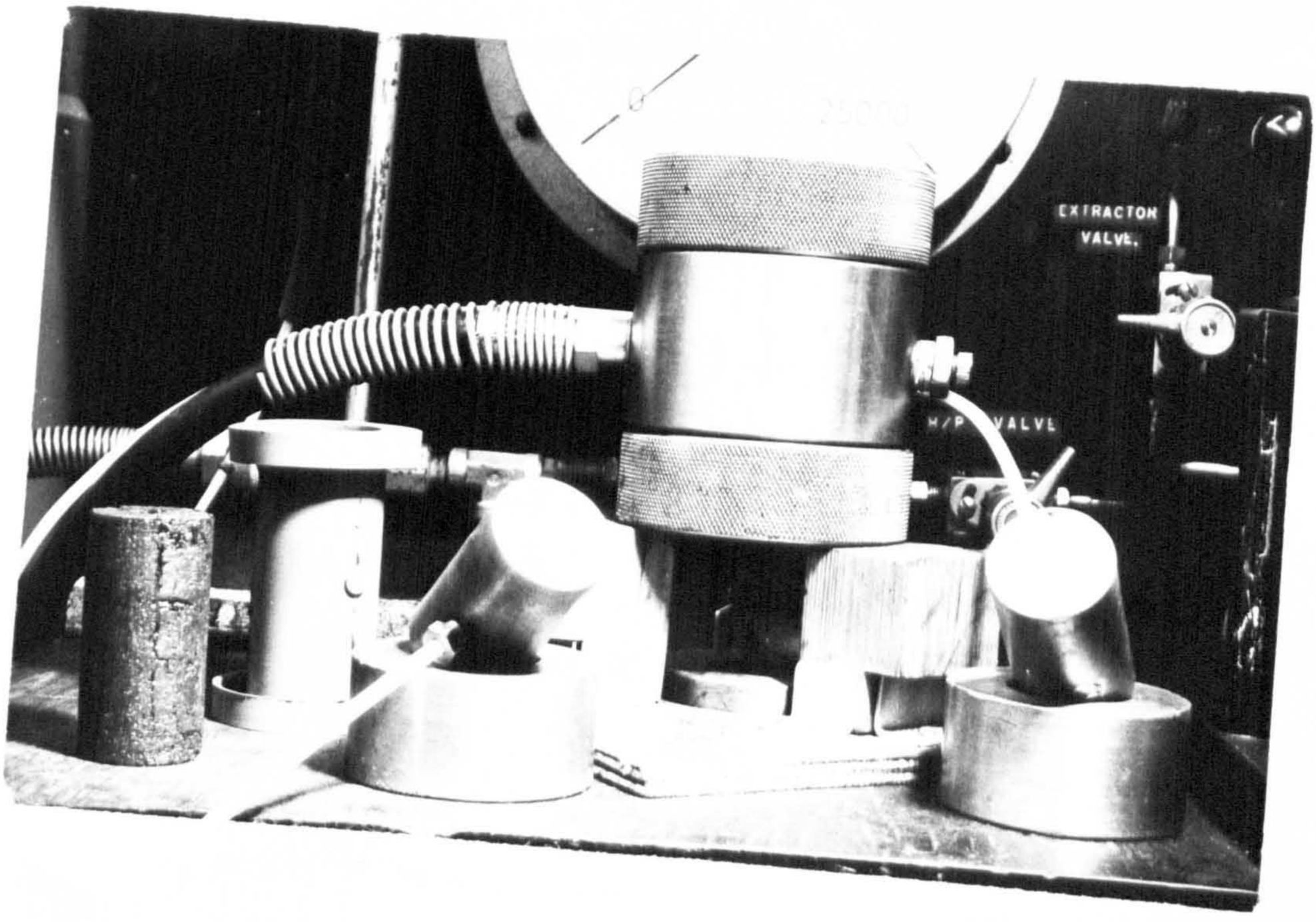
EXTRACTOR
VALVE.
VALVE

5.3 Experimental Apparatus for Stress-Permeability Measurements

5.3.1 Introduction

The main objective of this research, required an apparatus with which simultaneous measurements of stress and gas flow through coal could be made. This was achieved by slightly modifying a conventionally used triaxial testing apparatus to enable gas flow through the test specimen at various pressures. The three main components of the apparatus shown in Plate (5.2) and Figure (5.3.1) are the triaxial cell, the testing machine and the flow measuring apparatus. These parts will now be discussed in more detail.

5.3.2 The Triaxial Cell

The triaxial cell, which was originally designed by Hoek and Franklin (67) was constructed with some modifications in the Departmental workshop. The cell is illustrated diagrammatically in Figure (5.3.2) and the component parts are shown in Plate (5.3).

The main body of the cell was machined from bright drawn mild steel and consisted of a cylinder and two end caps screwed onto it. The cell weighed about 8.5 kg and could withstand confining pressure of about 82.6 MN/m^2. It was designed to take test specimens of maximum length 76.0 mm and of diameter 38.0 mm.

In order to seal the test specimen and to apply independent axial and radial stresses, a synthetic rubber sleeve, designed and

PLATE (5.2) The Assembled Picture of the Experimental Apparatus for Stress-Permeability Measurements.

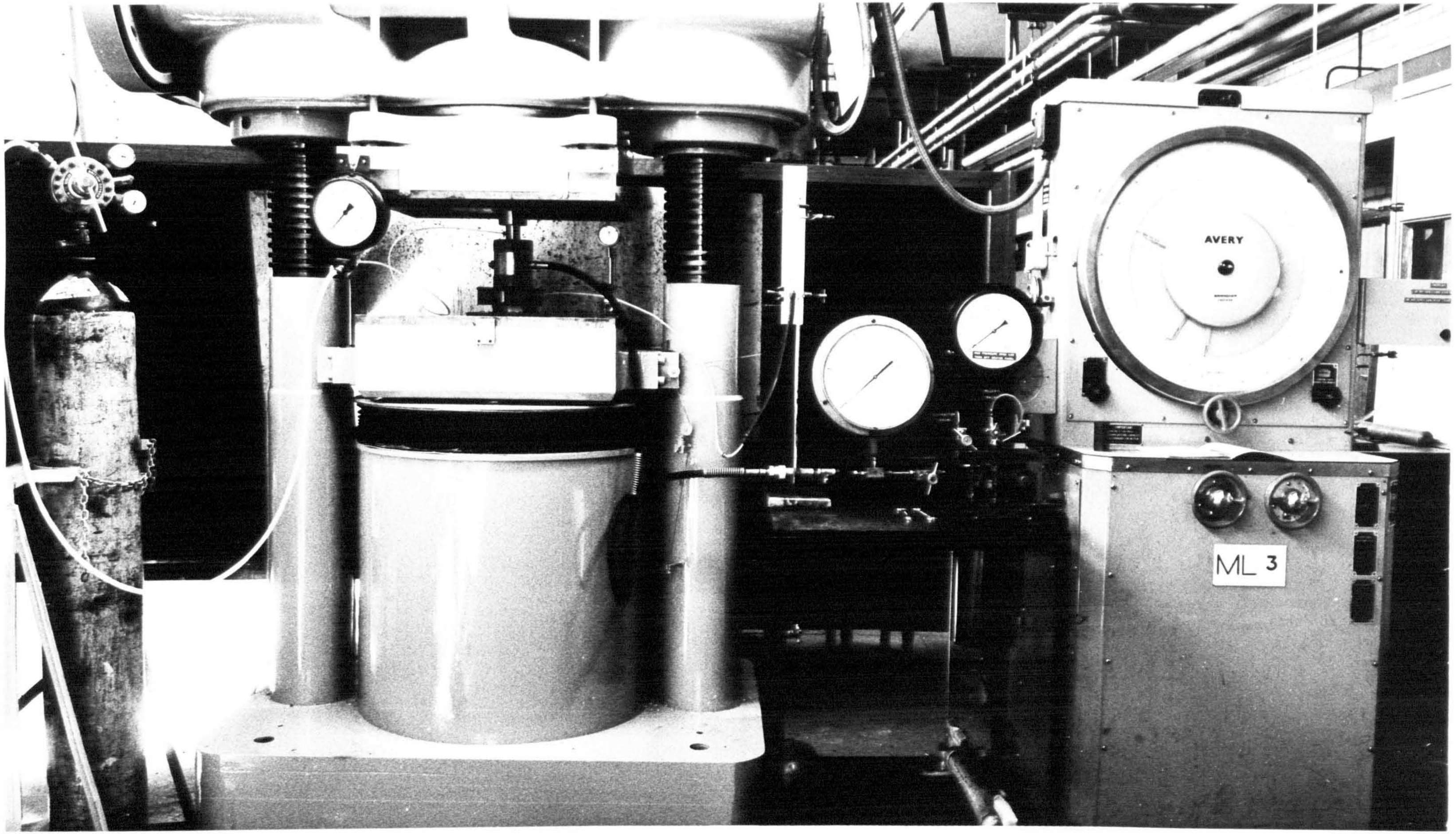
AVERY
ML 3

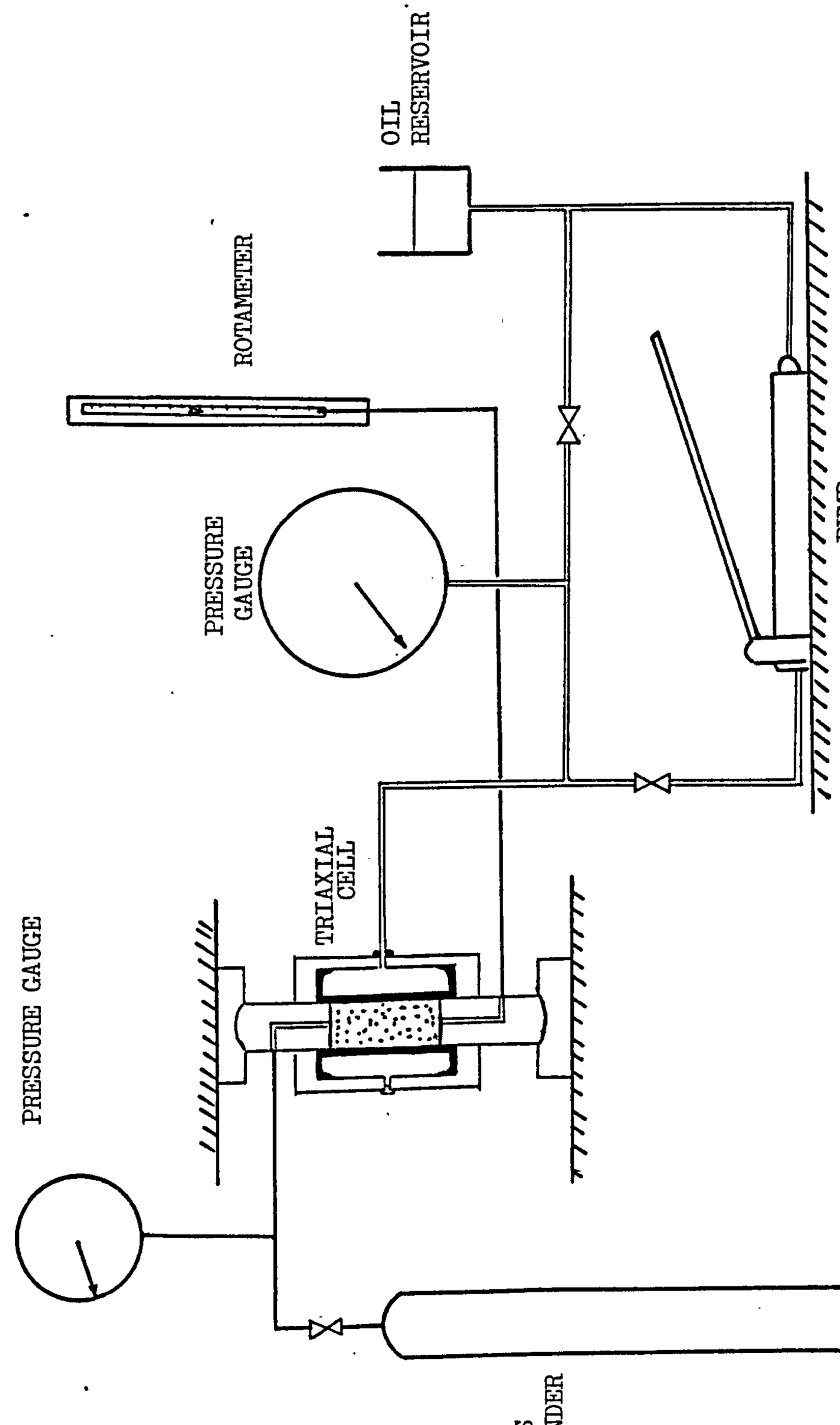

FIGURE (5.3.1) Schematic Diagram of the Experimental Apparatus (Not to Scale).

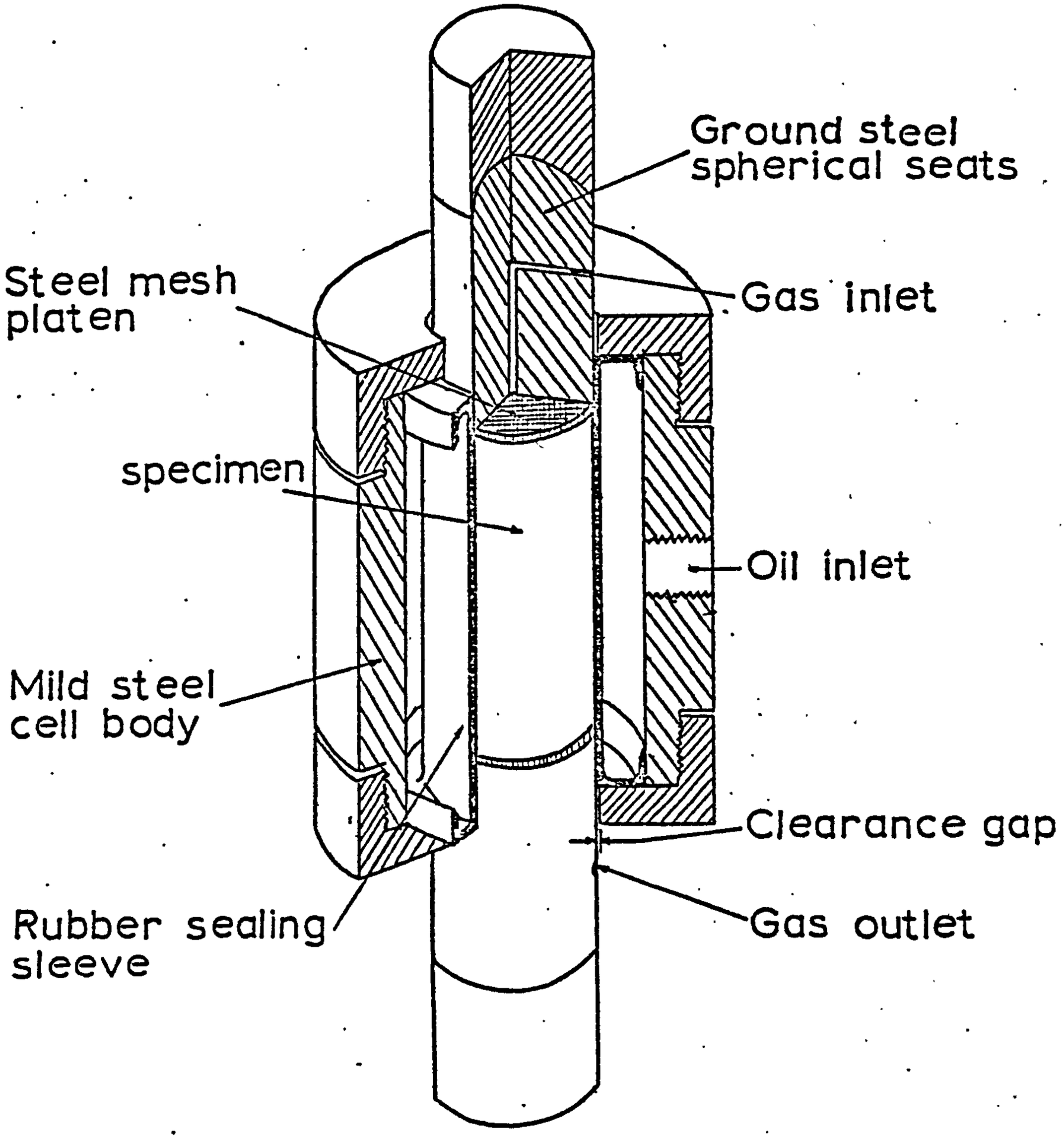

FIGURE (5.3.2) Diagram of the Triaxial Cell.

cast in the Departmental Workshop, was used. The rubber sleeve was capable of stretching to accomodate any deformation in the test specimen after failure. This provided successful measurements of fracture permeability under stress.

Radial stress was applied by the use of hydraulic oil pumped into the chamber between the rubber sleeve and the cell body using a hand operated 'Enerpec' pump. The pump is connected to the oil inlet in the cell wall via a 18 cm diameter 350 bar capacity pressure gauge to monitor the radial stress (σ_3). The connection between the gauge and the pump was by stainless steel tubing and a high pressure needle valve. Additional short circuiting tubing and a release valve, between the oil reservoir and the gauge, provided step by step lowering of the radial stress when necessary. The gauge and the triaxial cell were conncected by a flexible pressure hose.

Axial stress (σ_1) was applied by a conventional testing machine through two spherical seated platens placed at both ends of the cell so as to minimize bending stresses. These platens at the same time served as a gas inlet and an outlet for permeability measurements. Two right angled holes drilled through the cylindrical platens provided the continuity of gas flow between the inbye and outbye ends of the test specimen. 2 mm thick stainless steel mesh discs supplied by Sintered Products Ltd. were introduced between the steel platens and the coal specimen in order to spread gas evenly over the entire contact surface.

5.3.3 The Testing Machine

A 5000 KN Avery (71N25) compression testing machine having four load ranges from 0 - 500 KN to 0 - 5000 KN was used to apply axial load on the test specimen in the triaxial cell. The machine was equipped with hydraulic loading and unloading mechanisms with fine controls; this made it possible to investigate the elastic properties of coal under increasing and decreasing stresses and their effect on permeability.

5.3.4 Flow Measuring Apparatus

Permeability measurements carried out by Patching (17) and Somerton et al. (25) have shown that coal has different permeabilities for different gases. Patching carried out permeability tests on coal using helium, argon, nitrogen and carbon dioxide, the results showed a linear decrease in permeability with the increase in the square of the molecular diameters of the gases. On the other hand, Somerton et al. recorded a 20 to 40 per cent decrease in permeabilities of coal when the flowing gas was switched from nitrogen to methane. The reduction was too large to be explained on the basis of the molecular diameters alone and the sorption of methane was thought to play an important part in decreasing the permeability.

Although methane is the principle seam gas in coal mines, nitrogen was used as the flowing medium throughout this research to increase flow rates through low permeability coals hence simplifying the flow measurements. Nitrogen has a smaller molecular diameter as

compared to methane, it is less sorbable and safer to use. The gas was supplied in high pressure cylinders having an initial pressure of about 13.8 MN/m^2. Using a suitable pressure regulator, gas pressures of up to 2.74 MN/m^2 could be applied to the specimen.

Nitrogen was supplied to the top of the triaxial cell through a length of high pressure tubing. A 0 - 400 psi Burdon tube Sydney Smith test gauge was placed near the triaxial cell to monitor the upstream gas pressure into the test specimen. Passing through the gauge high pressure nitrogen was conducted to the top steel cylindrical platen and distributed over the surface of the coal specimen under stress. Atmospheric pressure nitrogen at the downstream end of the coal specimen was then picked up by the bottom steel cylindrical platen via a steel mesh disc and led to a flow rate measuring apparatus by plastic tubing.

A 40 - 500 cc/min rotameter supplied by Rotameter MFG Co. Ltd. and a 2 - 25 cc/min Precision Bore Flowrotor supplied by F & P Co. were used to measure flow rates of nitrogen at the downstream end. The smaller capacity rotameter was only used in extreme cases of measuring flow rates of gas through very low permeability coals under high stresses. Employing these previously calibrated sensitive rotameters, possible errors, due to manual timing of rising soap film in a bubble meter, used by previous research workers (25),(23),(26), were eliminated. The calibration curve for the rotameters used is given in Appendix I.

CHAPTER SIX

EXPERIMENTAL PROGRAMME AND METHODS OF MEASUREMENT

CHAPTER SIX

EXPERIMENTAL PROGRAMME AND METHODS OF MEASUREMENT

6.1 Introduction

It was found essential to gain information about the structural and mechanical properties of coals used. Therefore, prior to conducting stress-permeability experiments, measurements were carried out to determine the rank, mechanical strength and the effective porosities of the coals. This chapter describes the methods employed.

In this chapter consideration is also given to the choice of stress levels to be applied during stress-permeability experiments and to the effect of the direction of the maximum principal stress relative to the direction of gas flow. Following the discussion of these factors the finalised experimental programme is presented together with an outline of the experimental procedure.

The relevance of Klinkenberg's theory to coal permeability under stress is discussed in relation to the treatment of the experimental results.

6.2 Initial Measurements of Rank, Strength and Porosity

6.2.1 Initial Measurements of Coal Rank

Coal is formed by long term processing of plant and animal organisms throughout the geological times. The mechanical and chemical changes that have occurred during 'coalification' are very complex and are even now little understood in detail. It is agreed, however, that the general effect of this process has been to increase the proportion of carbon in the organic matter at the expense of hydrogen and oxygen. This increase is designated as an increase in the 'rank' of the coal which indicates the position of a coal in the continuous series ranging from peat, through brown coal and bituminous coal, to anthracite. A quantitative assessment of rank is made in terms of the volatile matter or the carbon content of the coal.

As was discussed in previous chapters, strength and elastic properties of different coals can be related to their ranks. Therefore to extend the basis for correlation the ranks of all the coals were determined prior to the stress-permeability experiments.

Immediately after the coal lumps reached the workshop, proximate analysis was carried out in accordance with the British Standards (68). Percentage volatile matter, carbon, ash and moisture were determined for all the coals tested.

6.2.2 Initial Measurements of Mechanical Strength

The strength of a rock is defined as the stress which is necessary to bring about rupture at given environmental conditions. It can either be established experimentally by means of laboratory testing of rock specimens or by rock testing in situ.

The uniaxial compressive testing of cylindrical rock specimens until failure is the most commonly used method of studying the strength and mechanical properties of rock. For any axial load applied to the rock specimen, the axial deformation is measured and the corresponding strain $\epsilon_1 = \frac{\Delta L}{L}$ is calculated. Stress-strain diagrams are obtained by plotting the stress and corresponding strains of the rock tested for failure.

Most solid materials, when subjected to stress, show a proportionate change in shape at first. This change is recoverable when the stress is removed. This property of recovering from strain of a material is termed elasticity. If a material recovers completely, it is called perfectly elastic. If the material does not recover completely, the strain that remains when the stress is removed is called permanent set, and the material is said to be in an elastic state (69).

If a solid material continuously and permanently changes shape without fracturing under a stress exceeding the yield value of the material, it is said to be in a plastic state. In other words, the plastic deformation of a material is the permanent deformation after complete removal of the externally applied stress.

Figure (6.2.1) shows an idealised stress-strain relationship diagram for rocks. Up to a certain externally applied stress σ_Y (yield point Y) on the rock, the stress σ is proportional to strain ε (Hooke's law);

$$\sigma = E \cdot \varepsilon$$

the proportionality constant E is known as Young's modulus of elasticity.

The transition from elastic to ductile behaviour takes place at point Y, which is called the yield point, and the corresponding stress σ_Y is termed the yield stress. On further loading up to the ultimate stress σ_{ult} at point U, failure of the material takes place, and with increasing strain beyond U the stress drops. The stress value σ_{ult} is known as the uniaxial compressive strength of the material.

If a material is loaded beyond the yield point Y and the stress-strain curve continues to rise within the inelastic domain the material is said to be strain hardened. As shown in Figure (6.2.2), only a part of the strain is recovered if the material is unloaded from σ_B to $\sigma_0 = 0$. The irreversible, permanent deformation of the magnitude ε_{ir} is known as plasticity deformation:

$$\varepsilon_{total} = \varepsilon_{ir} + \varepsilon_{el}$$

The ratio of the elastic strain ε_{el} to the total strain ε_{total} of the material is termed the degree of elasticity of the rock:

$$\text{Degree of Elasticity} = \frac{\varepsilon_{el}}{\varepsilon_{total}}$$

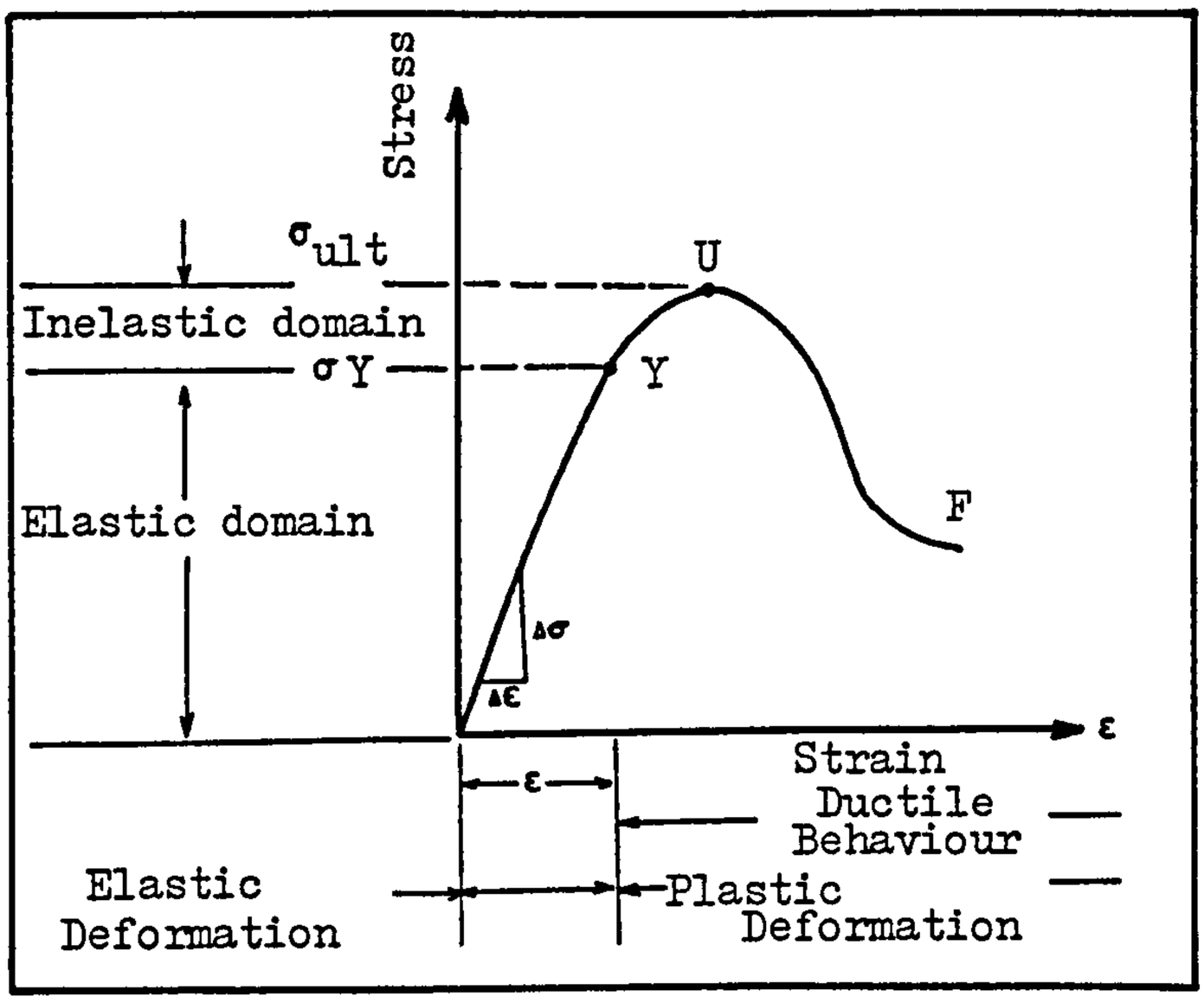

FIGURE (6.2.1) Stress-Strain Diagram for Rock

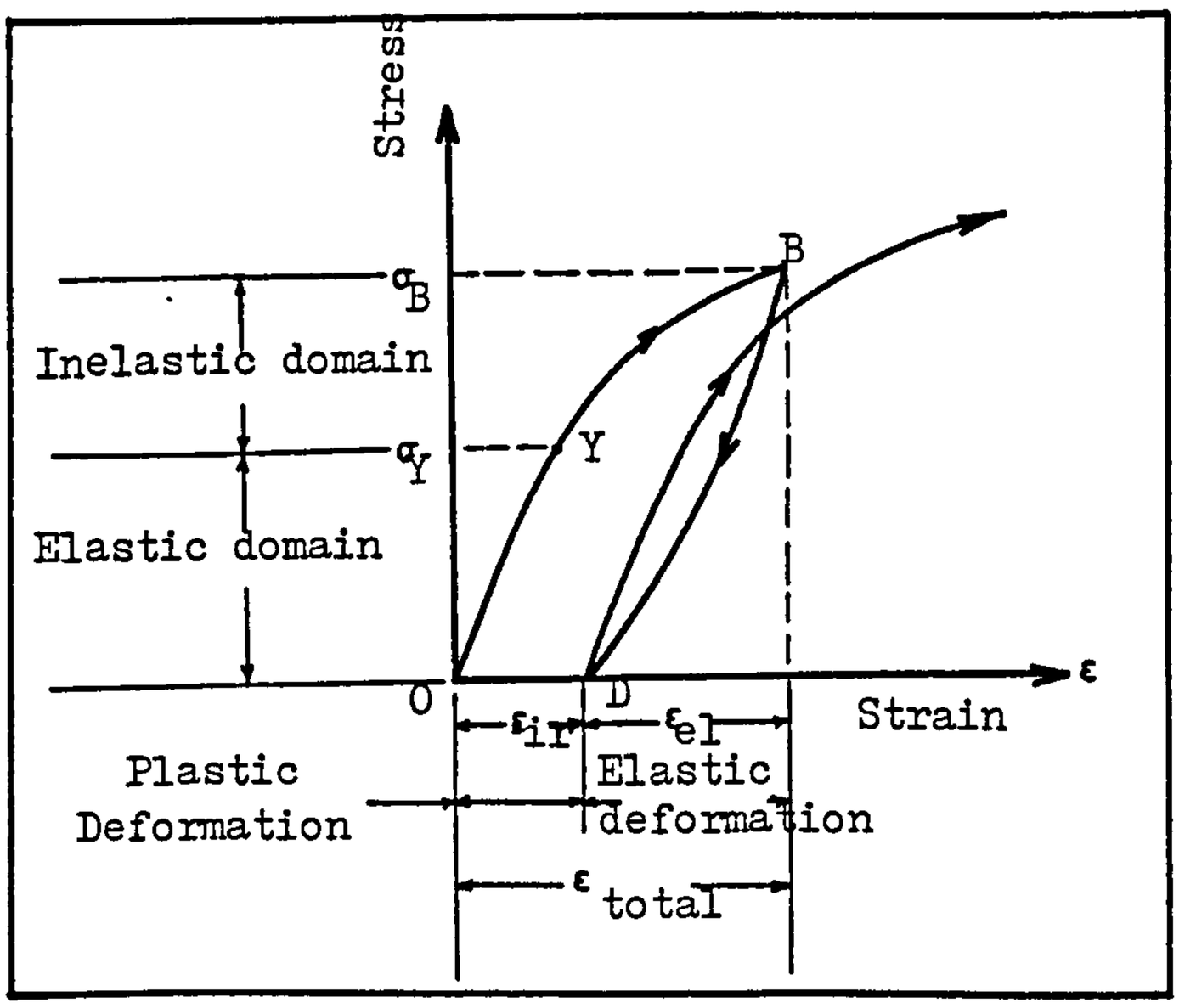

FIGURE (6.2.2) Stress-Strain Diagram of Strain Hardening Characteristic of a Ductile Material.

The ratio of the plasticity strain $\varepsilon_{pl} = \varepsilon_{ir}$ to the total strain ε_{total} of the material is termed the degree of plasticity of the material (69):

$$\text{Degree of plasticity} = \frac{\varepsilon_{pl}}{\varepsilon_{total}}$$

6.2.2.1 Apparatus and Procedure for Measurement of Coal Strength

Cylindrical test specimens, having a diameter to length ratio of one, were prepared from each coal to be tested for stress-permeability relationship. These specimens were then tested for uniaxial compressive strength by loading until failure in a Denison universal testing machine. Axial deformation measurements were made simultaneously using dial guages and the strains were calculated.

Stress-strain diagrams were produced for every coal tested and the patterns of deformation were observed. Young's modulus for every coal were then determined from the diagrams produced.

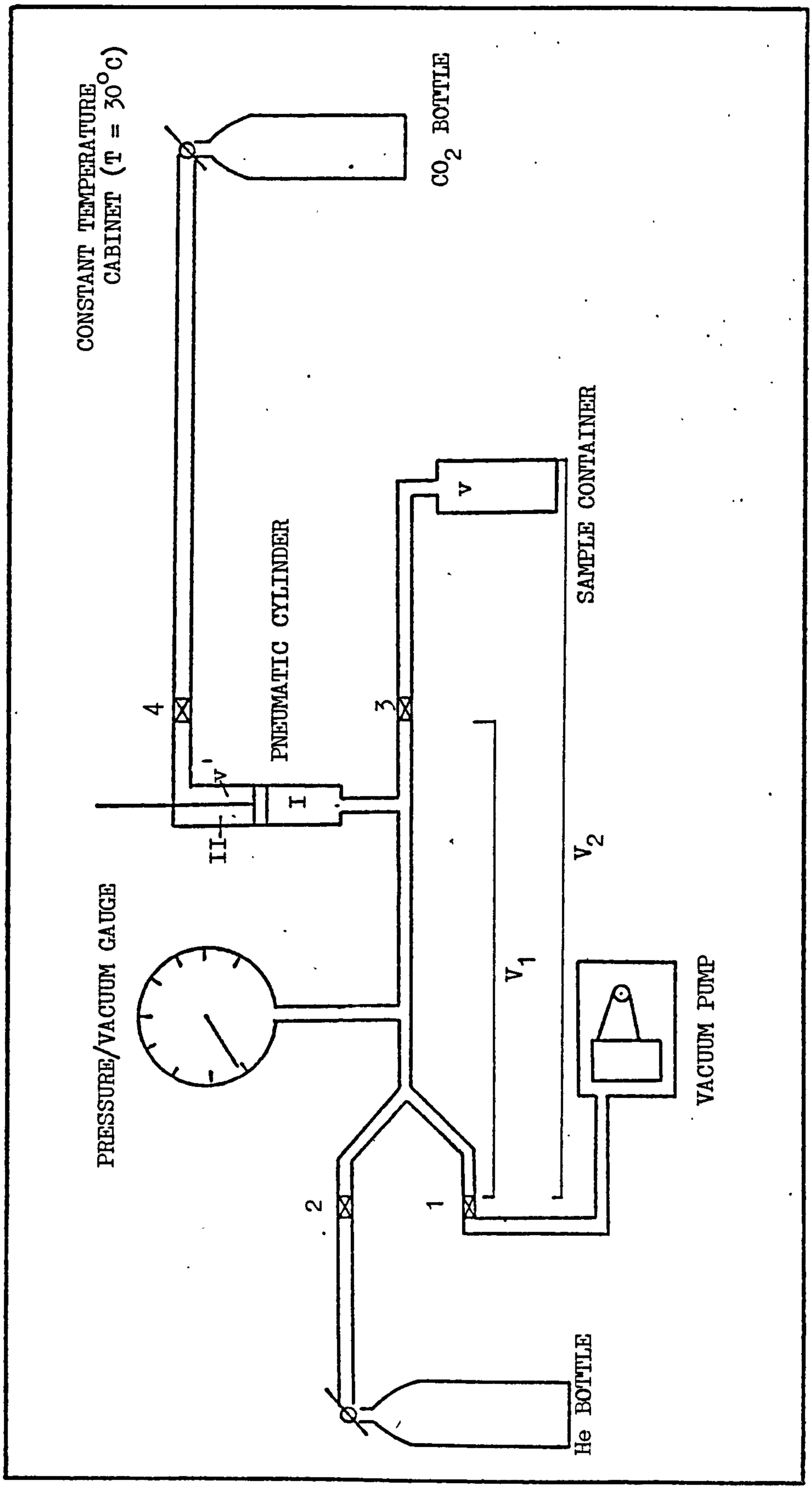

FIGURE (6.2.3) Schematic Diagram of the Experimental Set-Up for Effective Porosity Measurements.

6.2.3 Initial Measurements of Effective Porosity

A number of stress-permeability test specimens from each coal were selected and their effective porosities were determined before stressing. In order to avoid any damage to the internal structure of the test specimens, porosities were determined by the 'Gas Expansion Method'.

The porosity measurement apparatus shown in Figure (6.2.3) was specially designed for this purpose. The basic principle used is that of isothermal expansion of gas into the test specimen where the effective pore volume can be determined from the observed changes in the gas pressure using the Boyle-Mariotte gas law.

The apparatus consisted of the following parts:

(a) The sample container which is built to take a 38 mm diameter, 76 mm length cylindrical coal specimen with very little free space left. Volume of the sample container is V_c = 85·775 cc, Figure (6.2.4).

(b) Pneumatic cylinder equipped with two cup seals providing two airtight sections as the piston arm moves. The cross-sectional area of the cylinder is A = 11·341 sq. cm, Figure (6.2.5).

(c) Vacuum pump.

(d) Clockhouse Pore Pressure/Vacuum gauge.

(e) Four high pressure needle valves.

(f) Helium bottle.

(g) Carbon dioxide bottle.

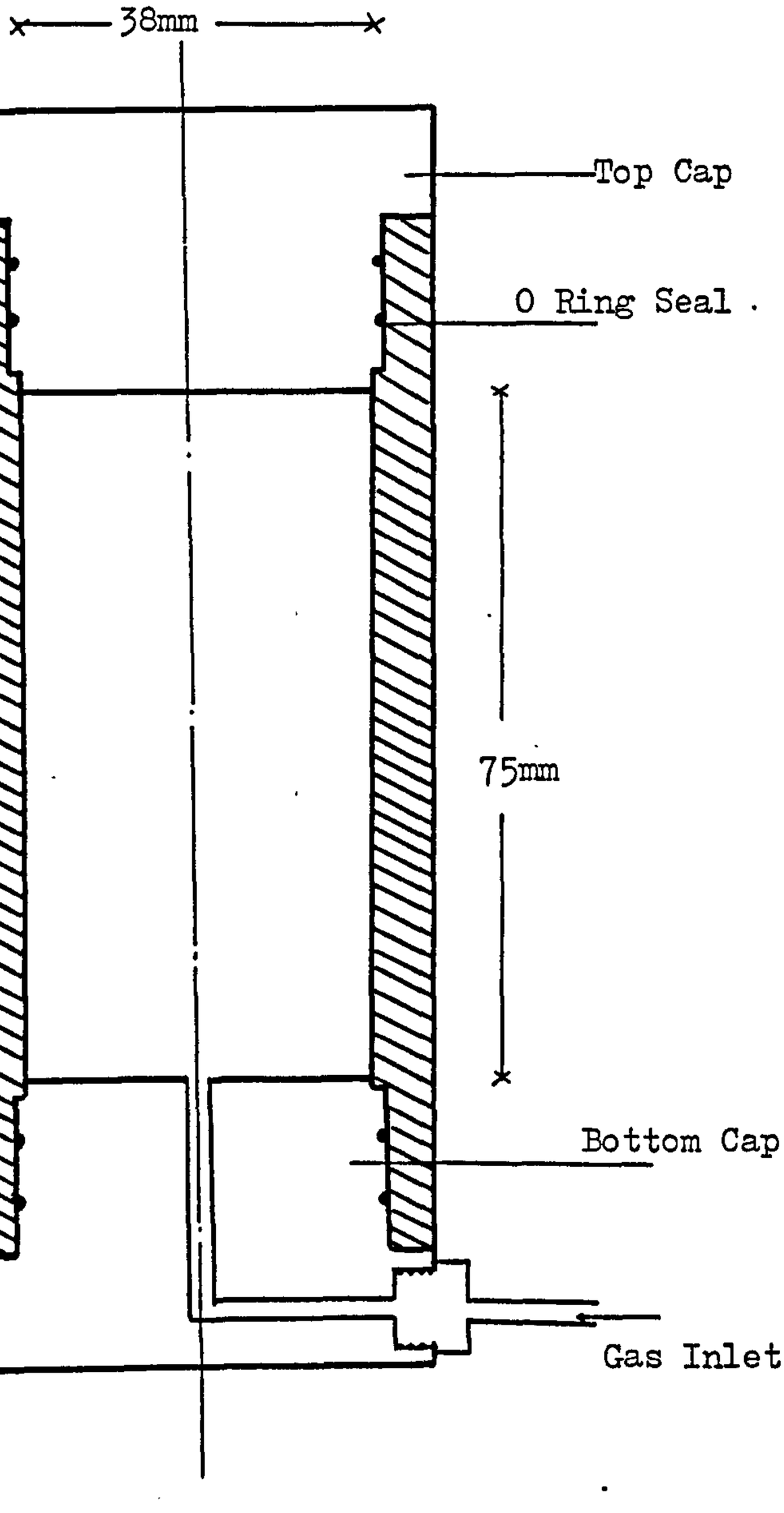

FIGURE (6.2.4) The Sample Container Used in Effective Porosity Measurements.

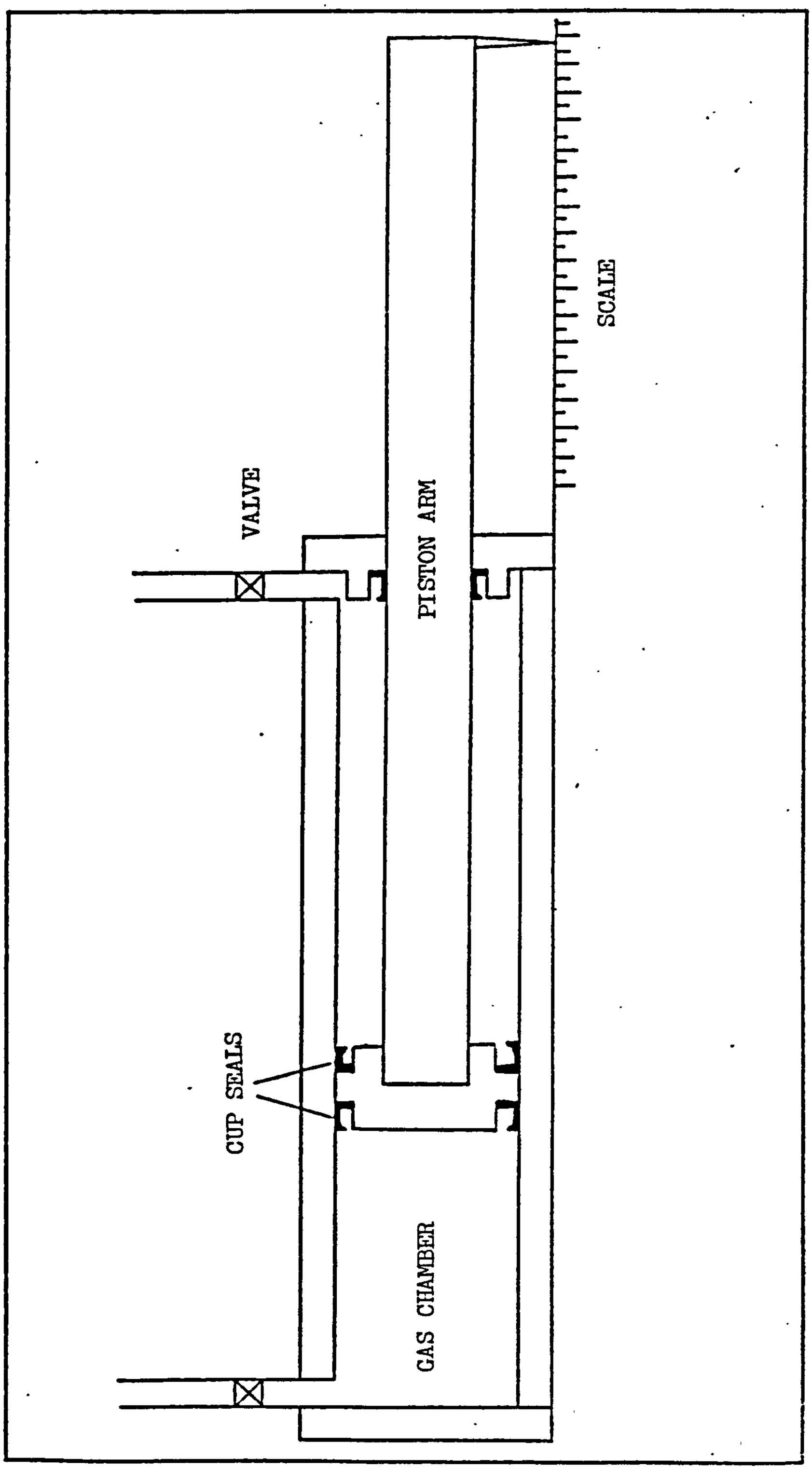

FIGURE (6.2.5) Pneumatic Cylinder Used in Effective Porosity Measurements.

Owing to its smallest molecular size, Helium was used as the flowing medium in porosity measurements. Carbon dioxide was readily available and was only used externally to provide high pressures in the pneumatic cylinder. The system was enclosed in a constant temperature cabinet which was kept at 30°C by a thermostat. Bulk volumes V_b of test specimens were determined by water displacement and then the specimens were dried in an oven at 80°C for 24 hours.

The dry specimen was placed in the sample container and the whole system was evacuated overnight. The sample container was then isolated from the system by closing the valve No 3, and the volume V_1 of the system was charged with helium at P_1 = 100 psi. The length of the piston arm L was measured and by opening the valve No 3, helium was allowed to expand into the sample container causing a drop in total gas pressure. Part II of the pneumatic cylinder was then charged with 100 psi carbon dioxide and pushing the piston arm forward the pressure P_2 of the helium gas in volume V_2 was brought to 100 psi. The system was left to reach equilibrium at constant temperature and by further advancing of the piston arm a final equilibrium for the system at P_2 = 100 psi was reached. The length L' of the piston arm was then measured.

Under isothermal flow conditions, volume v' displaced from the pneumatic cylinder during the process is equal to the volume v expanded into the sample container since:

$$P_1V_1 = P_2V_2$$

$$P_1 = P_2 = 100 \text{ psi}$$

therefore $$V_1 = V_2 \qquad \ldots\ldots\ldots \quad 6.2.1$$

substituting $V_2 = V_1 + v - v'$ in equation 6.2.1 we get,

$$V_1 = V_1 + v - v'$$

thus

$$v = v' \qquad \ldots\ldots\ldots \quad 6.2.2$$

The volume of gas displaced from the cylinder is found as;

$$v' = v = A(L - L')$$

where:

A the cross-sectional area of the cylinder, cm^2

L and L' the initial and final lengths of the piston arm, cm

Volume v expanded into the sample container fills both the free space around the coal specimen (v_f) and the effective pore volume $(V_v)_e$, then:

$$(V_v)_e = v - v_f = A(L - L') - v_f \qquad \ldots\ldots\ldots \quad 6.2.3$$

The volume of the free space v_f is the difference between the volume of the sample container V_c and the bulk volume V_b of the test specimen which were both predetermined, thus;

$$v_f = V_c - V_b \qquad \ldots\ldots\ldots \quad 6.2.4$$

substituting equation 6.2.4 in 6.2.3 we get,

$$(V_v)_e = A(L - L') - (V_c - V_b) \qquad \ldots\ldots\ldots \quad 6.2.5$$

which gives the effective pore volume of the test specimen to be used in stress-permeability experiments.

Effective porosities of the test specimens are expressed as the percentage of effective pore volume to the bulk volume or the effective pore volume per weight of coal, (cc/gm).

6.3 Measurement of Permeability Under Stress

6.3.1. Choice of Stress Levels

As discussed previously the stresses experienced around working coal faces can be examined in three major areas:

(a) the front abutment zone,

(b) the crushing zone,

(c) the recompaction zone.

Therefore, it was decided to conduct laboratory stress-permeability measurements simulating the stress conditions experienced in these zones. Considering that most of the coal seams worked in the United Kingdom are at depths less than 1000 m, radial stresses (σ_3) applied need not be so high. In deciding on the magnitudes of simulated maximum and minimum principal stresses σ_1 and σ_3 for these zones, both the results of the finite element analysis and the works of previous researchers were considered.

Under triaxial stress conditions, the radial stress, σ_3, is related to the axial stress, σ_1, by the relation (70):

$$\sigma_3 = \frac{\nu}{1-\nu}\,\sigma_1$$

where ν is Poisson's ratio:

$$\nu = \frac{\text{radial strain, } \varepsilon_3}{\text{axial strain, } \varepsilon_1}$$

Previous researchers such as Somerton et al. (25) and Gawuga (26) have used principal stress ratios (σ_3 / σ_1) of $\frac{1}{2}$ and $\frac{1}{3}$ respectively which were based on the above relation. Poisson's ratio for rock varies according to the nature of deformation and is also affected by the direction of loading and the rock grain interlocks. Poisson's ratio values, ranging between $\nu = 0{\cdot}24$ and $\nu = 0{\cdot}49$, have been reported for different coals in literature (56),(71),(18). Having to study seven different coals which would inevitably give rise to seven different Poisson's ratios, it was thought that using stress ratios based purely on the Poisson's ratio for each coal would offer no real basis for comparing the effects of stress on permeability of these coals. To facilitate correlation of the stress-permeability behaviour of different coals, the stress ratio σ_3/σ_1 should be kept constant for all seven coals used.

The finite element analysis of stresses around working longwall faces, discussed in Chapter 4, has shown that both σ_1 and σ_3 increase in the front abutment zone of a coal face. The magnitudes

of the maximum principal stresses increase with depth and the stress ratio σ_3/σ_1 changes between $\frac{1}{2}$ and $\frac{1}{3{\cdot}5}$ for the front abutment zones of coal faces 300 to 700 m deep.

Precise increments of 10·0 Bars (1·0 MN/m^2) for the radial stress and 1·0 KN for the axial load could be applied with the existing equipment. Using 37 to 38 mm diameter core specimens, 1·0 KN load creates approximately 0·90 MN/m^2 axial stress. Therefore, the stress ratio practically applicable on the specimens used is given by the relation:

$$\frac{\sigma_3}{\sigma_1} = \frac{\sigma_3}{0{\cdot}9F_1}$$

substituting σ_3 = 1·0 MN/m^2 and 1·0 KN increments of axial load for F_1 one obtains the stress ratios $\frac{1}{1{\cdot}8}, \frac{1}{2{\cdot}7}, \frac{1}{3{\cdot}6}, \frac{1}{4{\cdot}5}$ and so on.

A number of specimens were tested for stress-permeability relationship under the above determined stress ratios to see if it had any significant effect on the stress-permeability behaviour of coals. As shown in Figures (6.3.1) and (6.3.2), the reduction in permeability of a specimen increased slightly as the same specimen was loaded and unloaded in cycles of increasing stress ratios. Other than this, no significant change in the general stress-permeability behaviour of coal was noted. Unloading curves are not included in the figures.

In order to extract maximum information about the stress-permeability behaviour of coals, it was planned to test each specimen more than once. This necessitated the employment of

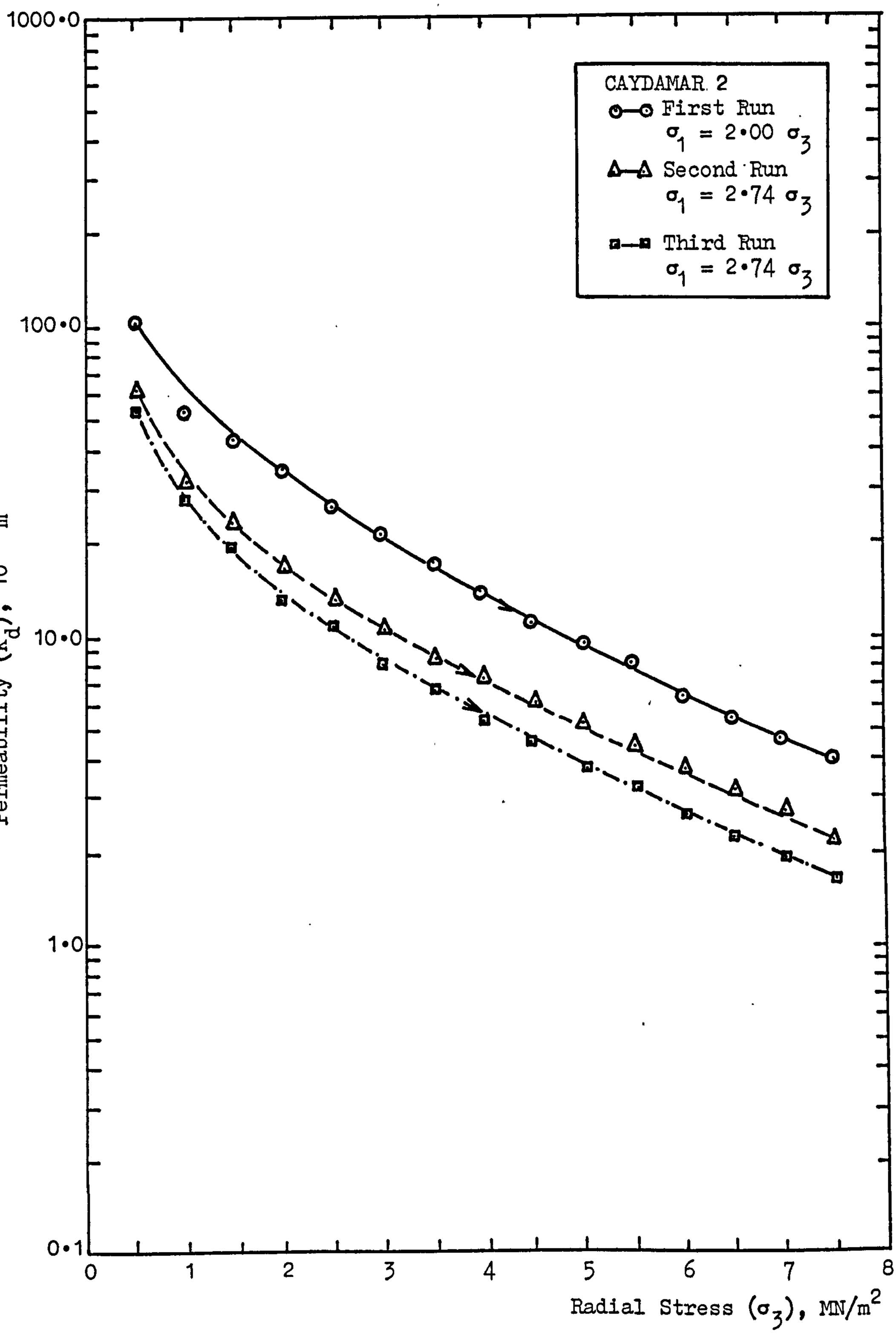

FIGURE (6.3.1) Stress-Permeability Curves for CAYDAMAR Coal at Different Stress Levels.

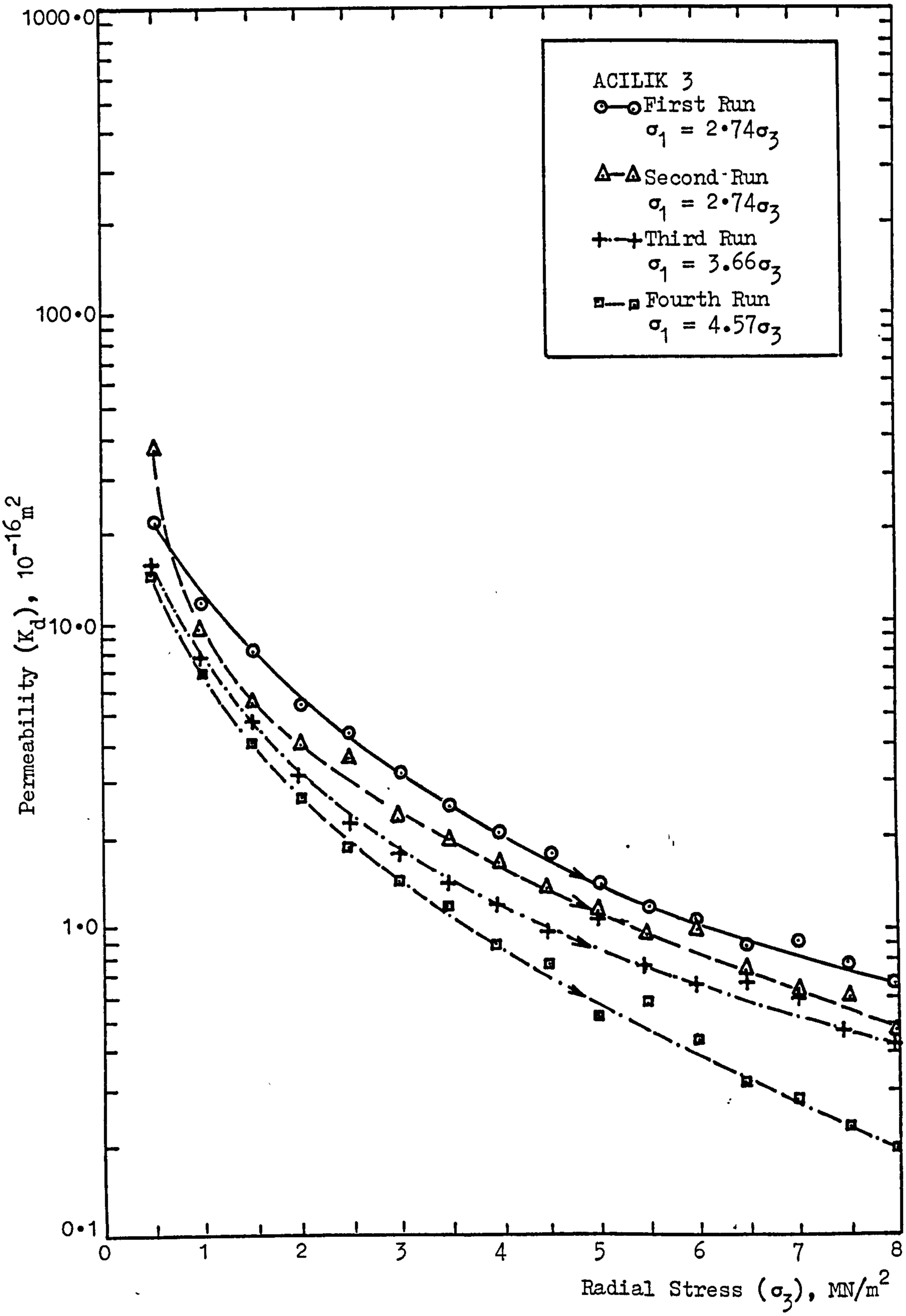

FIGURE (6.3.2) Stress-Permeability Curves for ACILIK Coal at Different Stress Levels.

axial and radial stresses well below the failure stresses of the coals used.

Considering all the facts mentioned above and taking into account the mechanical strength and the permeability of the specimens, it was decided to apply radial stresses up to a maximum of $\sigma_3 = 8{\cdot}00\ MN/m^2$ using a stress ratio of $\frac{\sigma_3}{\sigma_1} = \frac{1}{2{\cdot}7}$. This was thought to be a realistic simulation of the subsurface stress conditions yet avoided the possibility of damage of the specimens that might occur when using higher stress ratios.

The same ratio was applied in the stress-permeability experiments on fractured coal, simulating the stress conditions in the recompaction zone of a longwall face. Stress conditions for the crushing zone were created by loading the specimen to the predetermined maximum stress level, and, releasing the radial stress σ_3, suddenly, while keeping the axial stress σ_1 at its highest possible magnitude.

6.3.2 The Direction of Maximum Principal Stress

Nearly all the coal specimens used in this research have been cored parallel to the bedding planes. Therefore, the flow of gas, axially along the specimen, was also parallel to the bedding planes. Under similar flow conditions, Gawuga (26) conducted some tests on the effects of direction of maximum principal stress relative to the flow direction. He reported that with the maximum principal stress perpendicular to the flow direction, greater

reductions in permeability of the specimens were observed.

A series of experiments were carried out by the author in which a specimen was first tested with the maximum principal stress parallel to the flow direction; the experiment was then repeated with the maximum principal stress perpendicular to the flow direction. As shown in Figure (6.3.3), the slope of the second loading curve, where the maximum principal stress was perpendicular to the flow direction was greater than the first one. In general, lower permeabilities were observed when the maximum principal stress was perpendicular to the flow direction.

Unfortunately, due to the limitations imposed by the experimental equipment, it was found impractical to apply very high radial stresses which usually caused the rupture of the protective sleeve around the specimen. Another limitation was that the flow rate of gas through very low permeability specimens was impossible to measure under very high radial stresses. Consequently, the experimental conditions had to be such that the maximum principal stress direction was parallel with the bedding planes and the gas flow direction. As a result the measured permeability was probably in excess of the permeability parallel to the bedding planes in situ since the direction of maximum principal stress in situ is normally perpendicular to the bedding. However, it must be remembered that the in situ permeabilities of coal are expected to be higher than the experimental values obtained from test specimens which are generally free from major fractures.

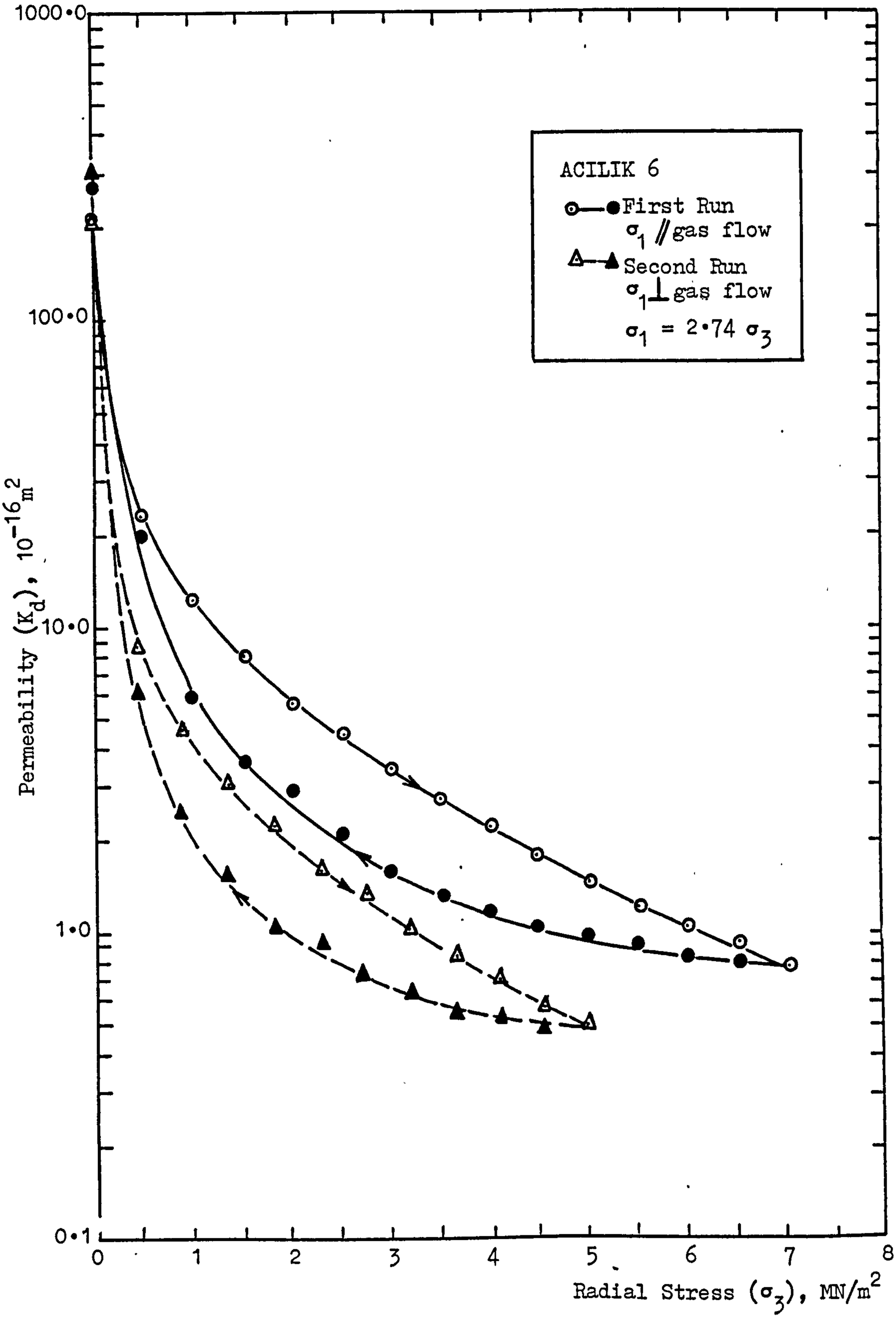

FIGURE (6.3.3) Directional Effect of Maximum Principal Stress on Permeability.

6.3.3 Experimental Programme

Previous research on coal permeability and the effect of stress on the permeability of coals has shown that it is impossible to reproduce permeability results even for specimens taken from the same lump of coal (25),(26),(17),(21). Due to the differences in orientation and the fracture characteristics of each individual coal specimen, it has not been possible to obtain identical values of permeability.

Although no real basis existed for comparing the stress-permeability results of different coals, it was found possible to establish a relative correlation between the generalised stress-permeability behaviour of coals. It is known that the permeability of coal is stress-history dependent, that is, when a coal sample is stressed and destressed, a relative change in permeability is created as a function of the elastic properties of coal material. Coals of the same elastic properties should experience similar changes under the same stress conditions. Therefore, a careful study of stress-history effect on permeabilities of different rank coals under the same stress conditions should produce the basis for correlating the stress-permeability behaviour of different coals. After such an understanding of the stress-permeability relationship is established, research could be extended into the explanation of permeability changes occuring around working longwall faces.

In view of the above suppositions, stress-permeability experiments were carried out in the following order:

(i) Determine the stress-history effect on coal permeability.

(ii) Determine the effect of fracturing on coal permeability.

(iii) Determine the fracture permeabilities of coal under stress.

(iv) Determine the effect of moisture on permeability of coal under stress.

(v) Determine the effect of directional anisotropy on the stress-permeability relationship of coal.

A number of test specimens, prepared from every lump taken from a different coal seam, were tested following the above programme. A more detailed discussion of the procedure followed in each step will be given in the following chapter in which the experimental results are discussed.

6.3.4 Experimental Procedure for Stress-Permeability Measurements

The general procedure of measuring the gas flow rates through triaxially stresses coal specimens was repeatedly used for all the samples tested.

The triaxial cell was prepared by inserting the coal specimen into the rubber sleeve and placing it in the cell body

as shown in Figure (6.3.4). After screwing both end caps onto the main body, the annalus between the cell body and the specimen was filled with oil. Air was bled from the valve provided for this purpose by slowly pumping oil into the cell while holding the cell horizontal with the open valve pointed upwards. When oil spurted out of the bleeding valve the cell was considered primed and the valve was closed, the cell being ready to use.

The bottom spherical seat was placed at the centre of the testing machine platen and three wooden blocks, which support the cell, were placed around it. The accompanying spherical based cylindrical platen was then placed onto the bottom seat and the cell body was slowly lowered over the cylindrical platen until it rested on the wooden blocks. The height of the wooden blocks was such that approximately 30 mm of the cylindrical platen was inside the cell and would be gripped by the rubber sleeve when oil pressure was applied. Finally the upper steel cylindrical platen was lowered into the cell and the top spherical seat was placed on top.

The whole assembly was then checked for true allignment and the machine cross-head was lowered until the upper platen was within a few millimetres of the top spherical seat. Using the hydraulic ram, the cross-head was lowered further to make contact with the top spherical seat. At this point, the coal specimen would be totally sealed and has zero stress applied to it.

Nitrogen gas was supplied to the specimen under pressure and the flow rate of gas through a non-stressed coal specimen

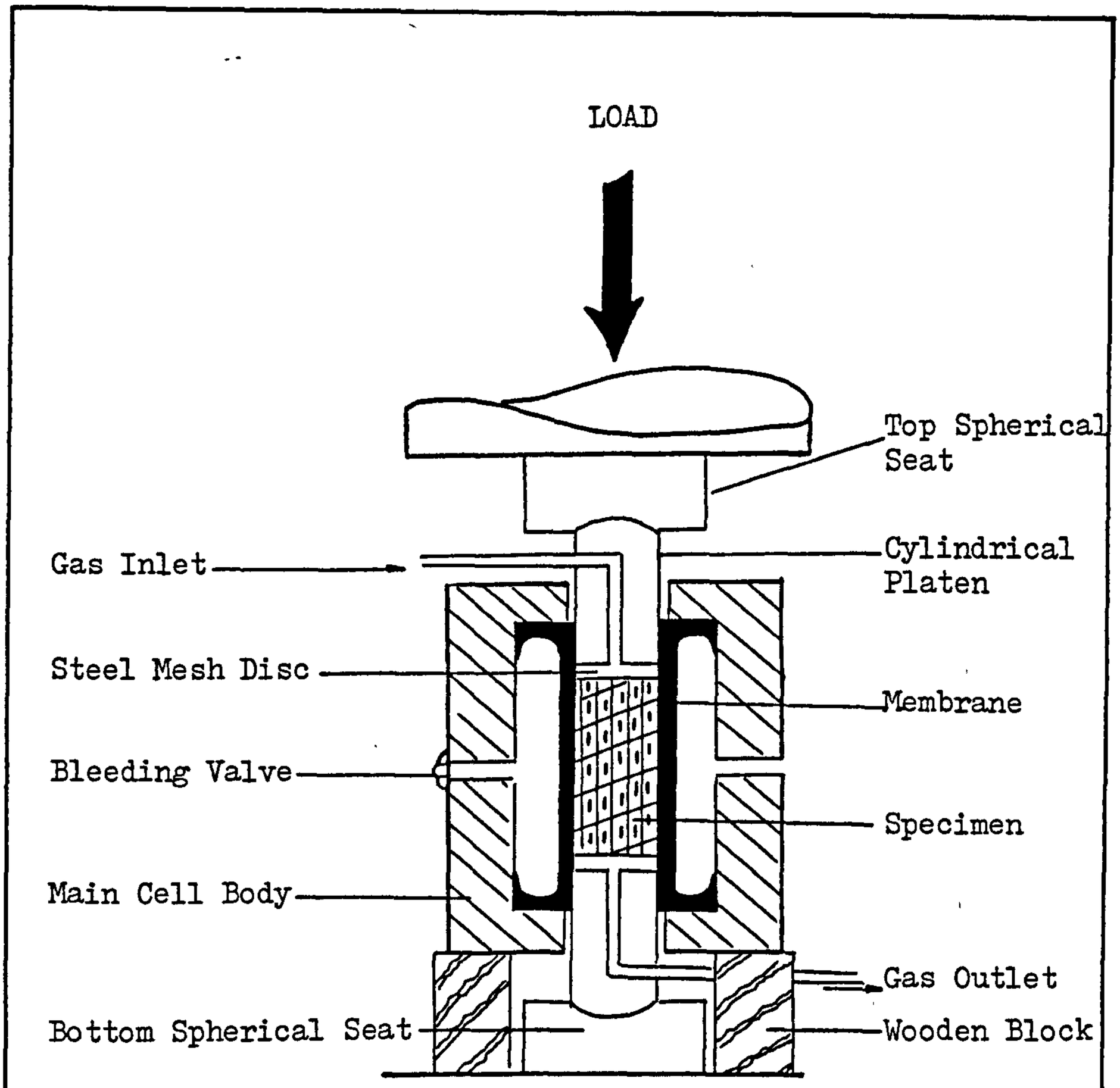

FIGURE (6.3.4) Schematic Representation of the Triaxial Cell.

(Base Permeability) was measured using one of the rotameters described in the previous chapter. In order to establish a relationship between permeability and applied stress, the specimen was loaded both axially (σ_1) and radially (σ_3) with the increments of $\sigma_3 = 0{\cdot}5$ MN/m^2 where the ratio $\frac{\sigma_3}{\sigma_1}$ was kept at a previously determined value of approximately $\frac{1}{2{\cdot}7}$. Simultaneously, the flow rates of nitrogen were measured for at least three gas pressure settings at each stress level.

Depending on the mechanical strength and the degree of reduction in permeability of coal dealt with, the loading procedure was terminated at radial and axial stresses of $\sigma_3 = 6{\cdot}5 - 8{\cdot}0$ MN/m^2 and $\sigma_1 = 17{\cdot}5 - 21{\cdot}6$ MN/m^2 respectively. Following a similar procedure, the test specimen was then unloaded with simultaneous measurements of gas flow rates at predetermined stress intervals.

In order to establish an understanding of the effects of elastic properties of coal on its permeability, most of the test specimens were tested more than once. Therefore, special attention was given to avoiding failure or damage of the test specimen in the early stages of the experiment.

Unlike previous research workers (26), (22), fracturing and failure of the coal specimens was caused by the sudden release of radial stress after the highest loading stresses were reached. This caused the induced tensile fracturing of the specimen similar to the fracturing process taking place at the coal face. The

process also avoids damage to the rubber sleeve so that the sample could be finally tested for fracture permeabilities under stress.

A John Bull dial gauge was mounted on a stand and used to monitor closure between the two machine platens, thus giving a measure of the axial displacement caused by the increasing stresses. For a number of specimens tested for failure, 120Ω Tinsley Telcon foil type strain gauges and a Vishay/Ellis Digital Strain Indicator were used to monitor the axial and radial strains simultaneously with the permeability measurements.

On completion of the test, the machine cross-head was raised, the top spherical seat and the cylindrical platen were removed and the cell body was lifted off the testing machine. In order not to cause any damage to the specimen, the cell was dismantled and the specimen was gently removed from the rubber sleeve and stored for further use.

The same loading-unloading procedure was applied in measuring the permeabilities of fractured coal specimens.

6.4 Treatment of Results

It is the usual practice to correct measured values of gas permeabilities of a porous media using the well established Klinkenberg equation. However, due to the unpredictable structural behaviour of coal, the validity of Klinkenberg's Theory for coal

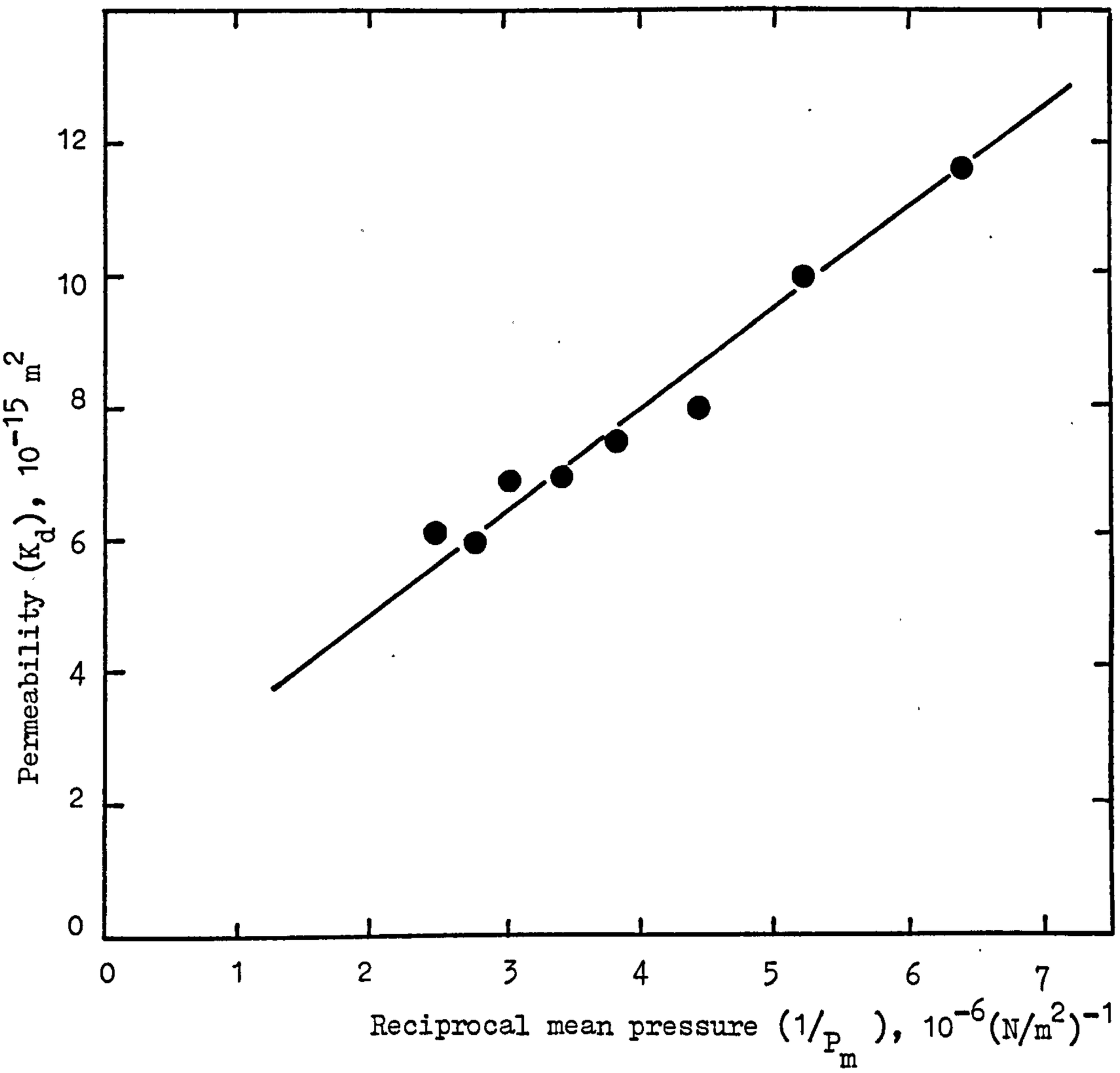

FIGURE (6.4.1) Variation of Permeability with Reciprocal Mean Pressure for Darley Dale Sandstone (After Gawuga (26)).

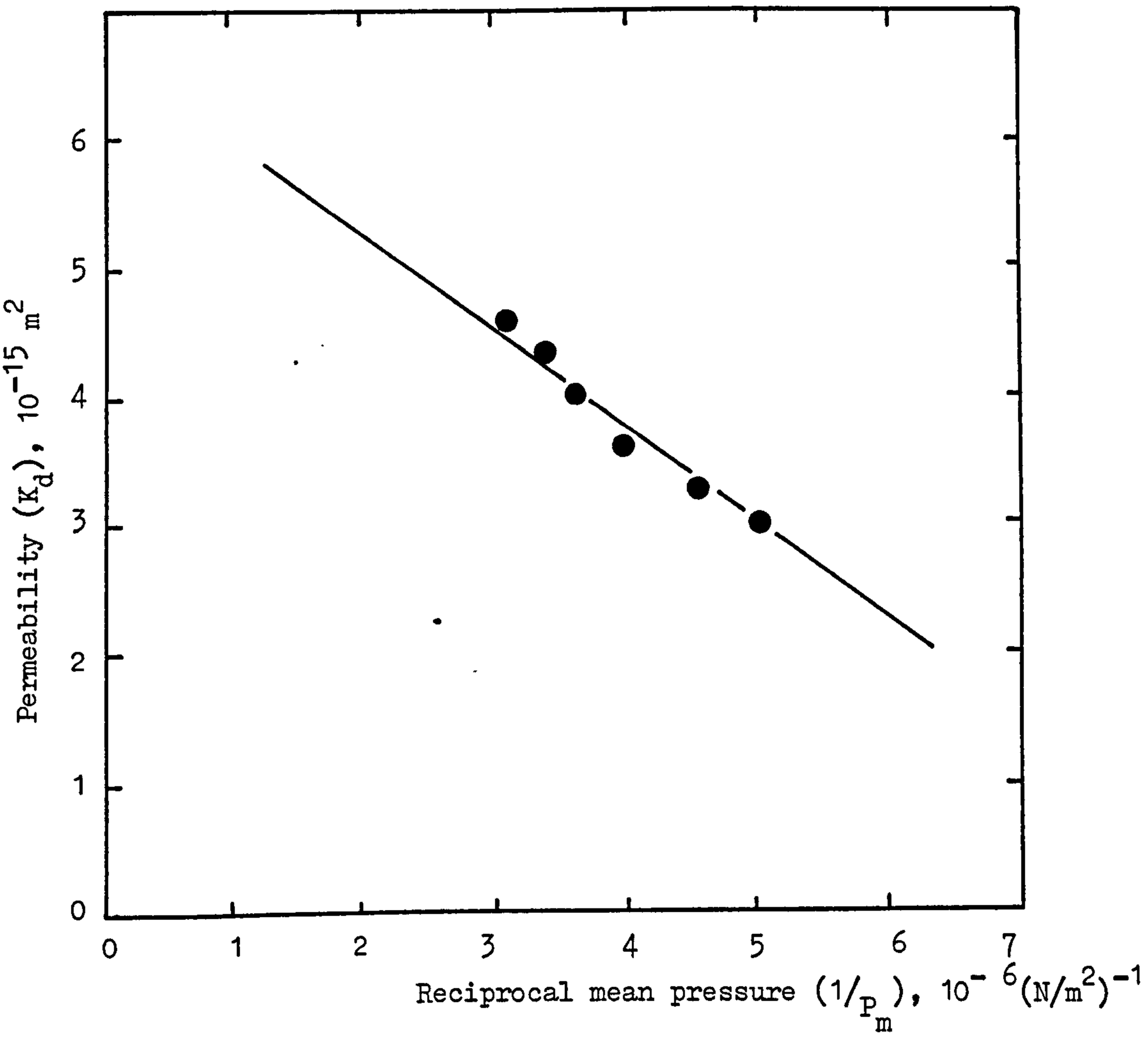

FIGURE (6.4.2) Variation of Permeability with Pressure for an Unstressed Coal Specimen (After Gawuga (26)).

permeability under stress has been questioned recently. Patching (17) suggested that the effect of molecular slip is of minor significance in comparison to the effect of confining pressure on permeability of coal. Further research has been done recently on this subject in the Department of Mining Engineering, University of Nottingham; the findings were considered before evaluating the permeability results obtained in this research.

6.4.1 The Validity of Klinkenberg's Theory for Permeability of Coal Under Stress

The effect of gas pressure on permeability of both stressed and unstressed coal was studied by Gawuga (26) and Yerebasmaz (66) in 1979 and 1981 respectively.

As shown in Figures (6.4.1) and (6.4.2), unstressed specimens of sandstone and coal exhibited opposite relations between the gas reciprocal mean pressure and permeability.

The decrease in permeability of sandstone with increasing gas pressure, as shown in Figure (6.4.1) is explained by the slip phenomenon. According to the theory, at low gas pressures the molecules closest to the walls of the pores slip along the pore walls causing the permeability to rise. As the gas pressure rises, the molecular free path of gas becomes smaller and the permeability decreases. However, the same did not apply to coal and its permeability increased as the gas pressure was increased. As shown in Figure (6.4.3), similar results were obtained by Yerebasmaz (66) in later research.

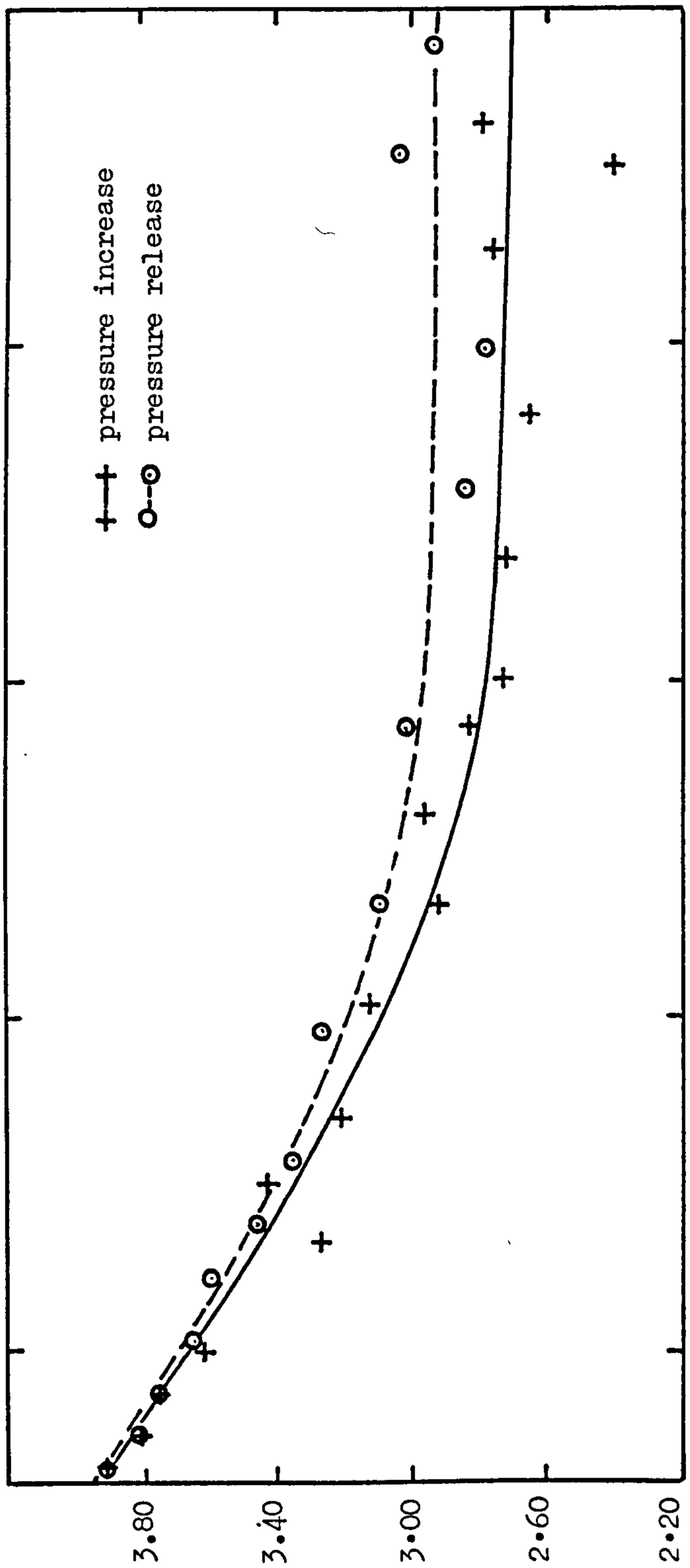

FIGURE (6.4.3) Variation of Permeability with Gas Pressure for Unstressed ACILIK Coal (After Yerebasmaz (66)).

The increase in permeability of coal with increasing gas pressure was explained by the expansion of the pore spaces and fissures under sufficiently high gas pressures thus creating wider flow channels. Figure (6.4.3) illustrates the irreversible character of the structural damage caused by high gas pressures.

When the same measurements were repeated under various stress conditions the permeability of coal was proved to be independent of gas pressure provided that sufficiently high stresses were applied. Figure (6.4.4) shows these results obtained by Gawuga.

Similar observations were made by the author. As shown in Figure (6.4.5), three different coal specimens were tested for the effect of gas pressure on permeability of coal under stress. The relation between the reciprocal mean gas pressure and the permeabilities of COCKSHEAD 2 and DEEP HARD 3 indicated that the permeability of stressed coal was independent of gas pressure. DUNSIL 6, on the other hand, showed a slight increase in permeability as the gas pressure increased.

In view of all these observations, one could say that the Klinkenberg Theory does not apply to coal. Under triaxial stress conditions, permeability is independent of gas pressure due to the compaction effect of stresses applied. Moreover, as will be discussed in the following chapter, the effect of externally applied stress on permeability of coal is so dominant that any minor changes in permeability due to gas pressure would be negligible. Therefore it was decided to ignore the Klinkenberg effect in permeability calculations.

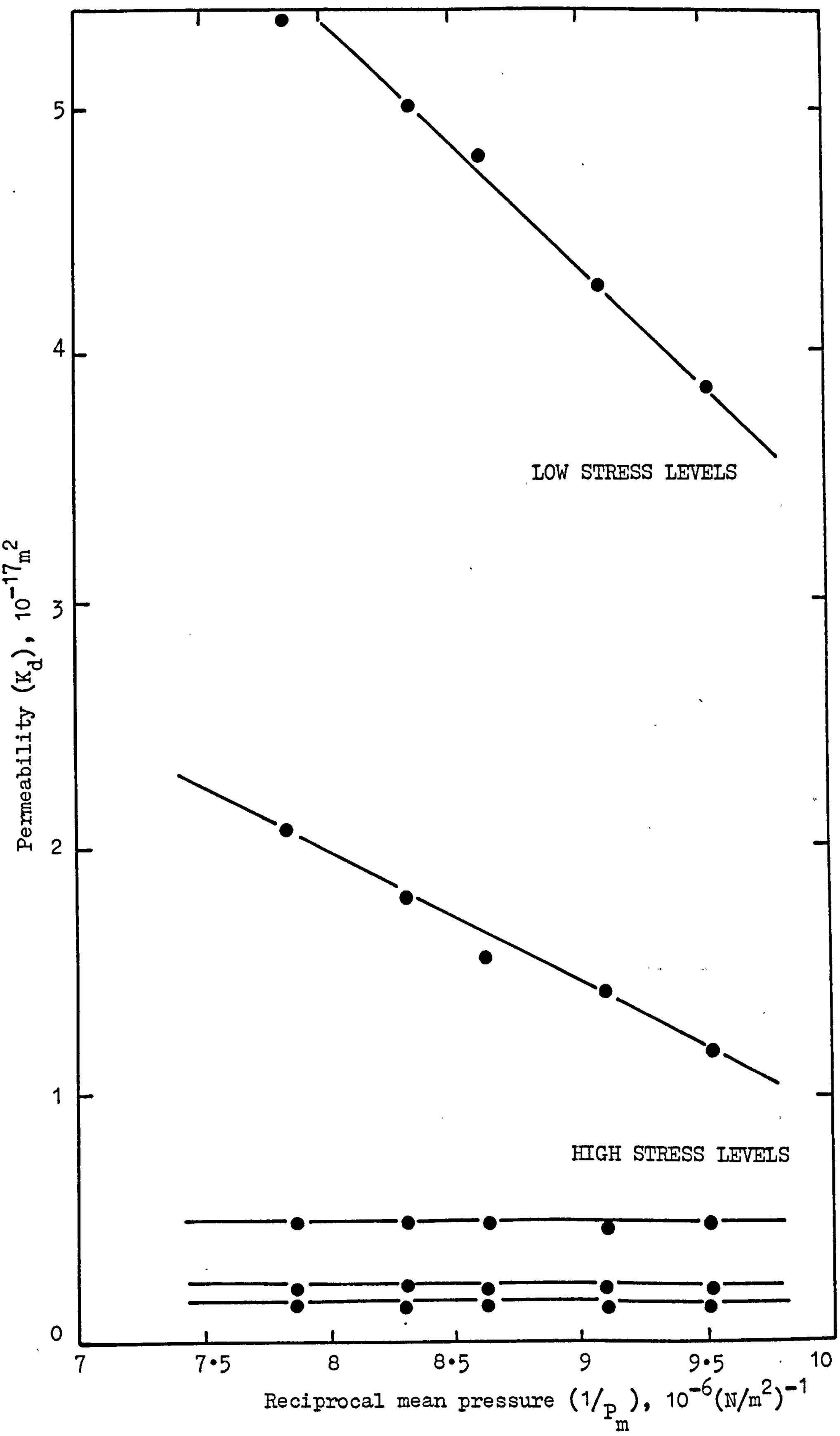

FIGURE (6.4.4) Variation of Permeability with Gas Pressure for Stressed Coal (After Gawuga (26)).

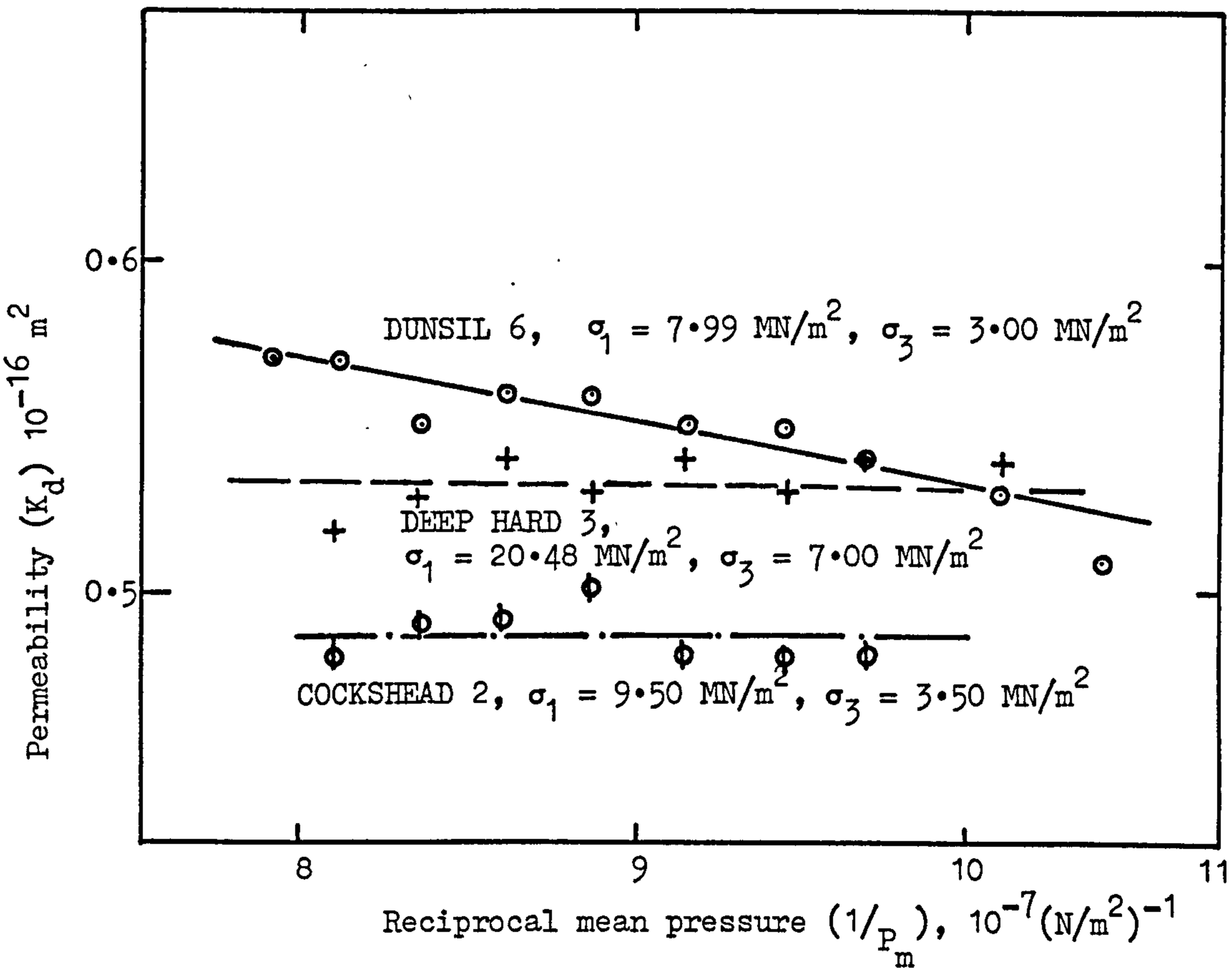

FIGURE (6.4.5) Variation of Permeability with Gas Pressure for Different Coals at Certain Stress Levels.

6.4.2 Computation of Results

Darcy's equation for the steady-state isothermal flow of compressible fluids through porous media:

$$Q_2 = \frac{K_d A}{\mu} \frac{\Delta P}{\Delta L} \frac{\bar{P}}{P_2} \qquad \ldots\ldots\ldots \quad 6.4.1$$

where

K_d permeability of the specimen

Q_2 volume flow rate at the downstream end of the specimen

μ viscosity of the flowing fluid, N_2

ΔL length of the specimen

P_2 gas pressure at downstream end where Q_2 is measured

A cross-sectional area of the specimen

ΔP differential pressure across the specimen

$\bar{P}$ mean gas pressure along the specimen

was used in calculating the permeabilities of the test specimens under stress, Figure (6.4.6).

Rewriting the equation 6.4.1 for permeability and adopting the SI system of units we get:

$$K_d = \frac{Q_2 \times \mu \times \Delta L \times P_2}{A \times \Delta P \times \bar{P}}$$

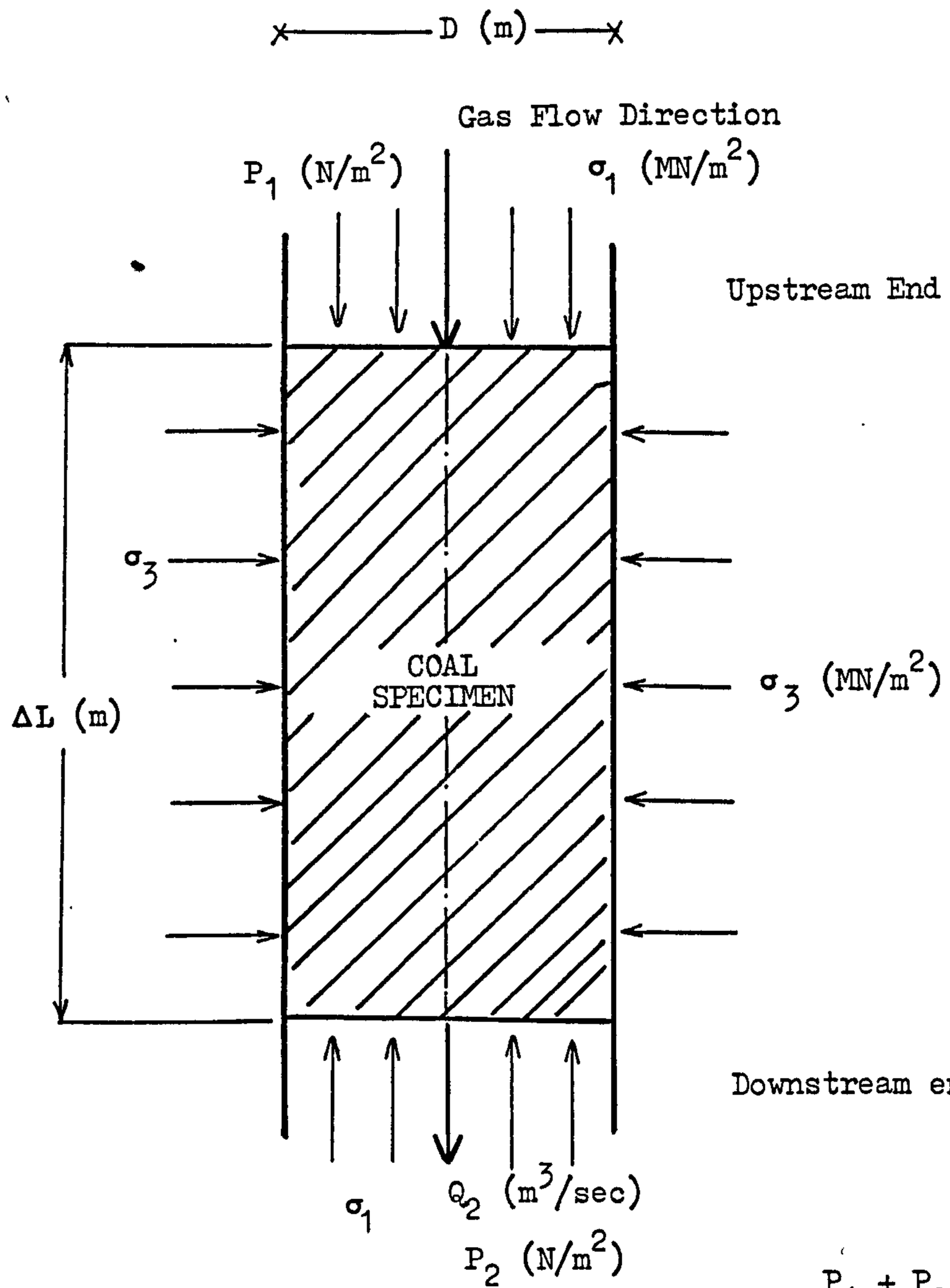

$P_1 > P_2$

$\Delta P = P_1 - P_2$

$$\bar{P} = \frac{P_1 + P_2}{2}$$

FIGURE (6.4.6) Parameters Used for Calculating the Permeability of Coal Specimens Under Triaxial Stress.

$$= \frac{\left[\frac{m^3}{s}\right]\cdot\left[\frac{Ns}{m^2}\right]\cdot\left[m\right]\cdot\left[\frac{N}{m^2}\right]}{\left[m^2\right]\cdot\left[\frac{N}{m^2}\right]\cdot\left[\frac{N}{m^2}\right]}$$

$$= \left[m^2\right]$$

Therefore the unit of permeability in the SI system of measurement is m^2 . This will be used as the unit of permeability (K_d) throughout this research. Another unit adopted for permeability, used particularly by the petroleum industry, is 'darcy' (3), where:

$$1 \text{ darcy} = 9{\cdot}87 \times 10^{-13} \ m^2$$

A computer program has been written to determine the permeabilities of coal specimens straight from the experimental readings where the inputs are in the form of:

- Radial stress (σ_3), Bar
- Axial load (F_1), KN
- Differential pressure across the specimen (ΔP), psi
- Volume flow rate of gas (Q_2), cc/min
- Length of the specimen (L), cm
- Diameter of the specimen (D), cm
- Viscosity of Nitrogen (μ), Ns/m^2 (72).

The program converts all the readings into the SI units and then calculates the desired variables.

The output is in the form of:

- Volume flow rate of gas (Q_2), m^3/s.
- Axial stress (σ_1), MN/m^2.
- Radial stress (σ_3), MN/m^2.
- Differential pressure across the specimen (ΔP), N/m^2.
- Permeability (K_d), m^2.

Stresses and the corresponding permeabilities of the specimen were then plotted on graphs and examined for stress-permeability relationship.

Appendix II presents an example of:

(i) A set of data obtained from one of the laboratory stress-permeability experiments.

(ii) An example calculation of permeability (K_d) from the laboratory data.

(iii) Computer output for the calculated permeabilities using the given data in (i).

CHAPTER SEVEN

PRESENTATION AND DISCUSSION OF EXPERIMENTAL RESULTS

CHAPTER SEVEN

PRESENTATION AND DISCUSSION OF EXPERIMENTAL RESULTS

7.1 Mechanical and Structural Properties of Coals Tested

Seven coals from different areas and coal seams were tested throughout this research; they are the two medium volatile bituminous coals ACILIK and CAYDAMAR and the five high volatile bituminous coals BARNSLEY, COCKSHEAD, BANBURY, DUNSIL and DEEP HARD. Tables (7.1.1) to (7.1.3) describe some structural and mechanical properties of the coals used. Plate (7.1) shows a test specimen from each coal.

Stress-strain curves obtained from the uniaxial compressive strength tests are illustrated in Figures (7.1.1) to (7.1.7).

7.2 Effects of Stress and Stress-History on the Internal Structure and Permeability of Different Coals

As discussed in the previous chapter, a detailed study of stress-history effect on coal permeability was decided upon as the most fruitful approach in establishing a reliable stress-permeability relationship for coals. Factors effecting the stress-permeability properties of different rank coals were identified by cycles of loading/unloading/relaxing experiments on a large number of coal

TABLE (7•1•1) Description of Coals Used During Stress-Permeability Experiments

COAL	COLLIERY	VOLATILE MATTER (m.f.b.) %	FIXED CARBON (m.f.b.) %	ASH (m.f.b.) %	MOISTURE %	DESCRIPTION
ACILIK	KOZLU, ZONGULDAK TURKEY	23•31	68•74	7•95	0•60	Well defined cleavage and cleat, no apparent fractures.
CAYDAMAR	KOZLU, ZONGULDAK TURKEY	28•70	67•56	3•74	0•39	Well defined cleavage and cleat, no apparent fractures, bright.
BARNSLEY	YORKSHIRE MAIN DONCASTER	33•74	61•07	5•19	8•13	Highly fissured, dull.
COCKSHEAD	WOLSTANTON STOKE-ON-TRENT	34•62	62•65	2•73	1•42	Defined cleavage and cleat, partly fissured, bright.
BANBURY	WOLSTANTON STOKE-ON-TRENT	36•23	58•27	5•10	1•60	Well defined cleavage and cleat, partly fissured.
DUNSIL	FURNACE HILLOCK CHESTERFIELD (O.C.S.)	39•94	54•46	5•60	6•51	Highly fissured, dull.
DEEP HARD	COTGRAVE NOTTINGHAM	43•52	49•65	6•83	11•22	Some cleavage and cleat, partly fissured.

TABLE (7.1.2) Mechanical Properties of Coals Used

TYPE OF COAL	NUMBER OF SPECIMENS	UNIAXIAL COMPRESSIVE STRENGTH σ_{ult} (MN/m^2)	STANDARD DEVIATION (MN/m^2)	YOUNG'S MODULUS E ($10^2 MN/m^2$)	STANDARD DEVIATION ($10^2 MN/m^2$)
ACILIK	6	10•98	1•39	4•76	0•46
CAYDAMAR	7	8•18	0•40	2•90	0•10
BARNSLEY	6	18•21	1•35	4•00	0•50
COCKSHEAD	5	17•11	4•05	2•72	0•30
BANBURY	6	6•32	1•30	2•00	0•20
DUNSIL	6	29•81	9•76	3•64	0•20
DEEP HARD	5	24•74	3•11	3•81	0•40

TABLE (7.1.3) Effective Porosities of Specimens Tested for Stress-Permeability Relationship

COAL SPECIMEN	VOLATILE MATTER (m.f.b.) %	EFFECTIVE POROSITY ϕ_e	
		%	cc/gm of coal
ACILIK 5	23•31	12•36	0•09
ACILIK 7		13•79	0•11
CAYDAMAR 4	28•70	10•69	0•09
CAYDAMAR 5		10•06	0•08
BARNSLEY 3	33•74	15•04	0•13
BARNSLEY 6		14•83	0•12
COCKSHEAD 3	34•62	6•61	0•05
COCKSHEAD 4		6•71	0•05
BANBURY 2	36•23	8•67	0•07
BANBURY 5		8•24	0•06
DUNSIL 2	39•94	11•55	0•09
DUNSIL 4		14•03	0•11
DEEP HARD 2	43•52	10•73	0•08
DEEP HARD 4		11•21	0•09

ACILIK CAYDAMAR COCKSHEAD BANBURY BARNSLEY DUNSIL DEEP HARD

PLATE (7.1) A Test Specimen from Each Coal Used

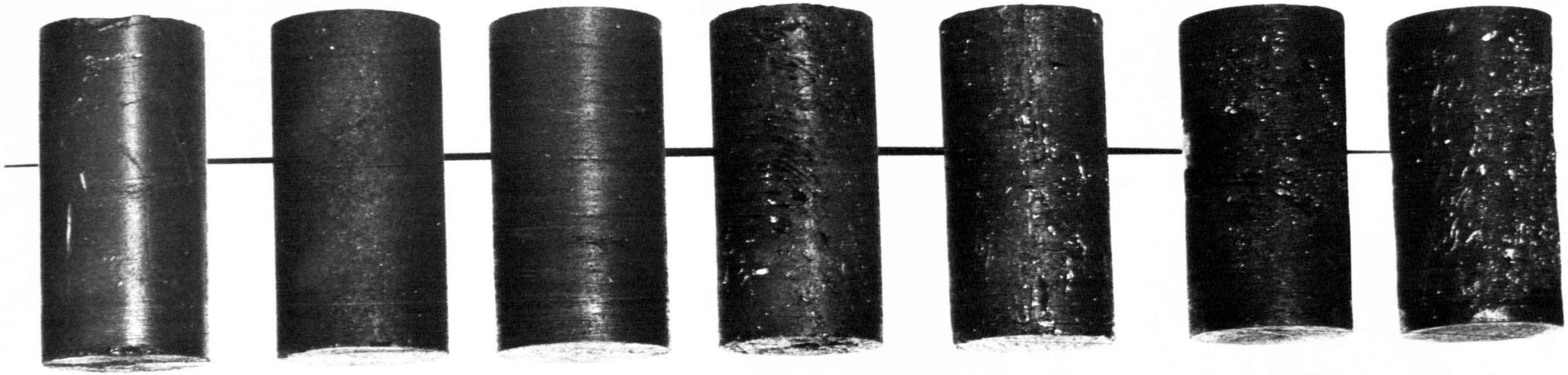

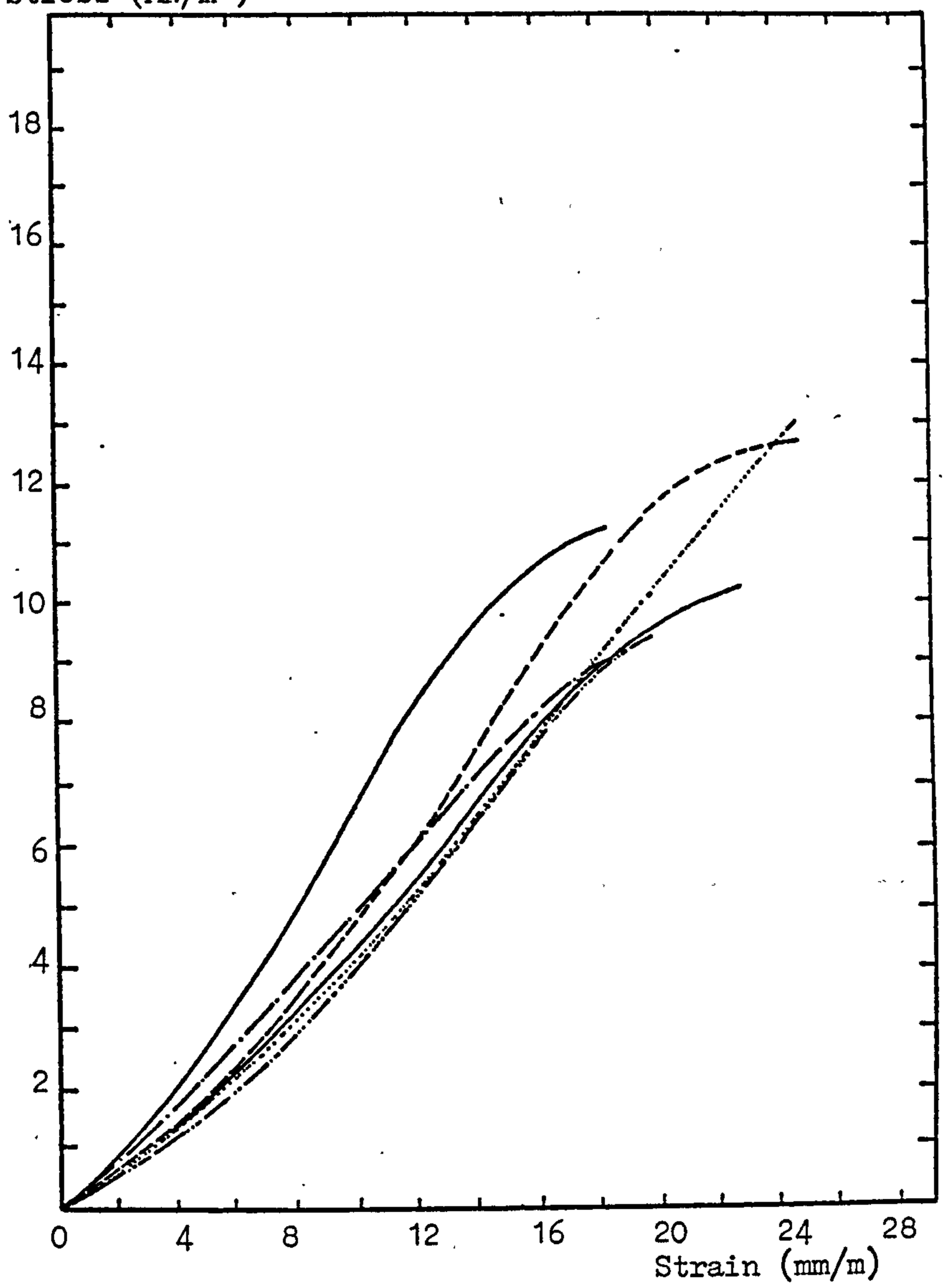

FIGURE (7.1.1) Stress-Strain Curves for ACILIK Coal.

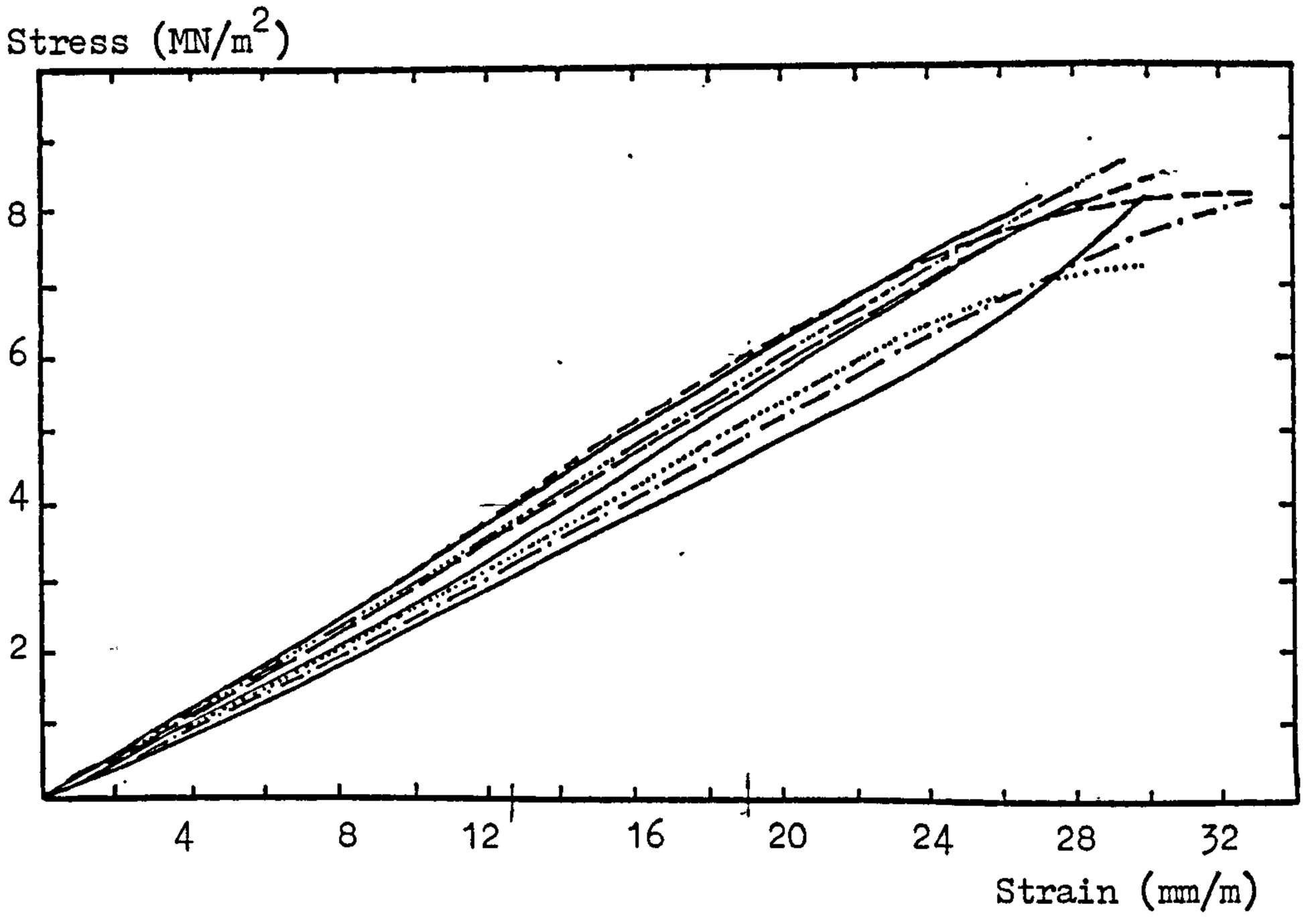

FIGURE (7.1.2) Stress-Strain Curves for CAYDAMAR Coal.

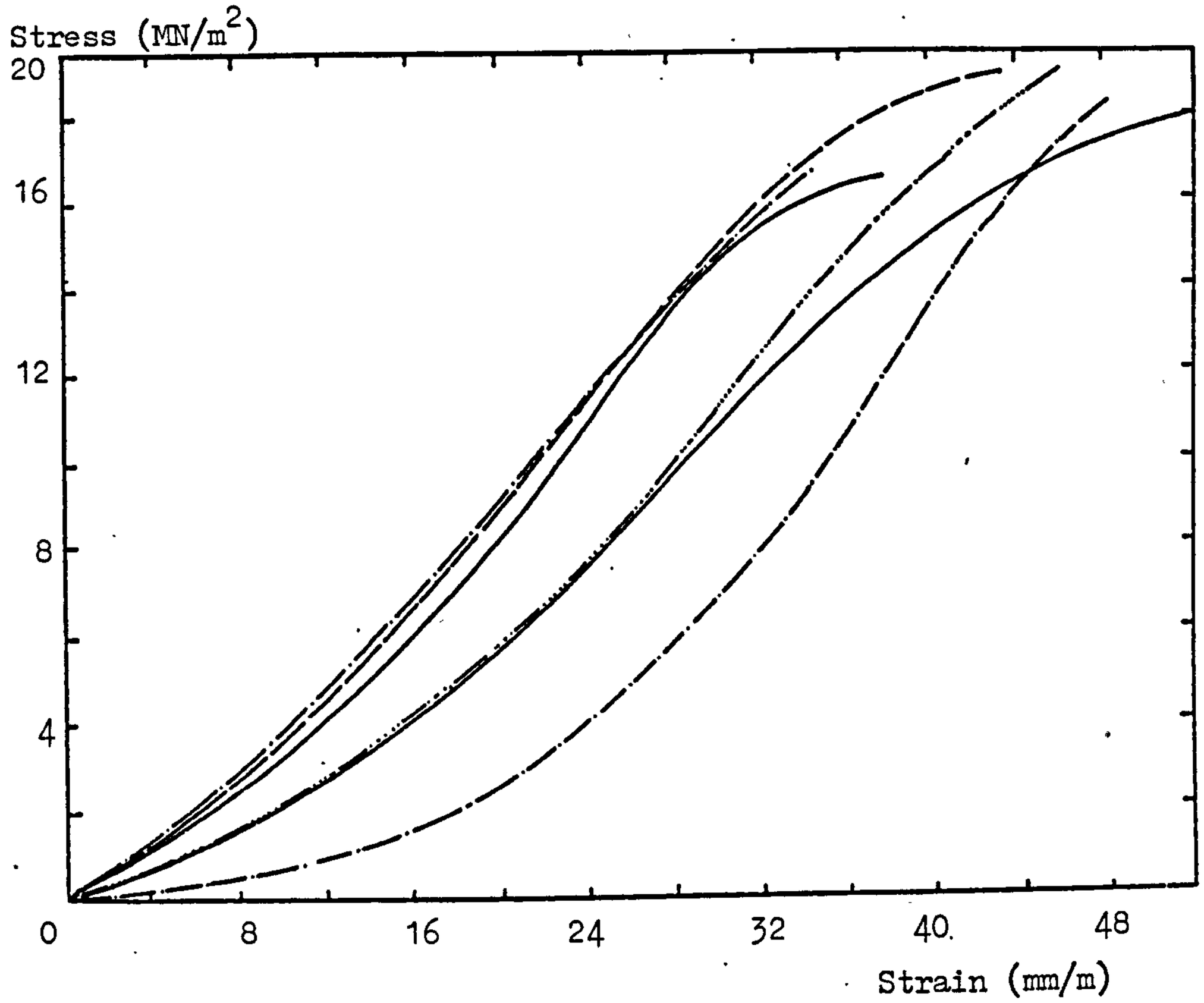

FIGURE (7.1.3) Stress-Strain Curves for BARNSLEY Coal.

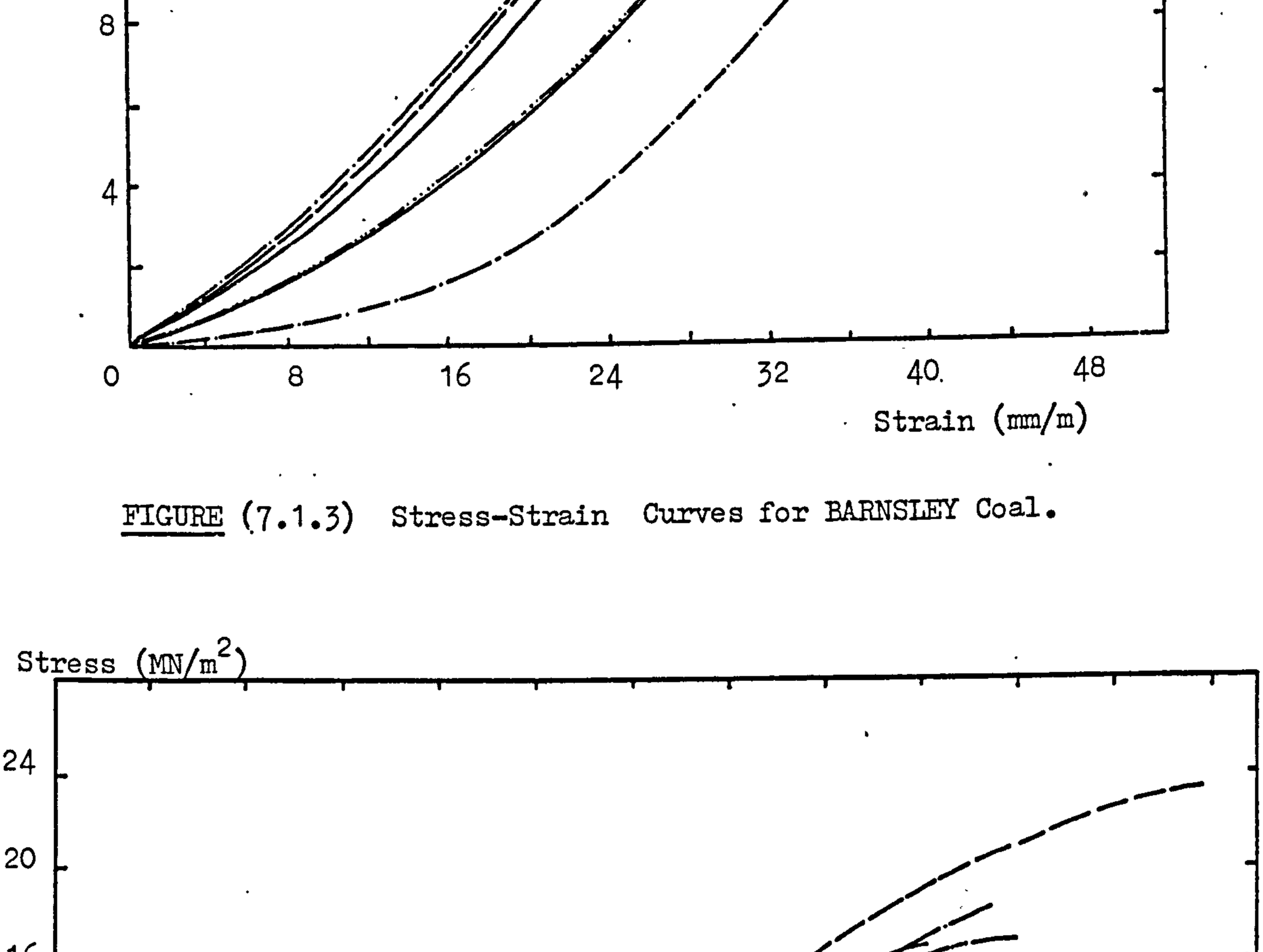

FIGURE (7.1.4) Stress-Strain Curves for COCKSHEAD Coal.

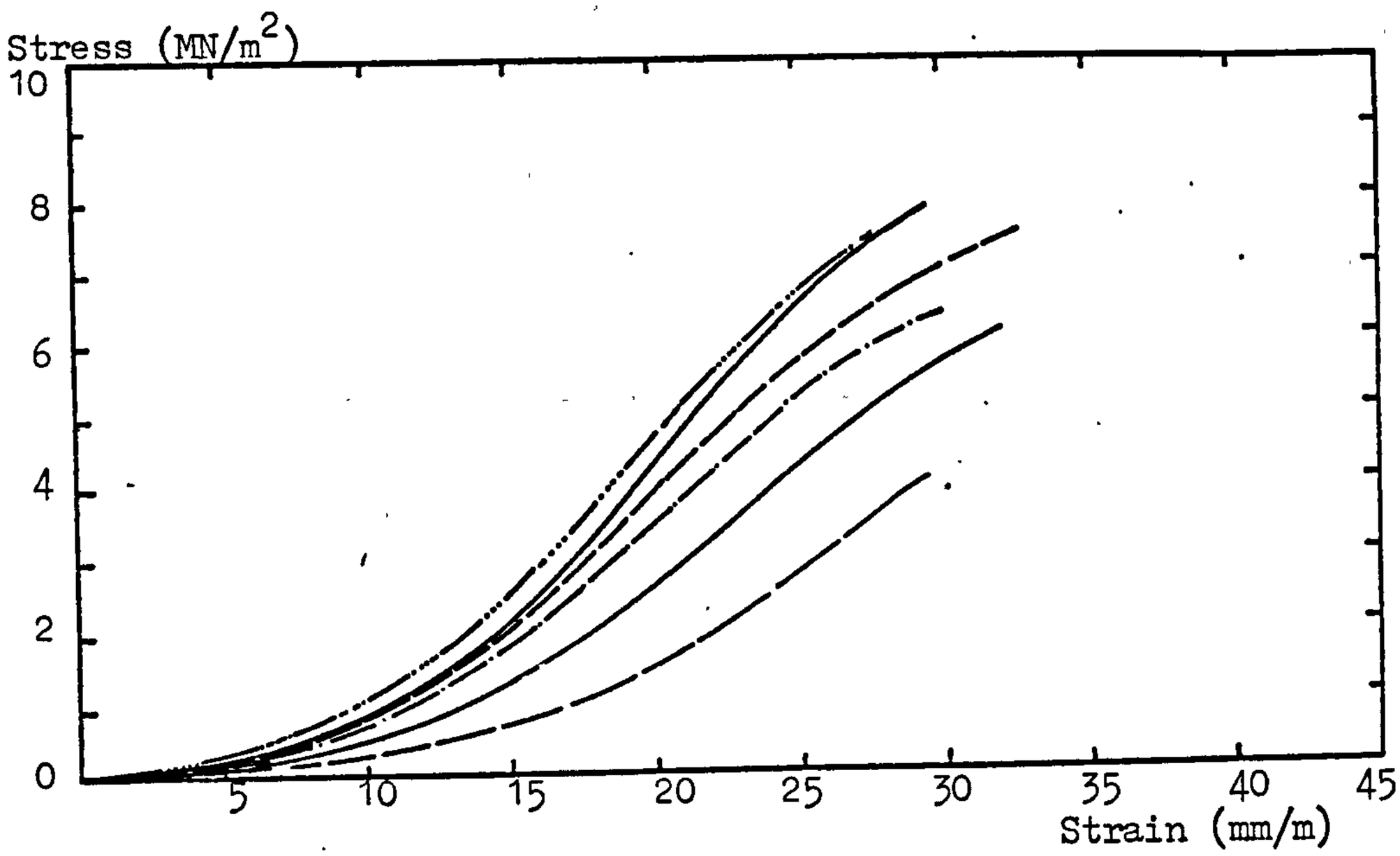

FIGURE (7.1.5) Stress-Strain Curves for BANBURY Coal.

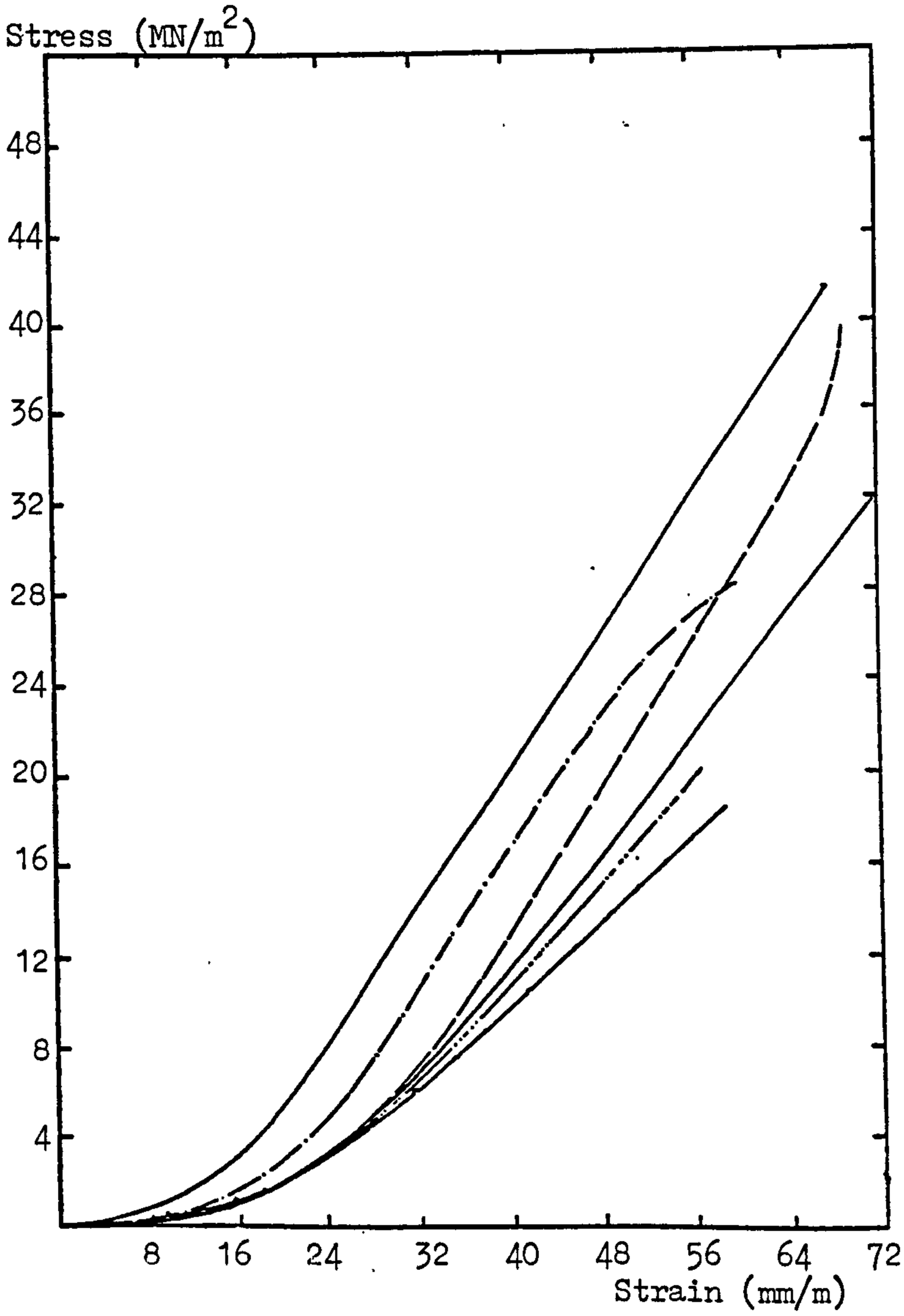

FIGURE (7.1.6) Stress-Strain Curves for DUNSIL Coal.

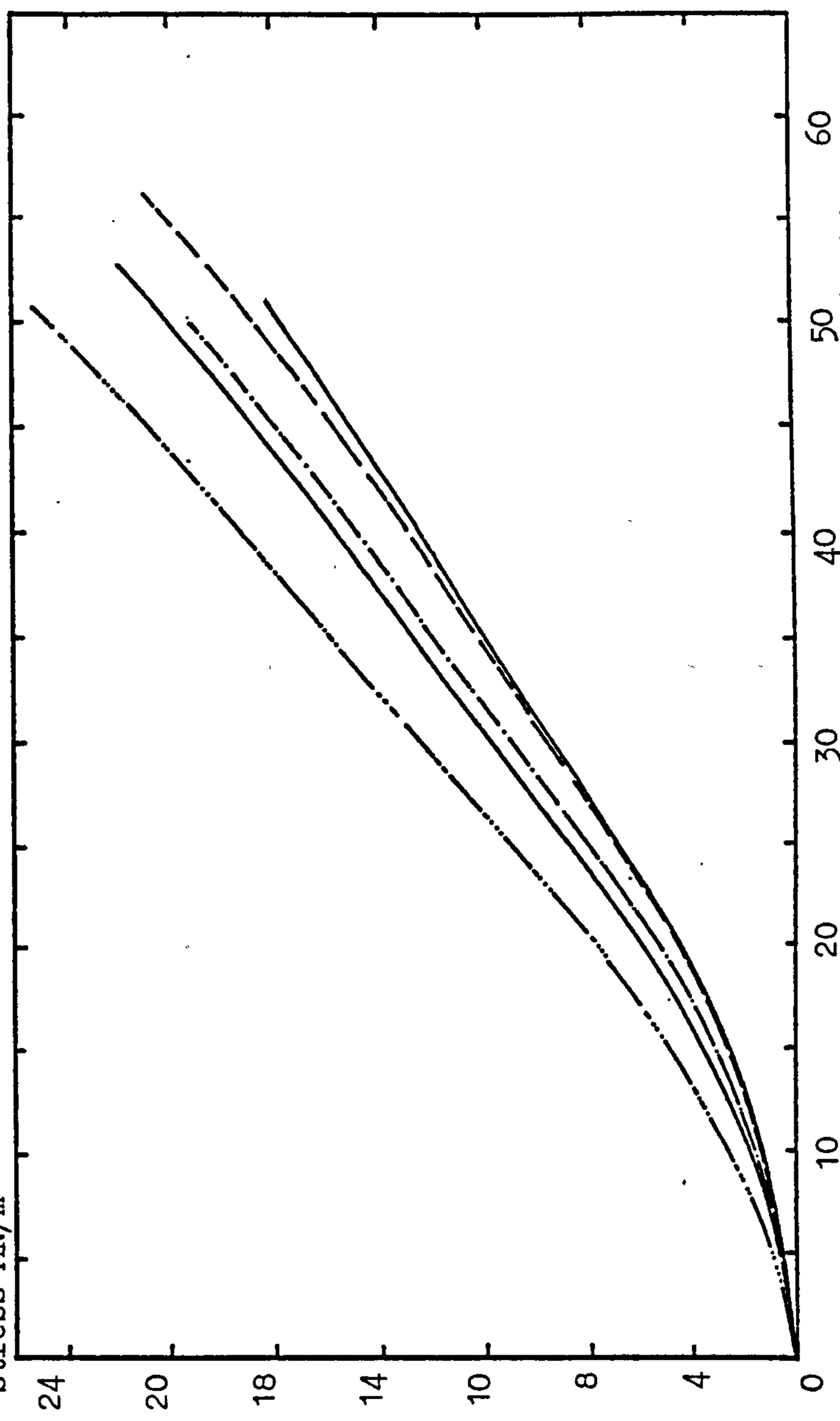

FIGURE (7.1.7) Stress-Strain Curves for DEEP HARD Coal.

specimens, taken from various coal seams. As will be discussed in further detail, the findings of these loading/unloading/reloading experiments also clarified the possible changes, both, in structure and, permeability, of coal seams in the front abutment zone of a coal face.

Although it was never possible to obtain identical stress-permeability curves for coals of the same origin, a high consistency in stress-permeability behaviour was achieved for specimens of the same kind. In the following pages, the stress-permeability curves, representing the general behaviour of each type of coal used, will be presented. These curves will form the basis of a discussion on the effects of stress-history on permeability of different coals.

Each specimen was subjected to a series of repeated loading/unloading/relaxing experiments under the same stress conditions. Experimental results are illustrated on graphs where Permeability (K_d) is plotted against the Radial Stress (σ_3). The ratio of Axial Stress to Radial Stress (σ_1/σ_3) varied between 1/2·66 and 1/2·75 in relation to the diameter of the test specimens used. This ratio is given on the top right hand corner of each graph. For clarity in presentation and to aid interpretation of the experimental results, permeabilities are shown on logarithmic scale. The direction of stressing is indicated by the arrows on stress permeability curves.

Accompanying each graph is a table of experimental results in which the name, the diameter and the length of the specimen are

shown on the top section. Radial and Axial Stresses for each loading/unloading cycle are given in the first two columns respectively. Subsequent columns present the permeabilities for each consecutive run on given dates.

The permeability of coal in general was found to be stress dependent, decreasing as the level of stress was increased. As can be seen in Figures (7.2.1) to (7.2.14), different coals showed different rates of reduction in permeability when subjected to the same level of stress.

When a coal specimen was loaded and unloaded two main patterns of structural changes were observed; these changes were dependent on the mechanical strength and the degree of propogation of existing hairline fractures under stress. Coals with a high degree of elasticity and no apparent fractures usually remained structurally unaffected after a series of loading/unloading cycles. On the other hand, highly fissured and/or low mechanical strength friable coals usually microfractured under the stress conditions created in the laboratory. Therefore, the change in permeability of a coal specimen was either caused by compression only or by the combined result of both compression and microfracturing of the coal material. These features will be discussed in more detail in relation to examples of typical stress-permeability behaviour curves for each type of coal used.

TABLE (7.2.1) Stress-Permeability Results for ACILIK 5 Specimen (Effect of Stress-History)

SAMPLE : ACILIK 5		D = 37•30 mm	L = 73•85 mm
	RADIAL STRESS σ_3 (MN/m^2)	AXIAL STRESS σ_1 (MN/m^2)	1st RUN/23.10.1980 PERMEABILITY K_d (10^{-16} m^2)	2nd RUN/3.11.1980 PERMEABILITY K_d (10^{-16} m^2)
LOADING	0•00	0•00	734•23	723•27
	0•50	1•37	13•34	13•06
	1•00	2•74	9•01	7•24
	1•50	4•11	6•14	4•38
	2•00	5•49	4•39	3•31
	2•50	6•86	3•37	2•53
	3•00	8•23	2•60	2•06
	3•50	9•60	2•10	1•71
	4•00	10•98	1•76	1•40
	4•50	12•35	1•48	1•21
	5•00	13•72	1•20	1•01
	5•50	15•10	1•01	0•86
	6•00	16•47	0•86	0•76
	6•50	17•83	0•73	0•67
	7•00	19•21	0•63	0•59
	7•50	20•59	0•54	0•52
UNLOADING	7•00	19•21	0•57	0•54
	6•50	17•83	0•62	0•58
	6•00	16•47	0•63	0•62
	5•50	15•10	0•67	0•64
	5•00	13•72	0•71	0•70
	4•50	12•35	0•86	0•79
	4•00	10•98	0•92	0•86
	3•50	9•60	1•06	1•04
	3•00	8•23	1•32	1•30
	2•50	6•86	1•83	1•59
	2•00	5•49	2•20	2•52
	1•50	4•11	3•13	3•17
	1•00	2•74	4•89	10•84
	0•50	1•37	8•60	15•43
	0•00	0•00	752•42	679•44

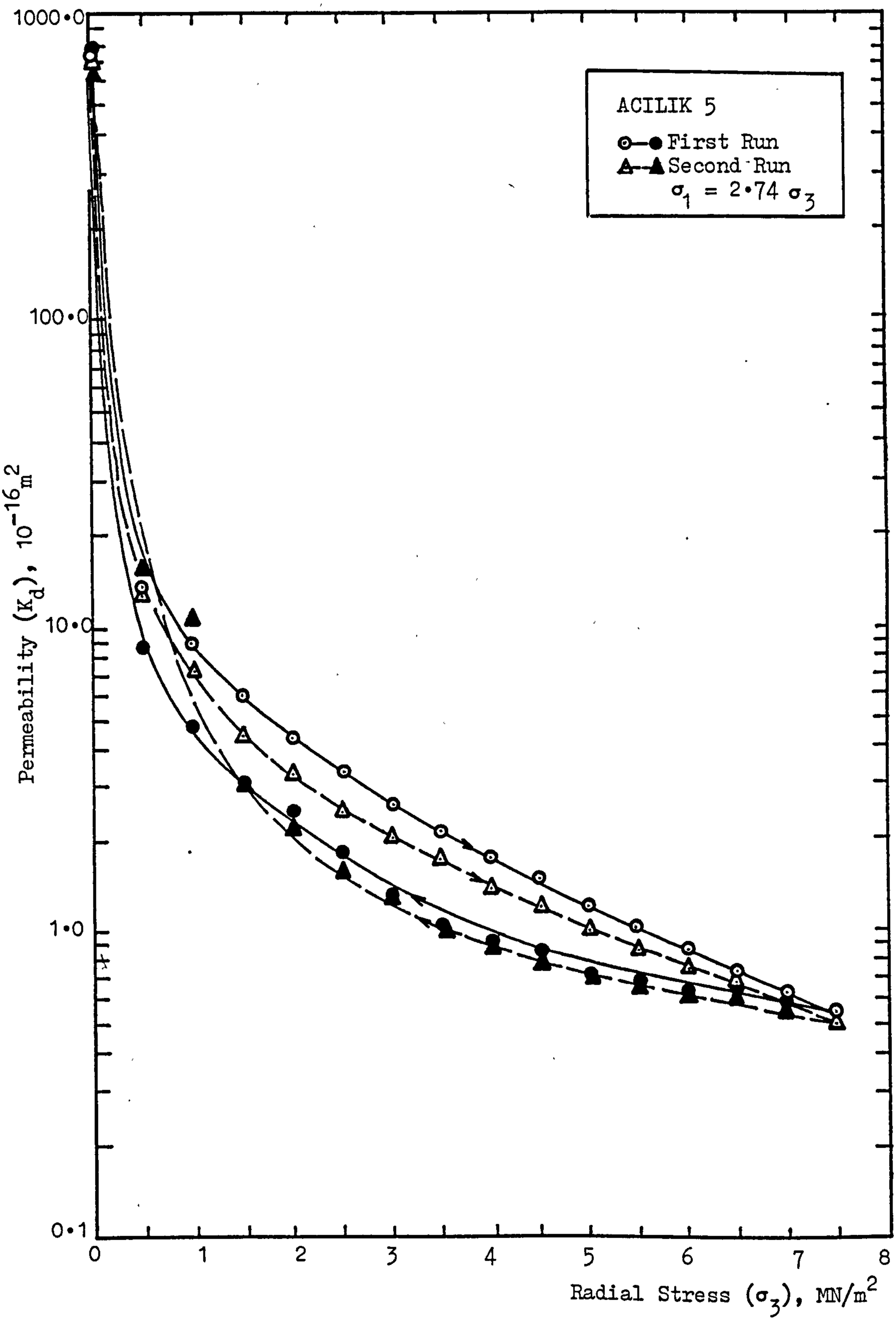

FIGURE (7.2.1) Effect of Stress-History on Permeability of ACILIK Coal

7.2.1 The Effect of Stress and Stress-History on Permeability of Non-Microfractured Coals.

Figures (7.2.1) to (7.2.6) illustrate the comparable stress-permeability curves obtained for the first and second loading/unloading experiments conducted on ACILIK, CAYDAMAR, DEEP HARD and DUNSIL specimens. In order to establish a better understanding of the stress-permeability behaviour of non-microfractured coal, the experimental procedure and the structural changes undergone by one of these specimens, ACILIK 5, will be discussed.

As shown in Figure (7.2.1), the permeability of ACILIK 5 specimen decreased under stress, first sharply, then gently, reaching a minimum at $\sigma_3 = 7{\cdot}50$ MN/m^2. At this level, the permeability of the specimen was found to be 1360 times lower than the base permeability. The specimen was then unloaded following the same stress path as in loading. This time the unloading stress-permeability curve followed a different path representing lower permeability values as compared to the loading curve.

After ten days of relaxation, ACILIK 5 was loaded and unloaded for the second time under the same stress conditions and the effects of the previous experiment, as well as of the relaxation, were observed. As can be seen in Figure (7.2.1), the second loading/unloading curve exhibits a similar stress-permeability relationship to that of the first. The significance of the second loading was that the time dependent recovery of permeability due to relaxation was clearly indicated by the placing of the

TABLE (7.2.2) Stress-Permeability Results for ACILIK 3 Specimen (Effect of Stress-History)

SAMPLE : ACILIK 3		D = 37•30 mm	L = 73•60 mm
	RADIAL STRESS σ_3 (MN/m^2)	AXIAL STRESS σ_1 (MN/m^2)	1st RUN/5.2.1980 PERMEABILITY K_d (10^{-16} m^2)	2nd RUN/11.2.1980 PERMEABILITY K_d (10^{-16} m^2)
LOADING	0•00	0•00	-	-
	0•50	1•37	21•33	37•50
	1•00	2•74	11•43	9•25
	1•50	4•11	8•19	5•71
	2•00	5•49	5•69	4•04
	2•50	6•86	4•47	3•72
	3•00	8•23	3•25	2•40
	3•50	9•62	2•48	1•98
	4•00	10•98	2•08	1•61
	4•50	12•35	1•78	1•37
	5•00	13•72	1•42	1•19
	5•50	15•10	1•17	0•98
	6•00	16•47	1•05	1•02
	6•50	17•84	0•88	0•74
	7•00	19•21	0•91	0•66
	7•50	20•59	0•77	0•61
UNLOADING	7•00	19•21	0•64	0•49
	6•50	17•84	0•67	0•48
	6•00	16•47	0•65	0•53
	5•50	15•10	0•71	0•53
	5•00	13•72	0•74	0•72
	4•50	12•35	0•83	0•79
	4•00	10•98	0•98	0•86
	3•50	9•62	1•15	1•01
	3•00	8•23	1•46	1•28
	2•50	6•86	1•81	1•73
	2•00	5•49	2•72	2•25
	1•50	4•11	4•33	3•74
	1•00	2•74	9•32	10•43
	0•50	1•37	24•36	38•11
	0•00	0•00	-	-

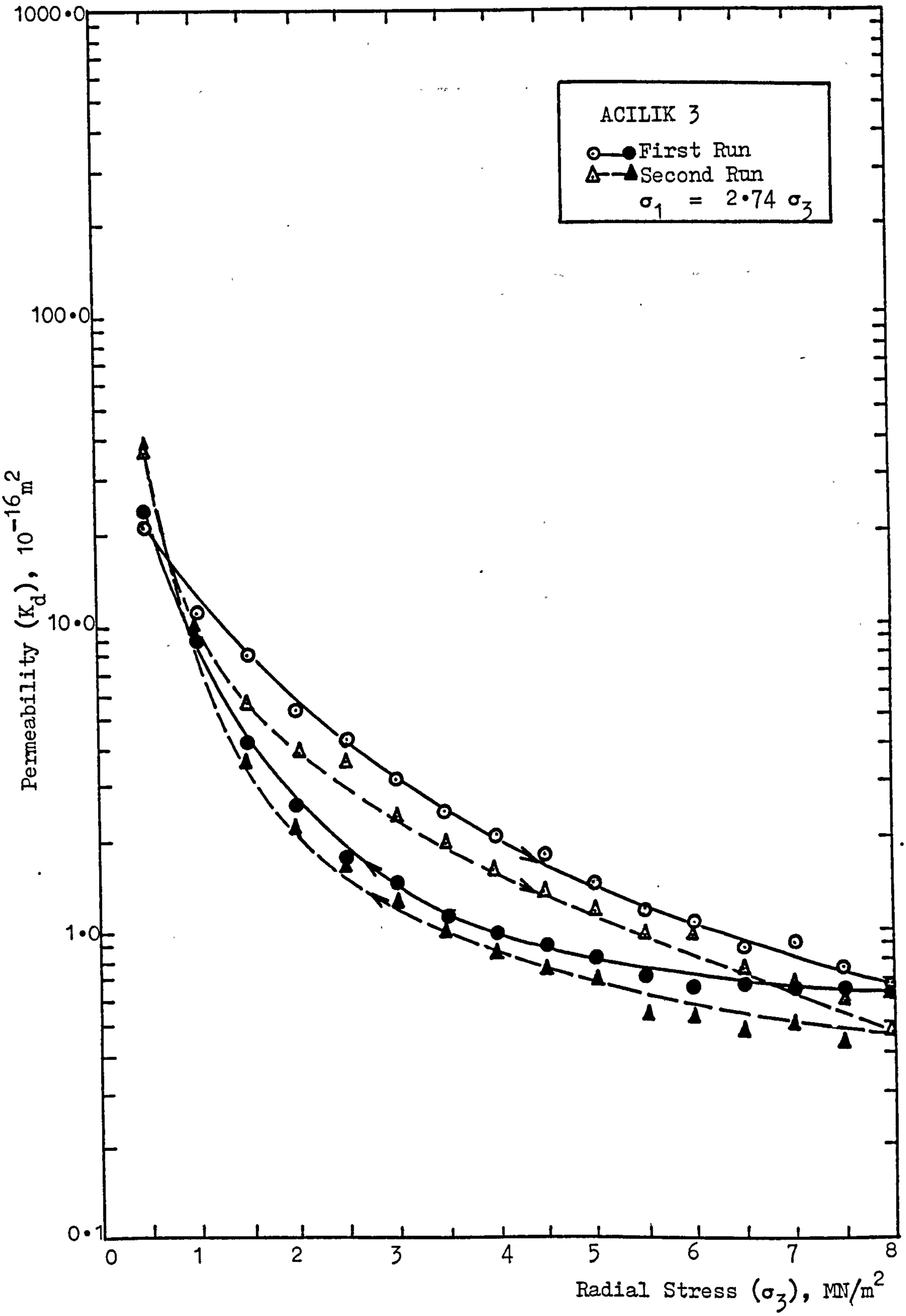

FIGURE (7.2.2) Effect of Stress-History on Permeability of ACILIK Coal.

TABLE (7.2.3) Stress-Permeability Results for CAYDAMAR 6 Specimen (Effect of Stress-History)

SAMPLE : CAYDAMAR 6		D = 37•25 mm	L = 72•50 mm
	RADIAL STRESS σ_3 (MN/m^2)	AXIAL STRESS σ_1 (MN/m^2)	1^{st} RUN/1.12.80 PERMEABILITY K_d (10^{-16} m^2)	2^{nd} RUN/8.12.80 PERMEABILITY K_d (10^{-16} m^2)
LOADING	0•00	0•00	181•71	84•21
	0•50	1•37	20•86	19•08
	1•00	2•75	17•27	11•54
	1•50	4•12	11•38	8•45
	2•00	5•50	8•31	5•62
	2•50	6•88	5•32	4•12
	3•00	8•25	3•81	3•20
	3•50	9•63	2•94	2•38
	4•00	11•01	2•21	1•80
	4•50	12•83	1•69	1•44
	5•00	13•76	1•38	1•12
	5•50	15•14	1•12	0•94
	6•00	16•51	0•90	0•80
	6•50	17•89	0•72	0•67
	7•00	19•27	0•63	0•53
	7•50	20•64	0•51	0•47
	7•00	19•27	0•56	0•50
	6•50	17•89	0•67	0•54
	6•00	16•51	0•75	0•62
	5•50	15•14	0•86	0•70
	5•00	13•76	1•00	0•81
	4•50	12•83	1•21	0•92
UNLOADING	4•00	11•01	1•50	1•06
	3•50	9•63	2•12	1•36
	3•00	8•25	2•41	1•62
	2•50	6•88	3•26	2•15
	2•00	5•50	4•98	2•76
	1•50	4•12	6•68	4•00
	1•00	2•75	9•34	7•03
	0•50	1•37	24•21	14•52
	0•00	0•00	150•54	77•15

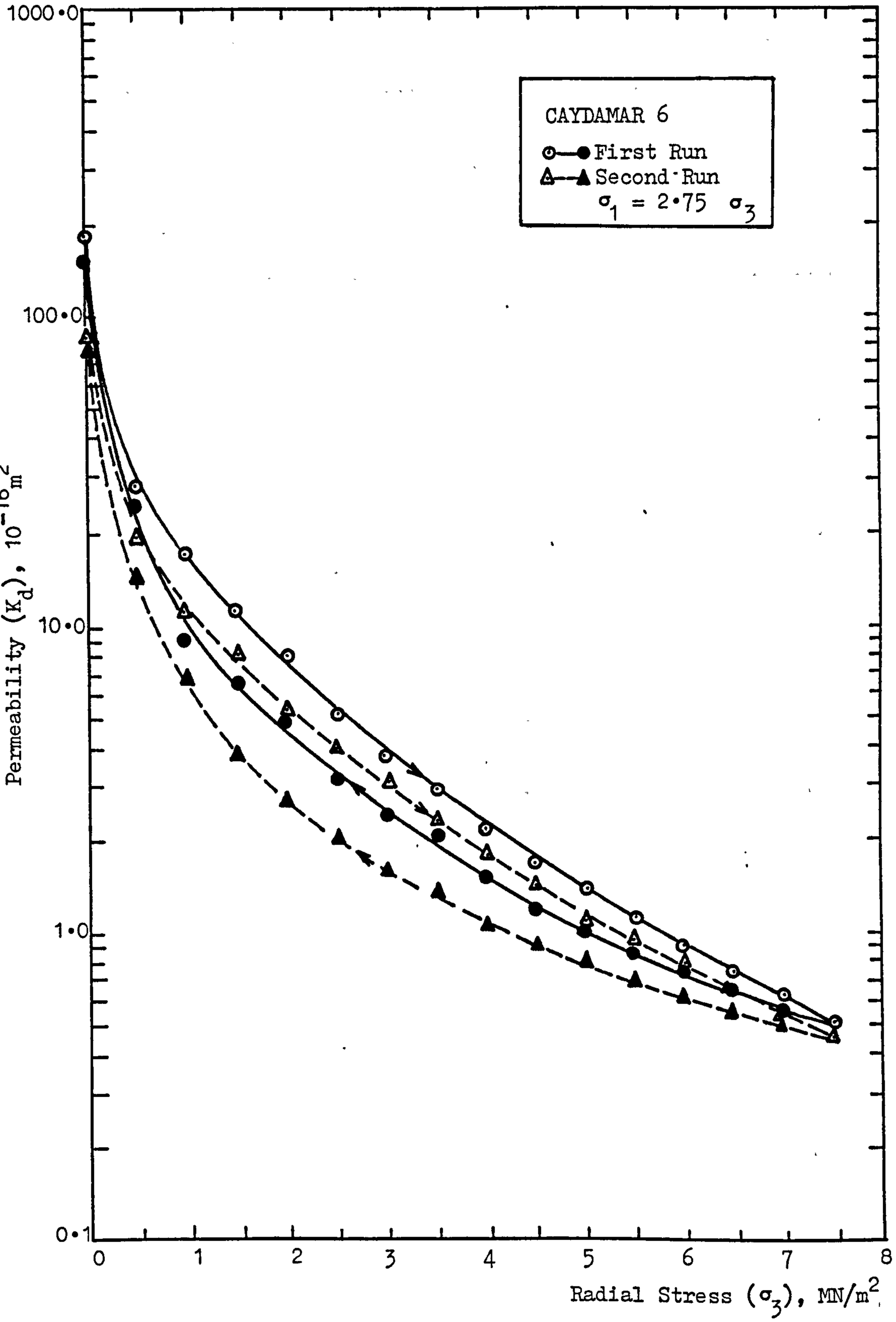

FIGURE (7.2.3) Effect of Stress-History on Permeability of CAYDAMAR Coal.

TABLE (7.2.4) Stress-Permeability Results for DEEP HARD 3 Specimen (Effect of Stress-History)

SAMPLE : DEEP HARD 3		D = 37·40 mm	L = 73·90 mm
	RADIAL STRESS σ_3 (MN/m^2)	AXIAL STRESS σ_1 (MN/m^2)	1st RUN/3.4.1981 PERMEABILITY K_d (10^{-16} m^2)	2nd RUN/10.4.1981 PERMEABILITY K_d (10^{-16} m^2)
LOADING	0·00	0·00	858·05	192·41
	0·50	1·36	43·22	40·63
	1·00	2·73	31·58	23·49
	1·50	4·09	19·82	14·81
	2·00	5·46	13·92	10·07
	2·50	6·82	8·69	6·19
	3·00	8·19	5·99	4·53
	3·50	9·55	4·11	2·83
	4·00	10·92	2·91	2·18
	4·50	12·28	2·10	1·61
	5·00	13·65	1·53	1·26
	5·50	15·10	1·15	0·98
	6·00	16·38	0·89	0·69
	6·50	17·75	0·68	0·59
	7·00	19·11	0·54	0·51
	7·50	-	-	-
	7·00	-	-	-
UNLOADING	6·50	17·75	0·57	0·54
	6·00	16·38	0·70	0·64
	5·50	15·10	0·87	0·76
	5·00	13·65	1·02	1·02
	4·50	12·28	1·35	1·39
	4·00	10·92	1·66	1·73
	3·50	9·55	2·59	2·26
	3·00	8·19	4·47	3·51
	2·50	6·82	5·71	5·62
	2·00	5·46	9·35	7·38
	1·50	4·09	16·24	10·28
	1·00	2·73	23·71	17·52
	0·50	1·36	38·35	25·59
	0·00	0·00	770·72	241·25

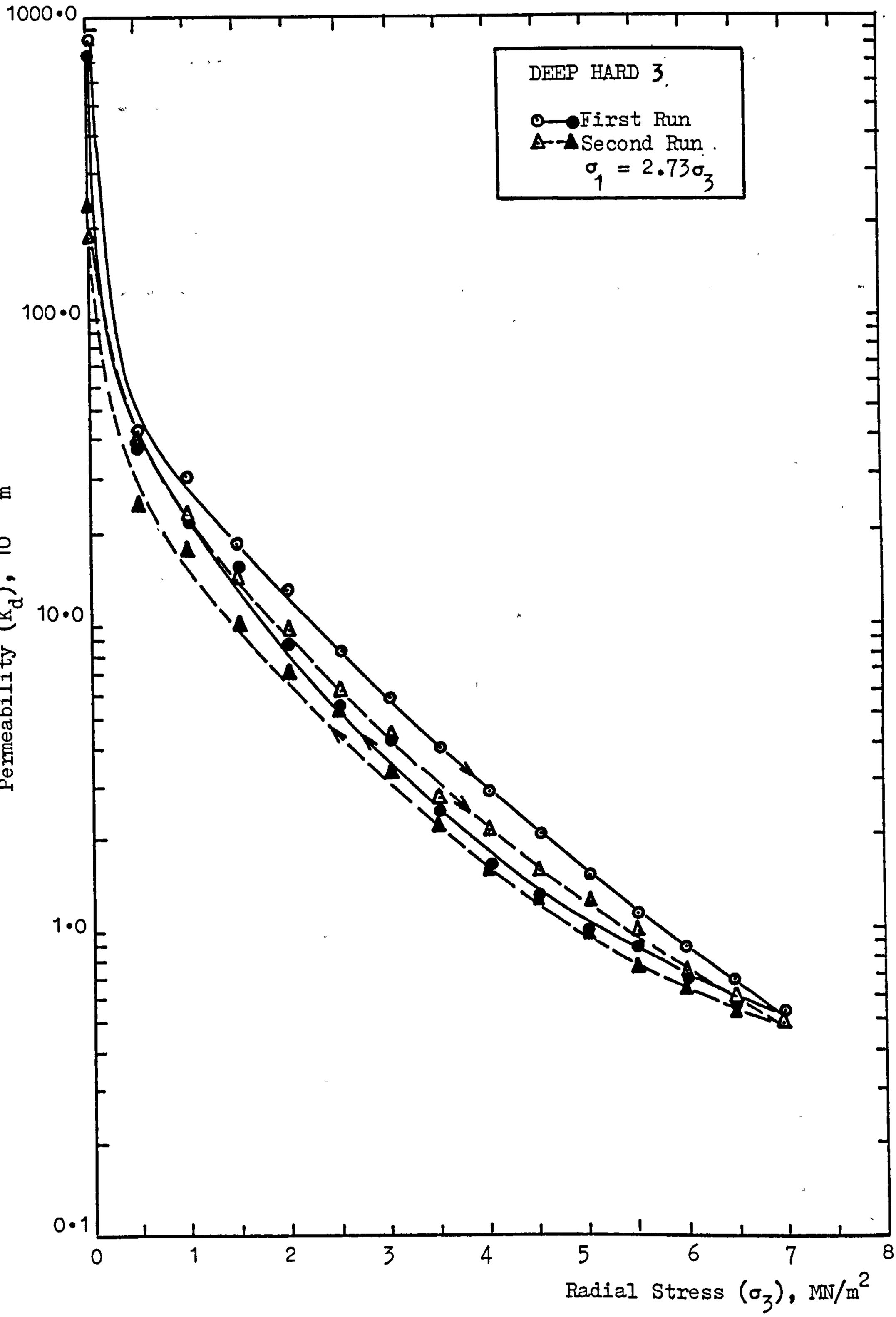

FIGURE (7.2.4) Effect of Stress-History on Permeability of DEEP HARD Coal.

TABLE (7.2.5) Stress-Permeability Results for DEEP HARD 5 Specimen (Effect of Stress-History)

SAMPLE : DEEP HARD 5		D = 37·45 mm	L = 74·90 mm
	RADIAL STRESS σ_3 (MN/m^2)	AXIAL STRESS σ_1 (MN/m^2)	1st RUN/7.4.1981 PERMEABILITY K_d (10^{-16} m^2)	2nd RUN/15.4.1981 PERMEABILITY K_d (10^{-16} m^2)
LOADING	0·00	0·00	757·02	256·70
	0·50	1·36	39·45	28·41
	1·00	2·72	22·90	13·90
	1·50	4·08	12·39	8·40
	2·00	5·44	8·40	5·19
	2·50	6·80	5·54	3·26
	3·00	8·17	3·59	2·29
	3·50	9·53	2·43	1·66
	4·00	10·89	1·63	1·30
	4·50	12·25	1·20	1·00
	5·00	13·61	0·87	0·78
	5·50	14·97	0·71	0·60
	6·00	16·34	0·55	0·48
	6·50	17·70	0·39	0·40
	7·00	19·06	0·32	0·34
	7·50	-	-	-
	7·00	-	-	-
UNLOADING	6·50	17·70	0·39	0·37
	6·00	16·34	0·47	0·42
	5·50	14·97	0·54	0·47
	5·00	13·61	0·68	0·61
	4·50	12·25	0·81	0·80
	4·00	10·89	1·16	0·99
	3·50	9·53	1·53	1·30
	3·00	8·17	2·32	1·69
	2·50	6·80	3·46	3·16
	2·00	5·44	5·09	4·82
	1·50	4·08	9·74	6·64
	1·00	2·72	16·41	12·06
	0·50	1·36	32·40	18·47
	0·00	0·00	482·84	495·60

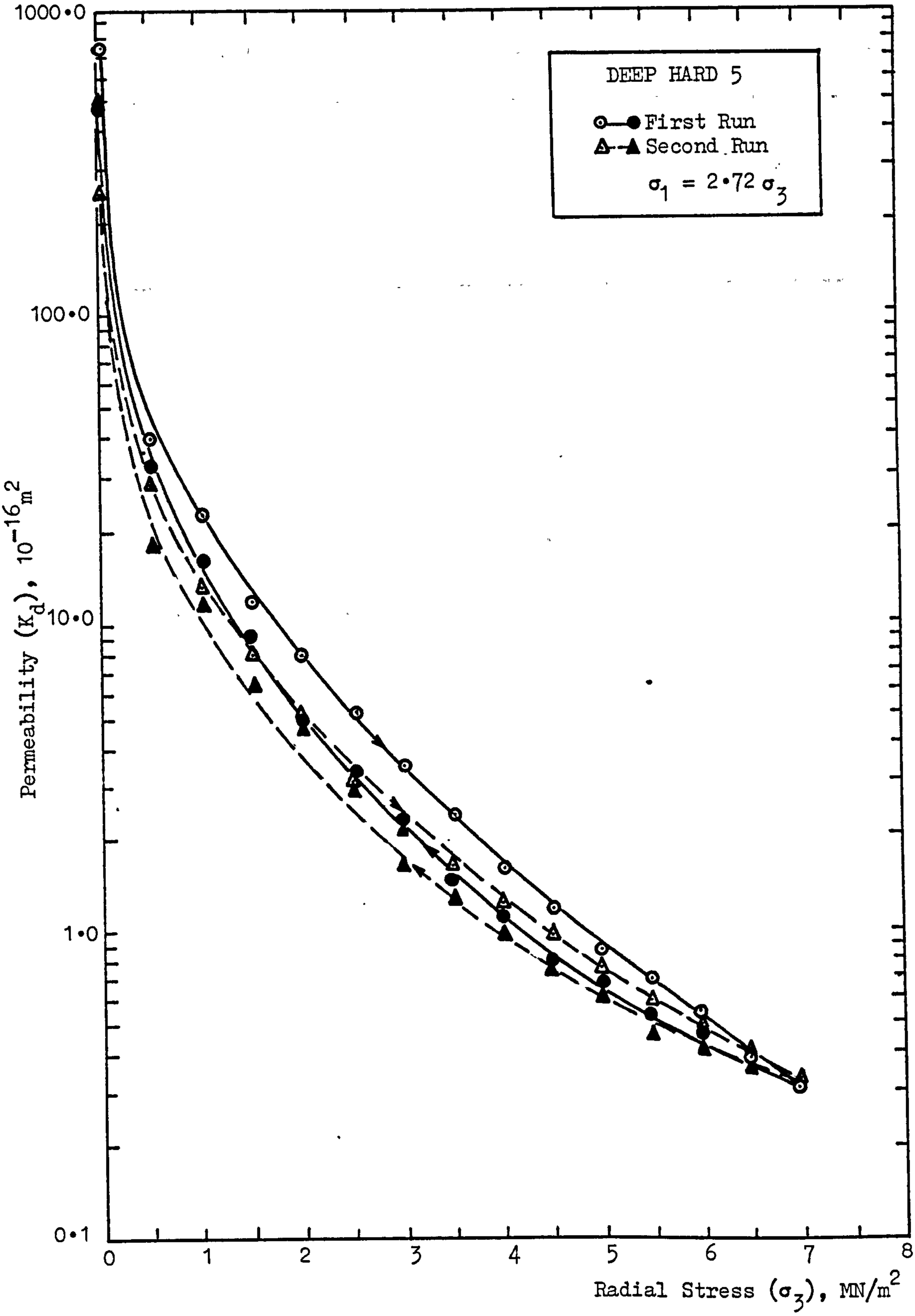

FIGURE (7.2.5) Effect of Stress-History on Permeability of DEEP HARD Coal.

TABLE (7.2.6) Stress-Permeability Results for DUNSIL 1 Specimen (Effect of Stress-History)

SAMPLE : DUNSIL 1		D = 37·80 mm	L = 74·90 mm
	RADIAL STRESS σ_3 (MN/m^2)	AXIAL STRESS σ_1 (MN/m^2)	1st RUN/18.2.1981 PERMEABILITY K_d (10^{-16} m^2)	2nd RUN/26.2.1981 PERMEABILITY K_d (10^{-16} m^2)
LOADING	0·00	0·00	851·29	48:29
	0:50	1·33	66·77	23:62
	1:00	2·67	44·79	16:29
	1·50	4:01	25·88	11:53
	2·00	5:34	18·96	8:97
	2·50	6·68	14·38	7:10
	3·00	8:02	10·70	5:70
	3·50	9·35	7·68	4:55
	4·00	10·69	6·29	3:73
	4·50	12·03	4·84	3:29
	5·00	13·36	4·00	2:65
	5·50	14·70	3·27	2:22
	6·00	16·04	2·63	1:95
	6·50	17·37	2·19	1:70
	7·00	18·71	1·86	1:54
	7·50	20·05	1:59	1:33
UNLOADING	7·00	18·71	1:75	1:40
	6·50	17·37	1·88	1:53
	6·00	16·04	2:09	1:63
	5·50	14·70	2·20	1:74
	5·00	13·36	2·43	2:03
	4·50	12·03	2·80	2:22
	4·00	10·69	3·20	2:48
	3·50	9·35	3·78	3:05
	3·00	8·02	4·93	3:78
	2·50	6·68	6·07	4:66
	2·00	5·34	8·43	6:28
	1·50	4·01	10·86	8:64
	1·00	2·67	17·88	12:44
	0·50	1·33	26·59	21·93
	0·00	0·00	800·42	73·18

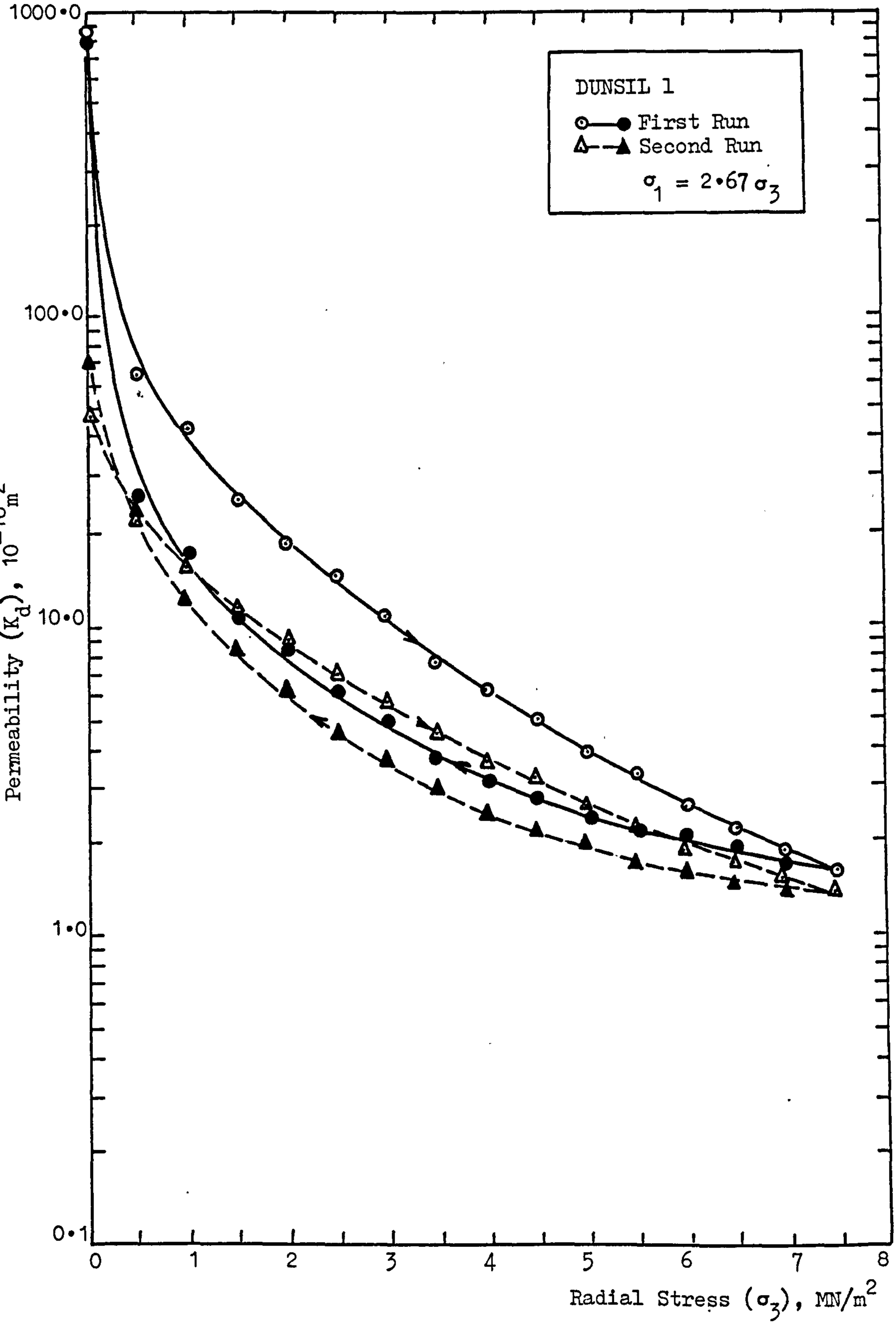

FIGURE (7.2.6) Effect of Stress-History on Permeability of DUNSIL Coal.

corresponding stress-permeability curve. The second loading curve lies between the first loading and unloading curves suggesting a partial recovery in permeability of the specimen. When ACILIK 5 was unloaded for the second time, the effect of the second loading was marked by a further decrease in permeability.

The shape of each individual loading/unloading curve suggests that unless microfractured, stressing and destressing causes a combined elastic-viscous-plastic compression and dilation of the coal material and its fissures (17). The time dependent partial recovery of permeability upon relaxation shows that the coals mentioned above have a high degree of elasticity to allow both stress and time dependent compression and decompression of the specimen.

Coals with a lower degree of elasticity which have, in the main, shown plastic deformation of the coal material, usually microfractured under the stress conditions created in the laboratory. Few of these specimens did not microfracture during the first loading/unloading cycle. When relaxed for a period of time, the effect of relaxation on permeability of these specimens was either negligible or non-existant. The stress-permeability curves for DUNSIL 1 and BARNSLEY 1, shown in Figures (7.2.6) and (7.2.7), illustrate the role of plastic deformation on stress-history dependent permeability behaviour of non-microfractured coals.

As shown in Figure (7.2.6), when DUNSIL 1 was relaxed for eight days after the first run, the rate of recovery in

TABLE (7.2.7) Stress-Permeability Results for BARNSLEY 1 Specimen (Effect of Stress-History)

SAMPLE : BARNSLEY 1		D = 37·55 mm	L = 73·85 mm
	RADIAL STRESS σ_3 (MN/m^2)	AXIAL STRESS σ_1 (MN/m^2)	1st RUN/19.8.80 PERMEABILITY K_d (10^{-16} m^2)	2nd RUN/27.8.80 PERMEABILITY K_d (10^{-16} m^2)
LOADING	0·00	0·00	99·84	108·18
	0·50	1·35	35·45	10·30
	1·00	2·70	18·81	4·67
	1·50	4·06	9·72	2·43
	2·00	5·41	5·73	1·55
	2·50	6·77	3·37	1·07
	3·00	8·12	2·39	0·74
	3·50	9·48	1·54	0·53
	4·00	10·83	0·94	0·33
	4·50	12·19	0·72	0·23
	5·00	13·54	0·38	0·18
	5·50	14·90	0·31	0·14
	6·00	16·25	0·24	0·12
	6·50	17·60	0·15	0·10
	7·00	18·96	0·12	-
	7·50	20·31	0·10	-
UNLOADING	7·00	18·96	0·11	-
	6·50	17·60	0·13	-
	6·00	16·25	0·13	0·11
	5·50	14·90	0·15	0·12
	5·00	13·54	0·22	0·13
	4·50	12·19	0·28	0·15
	4·00	10·83	0·37	0·18
	3·50	9·48	0·57	0·25
	3·00	8·12	1·17	0·34
	2·50	6·77	1·76	0·42
	2·00	5·41	2·95	1·00
	1·50	4·06	5·57	2·05
	1·00	2·70	10·83	3·76
	0·50	1·35	25·86	9·36
	0·00	0·00	34·43	958·00

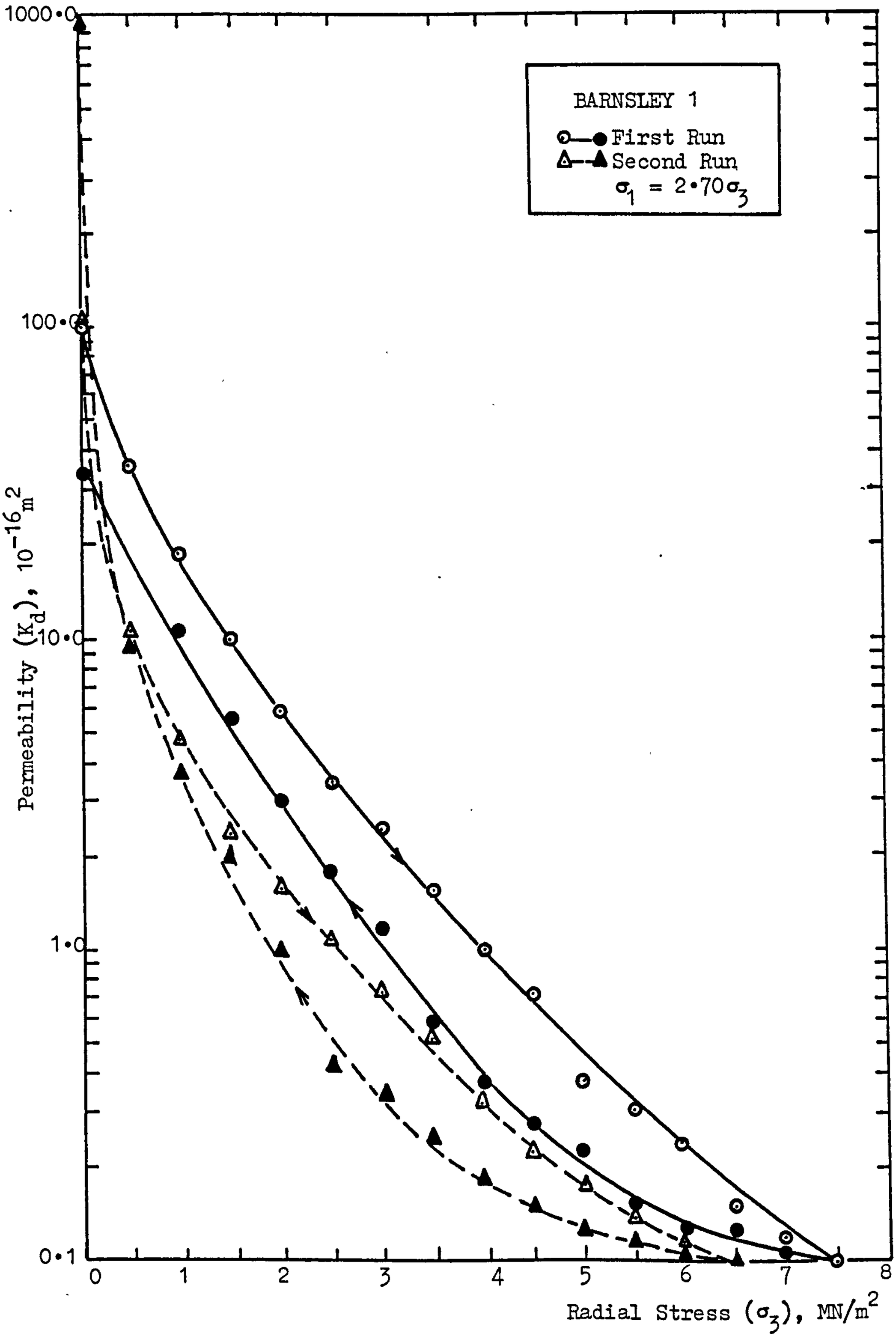

FIGURE (7.2.7) Effect of Stress-History on Permeability of BARNSLEY Coal.

permeability of the specimen was very low when compared to the time dependent relaxation behaviour of coals having a higher degree of elasticity.

The stress-permeability behaviour of BARNSLEY 1 under repeated loading/unloading cycles represented the extreme example of a high degree of plasticity. Figure (7.2.7) illustrates the results of two consecutive loading/unloading experiments carried out on the BARNSLEY 1 specimen. Contrary to the general behaviour of BARNSLEY coal, the specimen was not microfractured during the first run. After being relaxed for eight days, the specimen was loaded and unloaded for the second time. As shown in Figure (7.2.7), the second loading curve followed a lower path of permeabilities compared to the first unloading curve. Unlike the previously examined ACILIK, CAYDAMAR, DEEP HARD and DUNSIL coals, BARNSLEY 1 had shown no time dependent recovery of permeability upon relaxation. Unless microfractured, all BARNSLEY specimens have shown similar effects of stress-history on permeability suggesting that the compression and dilation of coals with a high degree of plasticity is stress dependent only. BARNSLEY 1 was microfractured during the second loading/unloading cycle.

7.2.2 The Effects of Stress and Stress History on Permeability of Microfractured Coals

The stress history behaviour of microfractured coals was found to be dependent on the intensity of microfracturing experienced by the coal material. When subjected to the same stress conditions, less fissured coals such as CAYDAMAR and COCKSHEAD have shown signs

of minor microfracturing whereas highly fissured coals, BARNSLEY, DUNSIL, and very low mechanical strength BANBURY were intensively microfractured.

Figures (7.2.8) to (7.2.10) show the results of successive loading/unloading experiments on CAYDAMAR and COCKSHEAD specimens which showed minor microfracturing after the first run. When these specimens were loaded and unloaded for the first time, the stress-permeability curves for the loading/unloading experiments showed no signs of structural change, suggesting a stress dependent deformation within elastic-plastic limits. However, when the specimens were relaxed for a certain period and loaded for the second time, the effects of microfracturing on permeabilities of the specimens became noticeable.

As in the case of CAYDAMAR 4 and COCKSHEAD 4, where microfracturing is negligible, the effect in permeability could only be noticed under high stresses. On the other hand, being slightly more microfractured during the first stress cycle, COCKSHEAD 2 had relatively higher permeabilities at all stages of the second loading.

In order to observe the effect of the second loading/unloading experiment on stress-permeability behaviour of both the coal material and the microfractures, CAYDAMAR 4 was tested for the third time after being relaxed for two days. Since there was no further microfracturing during the second loading/unloading experiment, the third loading curve followed a lower permeability path showing the usual time dependent recovery and stress-history

TABLE (7.2.8) Stress-Permeability Results for CAYDAMAR 4 Specimen (Effect of Stress-History)

SAMPLE : CAYDAMAR 4		D = 37•30 mm	L = 73•40 mm	
	RADIAL STRESS σ_3 (MN/m^2)	AXIAL STRESS σ_1 (MN/m^2)	1st RUN/15.7.80 PERMEABILITY K_d (10^{-16} m^2)	2nd RUN/8.10.80 PERMEABILITY K_d (10^{-16} m^2)	3rd RUN/10.10.80 PERMEABILITY K_d (10^{-16} m^2)
LOADING	0•00	0•00	-	632•50	564•20
	0•50	1•37	37•09	40•14	32•50
	1•00	2•75	25•49	19•34	16•07
	1•50	4•12	17•28	13•24	11•11
	2•00	5•50	11•80	9•43	7•87
	2•50	6•88	8•55	7•11	5•89
	3•00	8•25	6•77	6•13	4•79
	3•50	9•63	5•15	4•70	3•81
	4•00	11•01	4•02	3•68	3•15
	4•50	12•38	3•26	3•04	2•82
	5•00	13•76	2•48	2•59	2•34
	5•50	15•14	2•06	2•27	1•95
	6•00	16•51	1•73	1•90	1•72
	6•50	17•89	1•43	1•62	1•48
	7•00	19•27	1•16	1•43	1•34
	7•50	20•64	0•98	1•25	1•16
UNLOADING	7•00	19•27	1•07	1•31	-
	6•50	17•89	1•19	1•39	-
	6•00	16•51	1•30	1•60	-
	5•50	15•14	1•47	1•70	-
	5•00	13•76	1•16	1•96	-
	4•50	12•38	1•94	2•14	-
	4•00	11•01	2•27	2•74	-
	3•50	9•63	2•86	3•04	-
	3•00	8•25	3•61	3•52	-
	2•50	6•88	4•58	4•68	-
	2•00	5•50	5•76	6•60	-
	1•50	4•12	7•96	8•34	-
	1•00	2•75	12•80	14•30	-
	0•50	1•37	25•92	38•30	-
	0•00	0•00	-	615•39	-

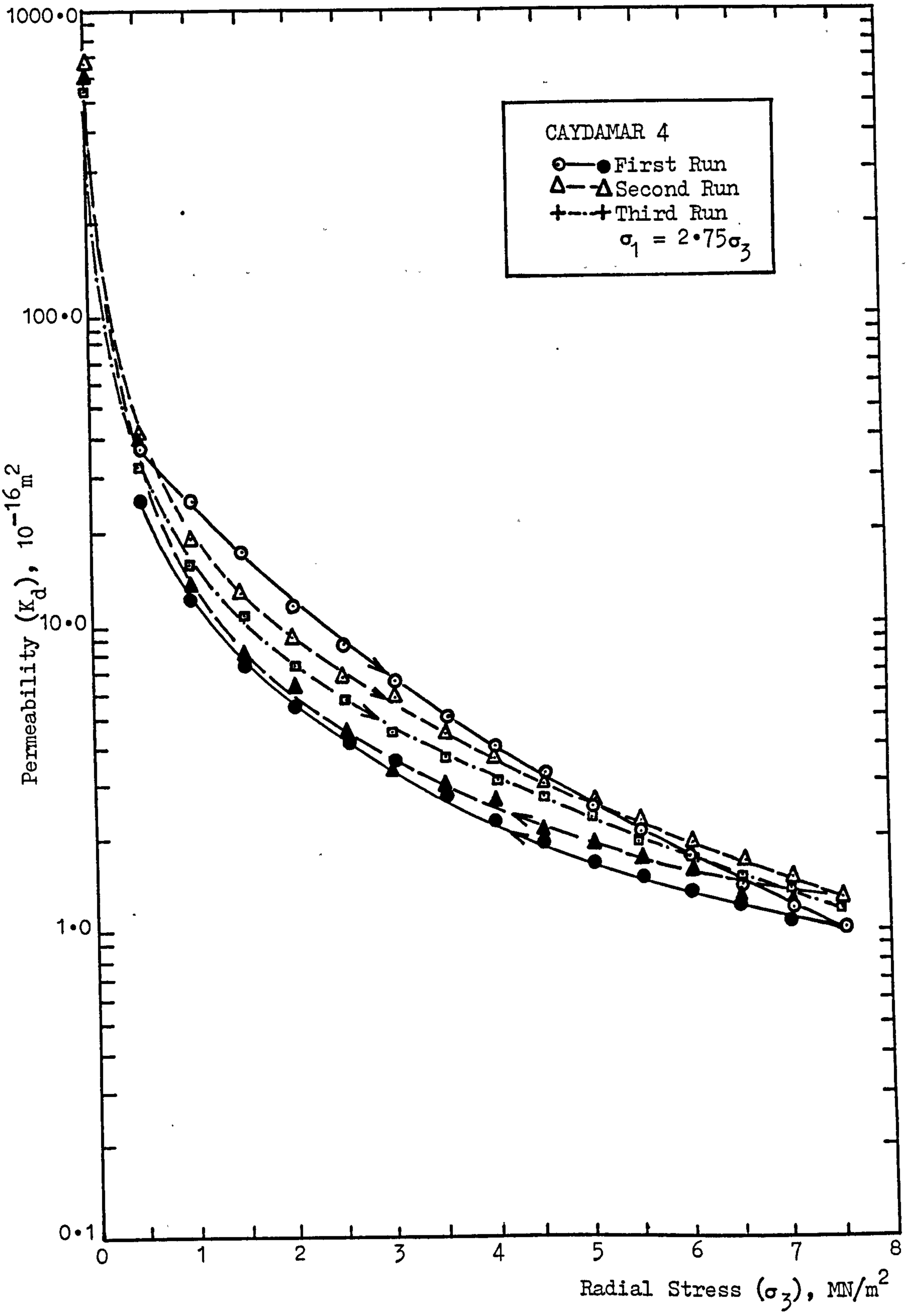

FIGURE (7.2.8) Effect of Stress-History on Permeability of Microfractured CAYDAMAR Coal.

TABLE (7.2.9) Stress-Permeability Results for COCKSHEAD 4 Specimen (Effect of Stress-History)

SAMPLE : COCKSHEAD 4		D = 37•40 mm	L = 73.94 mm
	RADIAL STRESS σ_3 (MN/m^2)	AXIAL STRESS σ_1 (MN/m^2)	1st RUN/18.5.1981 PERMEABILITY K_d (10^{-16} m^2)	2nd RUN/26.5.1981 PERMEABILITY K_d (10^{-16} m^2)
LOADING	0•00	0•00	397•76	399•62
	0•50	1•36	20•90	34•61
	1•00	2•73	7•96	5•41
	1•50	4•09	3•51	2•57
	2•00	5•46	1•91	1•55
	2•50	6•82	1•08	0•86
	3•00	8•19	0•83	0•69
	3•50	9•55	0•54	0•44
	4•00	10•92	0•37	0•35
	4•50	12•29	0•27	0•25
	5•00	13•65	0•19	0•20
	5•50	15•01	0•14	0•14
	6•00	16•38	0•10	0•11
	6•50	17•50	0•07	0•09
	7•00	19•11	0•06	0•07
	7•50	-	-	-
	7•00	-	-	-
UNLOADING	6•50	17•50	0•07	0•08
	6•00	16•38	0•08	0•08
	5•50	15•01	0•09	0•10
	5•00	13•65	0•11	0•12
	4•50	12•29	0•16	0•16
	4•00	10•92	0•25	0•23
	3•50	9•55	0•32	0•27
	3•00	8•19	0•48	0•49
	2•50	6•82	0•71	0•79
	2•00	5•46	1•20	1•22
	1•50	4•09	2•10	2•64
	1•00	2•73	4•04	3•90
	0•50	1•36	17•91	12•82
	0•00	0•00	383.11	395.69

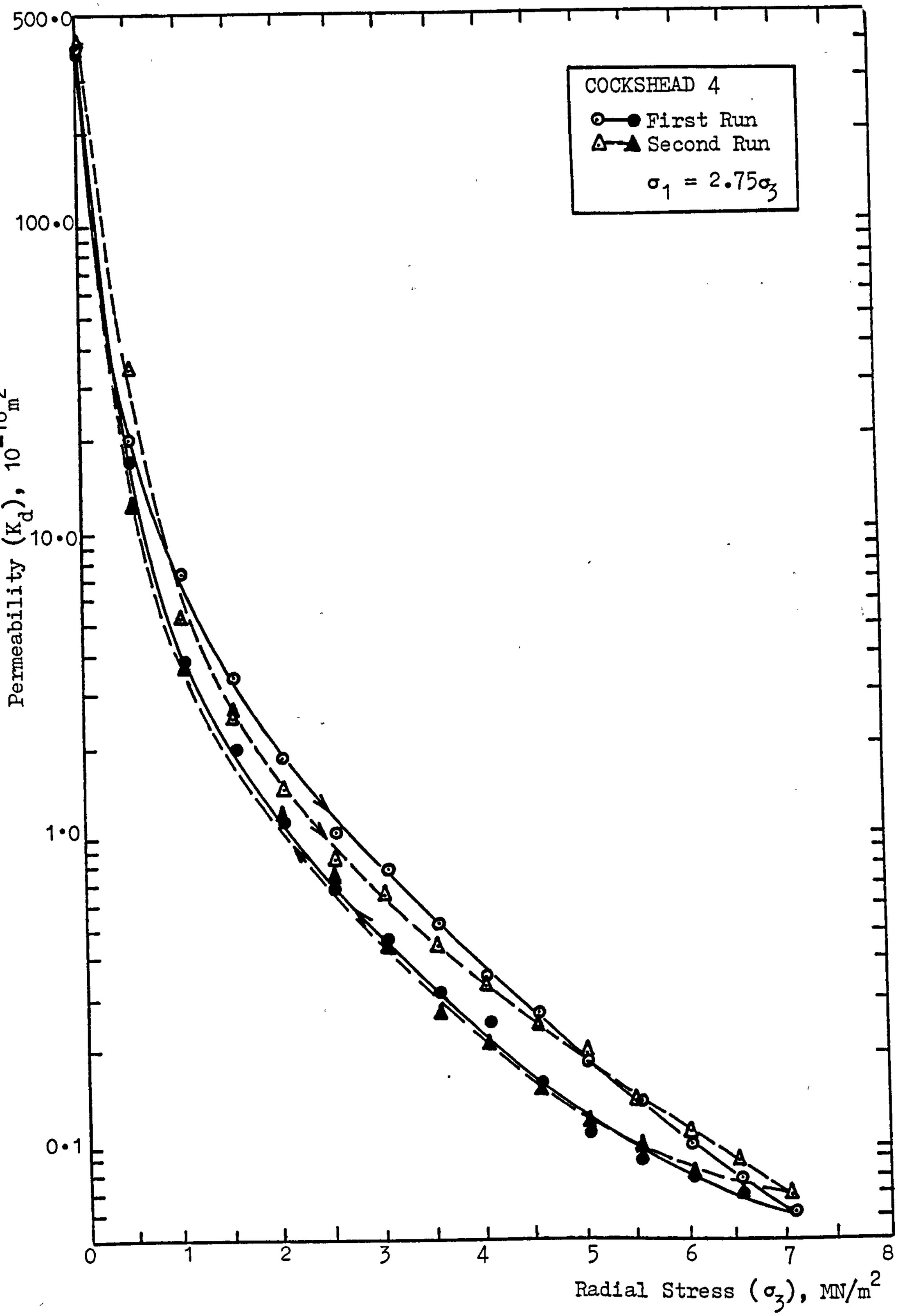

FIGURE (7.2.9) Effect of Stress-History on Permeability of Microfractured COCKSHEAD Coal.

TABLE (7.2.10) Stress-Permeability Results for COCKSHEAD 2 Specimen (Effect of Stress-History)

SAMPLE : COCKSHEAD 2		D = 37·50 mm	L = 73·65 mm
	RADIAL STRESS σ_3 (MN/m^2)	AXIAL STRESS σ_1 (MN/m^2)	1st RUN/15.5.1981 PERMEABILITY K_d (10^{-16} m^2)	2nd RUN/22.5.1981 PERMEABILITY K_d (10^{-16} m^2)
LOADING	0·00	0·00	398·36	375·20
	0·50	1·35	25·45	21·04
	1·00	2·71	5·13	3·80
	1·50	4·07	2·86	3·64
	2·00	5·43	1·80	2·01
	2·50	6·79	0·96	1·13
	3·00	8·14	0·64	0·76
	3·50	9·50	0·49	0·52
	4·00	10·86	0·38	0·40
	4·50	12·22	0·27	0·26
	5·00	13·58	0·25	0·27
	5·50	14·43	0·19	0·18
	6·00	16·29	0·13	0·13
	6·50	17·20	0·10	0·11
	7·00	19·01	0·08	0·09
	7·50	-	-	-
	7·00	-	-	-
	6·50	17·20	0·09	0·10
	6·00	16·29	0·11	0·11
	5·50	14·43	0·12	0·12
	5·00	13·58	0·14	0·16
UNLOADING	4·50	12·22	0·18	0·20
	4·00	10·86	0·24	0·28
	3·50	9·50	0·33	0·31
	3·00	8·14	0·47	0·55
	2·50	6·79	1·01	1·21
	2·00	5·43	1·11	1·33
	1·50	4·07	2·34	1·57
	1·00	2·71	4·73	3·16
	0·50	1·35	14·87	25·13
	0·00	0·00	389·26	383·38

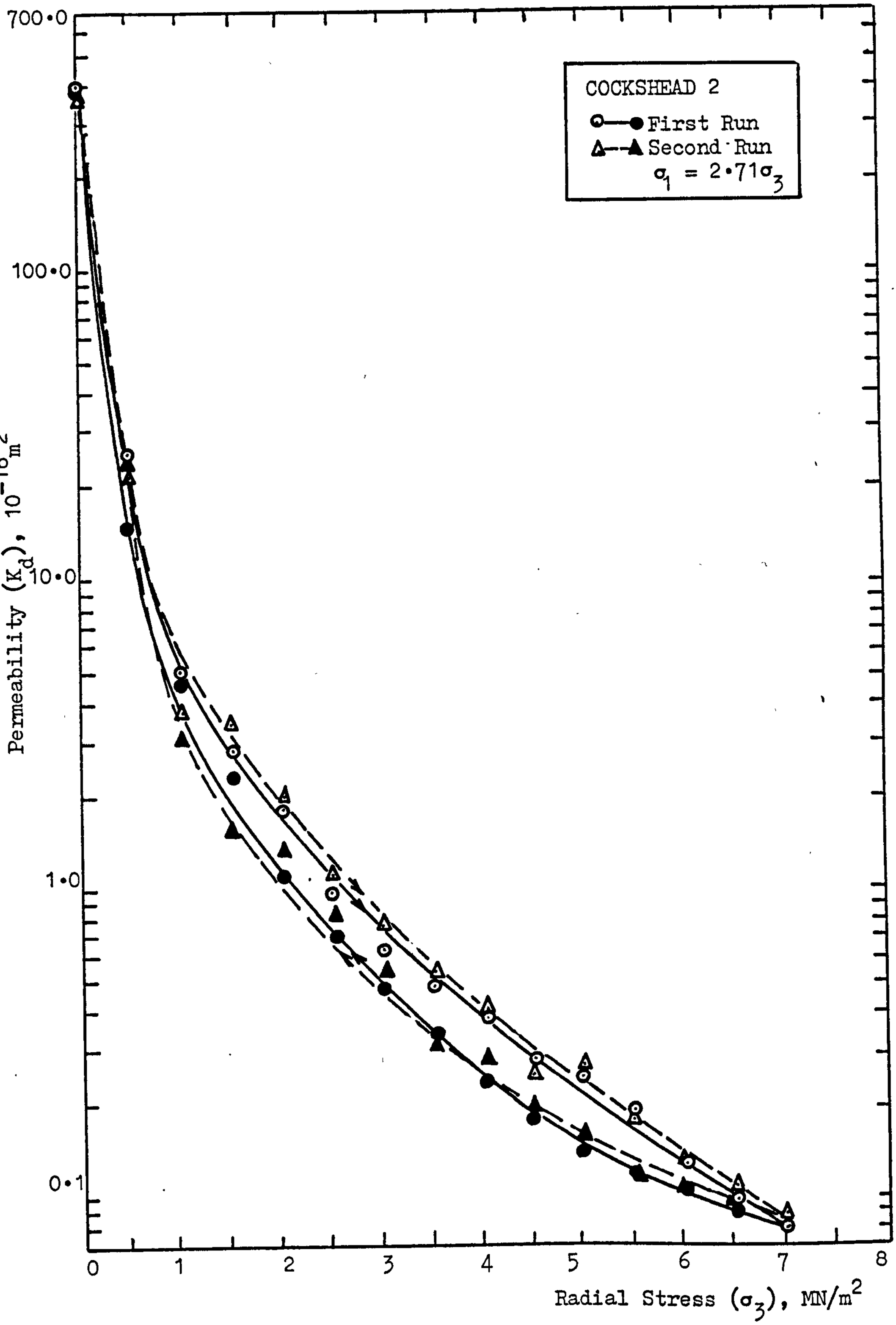

FIGURE (7.2.10) Effect of Stress-History on Permeability of Microfractured COCKSHEAD Coal.

effect on permeability of the whole structure. CAYDAMAR 4 was crushed while unloading during the third run.

CAYDAMAR 4 was the only specimen showing microfracturing characteristics amongst the seven CAYDAMAR specimens tested throughout this research. On the other hand, all the COCKSHEAD specimens showed similar microfracturing properties as illustrated in Figures (7.2.9) and (7.2.10). Depending on the intensity of microfracturing, permeabilities of coal specimens were increased after each run in which microfracturing took place.

As mentioned before, due to their highly fissured structure and/or low mechanical strength BARNSLEY, DUNSIL and BANBURY specimens usually microfractured intensively under high stresses. Figures (7.2.11) to (7.2.14) illustrate the comparable stress-permeability behaviour of BARNSLEY 5, DUNSIL 5, BANBURY 3 and BANBURY 4, which were highly microfractured during the first loading experiment. For a better understanding of the mechanism of microfracturing and its effect on permeability, the stress-permeability behaviour of BARNSLEY 5 will be discussed in detail.

As shown in Figure (7.2.11), the first loading of BARNSLEY 5 demonstrated the usual pattern of stress effect on permeability. When the specimen was unloaded, it first followed a lower permeability curve showing the effect of stressing. As the low stresses were reached, a sudden increase in permeability of the specimen was observed. On further unloading, the permeability of the specimen was generally higher than the loading permeabilities.

TABLE (7.2.11) Stress-Permeability Results for BARNSLEY 5 Specimen (Effect of Stress-History)

SAMPLE : BARNSLEY 5		D = 37·65 mm	L = 73·85 mm	
	RADIAL STRESS σ_3 (MN/m^2)	AXIAL STRESS σ_1 (MN/m^2)	1st RUN/16.10.80 PERMEABILITY K_d (10^{-16} m^2)	2nd RUN/22.10.80 PERMEABILITY K_d (10^{-16} m^2)	3rd RUN/12.11.80 PERMEABILITY K_d (10^{-16} m^2)
LOADING	0·00	0·00	681·06	710·75	644·88
	0·50	1·34	8·65	8·11	14·26
	1·00	2·69	2·50	3·73	3·10
	1·50	4·04	1·28	2·07	1·75
	2·00	5·38	0·93	1·54	1·30
	2·50	6·73	0·67	1·10	0·96
	3·00	8·04	0·50	0·82	0·75
	3·50	9·43	0·40	0·65	0·60
	4·00	10·77	0·30	0·53	0·50
	4·50	12·12	0·22	0·45	0·42
	5·00	13·47	0·17	0·38	0·34
	5·50	14·82	0·15	0·32	0·30
	6·00	16·16	0·12	0·28	0·27
	6·50	-	-	-	-
	7·00	-	-	-	-
	7·50	-	-	-	-
	7·00	-	-	-	-
	6·50	-	-	-	-
	6·00	-	-	-	-
	5·50	14·82	0·14	0·30	-
	5·00	13·47	0·16	0·34	-
	4·50	12·12	0·19	0·37	-
UNLOADING	4·00	10·77	0·22	0·41	-
	3·50	9·43	0·25	0·53	-
	3·00	8·04	0·29	0·68	-
	2·50	6·73	0·59	0·82	-
	2·00	5·38	0·75	1·37	-
	1·50	4·04	3·10	2·06	-
	1·00	2·69	4·24	3·40	-
	0·50	1·34	6·75	11·65	-
	0·00	0·00	774·42	797·73	-

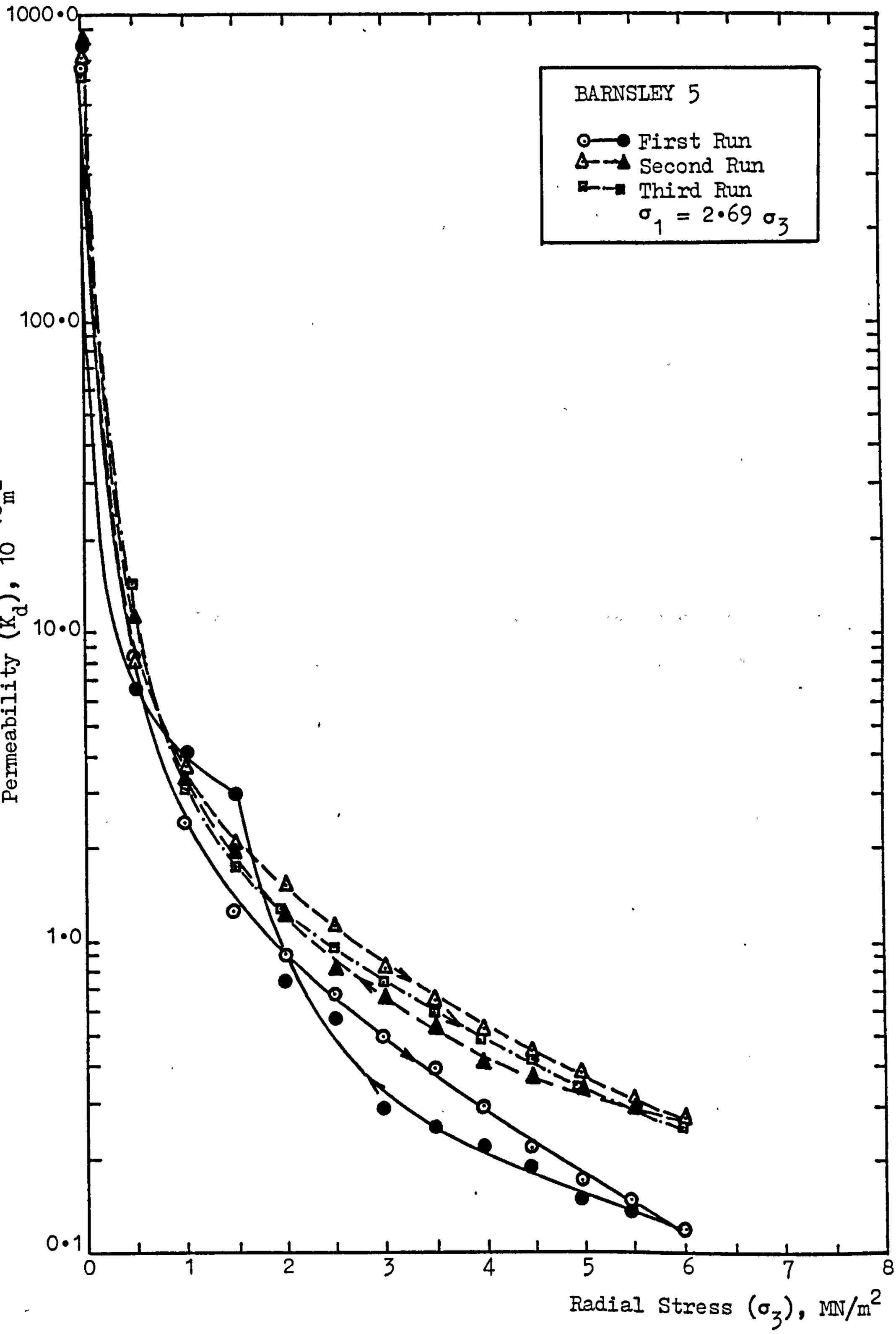

FIGURE (7.2.11) Effect of Stress-History on Permeability of Microfractured BARNSLEY Coal.

This indicated that BARNSLEY 5 was highly microfractured during the first run.

After being relaxed for six days, BARNSLEY 5 was loaded and unloaded for the second time. Due to the highly microfractured structure of the specimen, the second loading curve followed a considerably higher permeability path; the effect being more distinct under high stresses. The second unloading process had shown no further changes in the structure of the specimen and the stress-permeability curve followed a lower path compared to the loading curve.

Twenty days later, the same specimen was tested for the third time and the time dependent recovery in permeability of the whole structure was demonstrated by the position of the third loading curve. BARNSLEY 5 was crushed during the third unloading experiment.

As illustrated in Figures (7.2.11) to (7.2.14), microfracturing under increasing stresses does not cause an immediate increase in permeability of coal, as one might have expected. Due to the compaction effect of continuously increasing stresses, the permeability of coal decreases steadily even if it is highly microfractured during the process. It is only during the releasing of these stresses that the microfractured coal shows signs of increase in permeability. Furthermore, the actual open structured character of the microfractured coal and its permeability behaviour against the applied stresses can only be established

TABLE (7.2.12) Stress-Permeability Results for DUNSIL 5 Specimen (Effect of Stress-History)

SAMPLE : DUNSIL 5		D = 37·80 mm	L = 73·80 mm
	RADIAL STRESS σ_3 (MN/m^2)	AXIAL STRESS σ_1 (MN/m^2)	1st RUN/16.3.1981 PERMEABILITY K_d (10^{-16} m^2)	2nd RUN/24.3.1981 PERMEABILITY K_d (10^{-16} m^2)
LOADING	0·00	0·00	747·92	782·27
	0·50	1·34	57·04	37·58
	1·00	2·68	18·01	19·92
	1·50	4·03	8·16	11·17
	2·00	5·37	4·86	7·24
	2·50	6·71	3·06	5·07
	3·00	8·06	2·15	3·46
	3·50	9·40	1·56	2·65
	4·00	10·75	1·20	2·18
	4·50	12·09	0·93	1·68
	5·00	13·43	0·74	1·34
	5·50	14·78	0·59	1·16
	6·00	16·12	0·49	0·96
	6·50	17·46	0·41	0·79
	7·00	18·81	0·33	0·71
	7·50	20·15	0·29	0·60
UNLOADING	7·00	18·81	0·30	-
	6·50	17·46	0·35	-
	6·00	16·12	0·39	-
	5·50	14·78	0·43	-
	5·00	13·43	0·47	-
	4·50	12·09	0·59	-
	4·00	10·75	0·66	-
	3·50	9·40	0·86	-
	3·00	8·06	1·20	-
	2·50	6·71	1·50	-
	2·00	5·37	2·34	7·17
	1·50	4·03	3·84	-
	1·00	2·68	8·56	-
	0·50	1·34	24·25	90·17
	0·00	0·00	846·25	855·25

(20·15) (20·15)

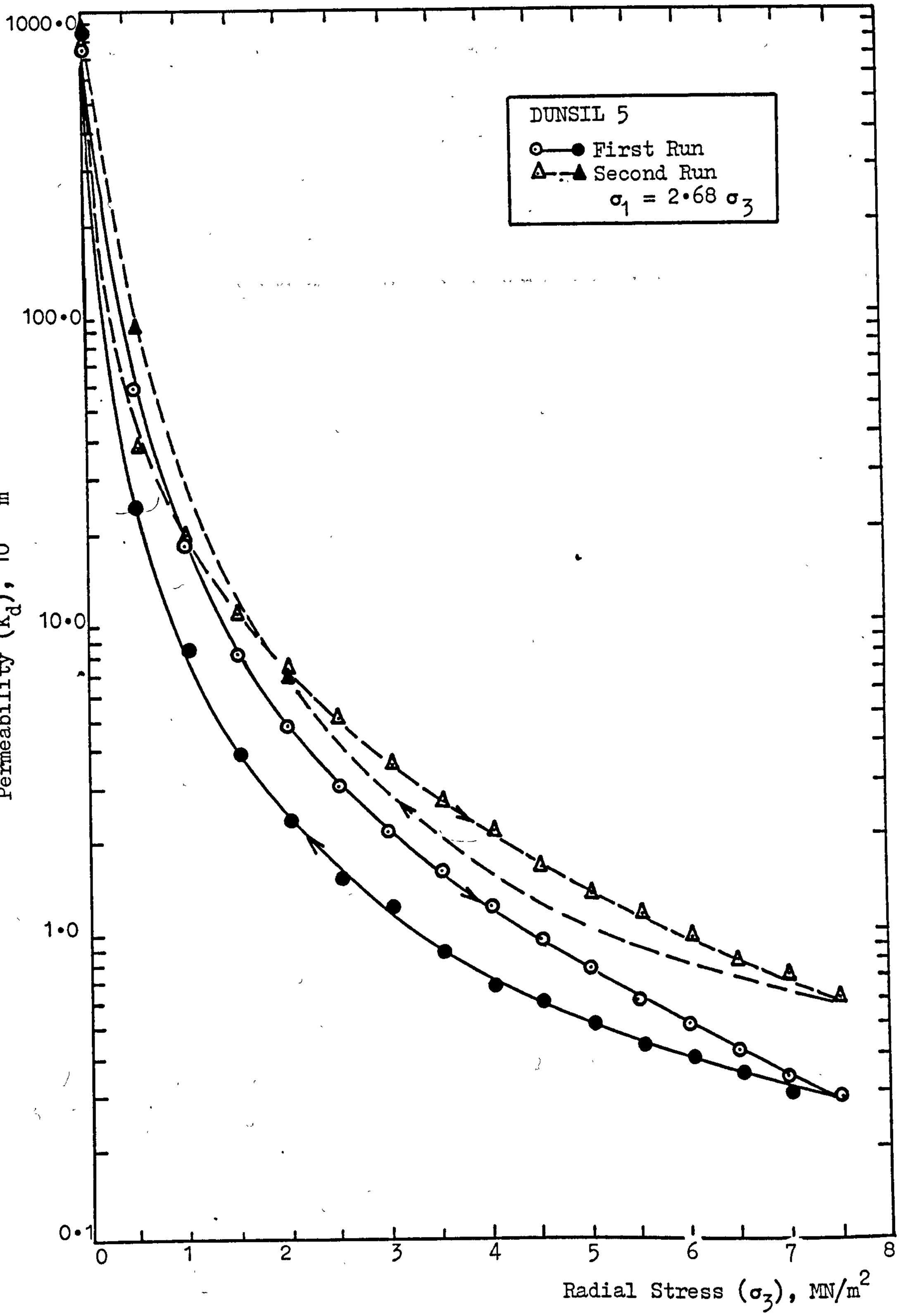

FIGURE (7.2.12) Effect of Stress-History on Permeability of Microfractured DUNSIL Coal.

TABLE (7.2.13) Stress-Permeability Results for BANBURY 3 Specimen (Effect of Stress-History)

SAMPLE : BANBURY 3		D = 37·35 mm	L = 73·75 mm
	RADIAL STRESS σ_3 (MN/m^2)	AXIAL STRESS σ_1 (MN/m^2)	1st RUN/12.5.81 PERMEABILITY K_d (10^{-16} m^2)	2nd RUN/19.5.81 PERMEABILITY K_d (10^{-16} m^2)
LOADING	0·00	0·00	399:63	402:59
	0·50	1:36	19:53	43:20
	1:00	2·73	5:01	17:80
	1·50	4·10	2:42	5:68
	2·00	5·47	1:59	3:55
	2·50	6·84	1:03	2:33
	3·00	8·21	0:77	1:68
	3·50	9·58	0:58	1:05
	4·00	10·95	0:40	0:92
	4·50	12·32	0:30	0·68
	5·00	13·69	0·24	0:54
	5·50	15·06	0:19	0:40
	6·00	16·42	0:16	0:32
	6·50	17·75	0:13	0:24
	7·00	19·16	0·10	0·21
	7·50	-	-	-
	7·00	-	-	-
UNLOADING	6·50	17·75	0:11	0:22
	6·00	16·42	0:13	0:28
	5·50	15·06	0·15	0:35
	5·00	13·69	0:20	0:42
	4·50	12·32	0:22	0:50
	4·00	10·95	0:29	0:68
	3·50	9·58	0:38	0:91
	3·00	8·21	0·47	1:15
	2·50	6·84	0:78	1:72
	2·00	5·47	1:32	2:65
	1·50	4·10	3:05	3·82
	1·00	2·73	12:25	8:21
	0:50	1·36	47:32	36:24
	0·00	0·00	428·15	464·93

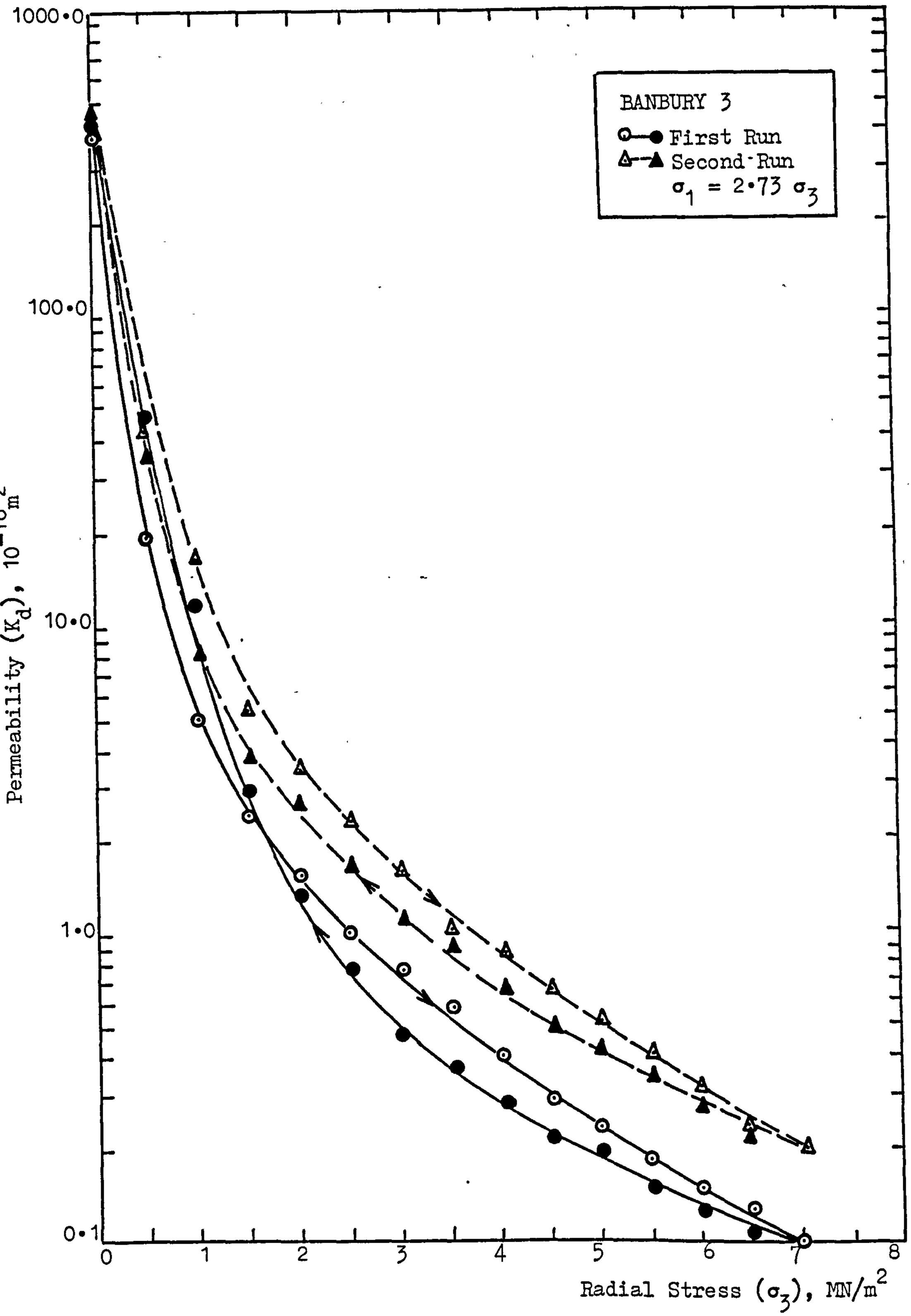

FIGURE (7.2.13) Effect of Stress-History on Permeability of Microfractured BANBURY Coal.

TABLE (7.2.14) Stress-Permeability Results for BANBURY 4 Specimen (Effect of Stress-History)

SAMPLE : BANBURY 4		D = 37•34 mm	L = 73•83 mm
	RADIAL STRESS σ_3 (MN/m^2)	AXIAL STRESS σ_1 (MN/m^2)	1st RUN/14.5.1981 PERMEABILITY K_d (10^{-16} m^2)	2nd RUN/20.5.1981 PERMEABILITY K_d (10^{-16} m^2)
LOADING	0•00	0•00	393:66	361:63
	0•50	1•37	10:54	42:34
	1:00	2•73	3:34	8:12
	1:50	4:10	1:69	5:58
	2•00	5•47	1:04	3:68
	2•50	6•84	0:73	2:40
	3•00	8•21	0:54	1:75
	3•50	9•58	0:38	1:12
	4•00	10•95	0:29	0:84
	4•50	12•32	0:23	0:74
	5•00	13•69	0:17	0:58
	5•50	15•06	0:14	0:42
	6•00	16•42	0:11	0:37
	6•50	17•79	0:09	0:30
	7:00	19•16	0•07	0•24
	7:50	-	-	-
	7•00	-	-	-
	6•50	17•79	0:07	0:28
	6•00	16•42	0:08	0:34
	5:50	15•06	0:09	0:38
	5•00	13•69	0:10	0:45
	4•50	12•32	0:12	0:54
UNLOADING	4•00	10•95	0:15	0:68
	3•50	9•58	0:21	0•86
	3:00	8•21	0:33	1:52
	2•50	6•84	2:20	1:63
	2•00	5•47	3•10	2:31
	1•50	4:10	4:72	4:87
	1•00	2:73	8:80	6:24
	0:50	1:37	28:23	24:22
	0•00	0•00	436•28	422•23

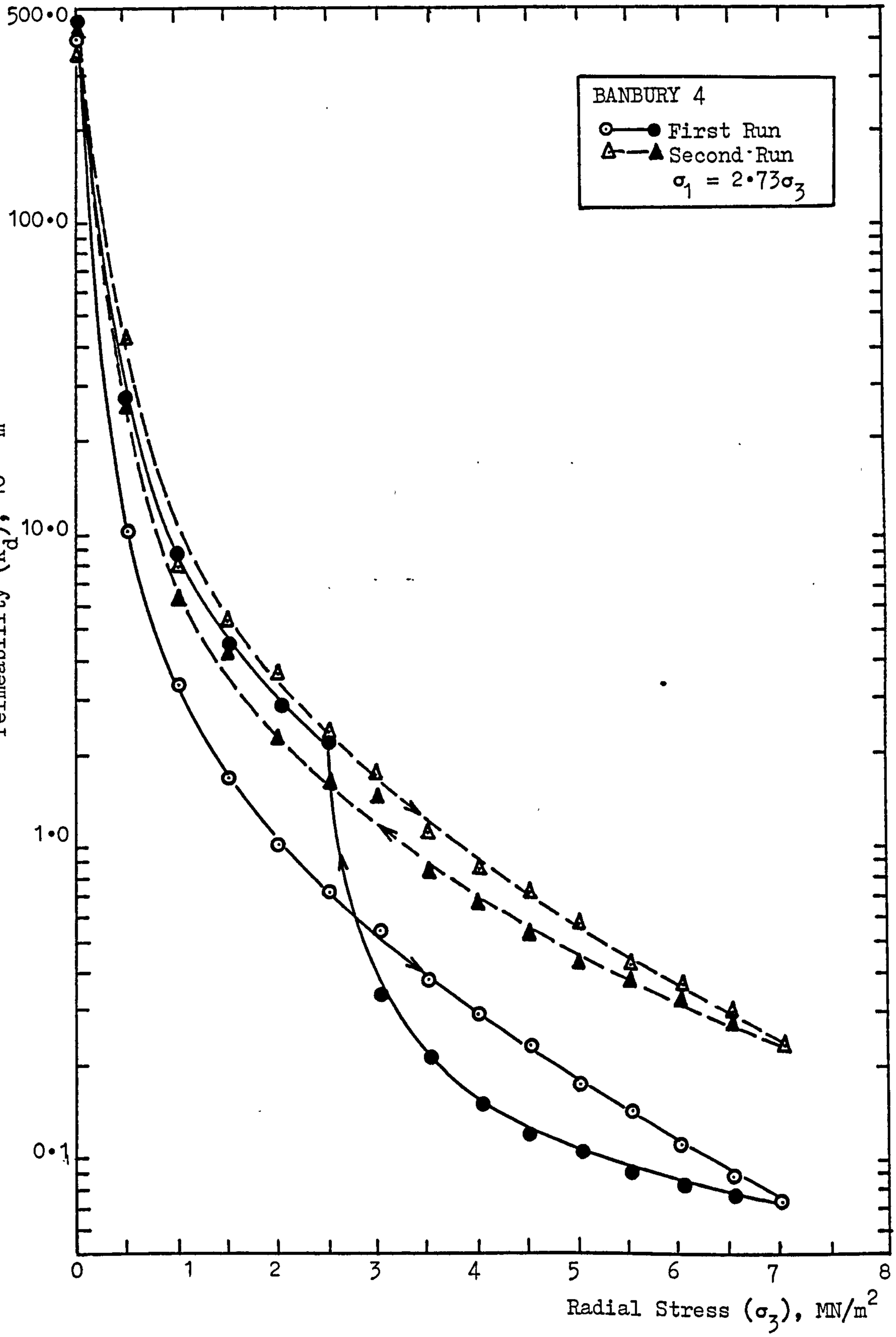

FIGURE (7.2.14) Effect of Stress-History on Permeability of Microfractured BANBURY Coal.

after a stress free relaxation. After being relaxed, microfractured coal has a higher degree of elasticity and permeability under stress.

7.2.3 Conclusions

In view of the observations made on the effects of stress and stress-history on permeability of seven different coals, the following conclusions can be drawn:

1. Permeability of coal decreases with increasing stress. The change in permeability can be attributed to the combined elastic-viscous-plastic compression and dilation of the coal material and its fissures under stress.
2. Permeability of coal is stress history dependent. Once coal is stressed and de-stressed, there is always a permanent change in its permeability. The nature of permeability change depends on the elastic properties and the microfracturing characteristics of coal under stress.
3. Coals with a high degree of elasticity such as ACILIK, CAYDAMAR and DEEP HARD do not microfracture under the simulated subsurface conditions*. For such coals, a time dependent partial recovery of permeability takes place when the stresses are relieved and the coal is

---

* Simulated triaxial stresses for the front abutment zone of a longwall face up to 700 m depth.

relaxed. The overall permeability decreases after each stress cycle.

4. Highly fissured and/or low mechanical strength coals such as BARNSLEY, DUNSIL, COCKSHEAD and BANBURY usually microfracture under the simulated subsurface conditions. Permeability of a microfractured coal increases only after the stresses are relieved and the coal is relaxed.
5. The rate of increase in permeability of a microfractured coal depends on the intensity of microfracturing. As the rate of propogation of microfractures increase, the effect of stress on permeability decreases.

When these conclusions are interpreted in terms of the stress conditions and the permeabilities of coal seams around working longwall faces, one can say that the permeability of coal seams should decrease between 10 to 100 times (depending on the depth and type of coal concerned) in the front abutment zone of a coal face. It must be remembered, however, that the stress conditions underground would be more complex than the simulated stress applied in the laboratory. Under such complex stresses and at very great depths it is more likely that all types of coals will microfracture at the front abutment zone, but this will not cause an immediate increase in permeability.

The fact that no major fracturing and failing incidents occurred under the stresses simulating the front abutment zone stress conditions, supported the belief that fracturing and failing of coal seams only takes place in the Crushing Zone (see page 76)

of a coal face. The nature of permeability changes in the crushing zone and the fracture permeabilities of coal will be discussed in the next section.

7.3 The Effect of Induced Tensile Fracturing on Permeability and the Fracture Permeabilities of Coals Tested.

As discussed in Chapter 4, the most dramatic change in permeability of coal seams is to be expected in the crushing zone. Stress conditions, similar to those experienced in the crushing zone, were created in the laboratory and the changes occuring in permeability of coal specimens were observed.

Stress-permeability experiments conducted on totally fractured specimens provided further information about the permeability behaviour of source seams in the recompaction zone.

Coal specimens that were to be tested for the effect of induced tensile fracturing on permeability were first loaded under simulated front abutment zone stress conditions. When a sufficiently high stress level was reached (i.e. $\sigma_3 = 7{\cdot}50$ MN/m^2, $\sigma_1 = 20{\cdot}50$ MN/M^2), the radial stress σ_3 was abruptly relieved keeping σ_1 as high as possible. The specimen usually failed with a cracking noise and the permeability increased considerably.

In an attempt to understand the deformation characteristics of coal during fracturing, two coal specimens ACILIK 2 and DUNSIL 5 were equipped with strain gauges and simultaneous readings of

TABLE (7.3.1) The Stress-Strain and Stress-Permeability Relationships for the ACILIK 2 Specimen During a Loading/Crushing Experiment

SAMPLE : ACILIK 2		D = 37•30 mm	L = 73•85 mm	
	RADIAL STRESS σ_3 (MN/m^2)	AXIAL STRESS σ_1 (MN/m^2)	3rd RUN PERMEABILITY K_d (10^{-16} m^2)	RADIAL STRAIN ε_3 (mm/m)	AXIAL STRAIN ε_1 (mm/m)
LOADING	0•00	0•00	335•99	-	-
	0•50	1•37	74•34	* -1•59	-1•34
	1•00	2•74	35•78	-2•78	-3•16
	1•50	4•11	22•75	-3•21	-5•29
	2•00	5•49	16•96	-3•57	-5•98
	2•50	6•86	12•40	-3•88	-6•98
	3•00	8•23	9•85	-4•14	-7•66
	3•50	9•60	7•76	-4•31	-8•22
	4•00	10•98	6•16	-4•46	-8•77
	4•50	12•35	5•11	-4•58	-9•28
	5•00	13•72	4•27	-4•62	-10•04
	5•50	15•10	3•52	-4•66	-10•62
	6•00	16•47	3•12	-4•71	-11•10
	6•50	17•84	2•66	-4•76	-11•62
	7•00	19•21	2•34	-4•77	-12•07
	7•50	20•59	2•04	-4•77	-12•41
UNLOADING	7•00	-	-	-	-
	6•50	-	-	-	-
	6•00	-	-	-	-
	5•50	-	-	-	-
	5•00	-	-	-	-
	4•50	-	-	-	-
	4•00	-	-	-	-
	3•50	-	-	-	-
	3•00	-	-	-	-
	2•50	-	-	-	-
	2•00	-	-	-	-
	1•50	-	-	-	-
	1•00	16•50	65•48	+2•60	-20•12
	0•50	-	-	-	-
	0•00	0•00	813•37	-	-

* Compressive strain is indicated by negative sign.

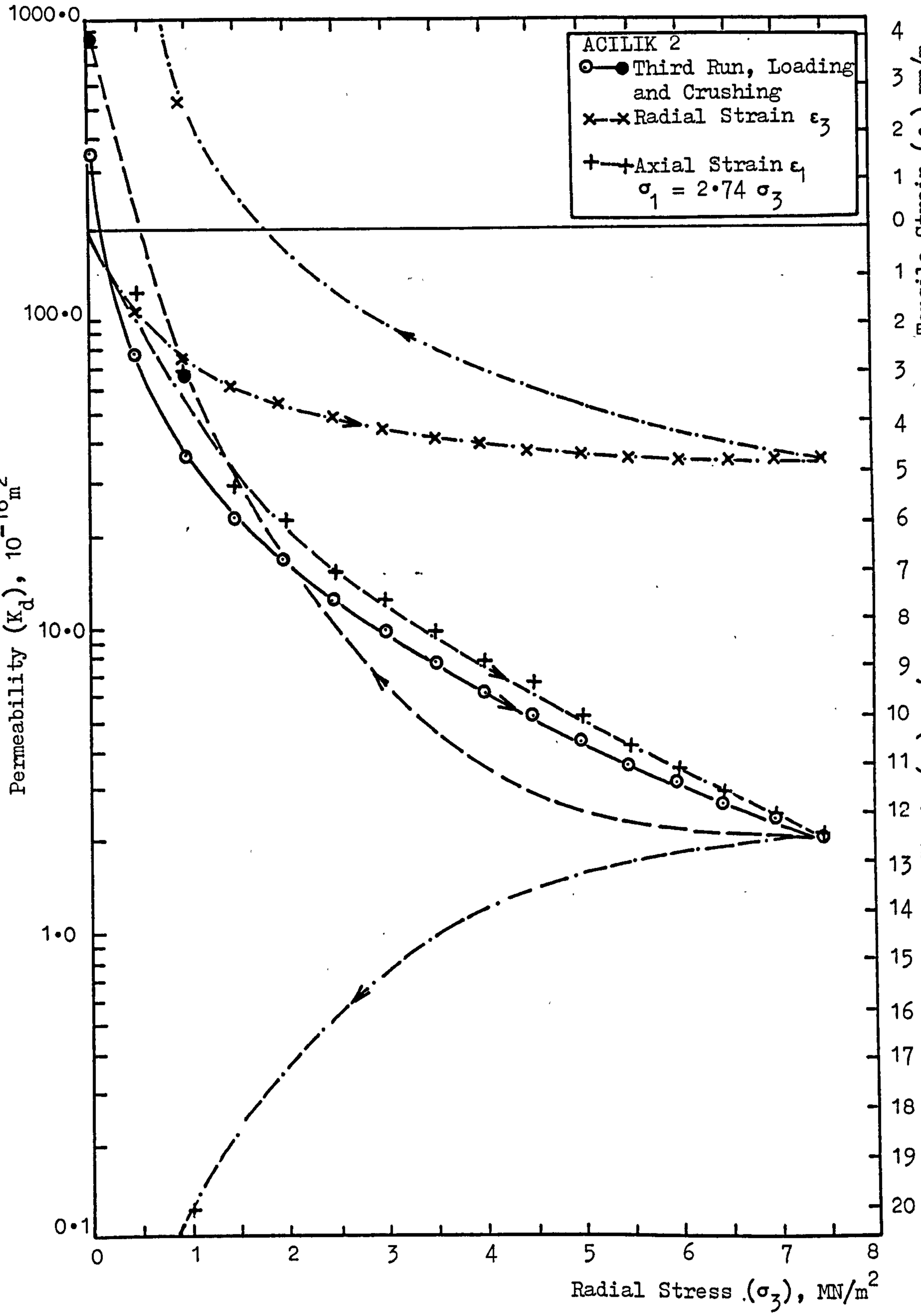

FIGURE (7.3.1) The Stress-Strain and Stress-Permeability Relationships for the ACILIK 2 Specimen During a Loading/Crushing Experiment.

TABLE (7.3.2) The Stress-Strain and Stress-Permeability Relationships for the DUNSIL 5 Specimen During a Loading/Crushing Experiment

SAMPLE : DUNSIL 5		D = 37•80 mm		L = 73•45 mm
	RADIAL STRESS σ_3 (MN/m^2)	AXIAL STRESS σ_1 (MN/m^2)	2nd RUN PERMEABILITY K_d (10^{-16} m^2)	RADIAL STRAIN ε_3 (mm/m)	AXIAL STRAIN ε_1 (mm/m)
LOADING	0•00	0•00	782•27	-	-
	0•50	1•33	37•50	-0•50	-2•90
	1•00	2•66	19•92	-0•67	-6•39
	1•50	3•99	11•17	-0•74	-7•29
	2•00	5•33	7•24	-0•73	-8•74
	2•50	6•66	5•07	-0•73	-9•44
	3•00	7•99	3•56	-0•73	-9•99
	3•50	9•33	2•65	-0•68	-10•54
	4•00	10•66	2•18	-0•66	-11•10
	4•50	11•99	1•68	-0•66	-11•65
	5•00	13•33	1•34	-0•63	-12•17
	5•50	14•66	1•16	-0•57	-12•67
	6•00	15•99	0•96	-0•56	-13•03
	6•50	17•33	0•79	-0•51	-13•59
	7•00	18•66	0•71	-0•45	-13•97
	7•50	19•99	0•60	-0•45	-14•36
	7•00	-	-	-	-
	6•50	-	-	-	-
	6•00	-	-	-	-
	5•50	-	-	-	-
	5•00	-	-	-	-
	4•50	-	-	-	-
UNLOADING	4•00	-	-	-	-
	3•50	-	-	-	-
	3•00	-	-	-	-
	2•50	-	-	-	-
	2•00	19•99	7•17	+0•97	-15•26
	1•50	-	-	-	-
	1•00	-	-	-	-
	0•50	19•99	90•17	+1•50	-15•95
	0•00	0•00	855•25	-	-

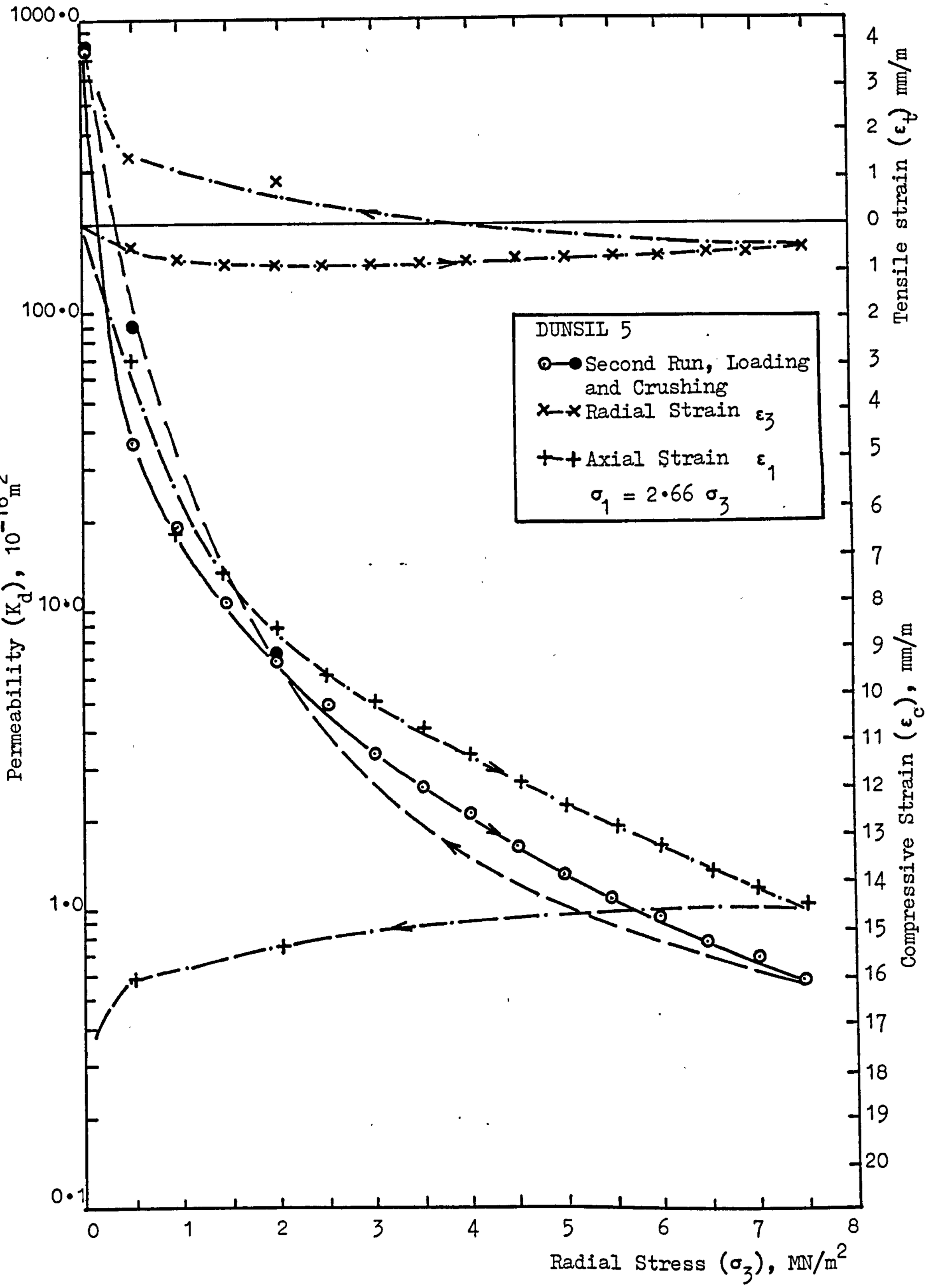

FIGURE (7.3.2) The Stress-Strain and Stress-Permeability Relationships for the DUNSIL 5 Specimen During a Loading/Crushing Experiment.

axial and radial strains were taken together with the stress-permeability measurements. The stress-strain and stress-permeability curves for the loading/crushing experiments on ACILIK 2 and DUNSIL 5 are illustrated in Figures (7.3.1) and (7.3.2).

As seen in both figures, coal is compressed in all directions while loading. Both the axial and radial compression contributes to the decrease in permeability though the major deformation is in the axial direction.

When the fracturing was initiated by an abrupt release of radial stress, the specimen bulged radially as indicated by the change in radial strain, and a rapid increase in permeability was observed. The mechanism of stress-strain and permeability changes illustrated in these figures is in fact the slow motion picture of the changes taking place in the crushing zone. Plate (7.2) shows some examples of test specimens which were fractured following the procedure discussed above.

Fractured coal specimens were relaxed for a period of time and then were finally tested for fracture permeabilities under increasing stresses. Stress-permeability curves for the fracturing and fracture permeability experiments were plotted on the same graph for ease of comparison. Axial stresses applied during the fracturing process are given in parenthesis beside the permeability values in the tables.

Figures (7.3.3) to (7.3.10) and the accompanying tables

PLATE (7.2) Test Specimens After Being Fractured During Stress-Permeability Experiments

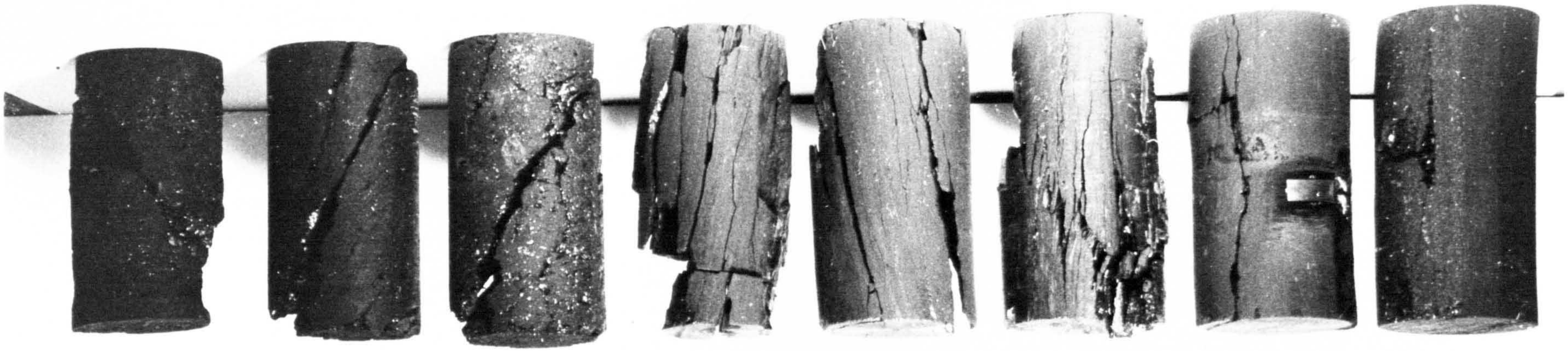

show the results of induced tensile fracturing and fracture permeability experiments conducted on the seven different coals used. As shown in the figures, permeabilities of the coal specimens increased dramatically during crushing. Due to the stress and time dependent relaxation of the coal material and the fractures, higher permeability values were obtained for the same coals tested for fracture permeabilities.

The fracturing experiments were usually carried out under identical stress conditions for all the specimens. Therefore, the intensity of fracturing was effected by the mechanical strength of the coal specimen. High mechanical strength coals like DUNSIL and DEEP HARD fractured less compared to the other coal specimens and exhibited lower fracture permeabilities. As shown in Figure (7.3.6), the first fracturing cycle for DUNSIL 3 only caused microfracturing of the specimen; the stress cycle had to be repeated to achieve full scale fracturing. Consequently, when crushed under high axial stresses, DUNSIL 7 had demonstrated similar fracturing behaviour to that exhibited by the low mechanical strength coals, see Figure (7.3.7).

The reduction in permeability of fractured coal under applied stress was very low as compared to the reductions observed for nonfractured coal. The stress-permeability curve for a fractured coal specimen followed a very gentle slope, the minimum permeabilities at $\sigma_3 = 7{\cdot}50$ MN/m^2 being only 5 to 35 times smaller than the base permeabilities. At the same stress levels, permeabilities of coal specimens were increased between 10 to 500 times after

TABLE (7.3.3) Stress-Permeability Results for ACILIK 6 Specimen (Effect of Fracturing and Fracture Permeabilities)

SAMPLE : ACILIK 6		D = 37•30 mm		L = 72•80 mm	
	RADIAL STRESS σ_3 (MN/m^2)	AXIAL STRESS σ_1 (MN/m^2)	3rd RUN/19.2.1980 PERMEABILITY K_d (10^{-16} m^2)	4th RUN/25.2.1980 PERMEABILITY K_d (10^{-16} m^2)	
LOADING	0•00	0•00	192•93	741•72	
	0•50	1•37	16•44	578•48	
	1•00	2•74	7•67	479•46	
	1•50	4•11	4•78	450•63	
	2•00	5•49	3•37	366•87	
	2•50	6•86	2•63	328•66	
	3•00	8•23	2•08	295•19	
	3•50	9•60	1•69	269•39	
	4•00	10•98	1•42	253•66	
	4•50	12•35	1•21	225•28	
	5•00	13•72	1•03	211•05	
	5•50	15•10	0•89	190•73	
	6•00	16•47	0•78	169•99	
	6•50	17•84	0•68	153•54	
	7•00	19•21	0•60	140•45	
	7•50	-	-	-	
	7•00	-	-	-	
	6•50	-	-	-	
	6•00	-	-	-	
	5•50	-	-	-	
	5•00	-	-	-	
	4•50	-	-	-	
UNLOADING	4•00	-	-	-	
	3•50	-	-	-	
	3•00	-	-	(19•21)	165•02
	2•50	-	(19•21) 4•84		-
	2•00	-	-		-
	1•50	-			-
	1•00	-	(16•47) 36•03	(8•23)	272•28
	0•50	-	-	(5•49)	311•46
	0•00	0•00	712•00		881•55

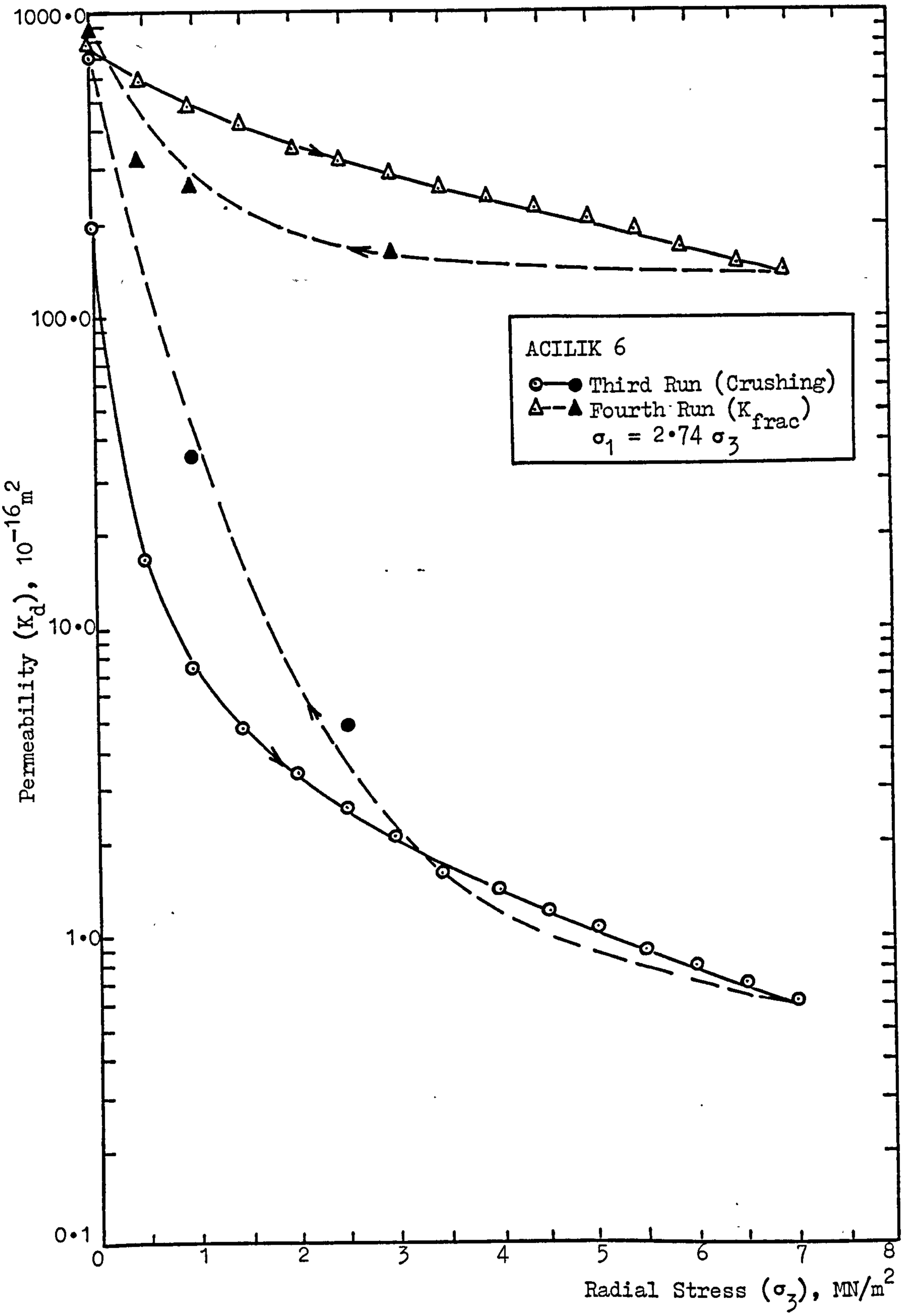

FIGURE (7.3.3) Effect of Fracturing on Permeability and Fracture Permeabilities for ACILIK Coal.

TABLE (7.3.4) Stress-Permeability Results for CAYDAMAR 2 Specimen (Effect of Fracturing and Fracture Permeabilities)

SAMPLE : CAYDAMAR 2		D = 37•25 mm		L = 72•30 mm	
	RADIAL STRESS σ_3 (MN/m^2)	AXIAL STRESS σ_1 (MN/m^2)	4^{th} RUN/26.6.1980 PERMEABILITY K_d (10^{-16} m^2)		5^{th} RUN/24.7.1980 PERMEABILITY K_d (10^{-16} m^2)
LOADING	0•00	0•00	-		947•70
	0•50	1•37	83•90		386•60
	1•00	2•75	32•30		236•40
	1•50	4•12	18•50		185•80
	2•00	5•50	11•80		146•30
	2•50	6•88	8•30		109•30
	3•00	8•25	6•60		94•80
	3•50	9•63	5•20		77•40
	4•00	11•01	4•10		67•60
	4•50	12•38	3•30		55•30
	5•00	13•76	2•80		49•00
	5•50	15•14	2•30		42•40
	6•00	16•51	2•00		38•30
	6•50	17•89	1•70		34•30
	7•00	19•27	1•40		29•10
	7•50	20•64	1•20		27•10
	7•00	-	-		-
	6•50	-	-		-
	6•00	-	(20.64) 1•40		-
	5•50	-	-	(20•64)	28•80
	5•00	-	-		-
UNLOADING	4•50	-	(20•64) 1.80		-
	4•00	-	-		-
	3•50	-	-		-
	3•00	-	-		-
	2•50	-	(19•27) 3•30		-
	2•00	-	-	(15•14)	62•30
	1•50	-	(15•14) 28•30		-
	1•00	-	-		-
	0•50	-	(4•12) 288•90	(4•12)	238•60
	0•00	0•00	-		1061•10

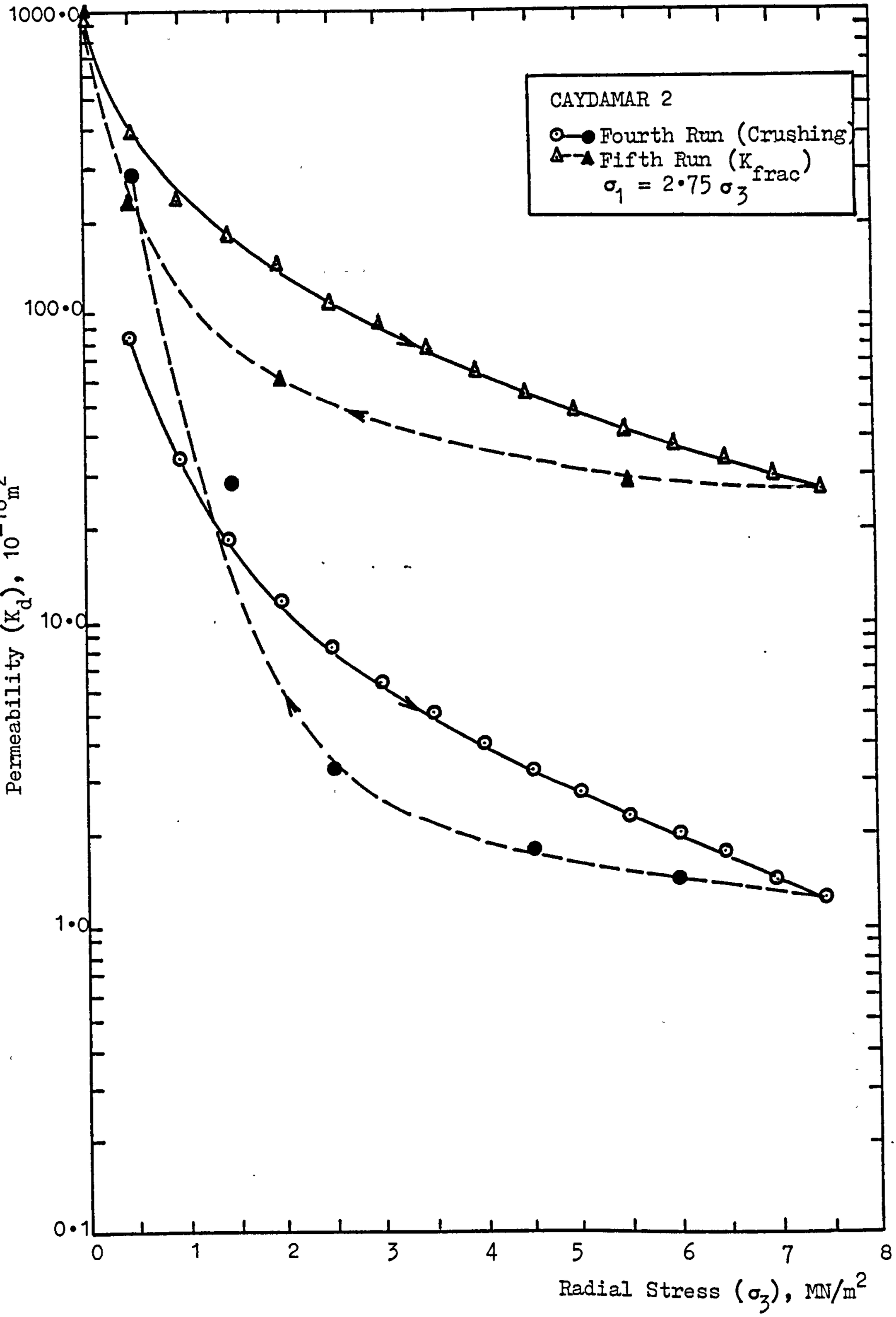

FIGURE (7.3.4) Effect of Fracturing on Permeability and Fracture Permeabilities for CAYDAMAR Coal.

TABLE (7.3.5) Stress-Permeability Results for BARNSLEY 4 Specimen (Effect of Fracturing and Fracture Permeabilities)

SAMPLE : BARNSLEY 4		D = 37·60 mm		L = 73·65 mm	
	RADIAL STRESS σ_3 (MN/m^2)	AXIAL STRESS σ_1 (MN/m^2)	1st RUN/15.10.1980 PERMEABILITY K_d (10^{-16} m^2)	2nd RUN/12.11.1980 PERMEABILITY K_d (10^{-16} m^2)	
LOADING	0·00	0·00	645·32	708·85	
	0·50	1·35	5·63	584·71	
	1·00	2·70	2·95	338·62	
	1·50	4·05	1·69	200·80	
	2·00	5·40	1·14	114·62	
	2·50	6·75	0·82	97·51	
	3·00	8·10	0·58	71·85	
	3·50	9·45	0·43	66·01	
	4·00	10·80	0·34	54·45	
	4·50	12·15	0·22	50·21	
	5·00	13·50	0·18	47·50	
	5·50	14·86	0·11	39·99	
	6·00	16·21	0·09	37·42	
	6·50	17·56	0·07	35·14	
	7·00	18·91	-	32·77	
	7·50	-	-	-	
	7·00	-	-	-	
	6·50	-	-	-	
	6·00	-	-	-	
	5·50	-	-	-	
	5·00	-	-	-	
	4·50	-	-	-	
UNLOADING	4·00	-	-	-	
	3·50	-	-	-	
	3·00	-	-	-	
	2·50	-	-	-	
	2·00	-	-	-	
	1·50	-	-	-	
	1·00	-	-	(18·91) 84·23	
	0·50	-	(17·56) 16·47	(18·91) 127·38	
	0·00	0·00	629·18	474.54	

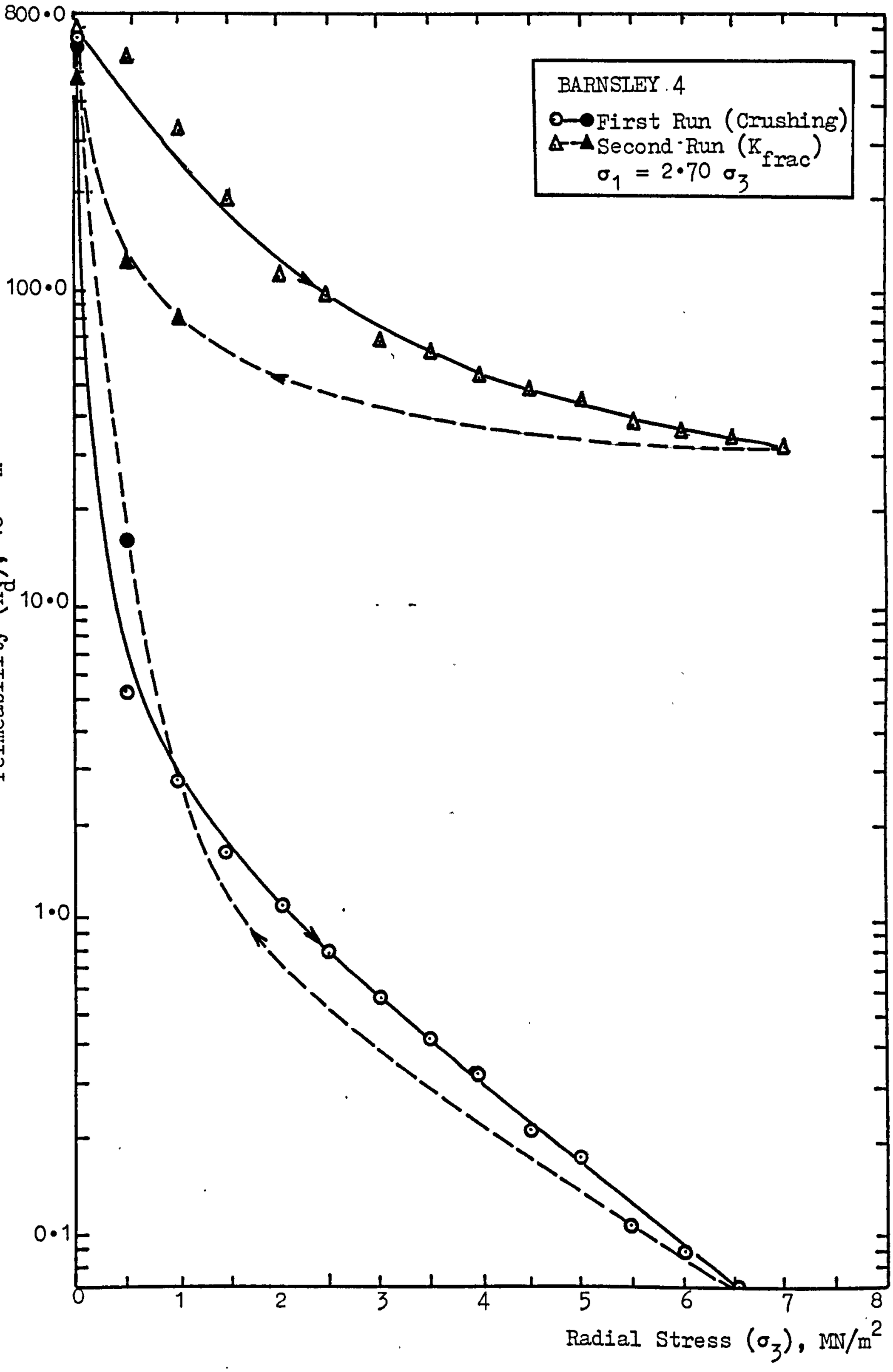

FIGURE (7.3.5) Effect of Fracturing on Permeability and Fracture Permeabilities for BARNSLEY Coal.

TABLE (7.3.6) Stress-Permeability Results for DUNSIL 3 Specimen (Effect of Fracturing and Fracture Permeabilities)

SAMPLE : DUNSIL 3		D = 37·80 mm		L = 73·85 mm	
	RADIAL STRESS σ_3 (MN/m^2)	AXIAL STRESS σ_1 (MN/m^2)	3rd RUN/27.2.81 PERMEABILITY K_d (10^{-16} m^2)	4th RUN/6.3.81 PERMEABILITY K_d (10^{-16} m^2)	5th RUN/9.3.81 PERMEABILITY K_d (10^{-16} m^2)
LOADING	0·00	0·00	167·44	189·87	64·50
	0·50	1·37	18·16	24·60	52·37
	1·00	2·67	10·35	11·52	42·63
	1·50	4·01	6·58	7·34	33·98
	2·00	5·34	4·61	5·26	30·96
	2·50	6·68	3·53	3·94	27·39
	3·00	8·02	2·67	2·91	24·43
	3·50	9·35	2·04	2·23	21·65
	4·00	10·69	1·60	1·74	19·50
	4·50	12·03	1·31	1·43	17·57
	5·00	13·36	1·03	1·11	15·87
	5·50	14·25	0·89	0·92	14·18
	6·00	16·04	0·75	0·77	12·70
	6·50	17·37	0·62	0·65	11·43
	7·00	18·71	0·52	0·55	10·10
	7·50	20·05	0·43	0·46	9·53
	7·00	-	-	-	-
	6·50	-	-	-	-
	6·00	-	-	-	-
	5·50	-	-	-	-
	5·00	-	-	-	-
	4·50	-	-	-	-
	4·00	-	-	-	-
	3·50	-	-	-	-
	3·00	-	-	-	-
	2·50	-	-	-	-
	2·00	-	-	(17·37) 3·37	-
UNLOADING	1·50	-	(16·04) 3·57	(12·03) 48·92	(13·36) 22·69
	1·00	-	-	-	-
	0·50	-	(16·04) 11·27	(12·03) 53·60	(9·33) 33·68
	0·00	0·00	341·46	64·67	75.10

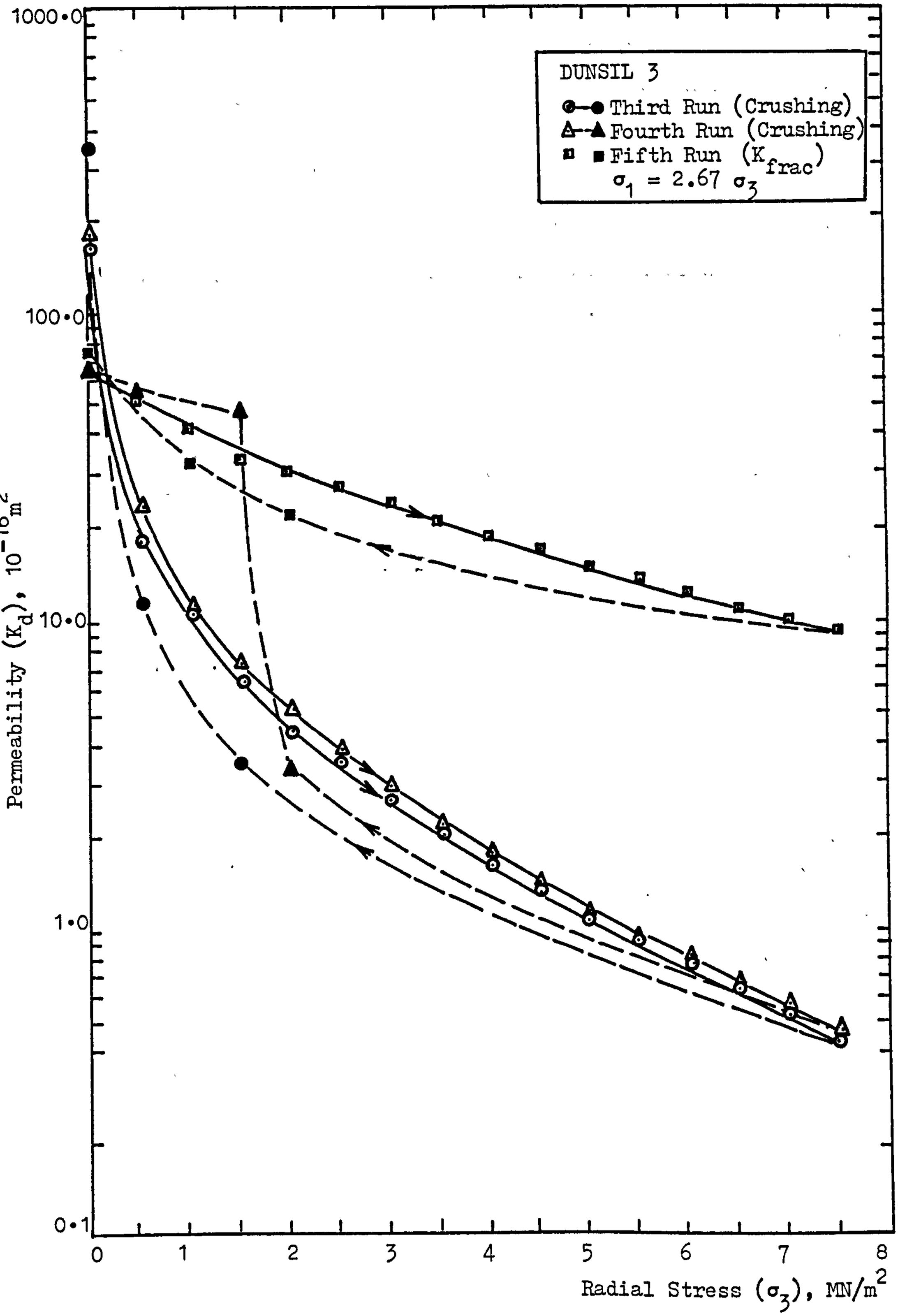

FIGURE (7.3.6) Effect of Fracturing on Permeability and Fracture Permeabilties for DUNSIL Coal.

TABLE (7.3.7) Stress-Permeability Results for DUNSIL 7 Specimen (Effect of Fracturing and Fracture Permeabilities)

SAMPLE : DUNSIL 7		D = 37•75 mm		L = 74•95 mm	
	RADIAL STRESS σ_3 (MN/m^2)	AXIAL STRESS σ_1 (MN/m^2)	1st RUN/6.3.1981 PERMEABILITY K_d (10^{-16} m^2)	2nd RUN/9.3.1981 PERMEABILITY K_d (10^{-16} m^2)	
LOADING	0•00	0:00	371:73	376•10	
	0:50	1:34	5:71	236:38	
	1:00	2:68	2:92	200:85	
	1:50	4:02	1:95	164:20	
	2:00	5:36	1:28	131:30	
	2:50	6:70	0:94	113:90	
	3:00	8:04	0:74	95:64	
	3:50	9:38	0:53	79:39	
	4:00	10:72	0:42	68:00	
	4:50	12:06	0:31	58:44	
	5:00	13:40	0:26	51:65	
	5:50	14:29	0:22	43:95	
	6:00	16:08	0:18	39:00	
	6:50	17:42	0:15	33:84	
	7:00	18:76	0:13	30:90	
	7:50	29:48	0:11	27:22	
UNLOADING	7:00	-	-	-	
	6:50	-	-	-	
	6:00	-	-	-	
	5:50	-	-	-	
	5:00	-	-	-	
	4:50	-	-	-	
	4:00	-	-	-	
	3:50	-	-	-	
	3:00	-	-	-	
	2:50	-	-	-	
	2:00	-	-	-	
	1:50	-	-	(17:42)	74:36
	1:00	-	(26:80)	124:37	-
	0:50	-	(20:10)	125:13	(16:08) 131:99
	0:00	0:00		371:32	356:88

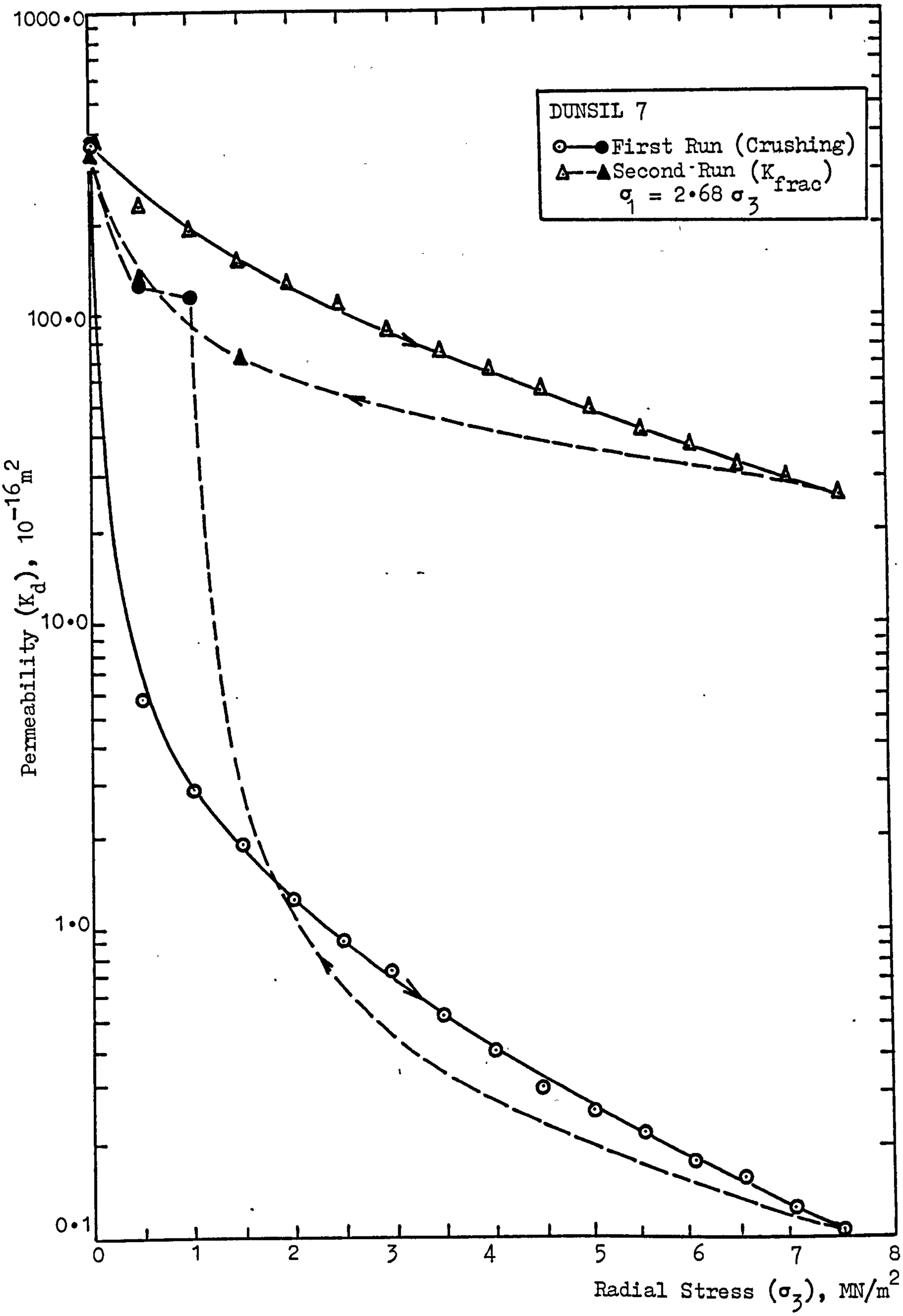

FIGURE (7.3.7) Effect of Fracturing on Permeability and Fracture Permeabilities for DUNSIL Coal.

TABLE (7.3.8) Stress-Permeability Results for DEEP HARD 1 Specimen (Effect of Fracturing and Fracture Permeabilities)

SAMPLE : DEEP HARD 1		D = 37·60 mm		L = 73·80 mm	
	RADIAL STRESS σ_3 (MN/m^2)	AXIAL STRESS σ_1 (MN/m^2)	3rd RUN/27.4.1981 PERMEABILITY K_d (10^{-16} m^2)	4th RUN/30.4.1981 PERMEABILITY K_d (10^{-16} m^2)	
LOADING	0·00	0·00	404·09	430·28	
	0·50	1·35	32·53	56·17	
	1·00	2·70	18·74	45·00	
	1·50	4·05	9·34	35·46	
	2·00	5·40	5·77	28·84	
	2·50	6·75	3·66	23·41	
	3·00	8·10	2·60	18·67	
	3·50	9·45	1·80	14·74	
	4·00	10·80	1·34	12·44	
	4·50	12·15	0·97	9·49	
	5·00	13·50	0·76	6·74	
	5·50	14·86	0·59	5·32	
	6·00	16·21	0·45	5·15	
	6·50	17·11	0·36	3·86	
	7·00	18·91	0·30	3·37	
	7·50	20·30	-	2·83	
	7·00	-	-	-	
	6·50	-	-	-	
	6·00	-	-	-	
	5·50	-	-	-	
	5·00	-	-	-	
	4·50	-	-	-	
UNLOADING	4·00	-	-	-	
	3·50	-	-	-	
	3·00	-	-	-	
	2·50	-	-	-	
	2·00	-	-	-	
	1·50	-	-	(17·11) 18·34	
	1·00	-	(18·91) 1·90	-	
	0·50	-	(18·91) 156·36	(17·11) 43·45	
	0·00	0·00	486·38	385·46	

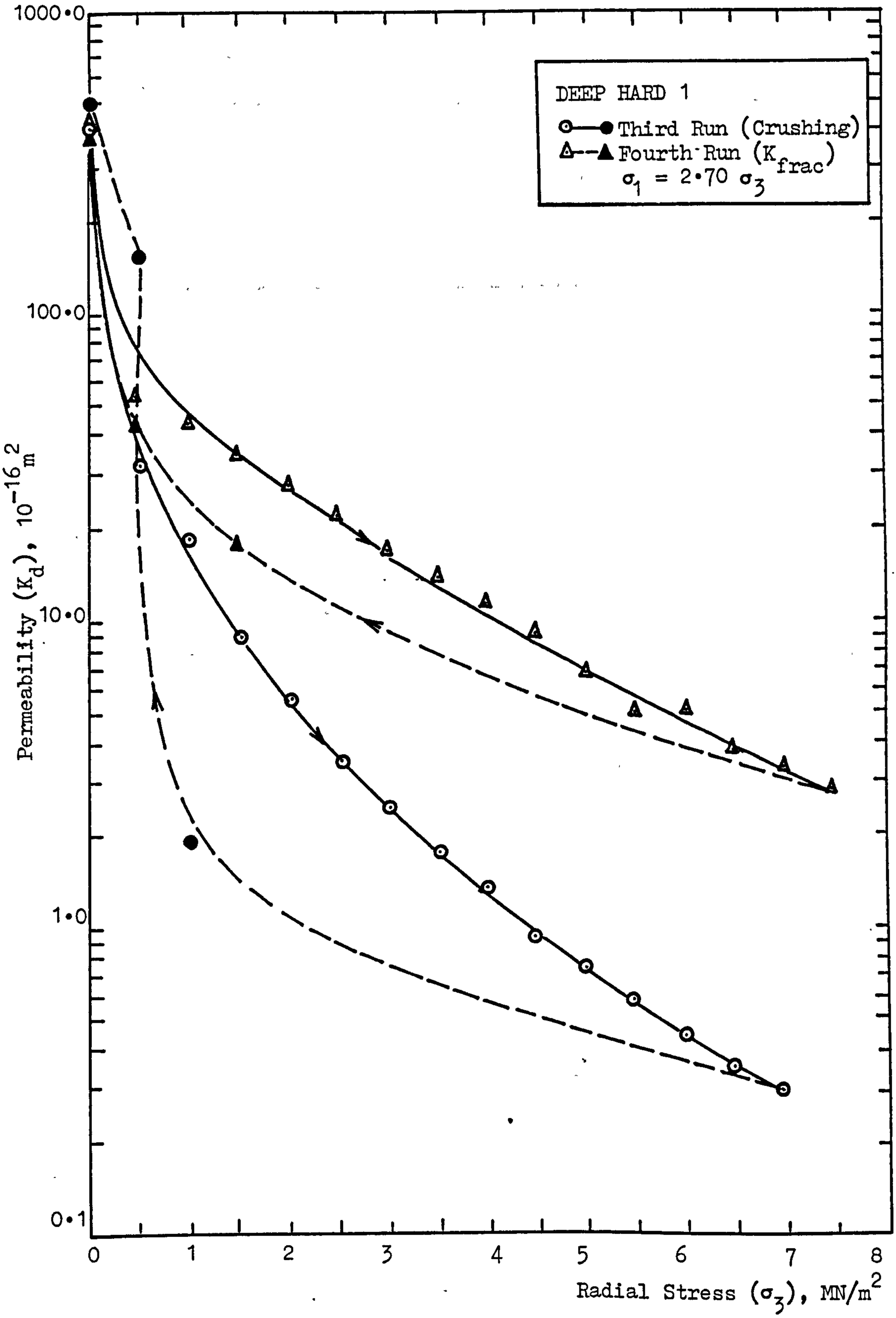

FIGURE (7.3.8) Effect of Fracturing on Permeability and Fracture Permeabilities for DEEP HARD Coal.

TABLE (7.3.9) Stress-Permeability Results for COCKSHEAD 5 Specimen (Effect of Fracturing and Fracture Permeabilities)

SAMPLE : COCKSHEAD 5		D = 37·30 mm		L = 73·85 mm	
	RADIAL STRESS σ_3 (MN/m^2)	AXIAL STRESS σ_1 (MN/m^2)	1st RUN/17.6.1981 PERMEABILITY K_d (10^{-16} m^2)	2nd RUN/22.6.1981 PERMEABILITY K_d (10^{-16} m^2)	
LOADING	0·00	0:00	195:06	398·45	
	0·50	1:37	95:43	59:41	
	1:00	2·74	42:36	61·19	
	1·50	4·11	19·32	59:41	
	2·00	5:49	13·10	58·70	
	2·50	6·86	9:25	57·99	
	3·00	8:23	6:34	57·63	
	3·50	9·60	4:14	57·10	
	4·00	10·98	2:93	56:03	
	4·50	12:35	2:04	55·42	
	5:00	13·72	1:63	54:97	
	5:50	15·10	1:50	53:63	
	6:00	16·47	1:13	53:23	
	6:50	17:38	0:91	52:43	
	7:00	19·28	0·74	51·63	
	7:50	-	-	-	
	7·00	-	-	-	
	6·50	-	-	-	
	6·00	-	-	-	
	5:50	-	-	-	
	5·00	-	-	-	
	4·50	-	-	-	
UNLOADING	4·00	-	-	-	
	3·50	-	-	-	
	3:00	-	-	-	
	2·50	-	-	-	
	2·00	-	-	-	
	1·50	-	(13·72) 6·71	(10·98) 50·70	
	1·00	-	-	-	
	0:50	-	(6·86) 17·94	(4·11) 54·96	
	0·00	0·00	395·42	411·26	

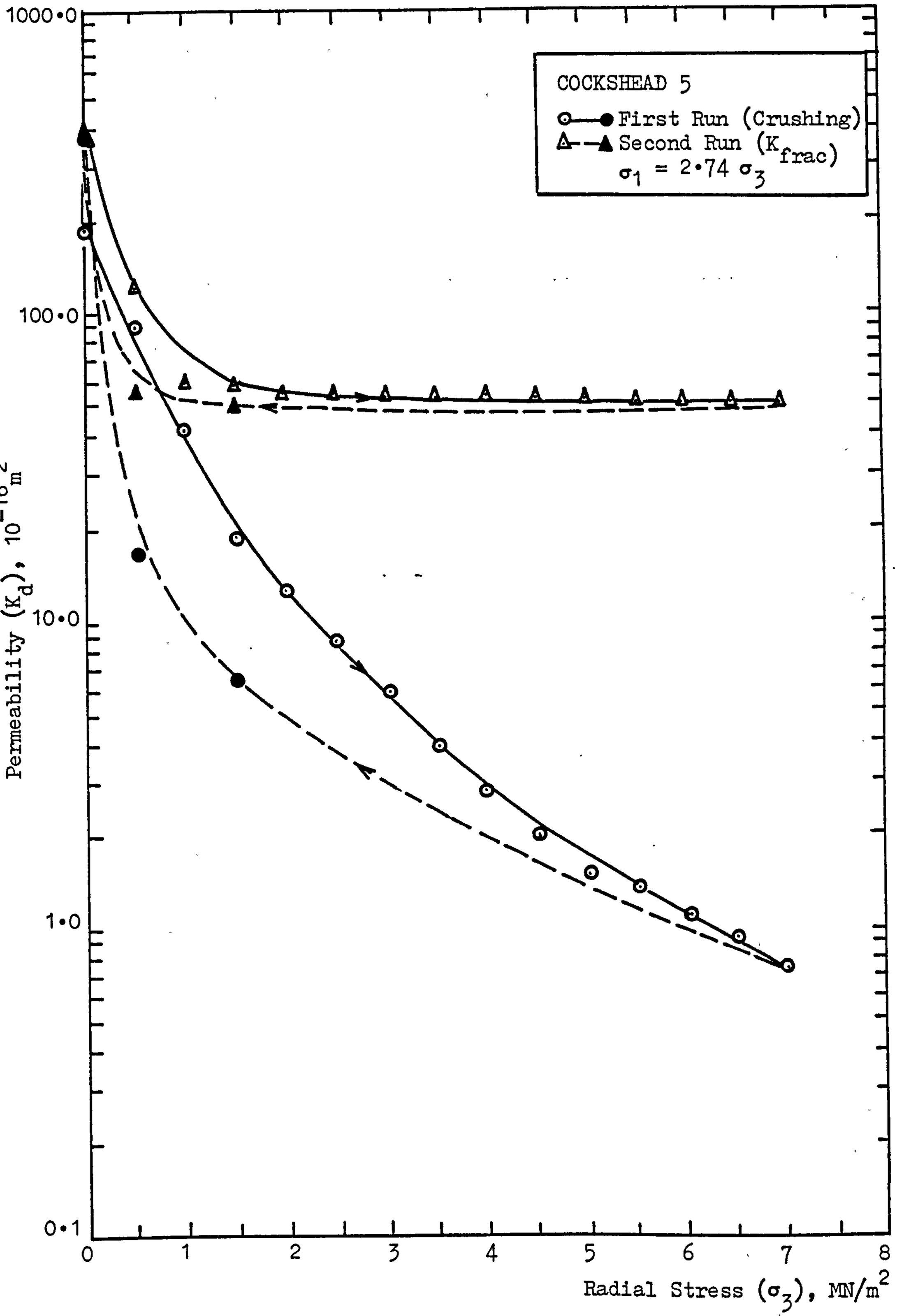

FIGURE (7.3.9) Effect of Fracturing on Permeability and Fracture Permeabilities for COCKSHEAD Coal.

TABLE (7.3.10) Stress-Permeability Results for BANBURY 1 Specimen (Effect of Fracturing and Fracture Permeabilities)

SAMPLE : BANBURY 1		D = 37·35 mm		L = 73·85 mm	
	RADIAL STRESS σ_3 (MN/m^2)	AXIAL STRESS σ_1 (MN/m^2)	3rd RUN/22.6.1981 PERMEABILITY K_d (10^{-16} m^2)	4th RUN/24.6.1981 PERMEABILITY K_d (10^{-16} m^2)	
LOADING	0·00	0·00	392·52	485·38	
	0·50	1·37	25·31	386·70	
	1·00	2·73	7·82	372·16	
	1·50	4·10	3·06	323·71	
	2·00	5·47	3·14	299·50	
	2·50	6·84	2·04	273·28	
	3·00	8·21	1·52	252·96	
	3·50	9·58	1·02	232·02	
	4·00	10·95	0·78	215·66	
	4·50	12·32	0·57	199·83	
	5·00	13·69	0·51	148·11	
	5·50	15·06	0·41	129·43	
	6·00	16·42	0·33	118·54	
	6·50	17·79	0·25	106·25	
	7·00	19·16	0·19	93·36	
	7·50	-	-	-	
UNLOADING	7·00	-	-	-	
	6·50	-	-	-	
	6·00	-	-	-	
	5·50	-	-	-	
	5·00	-	-	-	
	4·50	-	-	-	
	4·00	-	-	-	
	3·50	-	-	-	
	3·00	-	-	-	
	2·50	-	-	-	
	2·00	-	(12·32) 128·47	(9·60) 161·79	
	1·50	-	-	-	
	1·00	-	-	-	
	0·50	-	(4·10) 212·50	(4·10) 337·28	
	0·00	0·00	482·18	463·37	

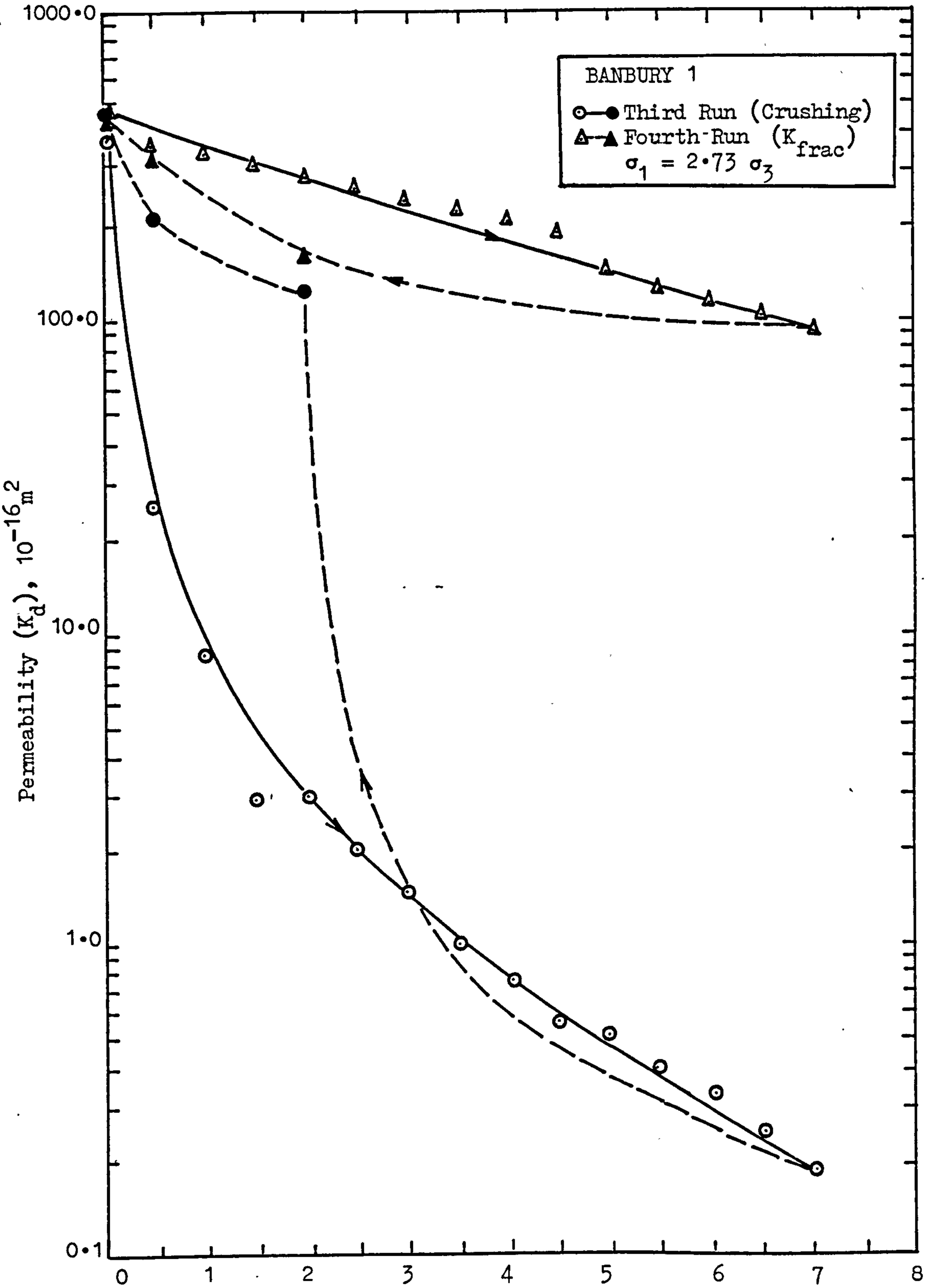

FIGURE (7.3.10) Effect of Fracturing on Permeability and Fracture Permeabilities for BANBURY Coal.

fracturing. Fracture permeabilities for all rank and structural property coals were of similar magnitudes. Therefore, some coals possessing very low permeabilities have shown higher rates of permeability increase .

In the light of the above observations, the following conclusions can be drawn:

1. Fracturing and failing of coal seams, in and around seams being worked, are most likely to happen in the crushing zone causing dramatic increases in permeability.
2. Fracture permeabilities of coal under stress are about 10 to 500 times higher than that of nonfractured coal. Fracture permeabilities of all rank coals are of very similar magnitudes as opposed to the high level of variation in permeabilities of different rank nonfractured coals under stress.
3. The effect of increasing stress on permeability of fractured coal is very small. This in practice can be seen in the recompaction zone, where very little change in permeability and most of the gas flow is to be expected.

7.4 The Effect of Moisture on Permeability of Coals Under Stress

It has been suggested (39),(40), that adsorbed moisture reduces the methane capacity of coal and plays a major role in retarding the flow of methane through the seam into the mining areas (15). A series of stress-permeability experiments were

carried out in an attempt to investigate the effect of moisture on permeability of coal under stress.

Having established an understanding of the effect of repeated loading on permeability of coal specimens, experiments were carried out where the moisture content of the coal specimen was changed between two consecutive test runs and relative change in permeability was observed. Experiments were, in the main part, carried out on coals with higher degrees of elasticity which normally exhibit a continuous decrease in permeability after each run.

Prior to the first loading/unloading experiment, the test specimens were saturated with water under vacuum for twenty four hours. The increase in moisture content was noted and the specimen was tested for stress-permeability relationship. Following the first loading/unloading experiment the specimen was oven dried at 80°C and relaxed for a period of time. After the second loading/unloading experiment on the dry specimen, any deflection from the usual stress-permeability behaviour of that coal was regarded as the effect of reduction in moisture.

Figure (7.4.1) shows the results of two consecutive stress-permeability experiments on ACILIK 8. The first run was with 1.63% moisture content and the second run was on dry coal. Due to the experimental experience gained on its stress-permeability behaviour, ACILIK coal was not expected to microfracture during the first run. If the specimen was not dried prior to testing for the second time one could hypothesise that it would follow a

TABLE (7.4.1) Stress-Permeability Results for ACILIK 8 Specimen (Effect of Moisture)

SAMPLE : ACILIK 8		D = 37•30 mm	L = 74•05 mm	
	RADIAL STRESS σ_3 (MN/m^2)	AXIAL STRESS σ_1 (MN/m^2)	1st RUN/1.2.80 PERMEABILITY K_d (10^{-16} m^2)	2nd RUN/8.2.80 PERMEABILITY K_d (10^{-16} m^2)	2nd RUN PERMEABILITY (HYPOTHETICAL) K_d (10^{-16} m^2)
LOADING	0•00	0•00	106•62	188•95	-
	0•50	1•37	22•14	26•70	-
	1•00	2•74	12•37	12•15	9•00
	1•50	4•11	7•56	7•22	6•00
	2•00	5•49	5•32	5•41	4•20
	2•50	6•86	4•06	4•22	3•10
	3•00	8•23	3•06	3•44	2•30
	3•50	9•60	2•34	2•71	1•70
	4•00	10•98	1•82	2•25	1•40
	4•50	12•35	1•48	1•88	1•15
	5•00	13•72	1•21	1•61	0•96
	5•50	15•10	0•95	1•41	0•80
	6•00	16•47	0•81	1•23	0•68
	6•50	17•84	0•69	1•08	0•58
	7•00	19•21	0•59	0•90	0•50
	7•50	20•59	0•52	0•85	0•42
UNLOADING	7•00	19•21	0•52	0•89	0•44
	6•50	17•84	0•55	0•95	0•47
	6•00	16•47	0•60	1•00	0•50
	5•50	15•10	0•63	1•08	0•53
	5•00	13•72	0•70	1•19	0•58
	4•50	12•35	0•77	1•27	0•64
	4•00	10•98	0•89	1•30	0•72
	3•50	9•60	1•07	1•72	0•84
	3•00	8•23	1•33	1•99	1•05
	2•50	6•86	1•58	2•60	1•40
	2•00	5•49	2•65	3•83	2•00
	1•50	4•11	4•66	4•30	3•20
	1•00	2•74	9•84	8•87	6•40
	0•50	1•37	15•02	24•32	-
	0•00	0•00	158•60	235•68	-

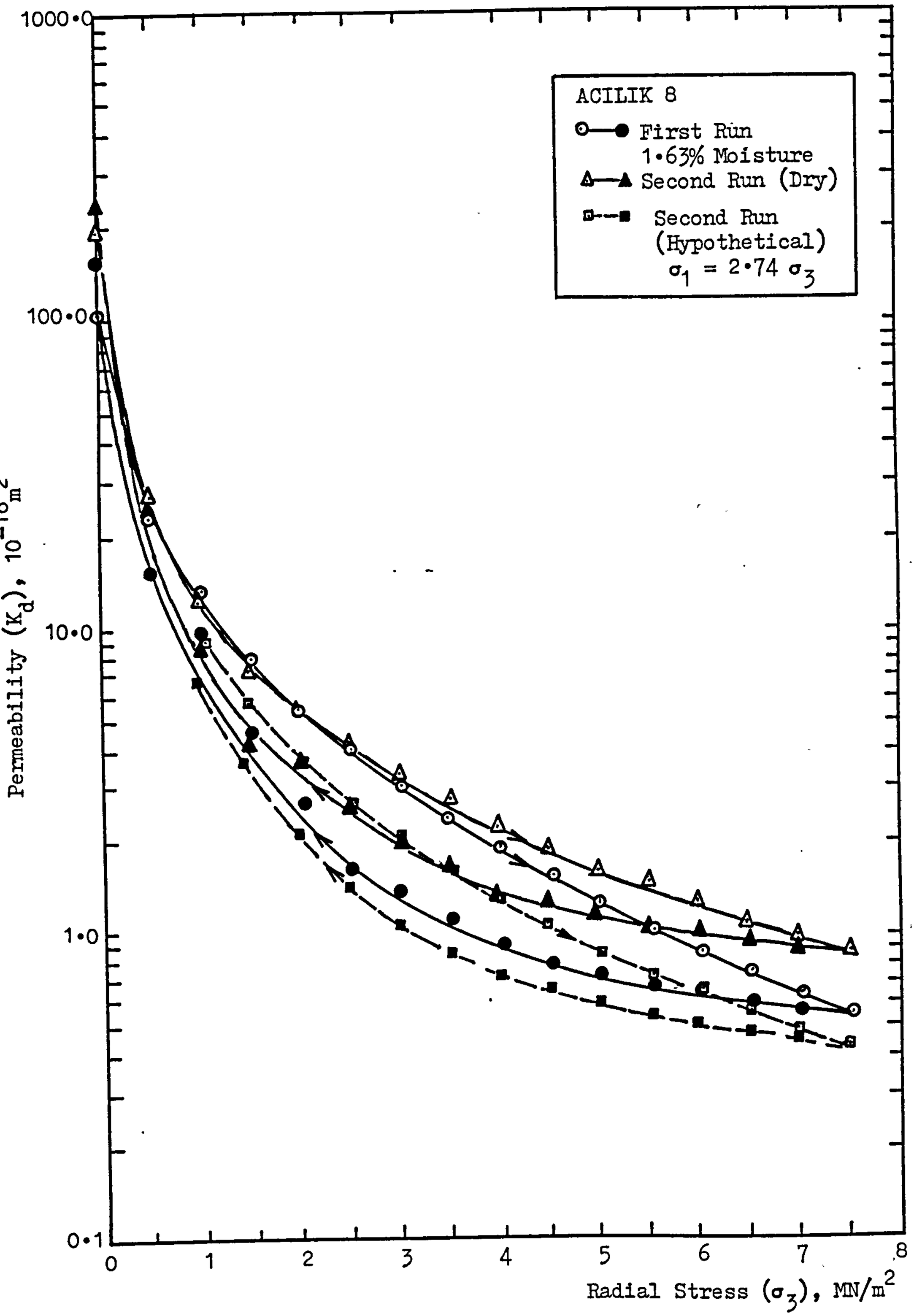

FIGURE (7.4.1) Effect of Moisture on Permeability of ACILIK Coal Under Stress.

lower permeability path similar to the one illustrated by broken lines. However, the second loading permeabilities for the dry coal were higher than the permeabilities for the first loading. When compared to the hypothetical permeability curve, permeability of the dry specimen had increased between $3{\cdot}00 \times 10^{-16}$ m^2 and $0{\cdot}40 \times 10^{-16}$ m^2 at stresses $\sigma_3 = 1{\cdot}00$ MN/m^2 and $\sigma_3 = 7{\cdot}50$ MN/m^2 respectively.

Figure (7.4.2) shows the stress-permeability curves for the three consecutive runs on BARNSLEY 2 where the saturated moisture in the specimen was dried off in two stages. On the assumption that no microfracturing took place during the whole experiment, the implications of the results were in total agreement with the methane sorption data reported by Joubert et al. (40). When a part of the artificially added moisture was removed from the specimen, it had no apparent effect on permeability; the second loading/unloading curve showed the highly plastic deformation character of BARNSLEY coal with a considerable decrease in permeability. It was only after the complete removal of moisture that the permeability of the specimen was increased as shown in the third loading/unloading curve.

In their research into the effect of moisture on the methane capacity of American coals, Joubert et al. (40) concluded that:

> "only adsorbed water affects the equilibrium capacity of a coal for methane; water present in excess of the adsorbed water has no effect on methane sorption".

TABLE (7.4.2) Stress-Permeability Results for BARNSLEY 2 Specimen (Effect of Moisture)

SAMPLE : BARNSLEY 2		D = 37·80 mm	L = 74·15 mm	
	RADIAL STRESS σ_3 (MN/m^2)	AXIAL STRESS σ_1 (MN/m^2)	1st RUN/27.8.80 PERMEABILITY K_d (10^{-16} m^2)	2nd RUN/29.8.80 PERMEABILITY K_d (10^{-16} m^2)	3rd RUN/4.9.80 PERMEABILITY K_d (10^{-16} m^2)
LOADING	0·00	0·00	341·12	327·76	290·88
	0·50	1·33	135·75	34·97	40·50
	1·00	2·66	87·05	14·93	14·22
	1·50	3·99	64·18	8·01	7·63
	2·00	5·33	41·37	4·30	5·00
	2·50	6·66	28·95	2·93	3·37
	3·00	7·99	18·22	2·10	2·56
	3·50	9·33	10·84	1·62	1·99
	4·00	10·66	7·17	1·19	1·53
	4·50	11·99	5·04	0·95	1·27
	5·00	13·33	3·53	0·69	1·10
	5·50	14·66	2·52	0·47	0·89
	6·00	15·99	1·92	0·32	0·63
	6·50	17·33	1·48	0·25	0·55
	7·00	18·66	1·18	0·21	0·48
	7·50	19·99	0·96	0·21	-
	7·00	18·66	0·99	0·21	-
	6·50	17·33	1·08	0·21	0·56
	6·00	15·99	1·22	0·24	0·56
	5·50	14·66	1·48	0·26	0·63
	5·00	13·33	1·77	0·28	0·74
UNLOADING	4·50	11·99	2·33	0·32	0·89
	4·00	10·66	2·94	0·36	0·99
	3·50	9·33	4·39	0·49	1·22
	3·00	7·99	7·65	0·87	1·53
	2·50	6·66	12·13	1·29	2·02
	2·00	5·33	18·16	2·00	2·58
	1·50	3·99	27·47	3·23	5·03
	1·00	2·66	39·02	7·77	7·41
	0·50	1·33	57·84	19·01	21·69
	0·00	0·00	245·18	91·58	960·06

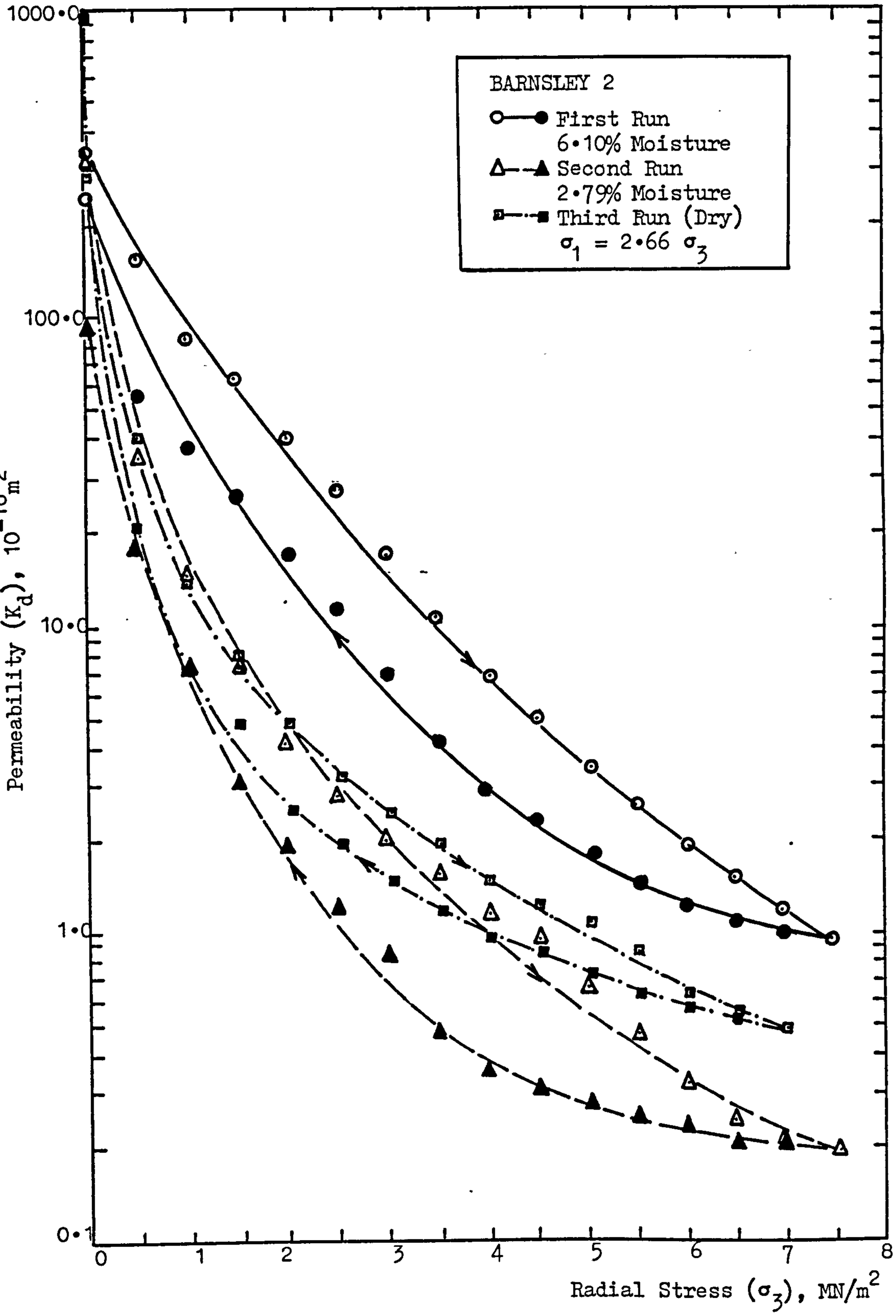

FIGURE (7.4.2) Effect of Moisture on Permeability of BARNSLEY Coal Under Stress.

In view of the above observations, the same might be held valid for the gas permeabilities of coal under stress. Unfortunately, the permeability results obtained for BARNSLEY 2 were the only ones of the kind and no generalisation could be made from these.

One very important outcome of the stress-permeability experiments on water saturated coals was that the observations pointed out that the two-phase flow characteristics of gas and water should be considered in models for predicting firedamp emissions. Kissel(15),(73)and Price et al. (74) reported that the gas permeability of seams in older regions of a mine increased vastly as the water and methane in the seam drained into the mine. This phenomenon was illustrated in a number of test specimens throughout this research, one will be discussed here.

CAYDAMAR 8 was saturated with 1•95% moisture and tested for the effect of moisture on permeability of coal under stress. During the early stages of the first loading experiment, it was noted that both water and gas were flowing from the downstream end of the specimen. As the free water in the pore spaces drained with the gas flow, a relative increase in permeability of the specimen was observed. The horizontal section of the first loading curve in Figure (7.4.3) illustrates the relative increase in permeability as the water is driven off. At the end of the first loading/unloading experiment, moisture content was measured and found to have decreased by 0•48%.

The above observations suggest that if a freshly mined

TABLE (7.4.3) Stress-Permeability Results for CAYDAMAR 8 Specimen (Effect of Moisture)

SAMPLE : CAYDAMAR 8		D = 37•45 mm	L = 73•20 mm
	RADIAL STRESS σ_3 (MN/m^2)	AXIAL STRESS σ_1 (MN/m^2)	1st RUN/28.11.1980 PERMEABILITY K_d (10^{-16} m^2)	2nd RUN/3.12.1980 PERMEABILITY K_d (10^{-16} m^2)
LOADING	0•00	0•00	162•21	217•14
	0•50	1•36	21•58	37•94
	1•00	2•72	20•83	28•40
	1•50	4•08	18•66	22•40
	2•00	5•44	17•27	19•61
	2•50	6•80	14•99	16•46
	3•00	8•17	13•03	13•82
	3•50	9•53	10•75	11•00
	4•00	10•89	8•79	8•97
	4•50	12•25	7•27	7•76
	5•00	13•61	5•86	6•29
	5•50	14•97	4•98	5•18
	6•00	16•34	4•19	4•40
	6•50	17•70	3•37	3•81
	7•00	19•06	2•73	3•20
	7•50	20•42	2•20	2•76
UNLOADING	7•00	19•06	2•44	3•07
	6•50	17•70	2•79	3•39
	6•00	16•37	3•22	3•87
	5•50	14•97	3•62	4•22
	5•00	13•61	4•17	4•81
	4•50	12•25	5•04	5•94
	4•00	10•89	5•95	6•28
	3•50	9•53	8•79	7•95
	3•00	8•17	8•75	9•94
	2•50	6•80	9•10	11•40
	2•00	5•44	10•18	14•43
	1•50	4•08	13•15	17•80
	1•00	2•72	15•88	22•05
	0•50	1•36	23•41	32•31
	0•00	0•00	138•90	250•31

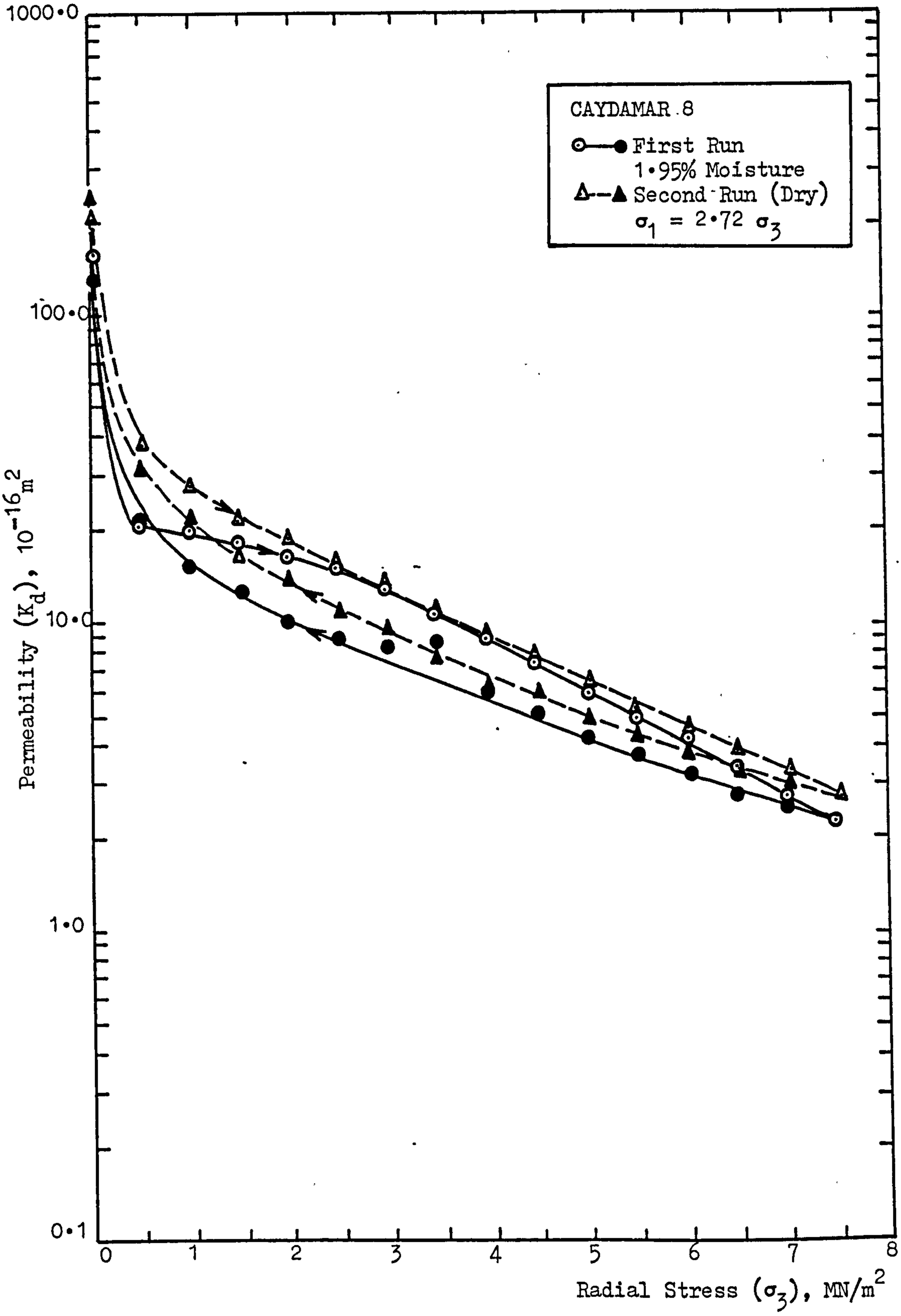

FIGURE (7.4.3) Effect of Moisture on Permeability of CAYDAMAR Coal Under Stress.

area of a coal seam contains water , its permeability to gas will be relatively low in the early stages. The increase in permeability of coal seams behind the face may be caused in part by the time dependent decrease of water due to drainage. Further research is to be carried out to determine the methane relative permeabilities and water relative permeabilities for coal and the two phase flow of gas and water is to be considered in simulation studies.

7.5 Directional Anisotropy of Coal Permeability Under Stress

Almost all the stress-permeability experiments in this research were carried out on coal specimens cored parallel to the bedding planes. This was mainly due to the fact that the maximum core recovery from a limited number of lumps was only possible by coring parallel to the bedding planes. Consequently, the flow of gas was also parallel to the bedding planes during the experiments.

In order to investigate the directional changes in permeability of coal under stress, a number of BARNSLEY specimens were cored perpendicular to the bedding planes. Figure (7.5.1) shows the results of stress-permeability measurements on BARNSLEY 10 specimen, where the gas flow and the maximum principal stress σ_1 were perpendicular to the bedding planes.

As seen in the figure, the base permeability for the specimen was $K_d = 150{\cdot}00 \times 10^{-16}$ m^2, similar to the base permeabilities obtained for other BARNSLEY specimens. As the applied stresses were increased to $\sigma_3 = 0{\cdot}50$ MN/m^2 , $\sigma_1 = 1{\cdot}35$ MN/m^2, no flow measurements were possible. The specimen was virtually impermeable

TABLE (7.5.1) Stress-Permeability Results for BARNSLEY 10 Specimen (Directional Anisotropy of Coal Permeability)

BARNSLEY 10	D = 37•65 mm L = 73•80 mm	
RADIAL STRESS σ_3 (MN/m^2)	AXIAL STRESS σ_1 (MN/m^2)	PERMEABILITY K_d ($10^{-16} m^2$)
0•00	0•00	150•00
0•50	1•37	0•00
7•50	20•21	0•00
0•50	16•16	16•24
7•50	28•00	0•00
0•50	20•21	19•34
7•50	35•00	0•00
0•50	29•19	24•12
7•50	38•00	0•00
0•50	31•88	32•07
0•00	0•00	612•19

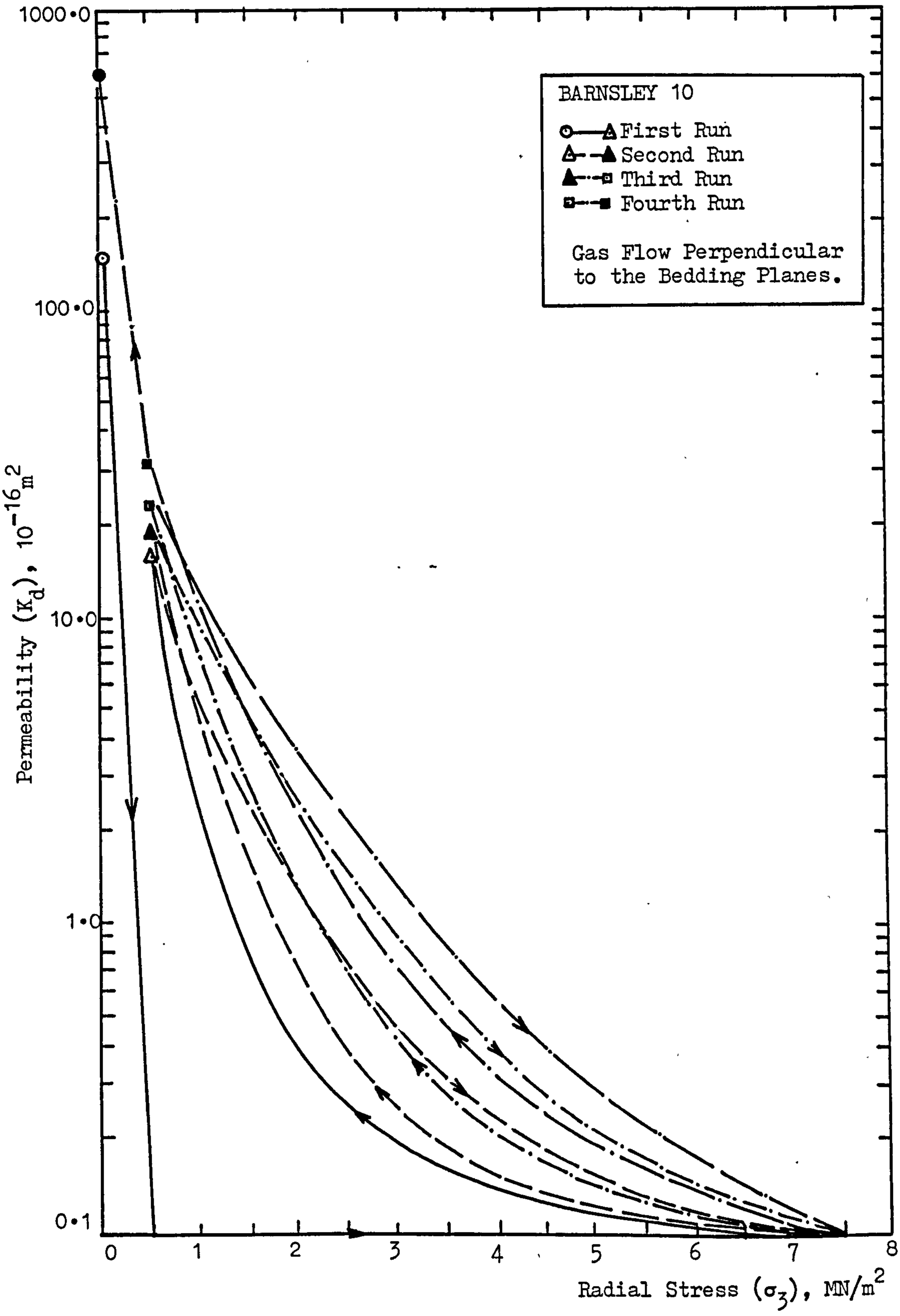

FIGURE (7.5.1) Stress-Permeability Results for BARNSLEY 10 Specimen.

perpendicular to the bedding planes. The stresses were then brought to $\sigma_3 = 7{\cdot}50$ MN/m^2 , $\sigma_1 = 20{\cdot}21$ MN/m^2, with no change in permeability observed, the specimen was crushed by releasing the radial stress. Permeability at $\sigma_3 = 0{\cdot}50$ MN/m^2 was increased to $K_d = 16{\cdot}24 \times 10^{-16}$ m^2. Cycles of increased stresses and crushing caused a further increase in permeability and the specimen was broken along the bedding plane, normal to the maximum principal stress.

Experiments have shown that the permeability of coal under stress is directionally anisotropic showing higher gas permeabilities along the bedding planes. Fracturing of coal is always along the planes of weakness independent of the direction of maximum principal stress. Unless highly fissured in the opposite direction, most of the gas flow should be expected along the bedding planes of the coal seams.

7.6 Observations on the Stress-Permeability Relationship of Coals with Different Physical and Mechanical Properties

It is a known fact that the mechanical strength of coal would effect its fracturing properties. Very low mechanical strength coals such as BANBURY, CAYDAMAR and ACILIK, were fractured easily under equivalent stress levels representing the stress conditions in the crushing zone of a working longwall face, whereas the highest mechanical strength coal, DUNSIL, necessitated the use of higher stress levels to achieve fracturing.

On the other hand, it was usually the very high or very low mechanical strength coals that microfractured during the loading/unloading experiments. This resulted in a relative increase in their permeability after relaxation. It was not possible to establish a clear relationship between the mechanical strength and microfracturing properties of coal, however it is believed that the properties of the mineral constituents, and the effects of techtonic activities on strength and brittleness of coal, would contribute to its microfracturing properties.

The effective porosities of some of the test specimens measured by the author, (see Table (7.1.3), indicated a similar relationship between the rank and porosity to that suggested by King and Wilkins (31). Figure (7.6.1) shows a comparison of these two sets of results. The degree of reduction in permeability of coals was found to be highest for low porosity coals. However, no single correlation between porosity and the stress-permeability behaviour of coals was made since other properties such as the compressibility of the coal material and the impurities (percent ash) in it would contribute to the rate of reduction in permeability under stress.

A more detailed discussion of the stress-permeability relationship of different coals will be presented in the following chapter.

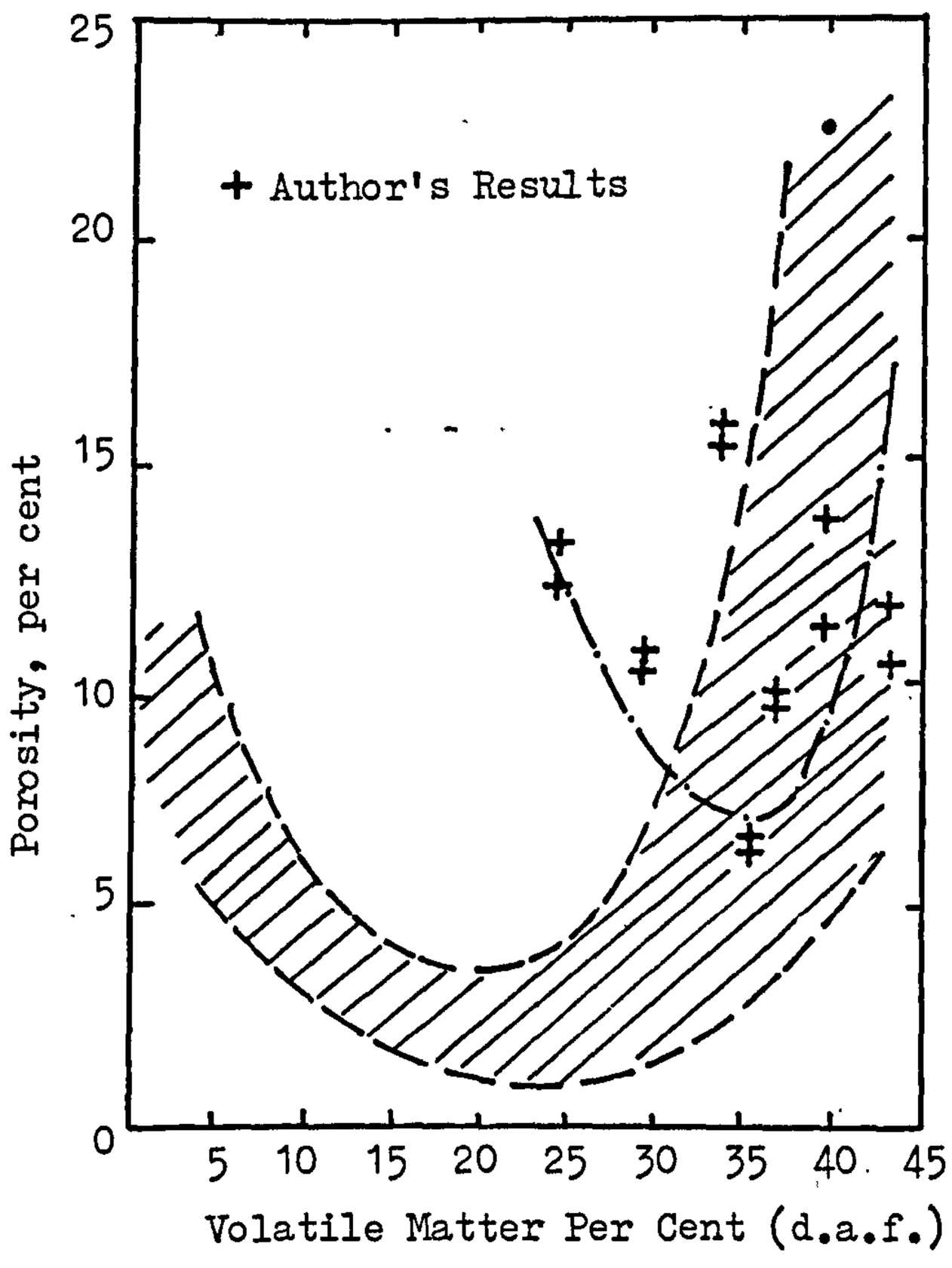

FIGURE (7.6.1) Comparison of Author's Results with Coal Porosities Obtained by King and Wilkins (31)).

CHAPTER EIGHT

DISCUSSION ON THE GENERALISED STRESS-PERMEABILITY BEHAVIOUR OF COALS TESTED

CHAPTER EIGHT

DISCUSSION ON THE GENERALISED STRESS-PERMEABILITY BEHAVIOUR OF COALS TESTED

8.1 Introduction

Although there has been a considerable amount of research concerned with ways of understanding the effect of applied stress on permeability of coals in general, no work on the correlation between the stress-permeability behaviour of different coals is reported in literature.

Within the frame of reference provided by the results obtained from stress-permeability experiments on seven different coals, it was observed that it was possible to establish a relationship between the rank and permeability of coal under stress.

This chapter discusses the above relationship and the attempts made throughout this research to establish an empirical relation between applied stress and permeability of the coals tested.

8.2 Permeabilities of Different Coals Under Stress

Due to the variations in the amount of minor fractures contained in every specimen, a large scatter of permeability results were obtained for each coal. Table (8.2.1) shows the minimum and maximum permeability values obtained from a number of specimens of each type of coal under certain stress levels. It was found that specimens yielding low permeability values were those containing the least number of fissures artificially created during coring and specimen preparation. On the assumption that the minimum permeability values for each coal would represent the permeability of the original coal material, these results were used for the purpose of correlation.

The minimum permeabilities of each coal at certain stress levels between $\sigma_3 = 1{\cdot}50$ MN/m^2 and $\sigma_3 = 7{\cdot}00$ MN/m^2 were plotted against the percentage volatile matter (m.f.b.). As shown in Figure (8.2.1), the permeability of coals under equivalent levels of stress decreased with decreasing rank up to 34 percent volatile matter and then increased towards the lower rank coals.

The variation in rate of reduction in permeability under stress, as illustrated in Table (8.2.1), was found to be the factor contributing to the wide variations found in permeabilities of different rank coals under high stresses. The rate of reduction in permeability of coal increased with decreasing rank up to a critical point (34 percent volatile matter) and then decreased twoards the higher percentage volatiles.

TABLE (8.2.1) Comparison of Minimum and Maximum Permeabilities at Certain Stress Levels, Rate of Reduction in Permeability Under Stress and Compressibility Values for Coals Tested

TYPE OF COAL (Number of specimens tested)	BASE PERMEABILITY (min) (max) ($10^{-16} m^2$)	PERMEABILITY σ_3 = 1·50 MN/m^2 (min) (max) ($10^{-16} m^2$)	PERMEABILITY σ_3 = 7·00 MN/m^2 (min) (max) ($10^{-16} m^2$)	RATE OF REDUCTION IN PERMEABILITY $\frac{K_{min}\ (7·00)}{K_{min}\ (1·50)}$	COMPRESSIBILITY C_x $(MN/m^2)^{-1}$
ACILIK (7)	106·62 - 734·23	2·88 - 8·19	0·27 - 0·91	1/10	0·164
CAYDAMAR (6)	181·71 - 632·50	2·84 - 43·70	0·12 - 4·50	1/24	0·174
BARNSLEY (7)	99·84 - 877·08	1·28 - 64·18	0·05 - 1·18	1/26	0·174
COCKSHEAD (6)	195·06 - 398·36	2·86 - 19·32	0·06 - 0·74	1/48	0·178
BANBURY (5)	399·63 - 452·37	1·69 - 7·62	0·07 - 0·21	1/24	0·174
DUNSIL (6)	189·92 - 851·29	1·95 - 25·88	0·13 - 1·86	1/15	0·169
DEEP HARD (5)	645·35 - 858·05	9·02 - 28·20	0·32 - 1·68	1/28	0·175

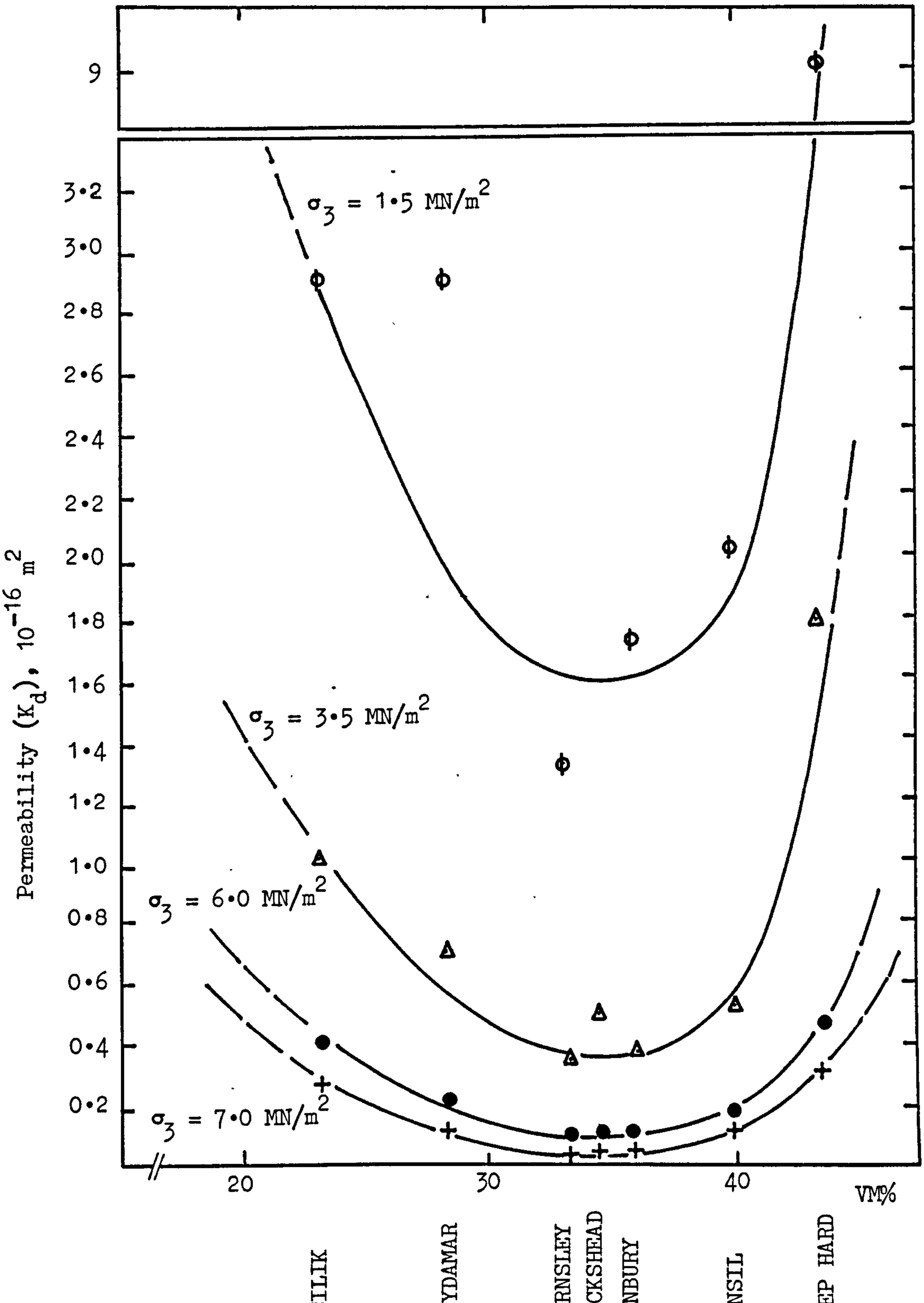

FIGURE (8.2.1) Variations of Coal Permeability Under Stress with Rank.

It was considered that differences in compressibility * (C_x) of different rank coals contributed to the variations in rate of reduction in permeability under stress. As mentioned in Chapter 7, microfracturing of some coals under stress did not result in an immediate effect on permeability. However, the overall compressibility of the coal material was affected by microfracturing and this fact was demonstrated by an increase in permeability when stress was released.

8·3 An Empirical Relationship Between the Applied Stress and Permeability of Different Coals

As illustrated in all the stress-permeability curves in Chapter 7, permeability of coal decreased first sharply, then gently, as the applied stress increased. The steep gradient of the first section of the curve, where a sharp decrease in permeability took place, was due to the closure of the minor fractures under low stresses. The magnitude of reduction in permeability, at this stage, depended on the amount of fractures that existed. After sufficiently high stresses were established (i.e. $\sigma_3 \geqslant 1{\cdot}50$ MN/m^2), the rate of reduction in permeability of the specimen was relatively lower. As this research was concerned with simulation

---

* Compressibility of rock in petroleum reservoir engineering is defined as "change in pore volume per unit pore volume per applied stress" (75), (76). As this research is concerned with the stress-permeability relationship of coals, compressibility of coal was defined in terms of the changes in permeability under stress instead of pore volume. Permeabilities at stress levels $\sigma_3 = 1{\cdot}50$ MN/m^2 and $\sigma_3 = 7{\cdot}00$ MN/m^2 were taken as the base values in calculating the compressibility for coal.

of the conditions underground, it was decided to concentrate on the second section of the stress-permeability curve as this would correspond to the stress levels experienced in mining practice.

For the purpose of comparison, first loading stress-permeability curves for every specimen of the same coal were plotted on one graph as shown in Figures (8.3.1) to (8.3.7). Although the stress-permeability curves for each specimen followed a different path, it was noticed that the slopes were similar. The slope of the stress-permeability curve was determined by the compressibility of the original coal material and was found to be comparable for each specimen.

It was thought that an empirical equation of the form:

$$y = ae^{-bx} \qquad \text{..... 8.3.1}$$

where

a and b are constants

y is the permeability

x is the applied stress

would represent the stress-permeability curves illustrated in the above mentioned figures.

In the early stages of employing curve fitting techniques, equation 8.3.1 took the form:

$$K_{\sigma_3} = K_{\sigma_B} e^{-C\sigma_3}$$

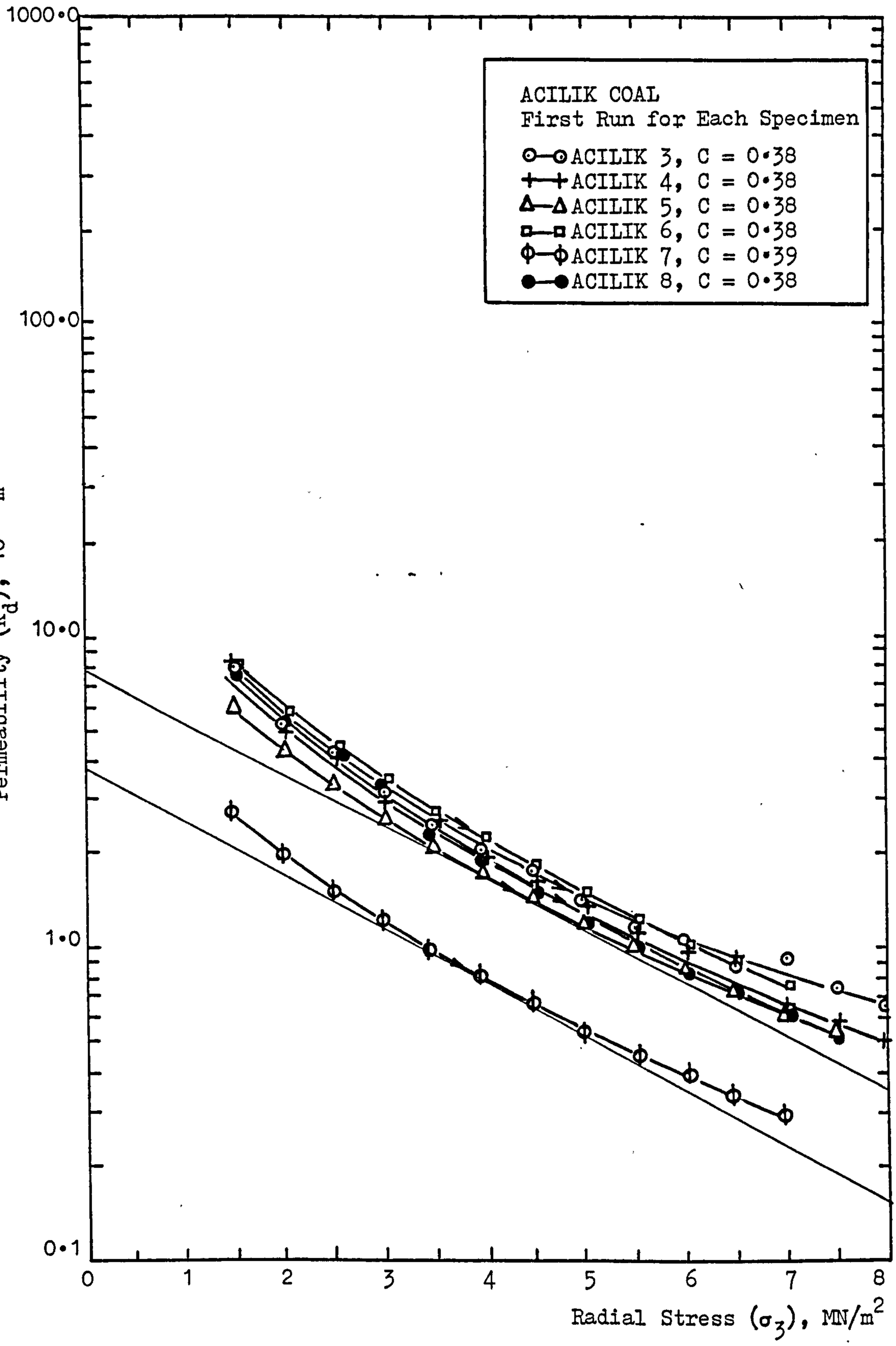

FIGURE (8.3.1) First Loading Curves for ACILIK Specimens.

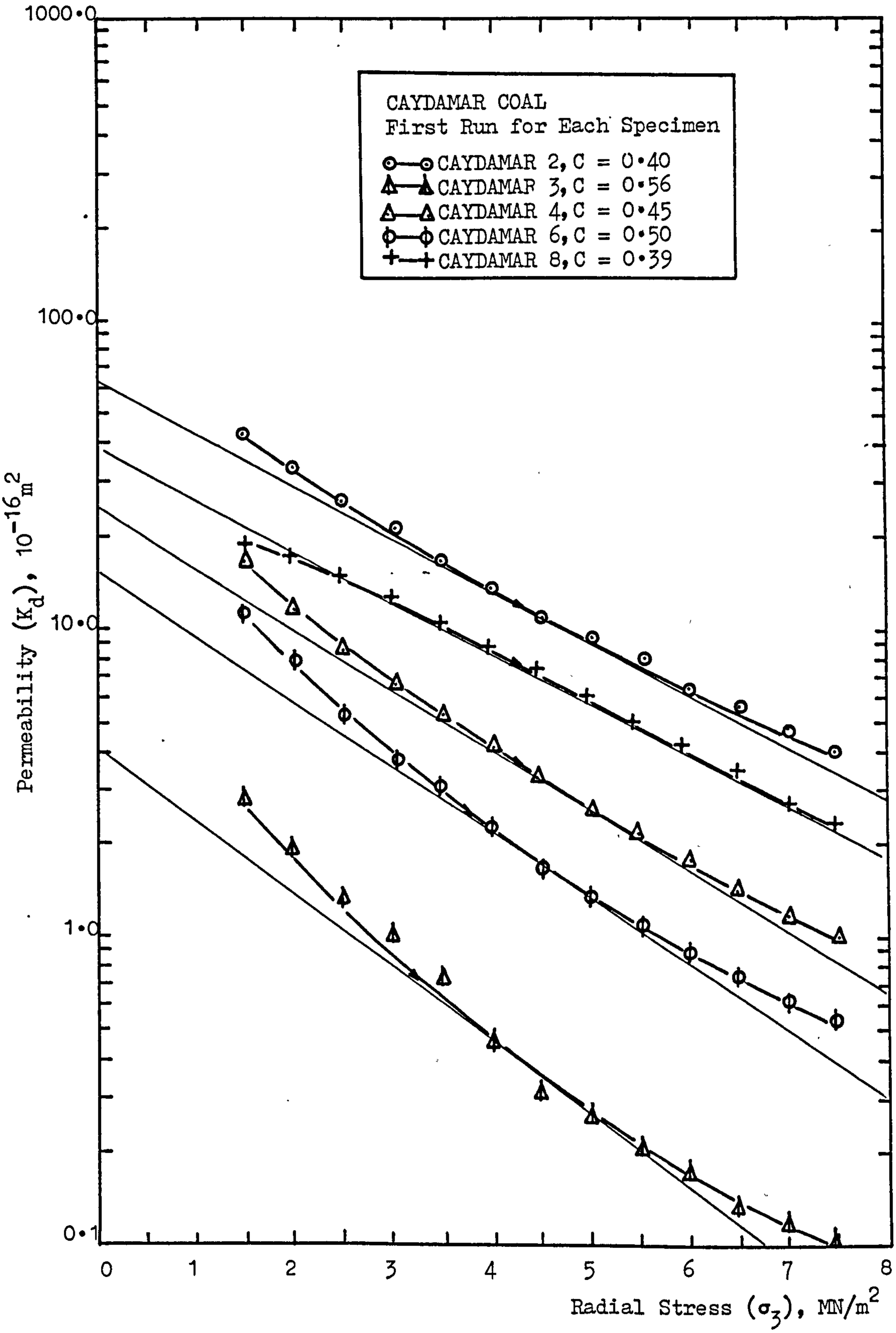

FIGURE (8.3.2) First Loading Curves for CAYDAMAR Specimens.

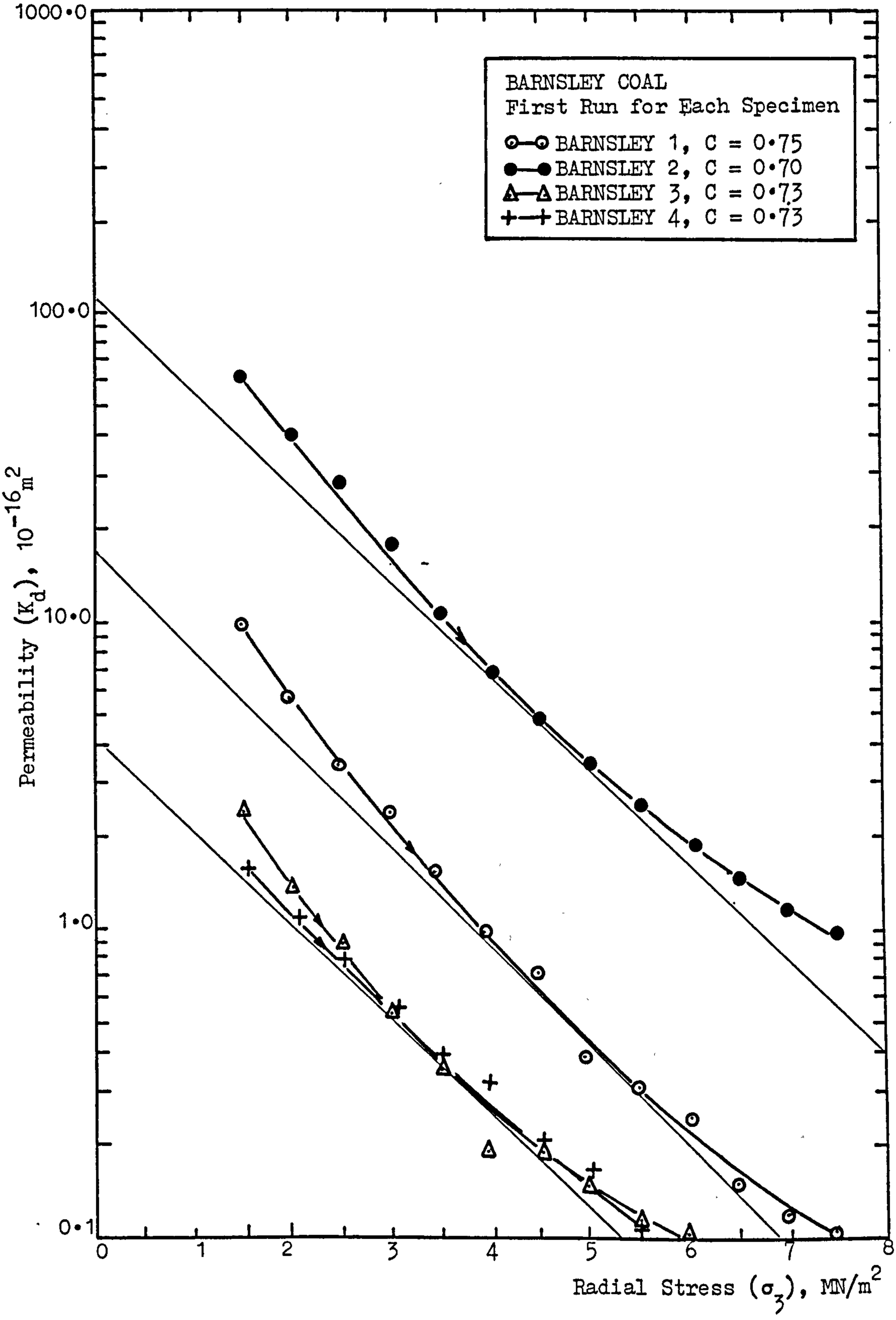

FIGURE (8.3.3) First Loading Curves for BARNSLEY Specimens. (Stress-Permeability Results of Highly Fissured BARNSLEY Specimens are Excluded from the Figure)

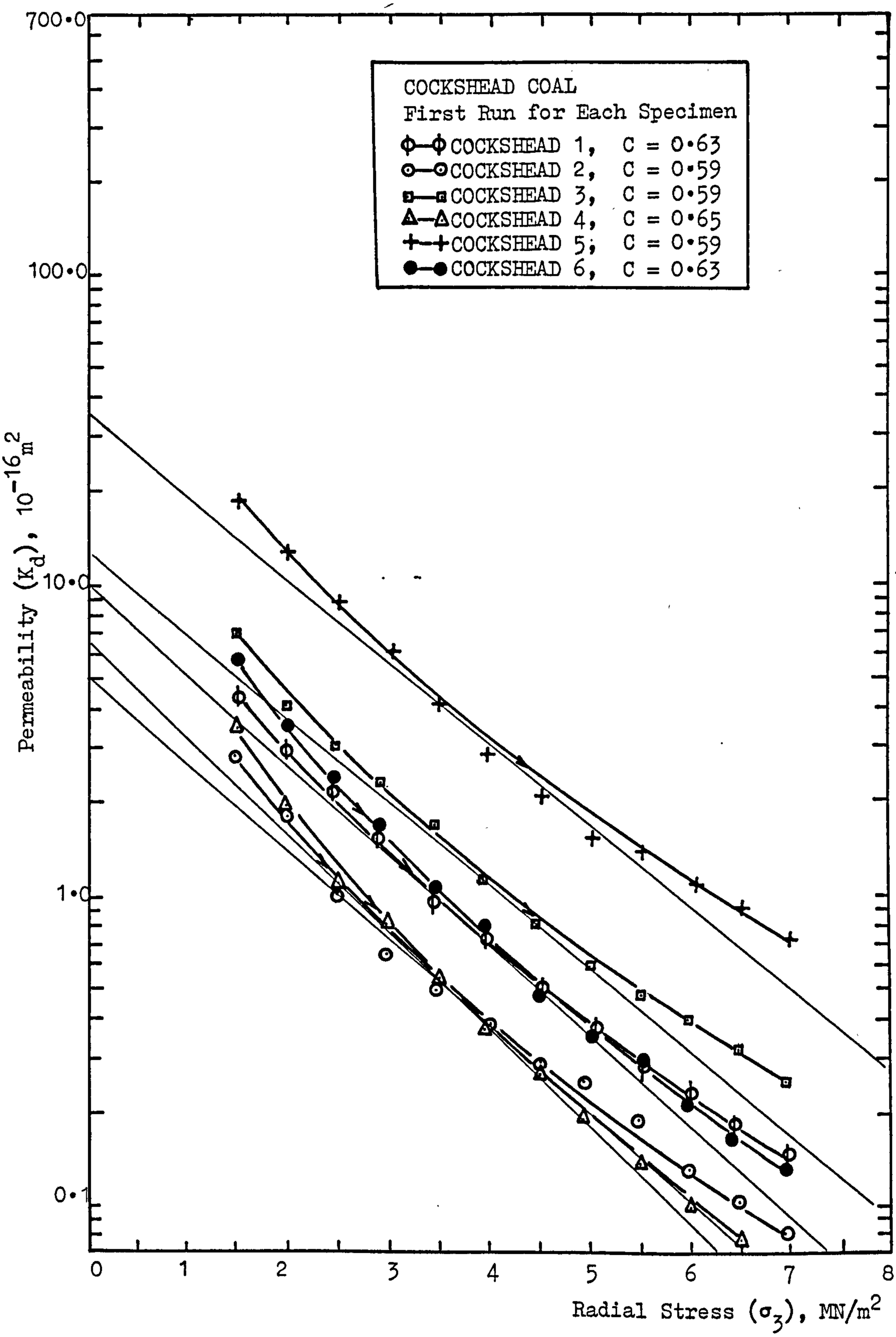

FIGURE (8·3·4) First Loading Curves for COCKSHEAD Specimens.

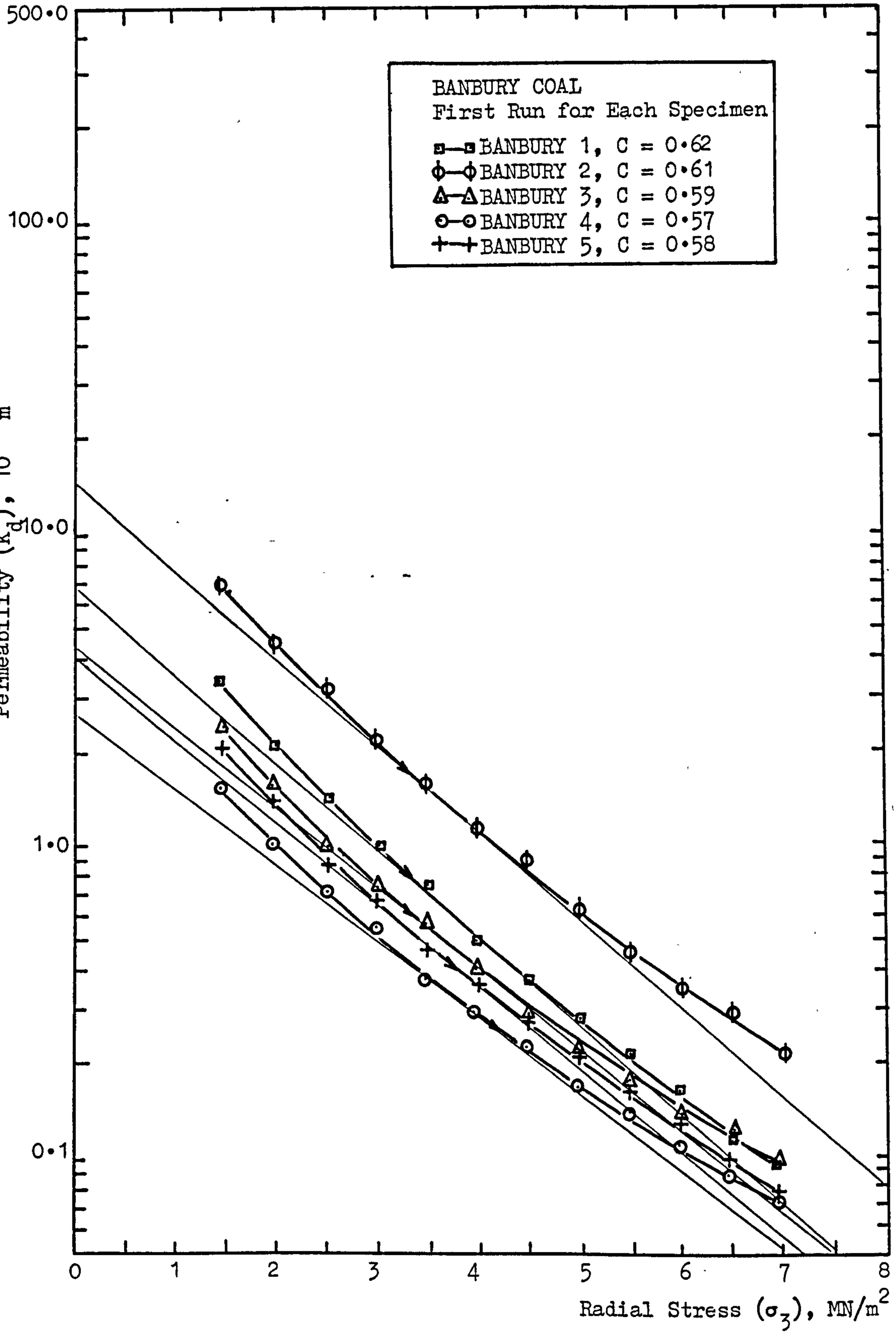

FIGURE (8.3.5) First Loading Curves for BANBURY Specimens.

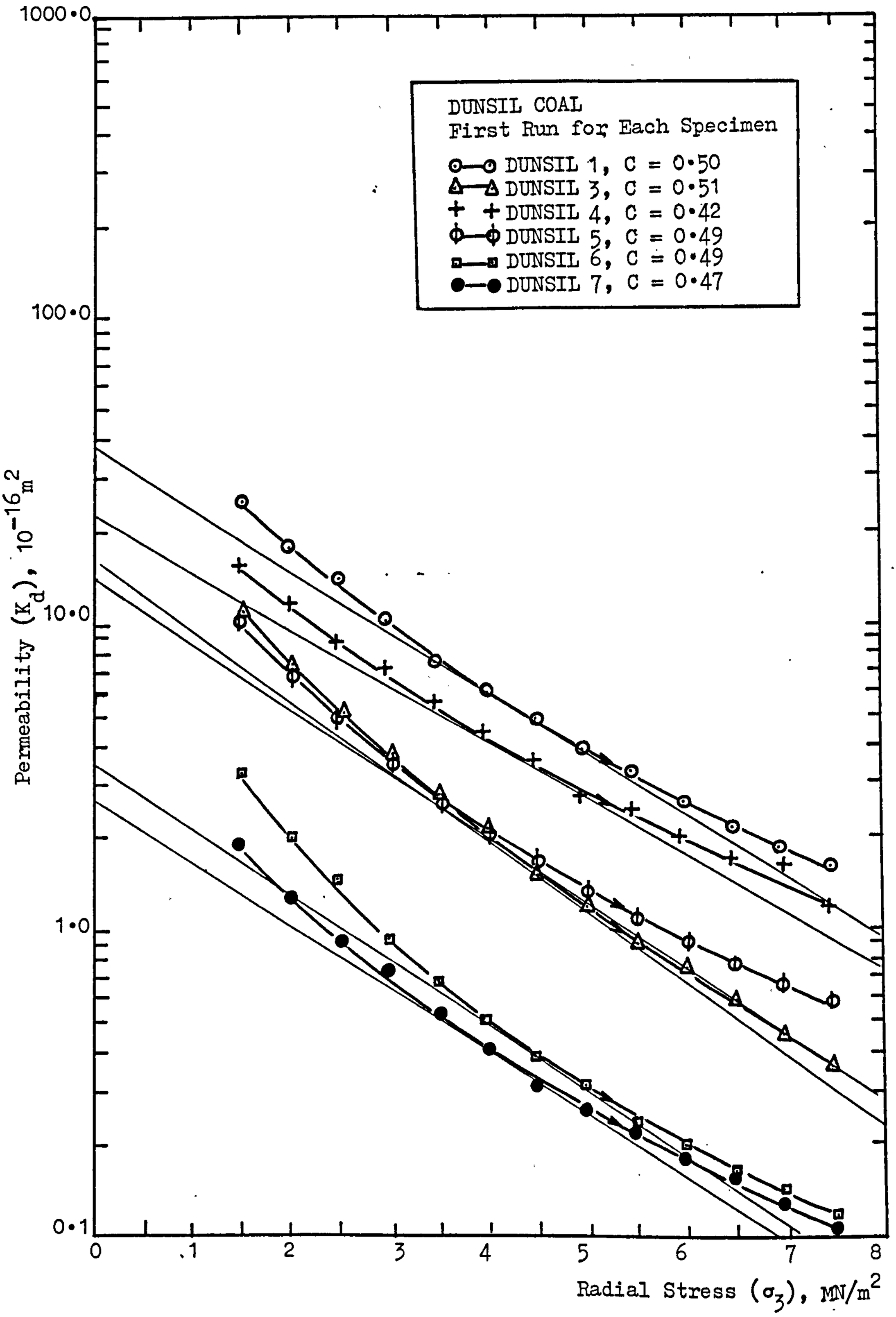

FIGURE (8.3.6) First Loading Curves for DUNSIL Specimens,

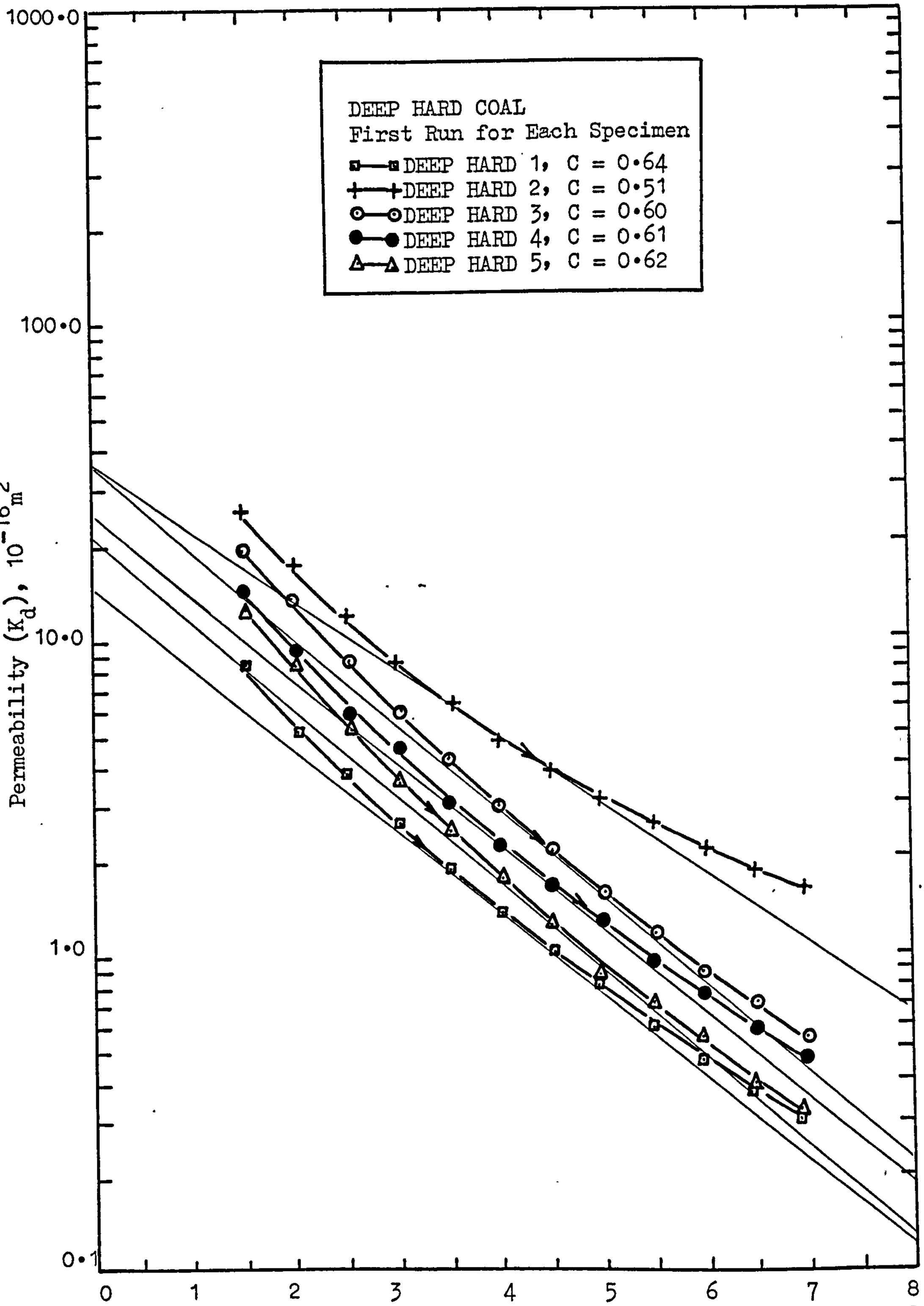

FIGURE (8.3.7) First Loading Curves for DEEP HARD Specimens.

which represented the tangent curves to the experimental stress-permeability curves at $\sigma_3 = 4{\cdot}00\ MN/m^2$ as shown in Figures (8.3.1) to (8.3.7). K_{σ_B} was a function of the fracture systems existing in each test specimen and constant C of the tangent curves was found to be of comparable values for each specimen of the same coal.

Careful examination of the experimental stress-permeability curves has shown that constants K_{σ_B} and C were changing along the curve being dependent on the applied stress. On further analysis of the experimental curves, a stress dependent variable of the form:

$$\alpha = (1{\cdot}12 - 0{\cdot}03\sigma_3)$$

was introduced and the exponential equation 8.3.1 took the final form:

$$K_{\sigma_3} = (1{\cdot}12 - 0{\cdot}03\sigma_3)K_{\sigma_B} e^{-(1{\cdot}12 - 0{\cdot}03\sigma_3)C\sigma_3} \quad \ldots\ldots\ldots \quad 8.3.2$$

so that

$$a = K_{\sigma_B}(1{\cdot}12 - 0{\cdot}03\sigma_3)$$

$$b = C\ (1{\cdot}12 - 0{\cdot}03\sigma_3)$$

where K_{σ_3} is the permeability at stress σ_3

σ_3 is the radial stress applied ($\sigma_1 = 2{\cdot}70\sigma_3$)

K_{σ_B} and C are constants obtained from the tangent curves at $\sigma_3 = 4{\cdot}00\ MN/m^2$ for each specimen

TABLE (8.3.1) Compressibility Factor C for the Coals Tested

TYPE OF COAL	VOLATILE MATTER %	COMPRESSIBILITY FACTOR C
ACILIK	23•31	0•38
CAYDAMAR	28•70	0•47
BARNSLEY	33•74	0•73
COCKSHEAD	34•62	0•61
BANBURY	36•23	0•59
DUNSIL	39•94	0•48
DEEP HARD	43•52	0•59

Mean values of C for each coal will be termed as 'the compressibility factor'. Table (8.3.1) lists the compressibility factors experimentally determined for the coals used in this research. As discussed in the previous section, the effect of increasing stress on permeabilities of the coals tested have been related to their rank. The compressibility factor, which defines the degree of reduction in permeability of coal under stress, increases as the rank decreases up to 34 percent volatile matter and then decreases towards the lower rank coals. Figure (8.3.8) illustrates the relation between the rank and compressibility factor of coals tested.

During the stress-permeability experiments conducted by the author, it was noticed that microfracturing and fracturing of each individual coal specimen effected its compressibility. The compressibility of coal decreased considerably if the specimen was microfractured or fractured after a loading/unloading experiment. It was found that the magnitude of the compressibility factor for fractured coal was solely dependent upon the degree of fracturing induced. The degree of fracturing was determined by the levels of stress applied during the crushing process. Coals of different mechanical strengths have shown different fracturing characteristics under equivalent levels of stress, (see Figures (7.3.6) and (7.3.7)).

The validity of equation 8.3.2 should be tested by further research on other coals of different ranks. Should it

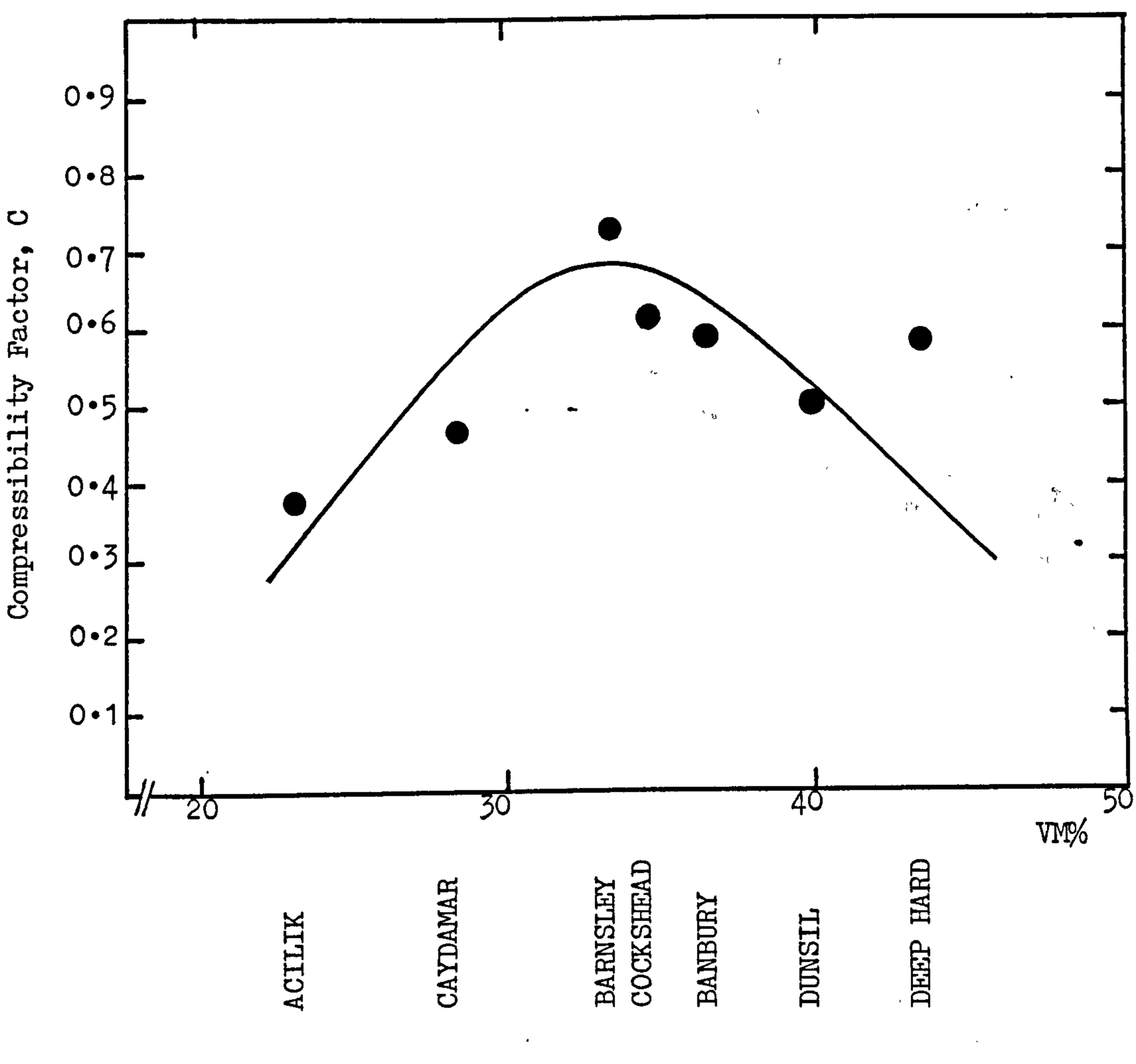

FIGURE (8.3.8) The Relationship Between the Compressibility Factor and the Rank of Coals Tested.

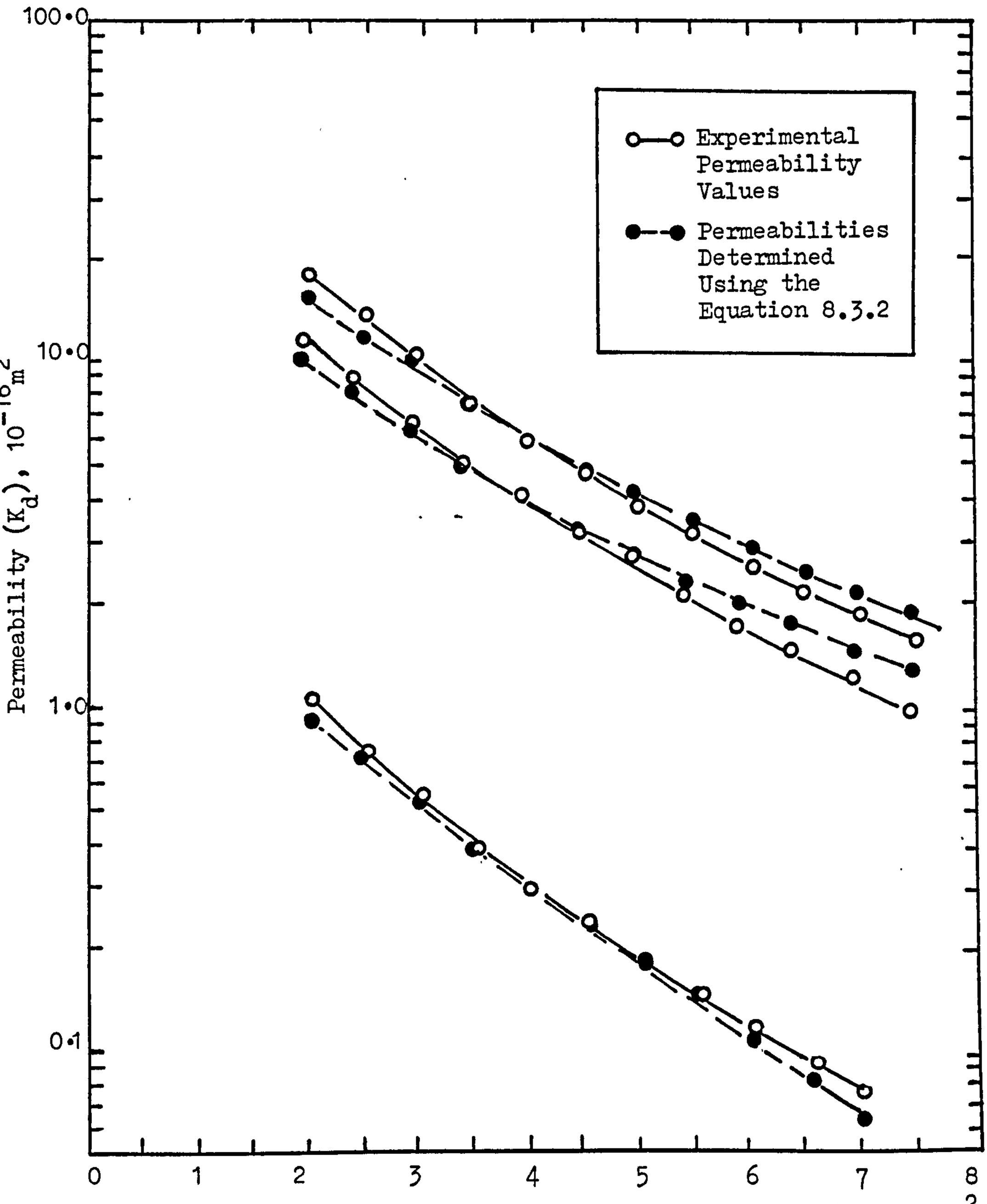

FIGURE (8.3.9) Comparison of Experimental and Theoretical Stress-Permeability Curves.

prove to be valid for all coals, then a stress-permeability relationship for any coal seam could be established if permeability at any stress level is measured in situ.

Figure (8.3.9) compares some of the experimental stress-permeability curves with curves based on the empirical equation 8.3.2. The empirical equation 8.3.2 was found to be accurate within $\pm$ 3·00 x 10^{-16} m^2 for coal specimens free from major fractures. The margin of error dimishes towards the high stress levels.

CHAPTER NINE

DISCUSSION ON THE FLOW PATTERNS OF METHANE AROUND WORKING LONGWALL FACES

CHAPTER NINE

DISCUSSION ON THE FLOW PATTERNS OF METHANE AROUND WORKING LONGWALL FACES

9.1 Permeability of Coal Seams in Relation to the Methods of Predicting Methane Flow

Migration of methane in and around working coal seams has been the subject of various research projects which have used mathematical models in an attempt to simulate mining conditions (77),(78),(79),(80),(81),(82). These studies were focussed on the three dimensional area surrounding the workings, called the zone of gas emission, from which methane is released as a result of mining. Demarcation of boundaries of the gas emission zone, and the methods employed in predicting methane flow within these boundaries, vary considerably from one country to another.

The two main methods employed in predicting the methane flow from the gas emission zone into the mine areas are:

(i) the degree of gas emission method and

(ii) methods based on the principles of gas flow in porous permeable media.

The first method, which is widely used in European countries, defines the degree of gas emission as the percentage

of the gas contained within the strata at a specific level which flows into the workings (77). As shown in Figure (9.1.1), the prediction methods based on this theory differ in their definition of the gas emission zone and in the assumed variation of the degree of gas emission within the zone. Methods employed in Belgium, France and the Federal Republic of Germany use the desorbable gas content as the gas content of a coal seam (82), whereas the total gas content, which is about $1m^3$/ton higher, is used in the United Kingdom (77). The strata other than coal are usually considered to have a certain percentage of the coal seam gas content (i.e. 10 m of sandstone or 100 m of shale are taken to have a gas content equivalent to 1 m of coal in France and Belgium (82)).

The values of degree of gas emission from the source seams at different depths are usually based on the residual gas content measurements in strata (81),(82). On the other hand, a new technique developed by the MRDE which is based on Airey's Theory of gas emission from broken lumps of coal (83), is being used in the United Kingdom in determining the degree of gas emission from coal seams (84). The application of Airey's Theory of gas emission in coal mining operations was discussed at some length in Gawuga's thesis (26).

Methane emission from a source seam is calculated by multiplying the degree of gas emission for the seam considered, by the gas content and the relative thickness, which is the ratio of the thickness of the source seam to the worked seam. The use

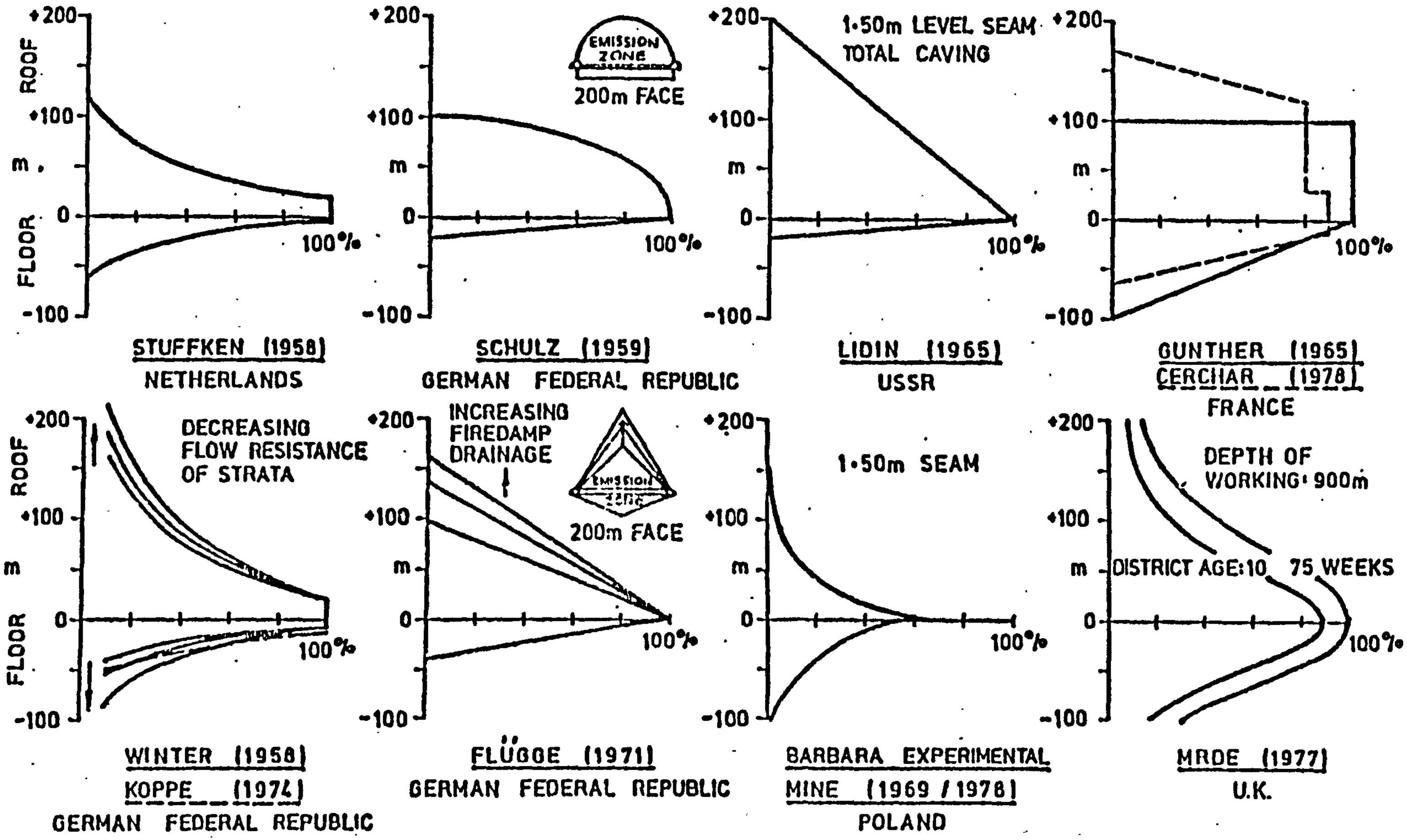

FIGURE (9.1.1) Adjacent Seam Gas Emission (%) as a Function of Distance from the Worked Seam, According to Various Authorities (77).

of relative thickness introduces the dependency of the methane emission on coal face production.

A more detailed discussion on the prediction methods using the degree of gas emission can be found in a report published by IEA recently (82).

The second method of predicting methane flow into mine workings is the computer solution of gas flow equations based on Darcy's Law (79),(80),(74). As an integral part of a total mine environment planning programme, computer models, simulating the flow of methane from the seam being worked and from the source seams in the adjacent strata, have been developed recently in the Department of Mining Engineering, University of Nottingham.

METNET 1, developed by Keen (79) in 1977 was mainly concerned with the problem of gas emission from working longwall faces. Later in 1980, O'Shaughnessy(80) developed a set of computer routines simulating the methane flow through the strata adjacent to a working longwall coal face which enables the calculation of methane flux into a mine roadway and any drainage borehole.

One of the main inputs needed in computer simulations of methane flow using Darcy's equation was the permeability of the strata concerned. Keen (79) proposed an empirical relationship from which a curve of permeability against the distance from the faceline could be deduced. The use of the permeability curve, shown in Figure (9.1.2), was later found to be impractical mainly

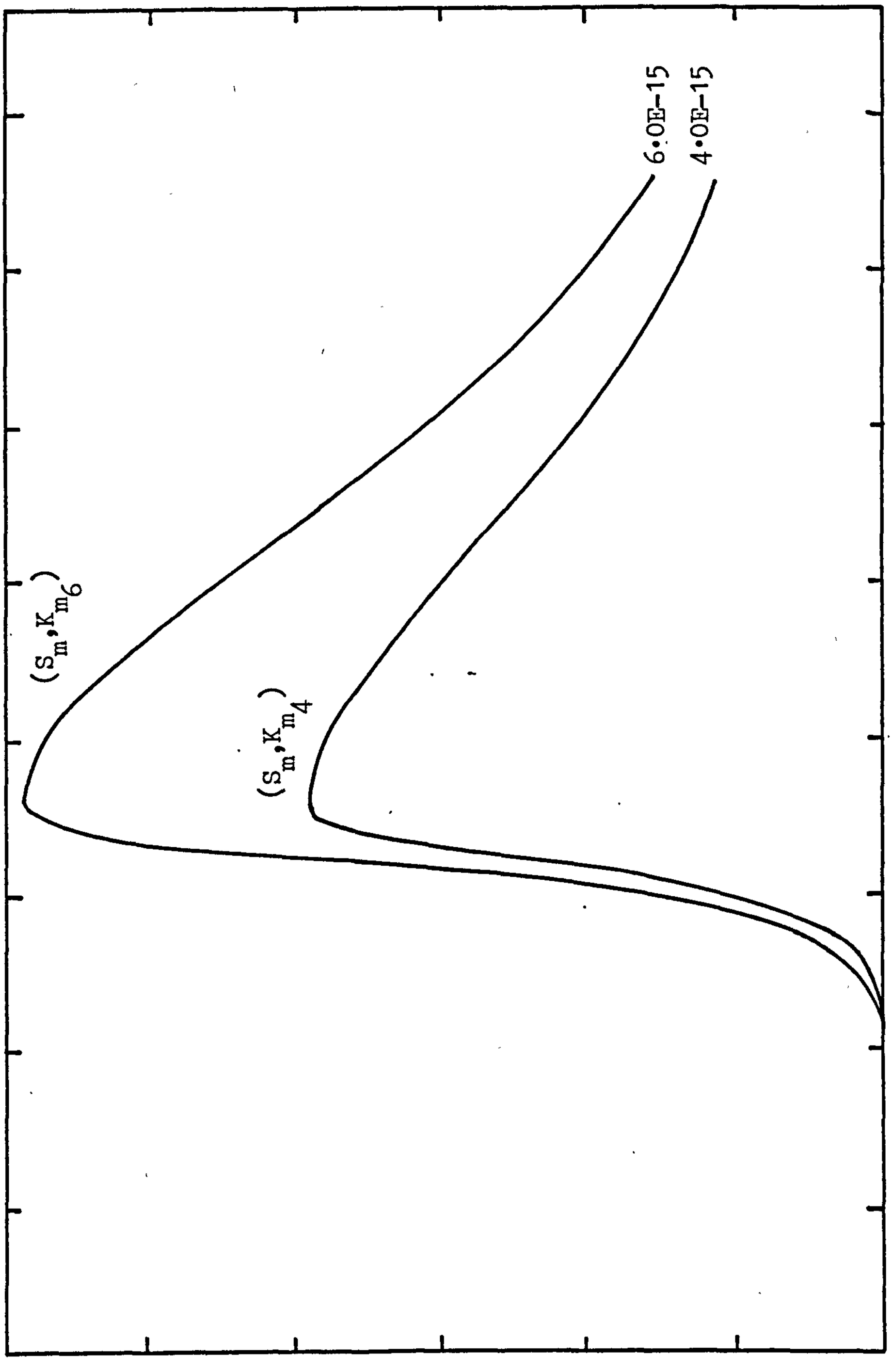

FIGURE (9.1.2) Permeability as a Function of Distance from Faceline, (After Keen (79)).

due to the lengthy and expensive calculations involved in solving the exponential equations by computers. Instead, the permeability data was directly input to a computer program in a manner similar to the way fan characteristics are input to a ventilation network program. Figure (9.1.3) illustrates the model and the assumed permeability values used by O'Shaughnessy in the steady and unsteady-state simulations of gas flow through strata adjacent to a working longwall face.

The need for a set of permeability curves representing various levels in the adjacent strata of a working longwall face was recognised by both Keen (79) and O'Shaughnessy (80) throughout their research.

It was therefore decided to produce empirical permeability profiles for coal seams lying at certain depths above and below the working longwall faces. The experimental stress permeability results obtained by the author were taken as the data base in producing these profiles and both the theoretical and practical research concerning the stresses and gas flow around working longwall faces were taken into account in interpretation.

9.2 A Study of High Permeability Zones in the Strata Above and Below Working Longwall Faces

The magnitude of gas release from a coal seam and its migration towards the low pressure working areas are controlled by the permeability of coal seams and the surrounding strata.

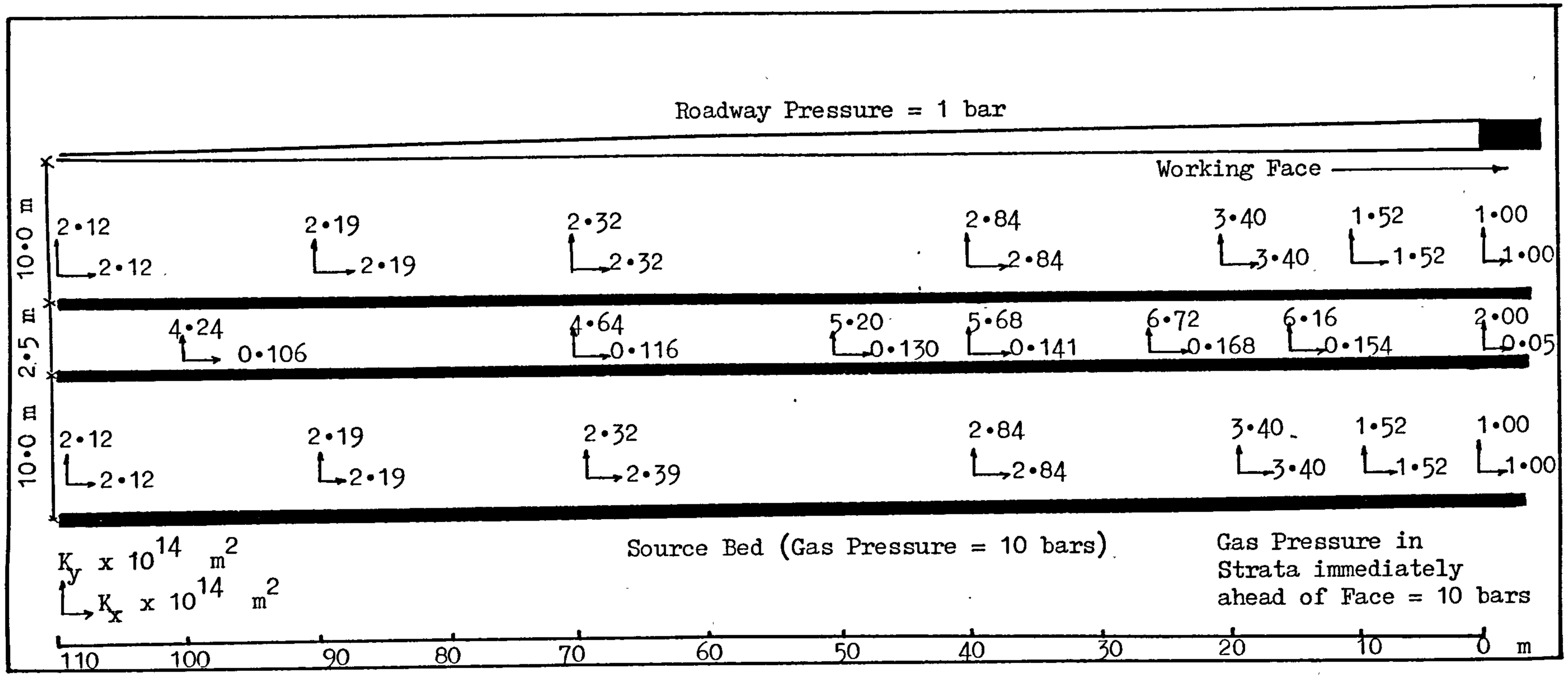

FIGURE (9.1.3) A Model Used in Computer Simulation of Gas Flow Around Working Longwall Faces (After O'Shaughnessy (80)).

As the experimental evidence provided in Chapter 7 suggests, the permeability of a coal seam will be highly effected by the stress disturbances taking place around a working longwall face.

Combining the experimental data provided in Chapter 7 with the stress conditions agreed upon in Chapter 4 a general stress-permeability profile for the immediate roof level of a working longwall face can be produced as shown in Figure (9.2.1). Stress conditions along the roof would be such that the different stress zones discussed in Chapter 4 would be created due to the extraction of the coal seam. As shown in the figure, the permeability of a coal seam dramatically increases in the crushing zone where the coal is fractured. The permeability of coal is expected to remain high in the stress relief zone and a slight decrease in permeability of fractured coal takes place as the coverload is established. It is believed that the accuracy of a prediction method totally depends on locating these maximum permeability zones relative to the postion of the face.

The position of the maximum permeability areas in coal seams around a working longwall face is determined by two main factors:

(i) the position of the bed relative to the worked seam,

(ii) the rate of face advance.

These points will now be expanded upon by means of discussion of theoretical and practical data reported in literature.

The greater the distance the bed is above or below the

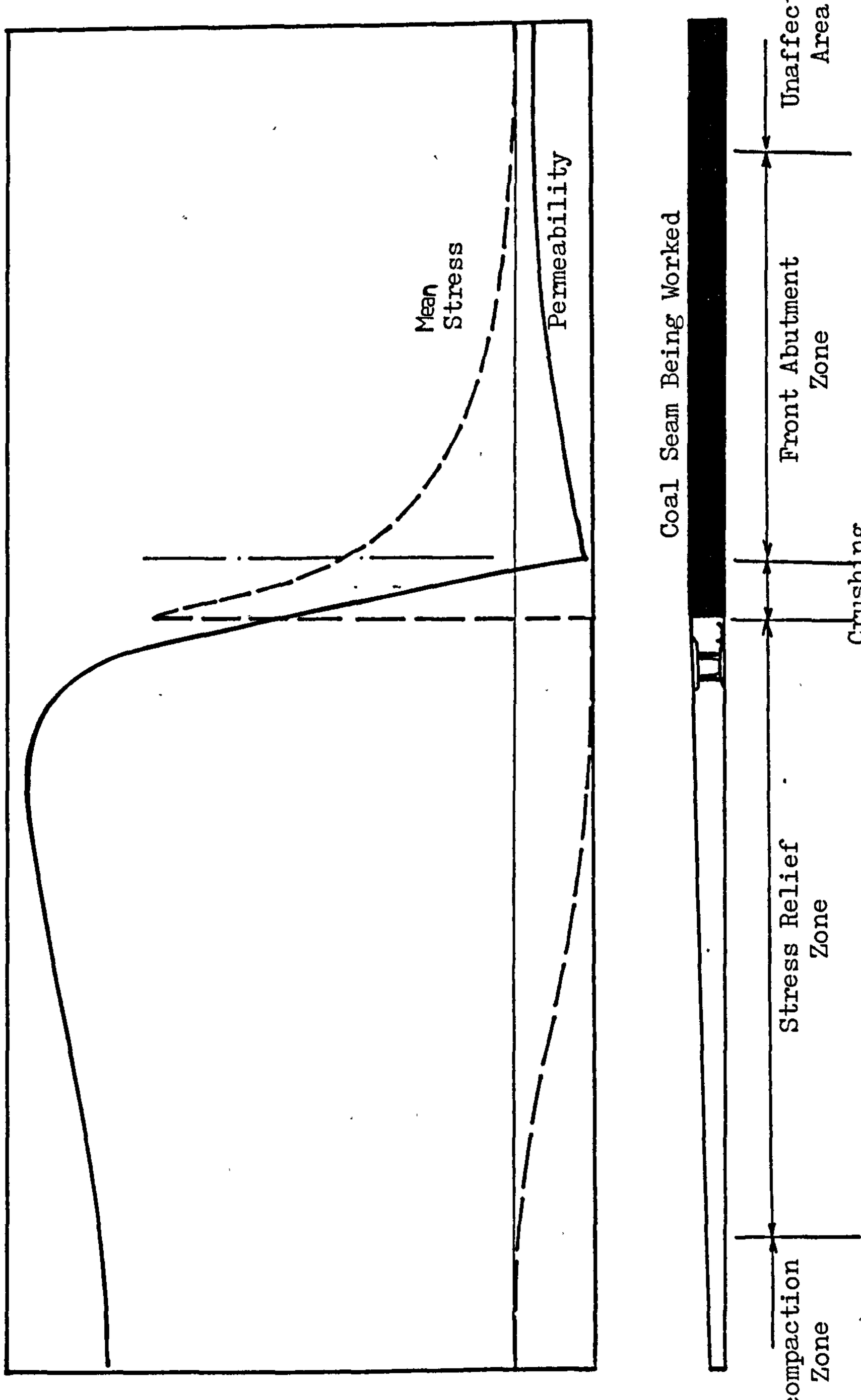

FIGURE (9.2.1) General Stress-Permeability Profile at the Roof Level of a Working Longwall Face (Not to Scale).

worked seam the less will be the effect of the stress disturbances. The most dramatical effect on permeability will be created by the fracturing of the seam at the crushing zone. The vertical distance from the face at which the effects of fracturing and stress relief are felt varies widely as reported by different authors. Reporting on the results of gas flow measurements in the strata above and below the working longwall faces, Noack (85) suggested that the effect of mining would be felt as far as 260 m above and 100 m below the worked seam, the zone 130 m above and 50 m below being mostly effected. Oldroyd (86) has carried out a series of borehole measurements in the floor strata of the Silkstone seam and reported that the effect of stress relief could be felt as far as 43 m below the seam being worked. The finite element analysis of the stresses around a longwall face by Hazine (62) has also shown that the stress conditions causing the fracturing of the coal seam at the crushing zone existed 100 m above and 50 m below the working horizon.

The rate of face advance determines how soon the fracturing and recompaction of the strata takes place with distance relative to the face line. Due to the dynamic conditions existing around working longwall faces stresses, and consequently permeability, at any one point do not remain constant, but change continuously as the face advances. The role of face advance in locating the maximum permeability regions in and around the worked seam will now be discussed in relation to experimental evidence provided by earlier research workers.

Figure (9.2.2) presents McC. Stewart's (87) results of gas

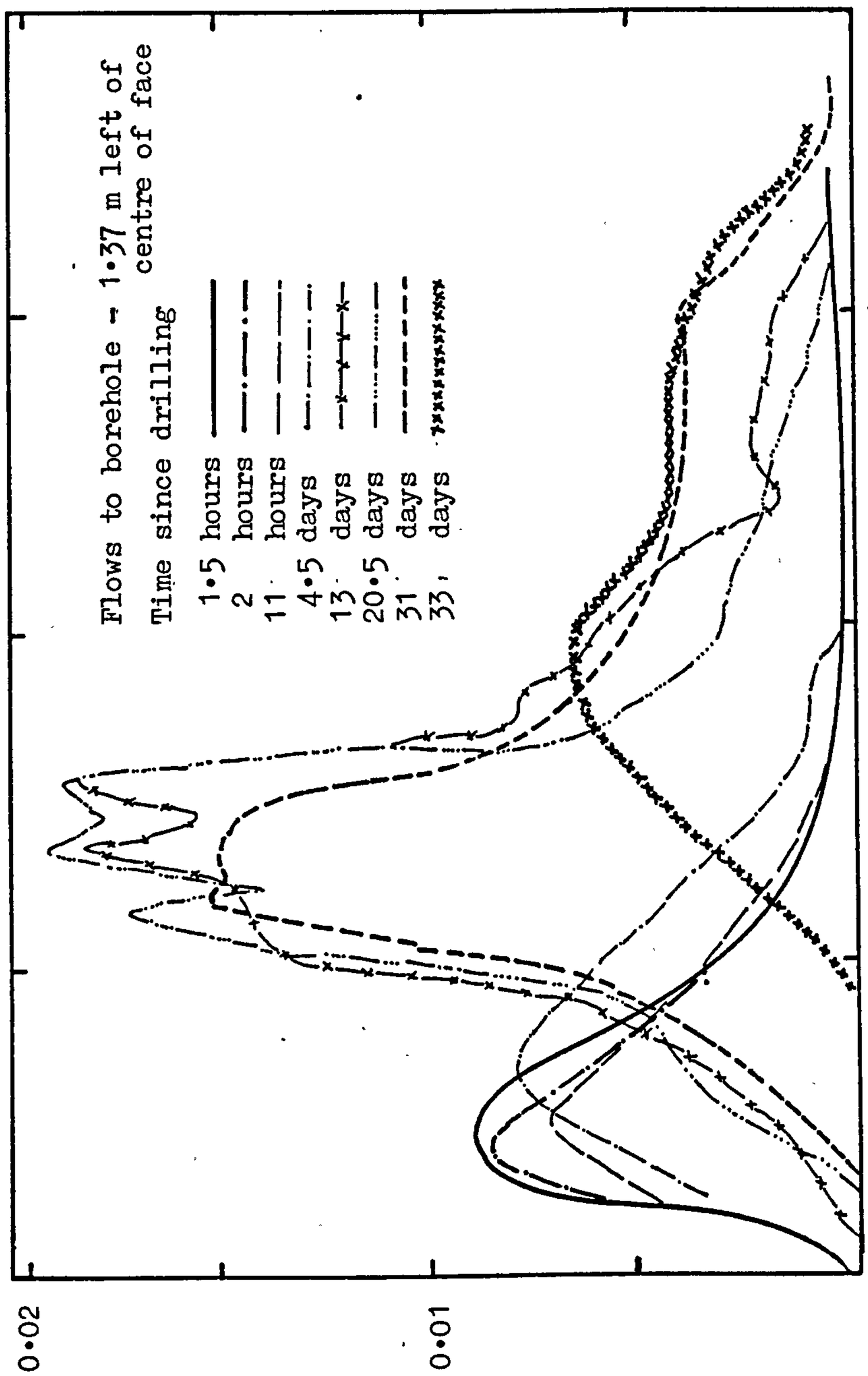

FIGURE (9.2.2) Example of Incremental Flow Measurements to a 50 mm Borehole in a Coal Seam Ahead of a Coalface (After McC. Stewart (87)).

flow measurements into a borehole ahead of a stationary face which illustrates the time dependent increase in permeability into the coal seam. The borehole was completed 21 hours after the face was stopped and the first flow measurements were made 1•5 hours after the drilling was completed. The maximum gas flow into the borehole was within the first 3 m for the first day, suggesting high permeability at this area. However, the region of maximum gas flow moved inward in four days and the peak flow increased. The author explains the phenomenon as the time dependent advance of 'de-stressing' into the coal seam. Further advancing of the face for approximately 5 m after 32 days caused the rapid drainage of the seam 5 m inwards from the new face and a new gas flow profile was established, similar to that before the face advanced.

In the case of a steadily advancing face, the distance between the face and the maximum gas emission region would decrease as the rate of face advance increases (88).

Richards (89), carried out borehole gas flow measurements at six different longwall coal faces in the United Kingdom and reported that the peak gas flow rate was observed between 1•82 m and 4•57 m into the face in different Collieries. It is believed that these figures can be taken as a basis for locating the crushing zone and, thus, the region of maximum permeability, in the seam being worked.

It is assumed in general that the position of maximum

permeability region in any seam near the worked seam will not lie vertically above or below the position of the maximum permeability region in the worked seam. Instead, its position will lag behind as the face advances, the horizontal distance from the faceline being dependent on the vertical distance to the face and the rate of face advance.

Figure (9.2.3) by Wolstenholme (14) and Figure (9.2.4) by Oldroyd (86) show graphs of gas flow rate from the floor strata of a working longwall face plotted against coal face advance. Wolstenholme reported that the rate of borehole flow increased with face advance to either a single or more rarely, a double maxima.

For the purposes of this research, it was deduced that a double maxima in the flow rate would mean that a sudden increase in permeability of the two coal seams lying 13 m and 20 m below the Deep Hard seam occurred as the face reached a distance of 17 m and 34 m, respectively, from the point of measurement. Therefore, one can say that the stress relief zones at the levels of the two underlying coal seams were 17 m and 34 m behind the face lying at angles of 38° and 30° with the horizontal. Similar observations were made on Oldroyd's results where the two peaks in gas flow in Figure (9.2.4) represented the high permeability zones in Seams B and C. It is believed that the high permeability zones within the floor strata of a working longwall face will lie on a parabolic curve, the curve getting smoother as the rate of face advance increases.

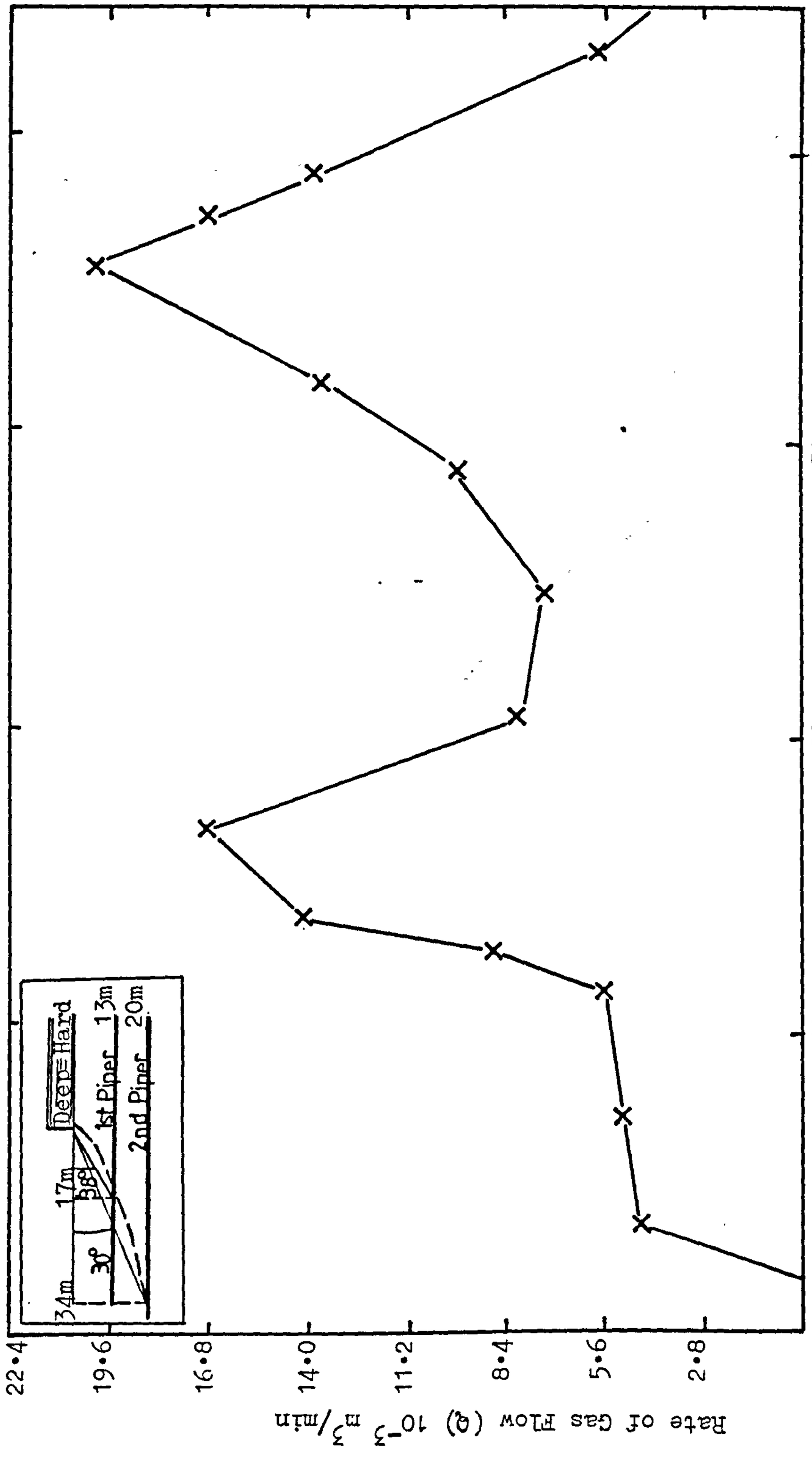

FIGURE (9.2.3) Variation of Gas Flow Rate from Boreholes with Coalface Advance (After Wolstenholme (14)).

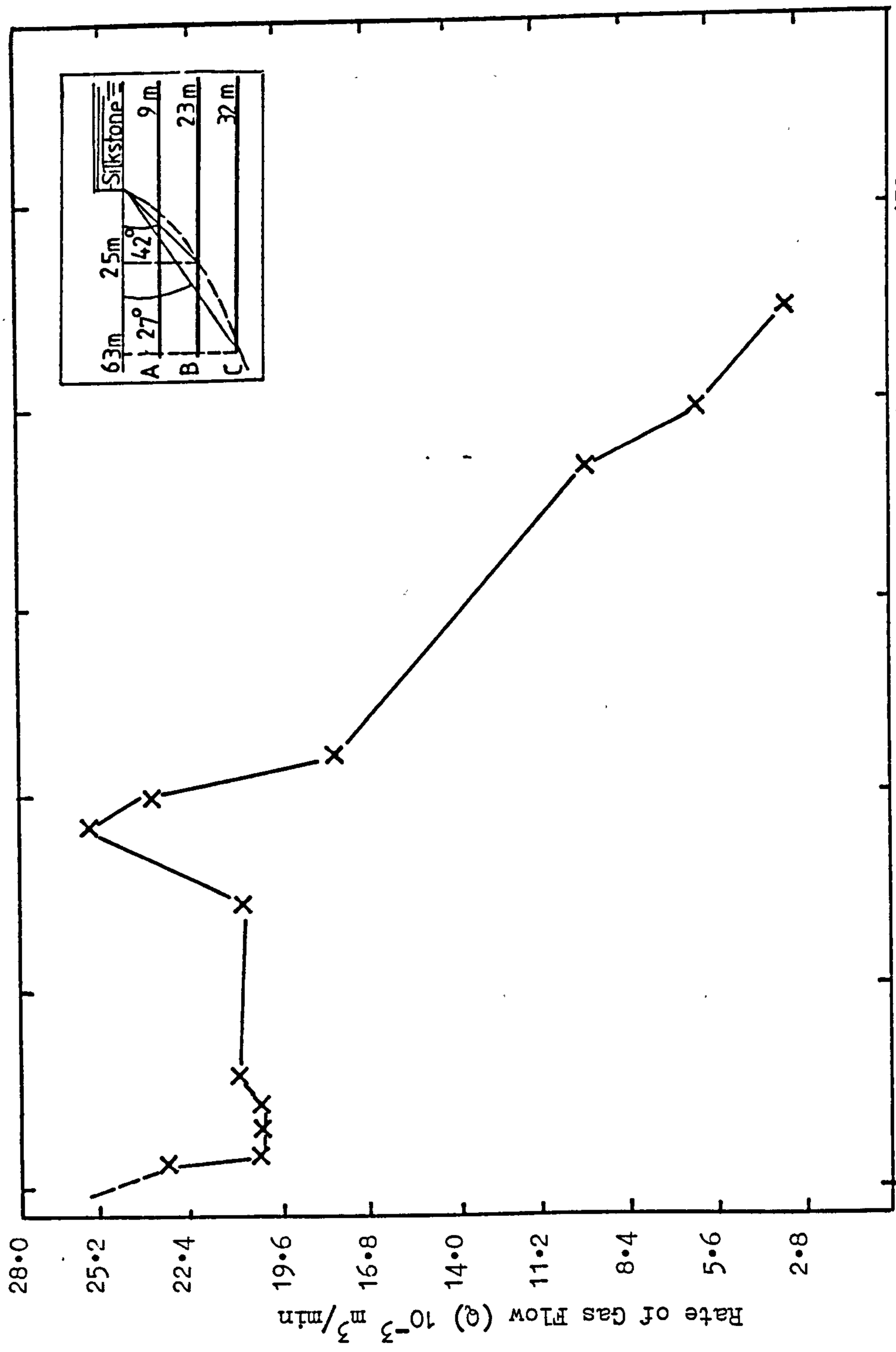

FIGURE (9.2.4) Variation of Gas Flow from Boreholes with Coalface Advance (After Oldroyd (86)).

Davis and Krickovic (90) conducted some underground subsidence and gas flow measurements in the roof level of a longwall coal face in the Pittsburgh seam, U.S.A. Ground movement above the working longwall face was monitored by using cobalt tracer bullets placed along a borehole. It is reported that the ground movement reached levels 33 m and 60 m above the working horizon as the face was 12 m and 50 m past the hole respectively. These points lie at angles of 70° and 50° with the horizontal. Similar research by Whittaker et al. (91) into the water permeability of the strata above a working longwall face suggested that the permeability of the strata at a test horizon 31 - 40 m above the longwall extraction was greatly affected about 15 m after undermining.

These data suggest a progressive upward movement of change in permeability behind the faceline which would also lie on a parabolic curve much steeper than the one for the floor strata.

Noack (85) carried out observations on gas flow from the seams above and below the working longwall faces in the Federal Republic of Germany. Working depth was between 644 to 827 m and the behaviour of areas up to 136 m above and 83 m below the coal faces with an advance rate of 15 - 42 m/month were observed. As shown in Figure (9.2.5). Noack defined a gas pocket around a working longwall face where the maximum gas emission zone extends above and below the waste at an angle of 60° with the horizontal.

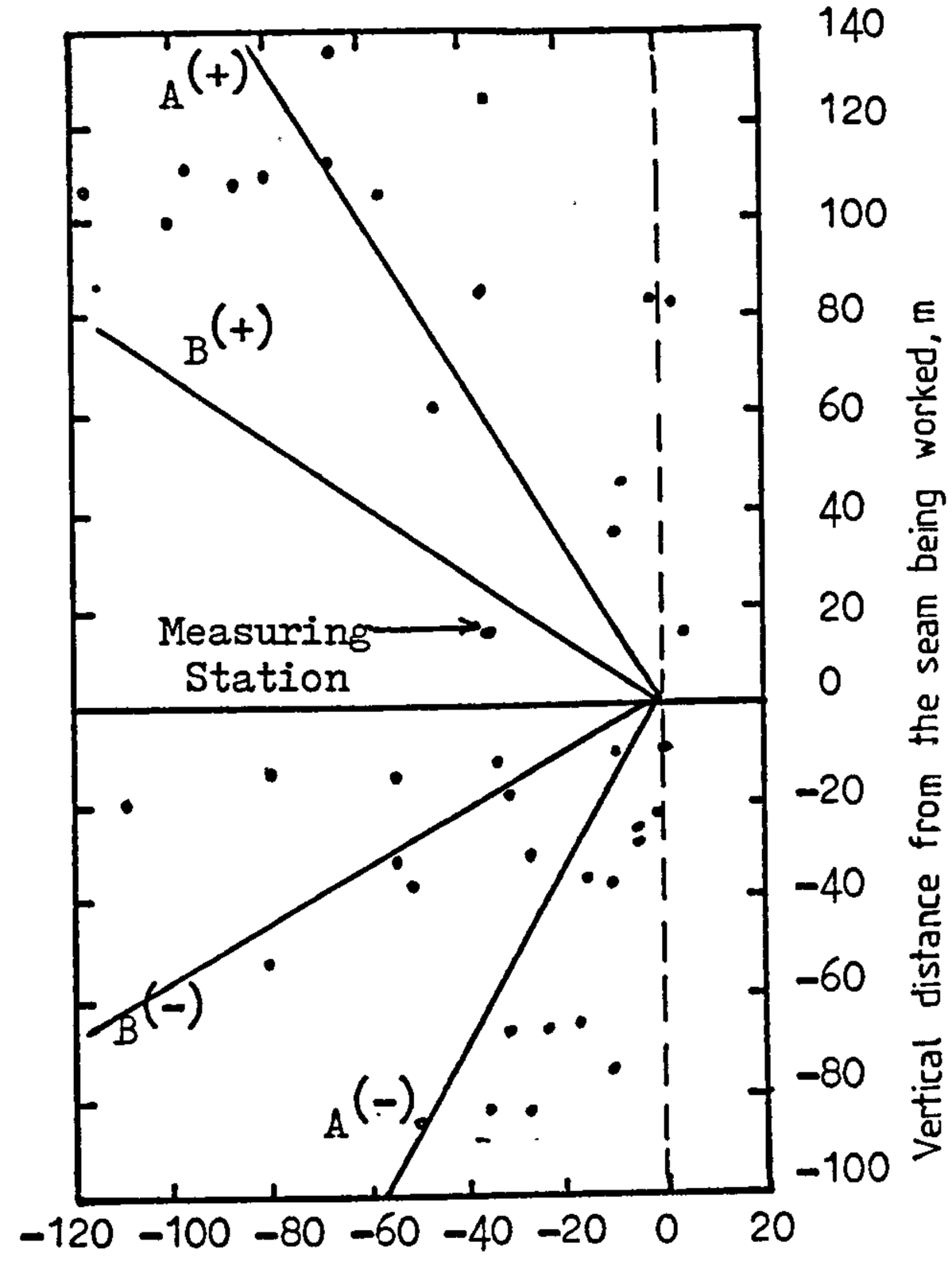

FIGURE (9.2.5) Section Through Plane of Maximum Emission A Rear Limit B of Gas Pocket (After Noack (85)).

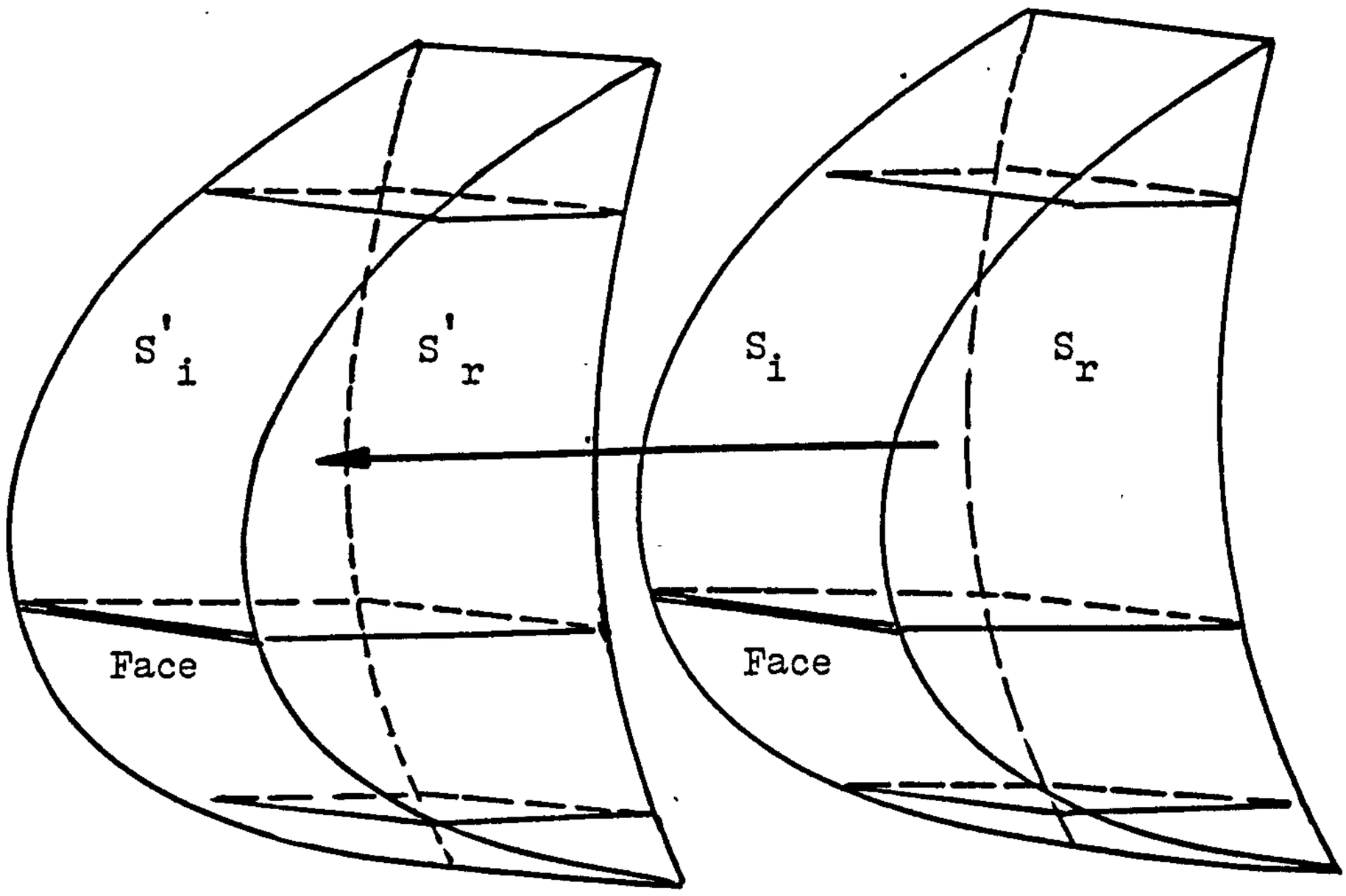

FIGURE (9.2.6) A Model Used in Predicting Methane Flow into Mine Workings (After Jeger (81) CERCHAR).

A most recent paper by Jeger (81), describing the methane flow prediction technique used by CERCHAR (Centre d'Etudes et de Recherces des Charbonnages de France), locates the points where permeability of the strata increases dramatically on a quasi-cylindrical surface S_i, as shown in Figure (9.2.6). It is suggested that the upper and lower flanks of this surface will get closer to the working horizon as the rate of face advance increases and will intersect with the rear surface S_r where gas emission is expected to be very slow due to the decrease in the gas content of the seams.

9.3 Stress and Permeability Profiles for Coal Seams Around Working Longwall Faces

In view of the experimental evidence discussed in the previous section, the theoretical profiles of stress distribution around a stationary longwall face, obtained by Hazine (62), were revised to accomodate the position of maximum permeability areas around a working longwall face. Stresses around 300, 500 and 700 m deep longwall faces were studied and it was observed that the effects of the stress disturbances could be felt as far as 100 m above and 50 m below the working horizon. Figure (9.3.1) and Tables (9.3.1) to (9.3.7) show the revised theoretical maximum and minimum principal stress values for coal seams around a 500 m deep working longwall face. As shown in the figure, the crushing zone for a gas source seam above or below the working horizon lies behind the face line at a certain angle with the horizontal. The magnitude of this angle is determined by the rate of face

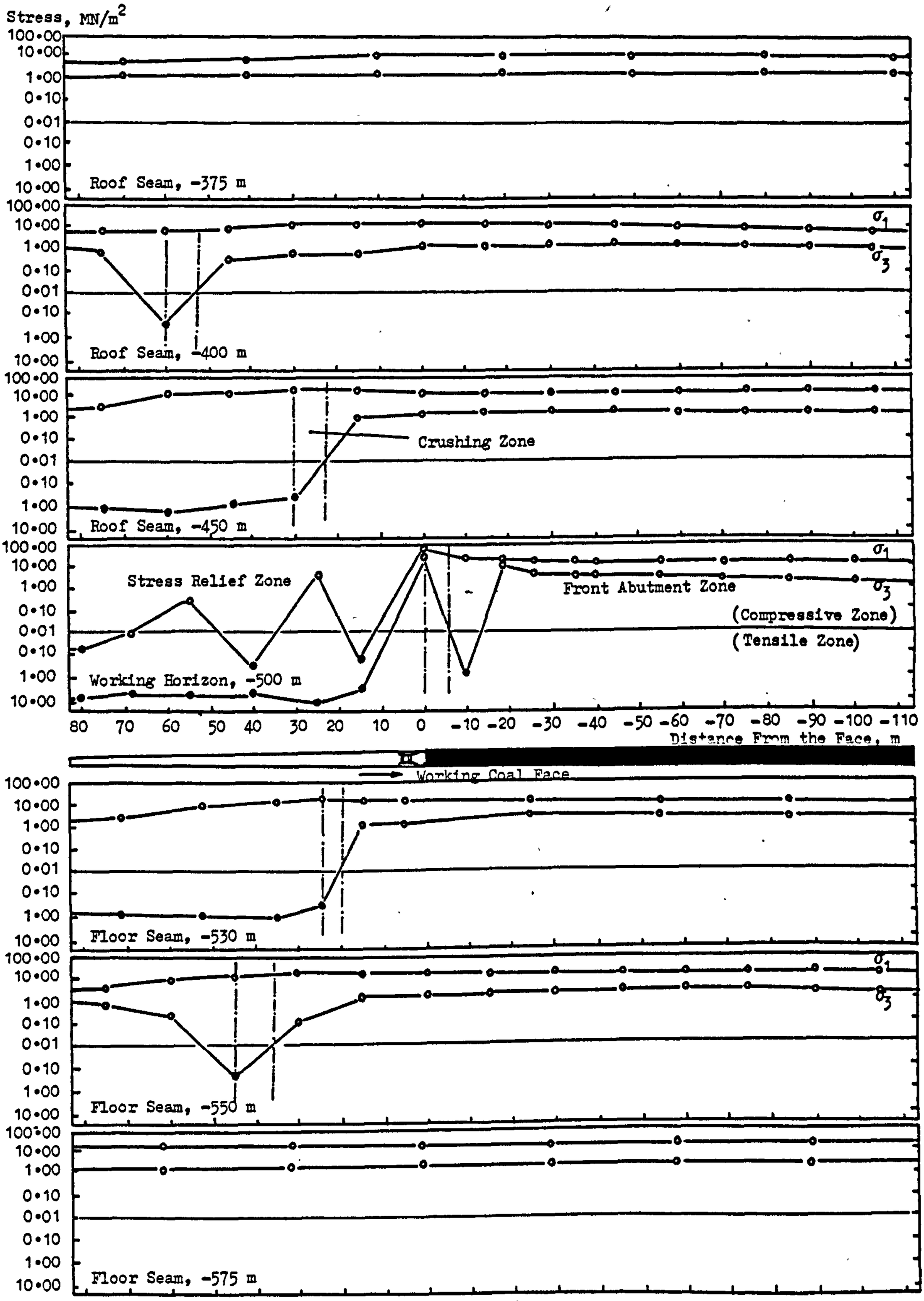

FIGURE (9.3.1) Revised Theoretical Maximum and Minimum Principal Stress Distribution Profiles Around a 500 m Deep Working Longwall Face

TABLE (9.3.1) Revised Theoretical Maximum and Minimum Principal Stress Values for a Coal Seam 125 m Above a 500 m Deep Working Longwall Face

DISTANCE FROM THE FACE LINE (m)	MAXIMUM PRINCIPAL STRESS σ_1 (MN/m^2)	MINIMUM PRINCIPAL STRESS σ_3 (MN/m^2)
70	-8•55	-1•03
40	-9•33	-1•04
10	-9•60	-1•29
-20	-9•59	-1•60
-50	-9•48	-1•86
-80	-9•35	-2•01
-110	-9•24	-2•11

TABLE (9.3.2) Revised Theoretical Maximum and Minimum Principal Stress Values for a Coal Seam 100 m Above a 500 m Deep Working Longwall Face

DISTANCE FROM THE FACE LINE (m)	MAXIMUM PRINCIPAL STRESS σ_1 (MN/m^2)	MINIMUM PRINCIPAL STRESS σ_3 (MN/m^2)
75	-7•96	-0•72
60	-8•80	0•58
45	-9•46	-0•47
30	-10•10	-0•57
15	-10•40	-0•84
0	-10•60	-1•23
-15	-10•60	-1•42
-30	-10•60	-1•70
-45	-10•50	-1•90
-60	-10•30	-2•03
-75	-10•20	-2•17
-90	-10•10	-2•24
-105	-9•99	-2•32

TABLE (9.3.4) Theoretical Values for Maximum and Minimum Principal Stresses Along the Roof of a 500 m Deep Longwall Face.

DISTANCE FROM THE FACE LINE (m)	MAXIMUM PRINCIPAL STRESS σ_1 (MN/m^2)	MINIMUM PRINCIPAL STRESS σ_3 (MN/m^2)
80	0•06	8•06
67	-0•01	7•59
54	-0•43	8•00
40	0•45	7•63
27	-1•67	10•70
15	0•21	4•29
0	-74•00	-22•20
-10	-20•40	0•74
-18	-18•90	-10•10
-25	-17•00	-8•43
-35	-15•90	-7•51
-40	-15•10	-6•56
-55	-13•90	-5•80
-70	-13•20	-5•01
-85	-12•80	-4•52
-100	-12•60	-4•16
-115	-12•40	-3•79
-130	-12•30	-3•78
-145	-12•20	-3•66
-160	-12•10	-3•54
-175	-12•10	-3•47
-190	-12•10	-3•39

TABLE (9.3.3) Revised Theoretical Maximum and Minimum Principal Stress Values for a Coal Seam 50 m Above a 500 m Deep Working Longwall Face

DISTANCE FROM THE FACE LINE (m)	MAXIMUM PRINCIPAL STRESS σ_1 (MN/m^2)	MINIMUM PRINCIPAL STRESS σ_3 (MN/m^2)
75	-6•82	1•07
60	-10•10	1•56
45	-12•00	0•94
30	-13•70	0•51
15	-13•90	-0•90
0	-13•70	-1•29
-15	-13•20	-2•22
-30	-12•60	-2•80
-45	-12•10	-2•91
-60	-11•70	-3•07
-75	-11•50	-3•06
-90	-11•30	-3•09
-105	-11•20	-3•05

TABLE (9.3.5) Revised Theoretical Maximum and Minimum Principal Stress Values for a Coal Seam 30 m Below a 500 m Deep Working Longwall Face

DISTANCE FROM THE FACE LINE (m)	MAXIMUM PRINCIPAL STRESS σ_1 (MN/m^2)	MINIMUM PRINCIPAL STRESS σ_3 (MN/m^2)
72	-4•52	0•92
52	-9•98	1•29
37	-13•20	1•40
25	-20•00	0•54
15	-19•60	-1•50
5	-17•50	-1•16
-25	-15•80	-4•56
-55	-14•10	-4•53
-85	-13•30	-4•05

TABLE (9.3.6) Revised Theoretical Maximum and Minimum Principal Stress Values for a Coal Seam 50 m Below a 500 m Deep Working Longwall Face

DISTANCE FROM THE FACE LINE (m)	MAXIMUM PRINCIPAL STRESS σ_1 (MN/m^2)	MINIMUM PRINCIPAL STRESS σ_3 (MN/m^2)
75	-5•52	-0•80
60	-7•90	-0•30
45	-11•40	0•34
30	-13•60	-0•10
15	-15•60	-0•37
0	-16•00	-1•67
-15	-15•90	-1•89
-30	-15•40	-2•79
-45	-14•80	-3•32
-60	-14•40	-3•42
-75	-14•10	-3•56
-90	-13•80	-3•55
-105	-13•70	-3•56

TABLE (9.3.7) Revised Theoretical Maximum and Minimum Principal Stress Values for a Coal Seam 75 m Below a 500 m Deep Working Longwall Face

DISTANCE FROM THE FACE LINE (m)	MAXIMUM PRINCIPAL STRESS σ_1 (MN/m^2)	MINIMUM PRINCIPAL STRESS σ_3 (MN/m^2)
62	-14•10	-1•23
32	-15•10	-2•00
2	-14•90	-2•75
-28	-14•50	-3•12
-58	-14•30	-3•31
-88	-14•10	-3•40

advance and the experimental data referred to previously suggests average angles of 60° and 45° for the strata above and below respectively. Fracturing of the strata should take place in this direction and the permeabilities of coal seams are expected to increase dramatically along the fracture planes. Plate (9.1) shows a model in which the nature of fracturing at the longwall face and the strata above it are demonstrated, (92).

Figure (9.3.2) shows the general stress-permeability profiles for coal seams around working longwall faces. These profiles are based on the experimental observations discussed in Chapter 7 and the revised theoretical stress profiles given in Figure (9.3.1). Permeabilities of coal seams in the virgin strata are determined by magnitude of the cover load, therefore, as the seam gets deeper lower permeabilities are expected. Permeability of a coal seam decreases sharply with increasing stress in the front abutment zone. As the crushing zone is reached, (3 - 5 m infront of the face at the working horizon) permeability of the seam increases dramatically due to fracturing. The intensity of fracturing in the crushing zone of a source seam depends on its distance to the working face. Therefore, the fracture permeability of source seams would decrease as the vertical distance to the face increases. Permeabilities of coal seams remain high in the stress relief zone and a slight decrease in permeability of fractured coal would be observed as the cover load is established.

Permeability of a coal seam at different stress zones would depend on the type and strength of coal itself. As discussed

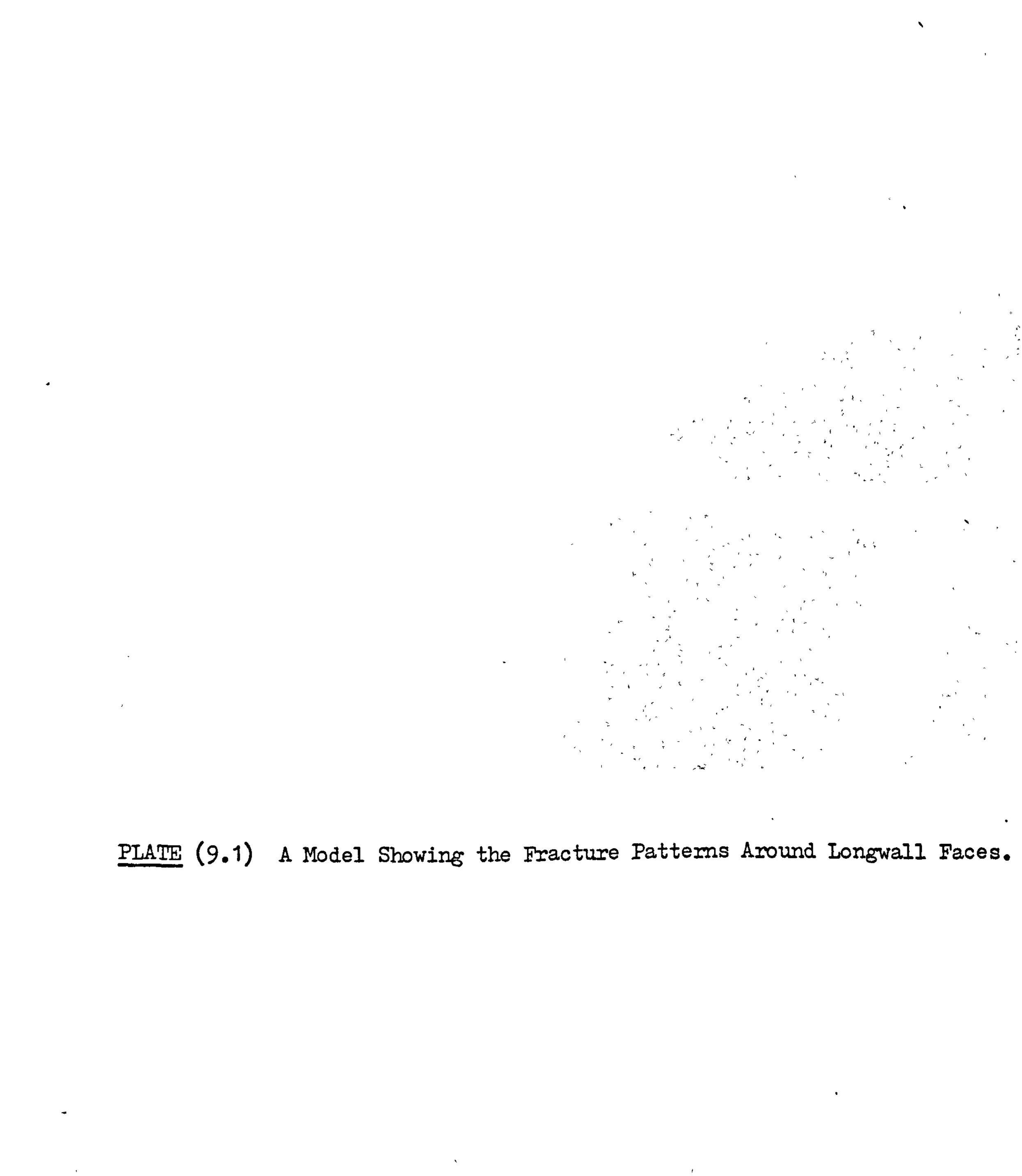

PLATE (9.1) A Model Showing the Fracture Patterns Around Longwall Faces.

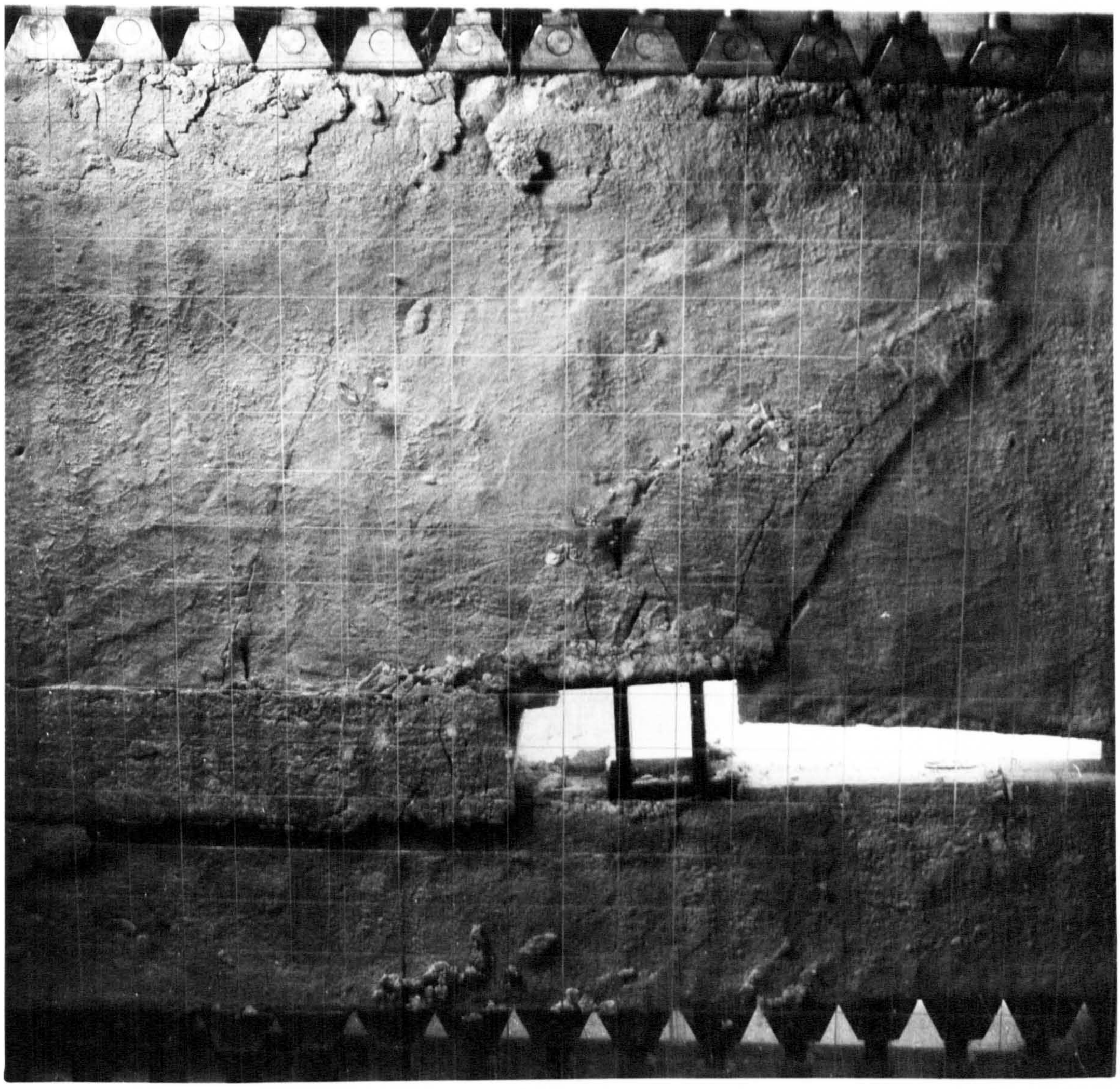

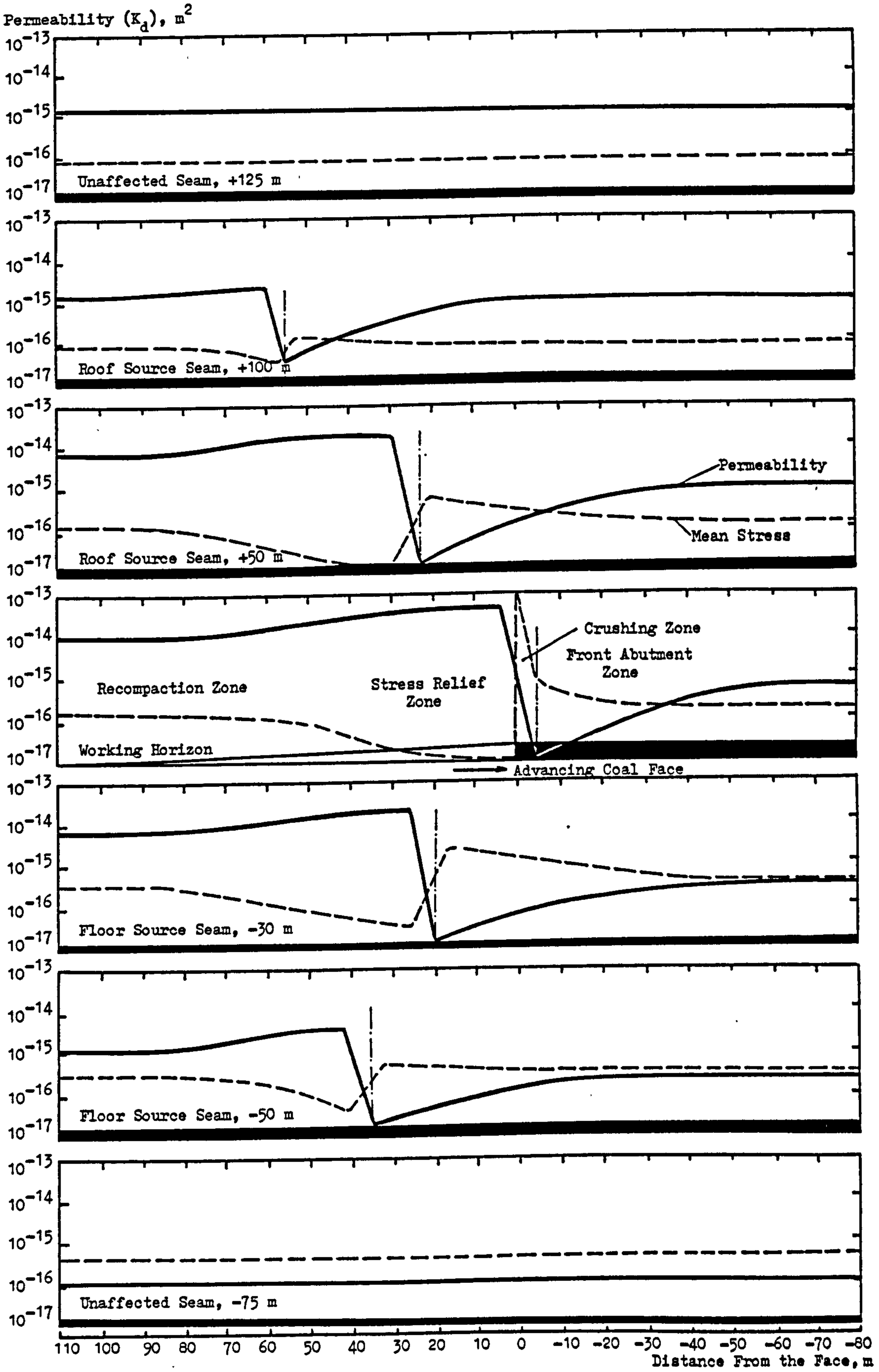

FIGURE (9.3.2) General Stress-Permeability Profiles for Coal Seams Around a Working Longwall Face at Any Depth. (Stresses are not to scale)

in Chapters 7 and 8, equivalent stress levels induced different magnitude permeabilities for different coals tested. Also, the intensity of fracturing was observed to be different in different mechanical strength coals. Table (9.3.8) lists the experimental permeability values, for the tested coals, under stress conditions simulating the different stress zones around 300, 500, 700 m deep coal seams.

So far, it was assumed that the coal seams concerned were in areas that had not been affected by under or over mining of the adjacent seams. If it is assumed that the coal seam being worked lies vertically below a seam that has been worked previously (distance between two seams <50 m), it should then be expected that the working seam would have higher induced permeabilities due to its stress history. Figure (9.3.3) shows the stress-permeability profiles for coal seams that are assumed to be affected previously by the stress disturbances created during the mining of an overlying seam.

As shown in Figure (9.3.3), permeability of the working seam, which lies 30 m below old workings, would be high due to the effects of previous stress disturbances. High stresses in the front abutment zone will not reduce the permeability to a great extent and further fracturing in the crushing zone will cause a slight increase in permeability of the seam. The floor source seam lying 20 m below the working horizon would have a relatively high induced permeability due to the old workings and it will increase further as the seam 20 m above is extracted. Relatively high permeabilities around these seams would not necessarily mean very high flow rates of methane since the gas

TABLE (9.3.8) Experimental Permeability Values Under Stress Conditions Simulating the Different Stress Zones Around 300, 500, 700 m Deep Coal Seams

TYPE OF COAL	PERMEABILITY, K_d ($10^{-16} m^2$)				
	AHEAD OF THE FACE			BEHIND THE FACE	
	STATIC LOAD ZONE	FRONT ABUTMENT ZONE	CRUSHING ZONE	STRESS RELIEF ZONE	RECOMPACTION ZONE
ACILIK					
300 m deep	1•60 - 4•41	0•40 - 1•05			260•00 - 328•00
500 m deep	1•30 - 3•44	0•30 - 0•91	110•00 - 170•00	712•00 - 820•00	230•00 - 295•00
700 m deep	1•00 - 2•73	0•26 - 0•77			200•00 - 269•00
CAYDAMAR					
300 m deep	1•60 -26•00	0•21 - 6•20			109•00 - 280•00
500 m deep	1•00 -21•00	0•14 - 4•70	120•00 - 288•00	470•00 - 947•00	94•00 - 270•00
700 m deep	0•70 -17•00	0•10 - 3•90			77•00 - 260•00
BARNSLEY					
300 m deep	0•67 -28•00	0•09 - 1•92			97•00 - 150•00
500 m deep	0•50 -18•22	0•05 - 1•30	70•00 - 190•00	600•00 - 650•00	71•00 - 125•00
700 m deep	0•35 -10•84	0•05 - 0•96			66•00 - 105•00
COCKSHEAD					
300 m deep	0•96 - 9•25	0•10 - 1•13			45•00 - 60•00
500 m deep	0•64 - 6•43	0•06 - 0•74	120•00 - 180•00	300•00 - 400•00	40•00 - 58•00
700 m deep	0•49 - 4•14	0•05 - 0•70			38•00 - 55.00
BANBURY					
300 m deep	0•73 - 3•40	0•11 - 0•26			273•00 - 280•00
500 m deep	0•54 - 2•30	0•07 - 0•21	200•00 - 212•00	460•00 - 482•00	252•00 - 270•00
700 m deep	0•38 - 1•80	0•05 - 0•16			232•00 - 260•00
DUNSIL					
300 m deep	0•94 -14•30	0•18 - 2•36			113•00 - 116•00
500 m deep	0•74 -10•40	0•13 - 1•86	53•00 - 125•00	371•00 - 855•00	95•00 - 120•00
700 m deep	0•53 - 7•60	0•09 - 1•59			79•00 - 100•00
DEEP HARD					
300 m deep	3•80 - 9•69	0•45 - 0•89			23•00 - 48•00
500 m deep	2•60 - 5•99	0•32 - 0•54	140•00 - 155•00	485•00 - 850•00	18•00 - 43•00
700 m deep	1•80 - 4•11	0•20 - 0•32			14•00 - 40•00

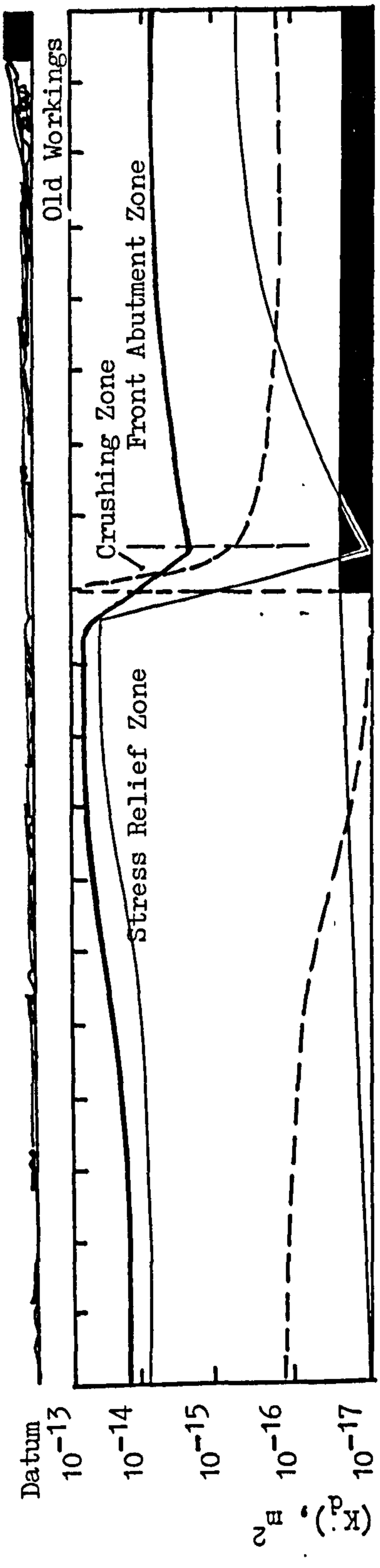

FIGURE (9.3.3) Stress-Permeability Profiles for Coal Seams that have been Affected by Previous Mining.

content and pressure in those seams would be lowered due to long term migration towards the old workings.

Figure (9.3.4) shows the different permeability zones and the suggested flow paths of methane around a working longwall face which is assumed to be a new mining area.

Ahead of the face, permeabilities of coal seams are very low due to high abutment pressures. The outer boundaries of this low permeability zone are defined by the parabola on the right hand side of the figure. Permeability of coal seams will start to increase in the crushing zone which lies between the inner parabola and the maximum permeability line. Behind the face, points of maximum permeability will lie at angles of 60° and 45° above and below the working horizon. The majority of the gas flowing into the workings would be expected from areas behind these points, within which permeability remains very high. Coal seams at distances more than 100 m above and 50 m below the working face are not expected to be highly effected by the stress disturbances. Permeabilities of these seams will generally remain constant with very little gas flow taking place towards the workings.

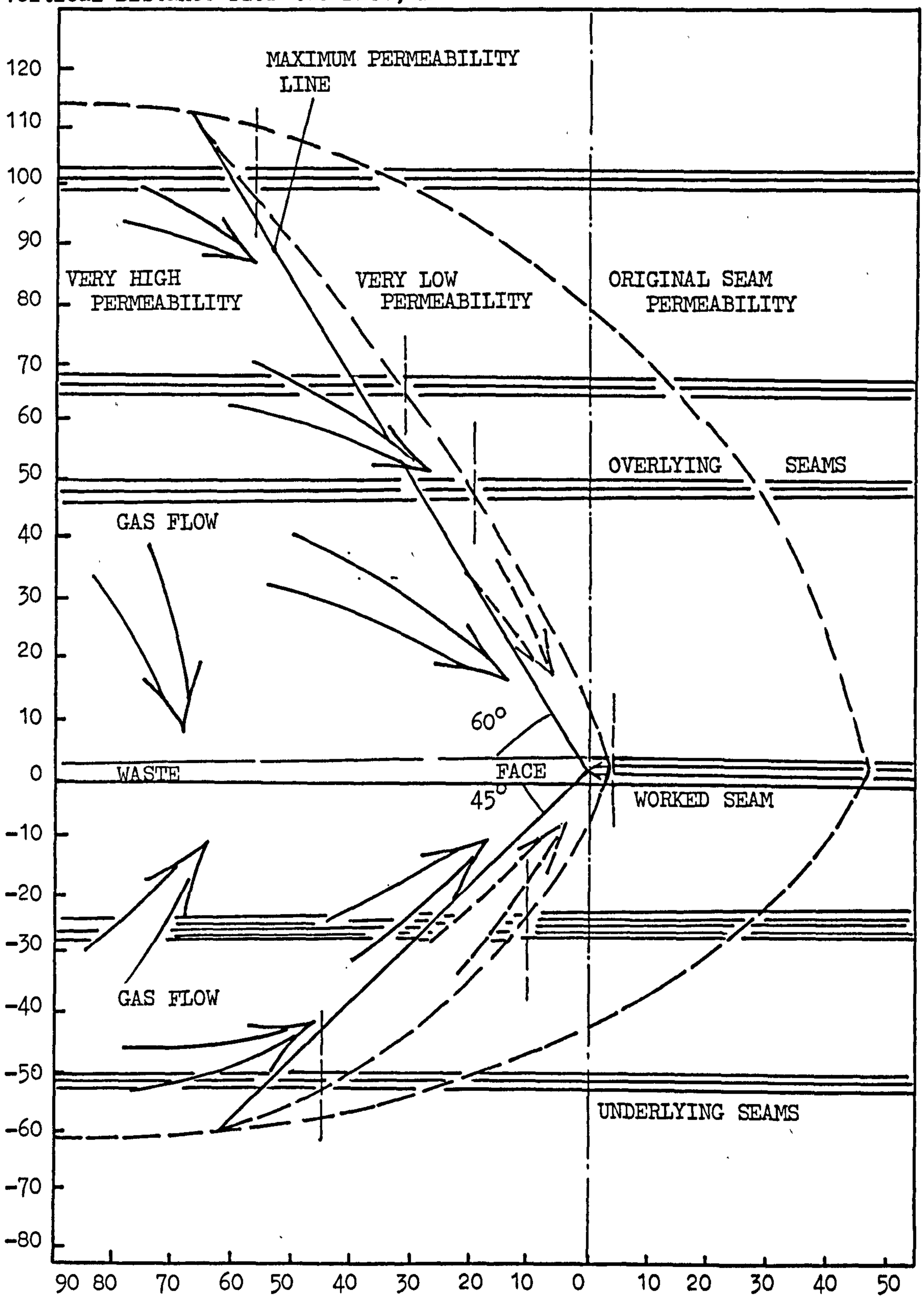

FIGURE (9.3.4) Different Permeability Zones and Suggested Flow Paths of Methane Around a Working Longwall Face.

CONCLUSIONS

CONCLUSIONS

This research was primarily concerned with the stress-permeability behaviour of different coals and a relationship between rank and permeability of coal under stress was established. The implications of the experimental results were discussed in relation to mining practice.

Laboratory investigations into the stress-permeability behaviour of seven different coals have shown that, in general, permeability of coal decreases as the applied stress increases. Microfracturing of coal under very high axial and radial stresses did not create an immediate increase in its permeability as one might have expected. It was only after the relieving of the stresses and complete relaxation of the specimen that the permeability of coal increased and exhibited higher permeability values when stressed for the second time. When fractured under the simulated stress conditions of a crushing zone, permeability of coal increased 10 to 500 times depending on the type of coal concerned. The effect of stress on permeability of fractured coal was very low and fracture permeabilities of all the coals tested were similar.

Permeability of coal, at very low stress levels was effected by the degree of fracturing of the specimens and a large scatter in base permeabilities of coals was observed. However,

the compressibility (i.e. the degree of reduction in permeability under stress) of the coal material was found to be the controlling factor in determining the effect of stress on permeabilities of different coals at high stress levels ($\sigma_3 \geqslant 1{\cdot}50$ MN/m^2). Compressibility of coal increased with decreasing rank up to 34 percent volatile matter and then decreased towards the lower rank coals. At high stress levels (i.e. the stresses representing the stress conditions at the front abutment zone of a working longwall face), the permeability of coals with low compressibility was about five times greater than that of highly compressible coals.

When these results are interpreted in relation to actual mining conditions, the permeability of coal seams should decrease between 10 to 100 times (depending on the compressibility of the coal concerned) in the front abutment zone of a working longwall face. Under equivalent stress conditions the permeability of the worked seam ahead of the face will be relatively higher for coals of lower compressibility. This may be one of the factors accounting for comparatively high rates of gas emission observed in some longwall faces.

Once the fracturing of a coal seam is initiated in the crushing zone, permeability of the seam will increase drastically and reach a peak in the stress relief zone. Permeability of a gas source seam at the stress relief zone of a working longwall face will be about 10 to 500 times higher than its inherent permeability. The majority of gas flow into the workings should therefore be expected from the stress relief zone behind the face.

Although there has been a considerable amount of underground research into the changing stresses, and the flow of methane around working longwall faces, these two subjects have usually been studied within the framework of different disciplines (rock mechanics and mine ventilation) in mining engineering. No reference to the simultaneous measurements of changes in stress and gas flow was made in literature. The author believes that a comprehensive study of the stress disturbances and induced permeabilities within the area affected by a working longwall face would provide the data needed for predicting the amount of methane flow into mine airways. This could be achieved by using boreholes drilled in different levels above and below the working horizon and by monitoring simultaneously the gas flow and pressure as well as the changing stresses as the face advances. Such an investigation will provide knowledge concerning the locations of the maximum permeability areas around working longwall faces. The author considered that the absence of such information constituted a deficiency in the field of mine environmental engineering.

Further laboratory investigation into the stress-permeability relationship of coals should take into account the adsorption of methane by coal. A comparative study of methane and nitrogen permeabilities of coal under stress may provide a correlation between the two.

The experimental apparatus should be improved to allow the application of very high stresses perpendicular to the bedding planes and to the direction of gas flow. It is believed that the

simultaneous measurements of axial and radial flow of gas would provide further information about the directional anisotropy of coal permeability under stress. A more sophisticated instrumentation is required to provide such measurements.

The effect of moisture on permeability of coal and the two-phase flow of methane and water should be studied in more detail. Experiments have shown that if a freshly mined area of a coal seam is saturated with water, its permeability to gas will be relatively low in the early stages. Methane relative permeabilities and water relative permeabilities of coal should be determined by a thorough laboratory investigation and these should be considered in simulating the actual mining conditions.

Finally, the stress-permeability behaviour of anthracites and semi-anthracites should also be studied since they were not included in this research.

ACKNOWLEDGEMENTS

The author would like to express his gratitude to Dr. M. J. McPherson and Mr. L. H. Morris for their supervision and guideance throughout the research, and to Professor T. Atkinson for allowing the project to be undertaken.

He wishes to thank the Scientific and Technical Research Council of Turkey (TUBITAK) for providing finance. For supplying coal samples he is grateful to Turkish Coal Enterprises and the National Coal Board.

He would also like to thank:

The technical staff of the Mining Department Workshop for their help in preparing test specimens and equipment used.

The research students and staff of the Department of Mining Engineering at the University of Nottingham.

Catherine Ellis for her care and patience in typing this thesis.

REFERENCES

(1) MUSKAT, M.
'Physical Principles of Oil Production',
McGraw-Hill Book Co., Inc., New York, 1949.

(2) AMYX, J. M., BASS, D. M., WHITTING, R. L.
'Petroleum Reservoir Engineering',
McGraw-Hill Book Co., Inc., New York, 1960.

(3) SCHEIDEGGER, A. E.
'The Physics of Flow Through Porous Media',
University of Toronto Press, Revised Edition, 1963.

(4) GRAHAM, J. I.
'The Permeability of Coal to Air or Gas, and the Solubilities of Different Gases in Coal',
Trans. Inst. Min. Engrs., Vol. 52, 1916-1917, pp 338-347.

(5) GRAHAM, J. I.
'The Permeability of Coal to Gases',
Trans. Inst. Min. Engrs., Vol. 58, 1918-1919, pp 32-39.

(6) GRAHAM, J. I.
'The Adsorption or Solution of Methane and Other Gases in Coal, Charcoal and Other Materials',
Trans. Inst. Min. Engrs., Vol. 62, 1921-1922, pp 298-322.

(7) AUDIBERT, E.
'A Hypothesis of Methane Emission',
Rev. Ind. Miner. Mem., Vol. 12, 1932, pp 41-42.

(8) BRIGGS, H. and SINHA, R. P.
'The Discharge of Firedamp From Coal',
Trans. Inst. Min. Engrs., Vol. 87, 1933-1934, pp 190-204.

(9) SEVENSTER, P. G.
'Diffusion of Gases Through Coal',
Fuel, Vol. 38, 1959, pp 403-418.

(10) HUANG, W. M. AND SHELTON, T. C.
'Experimental Reuslts of Coal Permeability Tests',
Mining Engineering, Vol. 14, 1962, pp 52-54.

(11) JONES, R. E.
'A Laboratory Investigation into the Permeability of Coal',
Ph. D. Thesis, University of Nottingham, 1969.

(12) KARN, F. S., FRIEDEL, B., THAMES, B. M. and SHARKEY, A. G.
'Gas Transport Through Sections of Solid Coal',
Fuel, Vol. 49, 1970, pp 249-256.

(13) THIMONS, E. D., KISSEL, F. N.
'Diffusion of Methane Through Coal',
Fuel, Vol. 52, 1973, pp 274-280.

(14) WOLSTENHOLME, E. F.
'A Study of the Movement of Firedamp Within the Floor Strata of a Coal Seam Liable to Outbursts',
Ph. D. Thesis, University of Nottingham, 1968.

(15) KISSEL, F. N.
'The Methane Migration and Storage Characteristics of the Pittsburgh, Pocahontas No. 3, and Oklahoma Hartshorne Coalbeds',
U.S. Bureau of Mines, Report of Investigations, No.7667, 1972, 22p.

(16) FATT, I. and DAVIS, D. H.
'Reduction in Permeability with Overburden Pressure',
Trans. AIME, Petroleum Branch, Vol. 195, 1952, p 329.

(17) PATCHING, T. H.
'Variations in the Permeability of Coal',
Proc. 3rd Rock Mech. Symp., University of Toronto,
January 1965, pp 185-199.

(18) GUNTHER, J.
'Investigation of the Relationship Between Coal and the Gas Contained in It',
Revue de l'industrie Minerale, Vol. 47, No.10, 1965, p.693,
S.M.R.E. Translation No. 5134.

(19) FATT, I.
'The Effect of Overburden Pressure on Relative Permeability',
Trans. AIME, Petroleum Branch, Vol. 198, 1953, pp 325-326.

(20) McLATCHIE, A. S., HEMSTOCK, R. A., YOUNG, J. W.
'The Effective Compressibility of Reservoir Rock and Its Effects on Permeability',
Trans. AIME, Petroleum Branch, Vol. 213, 1958, pp 386-388.

(21) DABBOUS, M. K., REZNIK, A. A., TABER, J. J. and FULTON, P. F.
'The Permeability of Coal to Gas and Water',
Trans. AIME, Petroleum Branch, Vol. 257, 1974, pp 563-572.

(22) MORDECAI, M.
'An Investigation into the Effect of Stress on Permeability of Rock Taken from Carboniferous Strata',
Ph. D. Thesis, University of Nottingham, 1971.

(23) MORDECAI, M., MORRIS, L. H.
'The Effects of Stress on the Flow of Gas through Coal Measure Strata',
Trans. Inst. Min. Engrs. Vol. 133, 1974, pp 435-443.

(24) POMEROY, C. D., and ROBINSON, D. J.
'The Effect of Applied Stresses on the Permeability of Middle Rank Coal to Water',
Int. J. Rock Mech. Min. Sci., Vol. 4, 1967, pp 329-343.

(25) SOMERTON, W. H., SOYLEMEZOGLU, I. M. and DUDLEY, R.C.
'Effect of Stress on Permeability of Coal',
Int. J. Rock Mech. Min. Sci. Geomech. Abstr.,
Vol. 12, 1975, pp 129-145.

(26) GAWUGA, J. K.
'Flow of Gas Through Stressed Carboniferous Strata',
Ph. D. Thesis, University of Nottingham, 1979.

(27) McPHERSON, M. J.
'The Occurence of Methane in Mine Workings',
Journ. of Mine Ventilation Society of South Africa,
Vol. 28, No. 8, 1975, pp 118-128.

(28) BANGHAM, D. H., FRANKLIN, R. E., HIRST, W. and MAGGS, A. P.
'A Structural Model for Coal Substance',
Fuel, Vol. 28, No. 10, 1949, pp 231-238.

(29) BLAYDEN, D. H., GIBSON, J. and RILEY, H. L.
'An X-Ray Study of the Structure of Coals, Cokes and Chars',
Proc. Conf. Ultra-Fine Structure of Coals and Cokes,
B.C.U.R.A., London, 1944, pp 176-231.

(30) BROWN, J. K. and HIRSCH, P. B.
'Recent Infra-Red and X-Ray Studies of Coal',
Nature, Vol. 175, No. 4449, February 1955, pp 229-233.

(31) KING, J. G. and WILKINS, E. T.
'The Internal Structure of Coal',
Proc. Conf. Ultra-Fine Structure of Coals and Cokes,
B.C.U.R.A., London, 1944, pp 46-56.

(32) GAN, H., NANDI, S. P. and WALKER, P. L.
'Nature of Porosity in American Coals',
Fuel, Vol. 51, 1972, pp 272-277.

(33) ZWIETERING, P. and VAN KREVELEN, D. W.
'Chemical Structure and Properties of Coal IV-Pore Structure',
Fuel, Vol. 33, 1954, pp 331-337.

(34) TODA, Y. and TOYODA, S.
'Application of Mercury Porosimetry to Coal',
Fuel, Vol. 51, 1972, pp 199-201.

(35) GRIFFITH, M. and HIRST, W.
'The Heat of Wetting of Coals in Organic Liquids',
Proc. Conf. Ultra-Fine Structure of Coals and Cokes,
B.C.U.R.A., London, 1944, pp 80-94.

(36) LANGMUIR, I.
'The Constitution and Fundamental Properties of Solids and Liquids',
J. Amer. Chem. Soc., Vol. 38, 1916, pp 2221-2295.

(37) BRUNNAUER, S., EMMET, P. H. and TELLER, E.
'Adsorption of Gases in Multi-Molecular Layers',
J. Amer. Chem. Soc., Vol. 60, 1938, pp 309-319.

(38) JOLLY, D. C.
'An Investigation into the Relationship Between the Methane Sorption Capacity of Coal and Gas Pressure',
Ph. D. Thesis, University of Nottingham, 1967.

(39) JOUBERT, J. I., GREIN, C. T. and BIENSTOCK, D.
'Sorption of Methane in Moist Coal',
Fuel, Vol. 52, 1973. pp 181-185.

(40) JOUBERT, J. I., GREIN, C. T. and BIENSTOCK, D.
'Effect of Moisture on the Methane Capacity of American Coals',
Fuel, Vol. 53, 1974, pp 186-191.

(41) ETTINGER, I. L. and LIDIN, G. D.
Izv. Akad. Nauk. SSSR, Otd. Tekh. Nauk 1950, No. 8, 1198.

(42) ETTINGER, I. L., LIDIN, G. D., DMITRIEV, A. M. and ZHUPAKHINA, E. S.
'Systematic Handbook for the Determination of the Methane Content of Coal Seams From the Seam Pressure of the Gas and the Methane Capacity of the Coal',
Moscow, 1958, National Coal Board Translation No. A1606/SEH.

(43) BARRER, R. M.
'Diffusion in and through Solids',
Cambridge University Press, London, 1941.

(44) LOEB, L. B.
'Kinetic Theory of Gases',
McGraw-Hill Book Co., Inc., New York, First Edition, 1927.

(45) LAMB, H.
'Hydrodynamics',
Cambridge University Press, London, 6th Ed., 1932.

(46) KNUDSEN, M.
'Die Gesetze der Molekularstromung und der inneren Reibungsstromung der Gase durch Rohren',
Annalen der Physik, Vol. 28, Leipzig, 1909, pp 75-130.

(47) ADZUMI, H.
'On the Flow of Gases through a Porous Wall',
Bulletin of Chemical Society of Japan, Vol. 12, No. 6, June 1937, pp 304-312.

(48) DARCY, H.
'Les Fontaines Publiques de la Ville de Dijon',
V. Dalmont, Paris, 1856.

(49) HUBBERT, M. K.
'Darcy's Law and the Field Equations of the Flow of Underground Fluids',
Trans. AIME, Petroleum Branch, Vol. 207, 1956, pp 222-239.

(50) CARMAN, P. C.
'Flow of Gases through Porous Media',
Butterworths Scientific Publications, London, 1956.

(51) NUTTING, P. G.
'Physical Analysis of Oil Sands',
Bull. Amer. Assoc. Petrol. Geol., Vol. 14, 1930, pp 1337-1349

(52) FANCHER, G. H., LEWIS, J. A. and BARNES, K. B.
'Some Physical Characteristics of Oil Sands',
Proc. 3rd Penn. Min. Ind. Conf., Penn-State Coll. Bull., No. 12, 1933, pp 65-167.

(53) KLINKENBERG, L. J.
'The Permeability of Porous Media to Liquids and Gases',
Drilling and Production Practice, Published by the American Petroleum Institute, 1941, pp 200-211.

(54) ROSE, W. D.
'Permeability and Gas-Slippage Phenomena',
Drilling and Production Practice, Published by the American Petroleum Institute, 1948, pp 209-217.

(55) SOWIER, T. S.
'Steady-State and Non-Steady-State Flows of Compressible Fluids through Sorptive Porous Media',
Ph. D. Thesis, University of Nottingham, 1973.

(56) EVANS I. and POMEROY, C. D.
'The Strength, Fracture and Workability of Coal',
National Coal Board, MRDE, Burton-on-Trent, Corrected Reprint, 1973.

(57) WHITTAKER, B. N.
'An Appraisal of Strata Control Practice',
Trans. Inst. Min. Engrs., Vol. 166, 1974, pp 9-24.

(58) PENG, S. S.
'Coal Mine Ground Control',
John Wiley and Sons Inc., New York, 1978.

(59) PENG, S. S.
'Roof Control Studies at Olga No. 1 Mine, Coalwood WV',
Final Report to the U.S. Bureau of Mines, Contract No. J0155125, July 1976, 22p.

(60) METCALF, J. R.
'The Front Abutment of a Longwall Face',
Int. J. Rock. Mech. Min. Sci., Vol. 4, 1967, pp 95-207.

(61) HAZINE, H. I.
'A Study of the Development of the Surface Strains Produced by Mining Subsidence',
M. Phil. Thesis, University of Nottingham, 1977.

(62) HAZINE, H. I.
Ongoing Research into the Stress and Strain Developments at Face Ends,
Department of Mining Engineering, University of Nottingham.

(63) WOODRUFF, S. D.
'Methods of Working Coal and Metal Mines',
3 Volumes, Pergamon Press, London, 1966.

(64) GRIFFITH, A. A.
'Theory of Rupture',
Proc. 1st Int. Conf. of Applied Mechanics, Delft, 1924, pp 55-64.

(65) PALVELEV, V. T.
'Methane Sorption by Mineral Coals of the Don Bass at High Pressure',
National Coal Board Translation A 371.

(66) YEREBASMAZ, G.
'An Investigation into the Flow of Methane through Coal Samples',
M. Phil. Thesis, University of Nottingham, 1981.

(67) HOEK, E. and FRANKLIN, J. A.
'Simple Triaxial Cell for Field or Laboratory Testing of Rock',
Trans. Inst. Min. Metall. Vol. 77, 1968, pp A22-6.

(68) 'British Standards',
BS1016: Part 3, 1973.

(69) JUMIKIS, A. R.
'Rock Mechanics',
Trans. Tech. Publications, Rockport MA, First Edition, 1979.

(70) DUNCAN, N.
'Engineering Geology and Rock Mechanics',
Vol. 2. Leonard Hill, London, 1969.

(71) SCHUYER,J. DIJKSTRA, H. and VAN KREVELEN, D. W.
'Chemical Structure and Properties of Coal - VII Elastic Constants',
Fuel, Vol. 33, 1954,

(72) GRAY, D. E., et al.
'American Institute of Physics Handbook',
McGraw-Hill Book Co., Inc., New York, 1957.

(73) KISSEL, F. N. and EDWARDS, J. C.
'Two-Phase Flow in Coalbeds',
U.S. Bureau of Mines, Report of Investigation, RI 8066,
September 1975, 22p.

(74) PRICE, H. S., McCULLOCH, R. C., EDWARDS, J. C. and
KISSEL, F. N.
'A Computer Model Study of Methane Migration in Coal Beds',
CIM Bulletin, Vol. 66, September 1973, pp 103-112.

(75) HALL, H. N.
'Compressibility of Reservoir Rocks',
Trans. AIME, Petroleum Branch, Vol 198, 1953, pp 309-311.

(76) FATT, I.
'Pore Volume Compressibilities of Sandstone Reservoir Rocks',
Trans. AIME, Petroleum Branch, Vol. 213, 1958, pp 382-364.

(77) NATIONAL COAL BOARD - MRDE
'Prediction of Firedamp Emission',
Final Report on ECSC Research Project, 7220-AC/B01,
December 1978, 102p.

(78) DUNMORE, R.
'Towards a Method of Prediction of Firedamp Emission
for British Coal Mines',
Proc. 2nd Mine Ventilation Congress, Session IX, 1979, pp 1-4.

(79) KEEN, T. F.
'The Simulation of Methane Flow in Carboniferous Strata',
Ph. D. Thesis, University of Nottingham, 1977.

(80) O'SHAUGHNESSY, S. M.
'The Computer Simulation of Methane Flow through Strata
Adjacent to a Working Longwall Coalface',
Ph. D. Thesis, University of Nottingham, 1980.

(81) JEGER, J.
'New Aspects of the Prediction of Methane Emission at
Faces in Level Measures and in Headings Situated in the
De-Stressed Zones Associated with Such Faces',
Proc. of Inf. Symp. on Methane, Climate, Ventilation
in the Coal Mines of the European Communities, Luxembourg,
November 1980, Published by the Colliery Guardian,
Vol. 2, pp 10-50.

(82) IEA COAL RESEARCH
'Methane Prediction in Coal Mines',
IEA, 1978, 77p.

(83) AIREY, E. M.
'Gas Emission from Broken Coal. An Experimental and
Theoretical Investigation',
Int. J. Rock Mech. Min. Sci., Vol. 5, 1968, pp 475-496.

(84) AIREY, E. M.
'A Theory of Gas Emission in Coal Mining Operations',
National Coal Board, MRDE Report, No. 21, May 1971, 25p.

(85) NOACK, K.
'Research into the Shape and Extent of Induced, Drainable Gas Pockets in the Locality of Level to Semi-Steep Workings of the Ruhr Carboniferous',
National Coal Board Translation, A2963/FWH, June 1970.

(86) OLDROYD, G. C.
'The Investigation into the Mechanism of Methane Outbursts from the Floor Strata of the Silkstone Seam',
Ph. D. Thesis, University of Nottingham, 1969.

(87) McC. STEWART, I.
'Diffusional Analysis of Seam Gas Emission in Coal Mines',
CIM Bulletin, Vol. 64, April 1971, pp 62-70.

(88) MYASNIKOV, A. A. and MASCHENKO, I. D.
'The Methane Emission of a Seam in Relation to the Rate of Face Advance',
Trudy Vost NII, Vol. 4, Moscow, 1964, pp3-12,
SMRE Translation No.5107.

(89) RICHARDS, M. J.
'An Investigation into the Movement of Firedamp from the Strata in the Region of Working Longwall Faces',
Ph. D. Thesis, University of Nottingham, 1975.

(90) DAVIS, J. G. and KRICKOVIC, S.
'Gob Degasification Research. A Case History',
Methane Control in Eastern U.S. Coal Mines. Proc. of the Symp. of the Bureau of Mines/Ind. Tech. Transf. Seminar, Morgantown WV, May 1973, 96p.

(91) WHITTAKER, B. N., SINGH, R. N. and NEATE, C. J.
'Effect of Longwall Mining on Ground Permeability and Subsurface Drainage',
Proc. 1st Int. Mine Drainage Symp., Denver, USA, May 1979, pp 161-183.

(92) HUMPHREYS, K. N.
'Performance of Powered Supports in Longwall Mining',
B. Sc. Dissertation, University of Nottingham, 1981.

APPENDIX I

THE CALIBRATION CURVE FOR THE ROTAMETERS USED

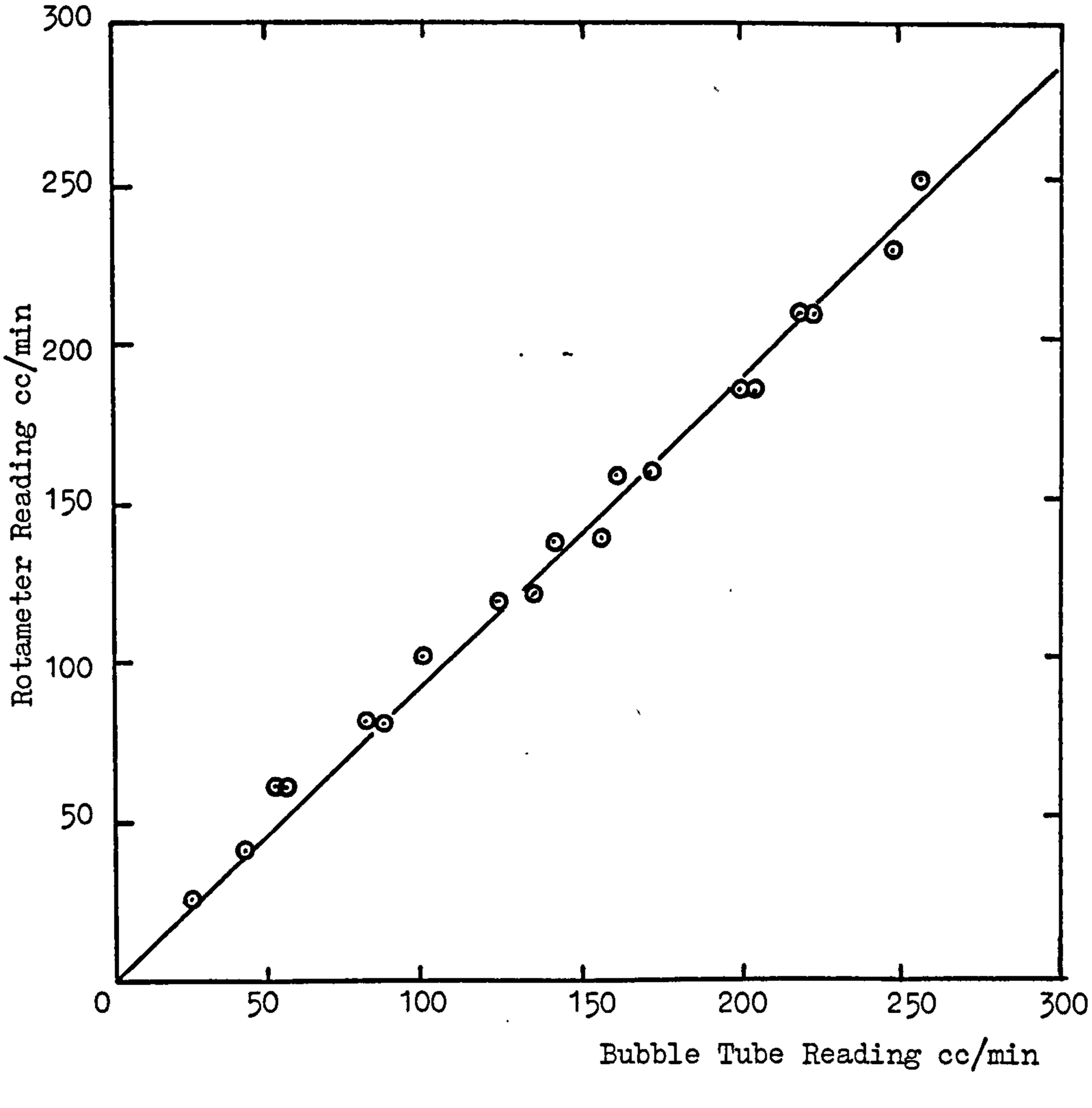

Rotameters are calibrated, by the manufacturers, for air flow. The errors in Rotameter readings were believed to arise from the use of Nitrogen as the flowing media. To compensate for these errors a correction factor $\Psi = 1.0338$, the ratio of air density to Nitrogen density, was applied. This correction factor was found to be accurate.

APPENDIX II

COMPUTATION OF EXPERIMENTAL RESULTS

TABLE (AII.1) Laboratory Data for Stress-Permeability Measurements on DEEP HARD Specimen.

Specimen: DEEP HARD 1, Third Run, Fracturing.
Date 27.4.1981
D = 3.76 cm
L = 7.38 cm

RADIAL STRESS (σ_3) bar	AXIAL LOAD (F_1) KN	GAS PRESSURE (Gauge Reading) (ΔP) psi	VOLUME FLOW Rate of Gas (Q_2) cc/min
0•0	0•0	10	142•22
		20	468•57
5•0	1•5	30	67•70
		40	106•00
		50	157•75
10•0	3•0	50	84•61
		60	118•00
		70	166•60
15•0	4•5	70	75•38
		80	95•90
		90	120•00
20•0	6•0	90	73•84
		100	87•70
		110	104•00
25•0	7•5	110	67•70
		120	76•92
		130	86•15
30•0	9•0	130	66•15
		140	72•30
		150	78•46
35•0	10•5	150	60•00
		160	64•61
		170	70•76
40•0	12•0	170	52•30
		180	59•46
		190	64•61

TABLE (AII.1) Continued .....

RADIAL STRESS (σ_3)	AXIAL LOAD (F_1)	GAS PRESSURE (Gauge Reading) (ΔP)	VOLUME FLOW Rate of Gas (Q_2)
bar	KN	psi	cc/min
45•0	13•5	190 200 210	49•23 52•30 55•38
50•0	15•0	210 220 230	46•15 49•23 52•30
55•0	16•5	230 240 250	41•53 44•61 47•70
60•0	18•0	270 280 290	43•07 46•15 49•23
65•0	19•5	300 310 320	43•06 45•25 47•70
70•0	21•0	320 330 340	40•00 42•25 44•61
10•0	21•0	150 160 170	56•92 67•70 80•00
5•0	21•0	10 20 30	72•30 182•20 300•00
0•0	0•0	10	224•90

As shown in Table (AII.1), the volume flow rate (Q_2) of Nitrogen through the test specimen was measured at three different gas pressures for each stress level applied. This data was directly fed to a computer program where all the units are converted into SI units and the permeabilities at each setting were calculated. Since the procedure followed in calculating the permeability was the same for each set of data, one example will be presented here:

Laboratory Data for the Permeability of DEEP HARD 1 Specimen at 2•0 MN/m^2 Radial Stress:

Radial Stress (σ_3) = 20•0 bars

Axial Load (F_1) = 6•0 KN

Gas Pressure (ΔP) = 100 psi

Volume Flow Rate (Q_2) = 87•70 cc/min

Length of the Specimen (ΔL) = 7.38 cm

Diameter of the Specimen (D) = 3.76 cm

Viscosity of Nitrogen (μ) = $1•745 \times 10^{-5}$ Ns/m^2

Computations

- Cross-sectional area of the specimen:

$$A = \frac{\pi D^2}{4}$$

$$A = \frac{\pi(3•76)^2}{4} \times 10^{-4} \ m^2$$

$$\underline{A = 1.1103645 \times 10^{-3} \ m^2}$$

- Length of the specimen:

$$\underline{\Delta L = 7{\cdot}38 \times 10^{-2} \text{ m}}$$

- Volume flow rate of gas corrected and converted into m^3/sec:

$$Q_2 = 87{\cdot}70 \times 1{\cdot}0338 \times \frac{1}{60} \times 10^{-6} \text{ m}^3/\text{sec}$$

$$\underline{Q_2 = 15{\cdot}111 \times 10^{-7} \text{ m}^3/\text{sec}}$$

- Differential gas pressure across the specimen:

$$\Delta P = 100 \text{ psi}$$

$$1 \text{ psi} = 6{\cdot}89476 \times 10^3 \text{ N/m}^2$$

therefore

$$\underline{\Delta P = 6{\cdot}89476 \times 10^5 \text{ N/m}^2}$$

- Gas pressure at the downstream end:

$$P_2 = 1 \text{ atm}$$

$$\underline{P_2 = 1{\cdot}01325 \times 10^5 \text{ N/m}^2}$$

- Mean gas pressure along the specimen:

$$\bar{P} = \frac{P_1 + P_2}{2}$$

$$P_1 = 1 \text{ atm} + \Delta P$$

therefore

$$\bar{P} = \frac{(1{\cdot}01325 + 6{\cdot}89476)\ 10^5 + (1{\cdot}01325 \times 10^5)}{2}$$

$$\underline{\bar{P} = 4{\cdot}46063 \times 10^5 \text{ N/m}^2}$$

- Permeability:

$$K_d = \frac{Q_2 \times \mu \times \Delta L \times P_2}{A \times \Delta P \times \bar{P}} =$$

$$K_d = \frac{15{\cdot}111 \times 10^{-7} \times 1{\cdot}745 \times 10^{-5} \times 7{\cdot}38 \times 10^{-2} \times 1{\cdot}01325 \times 10^{5}}{1{\cdot}1103645 \times 10^{-3} \times 6{\cdot}89476 \times 10^{5} \times 4{\cdot}46063 \times 10^{5}}$$

$$\underline{K_d = 5{\cdot}77 \times 10^{-16} \ m^2}$$

- Axial Stress:

$$\sigma_1 = \frac{F_1}{A}$$

$$= \frac{6{\cdot}0}{1{\cdot}1103645 \times 10^{-3}}$$

$$= 5{\cdot}40 \times 10^{-3} \ KN/m^2$$

$$\underline{\sigma_1 = 5{\cdot}40 \ MN/m^2}$$

- Radial Stress:

$$1 \text{ bar} = 0{\cdot}1 \ MN/m^2$$

$$\underline{\sigma_3 = 20{\cdot}0 \times 0{\cdot}1 = 2 \ MN/m^2}$$

The above computations are repeated for each set of data and the stress-permeability results are given in the form demonstrated in Table (AII.2).

TABLE (AII.2) An Example Computer Output Showing the Calculated Permeabilities for a Coal Specimen Under Stress.

SPECIMEN : DEEP HARD 1, THIRD RUN, FRACTURING

GAS FLOW (10**-7 M**2)	AXIAL STRESS (MN/M**2)	RADIAL STRESS (MN/M**2)	GAS PRESSURE (10**3N/M**2)	PERMEABILITY (10**-16M**2)
24.505	0.00	0.00	68.947	307.57
80.736	0.00	0.00	137.895	404.09
11.665	1.35	0.50	206.842	32.37
18.264	1.35	0.50	275.790	32.53
27.182	1.35	0.50	344.738	33.80
14.578	2.70	1.00	344.738	18.16
20.331	2.70	1.00	413.685	18.74
28.705	2.70	1.00	482.633	20.40
12.988	4.05	1.50	482.633	9.23
16.524	4.05	1.50	551.580	9.34
20.676	4.05	1.50	620.528	9.51
12.723	5.40	2.00	620.528	5.85
15.111	5.40	2.00	689.476	5.77
17.919	5.40	2.00	758.423	5.78
11.665	6.75	2.50	758.423	3.76
13.253	6.75	2.50	827.371	3.66
14.844	6.75	2.50	896.318	3.54
11.397	8.10	3.00	896.318	2.72
12.457	8.10	3.00	965.266	2.60
13.519	8.10	3.00	1034.214	2.48
10.338	9.45	3.50	1034.214	1.90
11.132	9.45	3.50	1103.161	1.80
12.192	9.45	3.50	1172.109	1.78
9.011	10.80	4.00	1172.109	1.31
10.245	10.80	4.00	1241.056	1.34
11.132	10.80	4.00	1310.004	1.32
8.482	12.15	4.50	1310.004	1.01
9.011	12.15	4.50	1378.952	0.97
9.542	12.15	4.50	1447.900	0.94
7.957	13.50	5.00	1447.900	0.78
8.482	13.50	5.00	1516.847	0.76
9.011	13.50	5.00	1585.794	0.75
7.155	14.86	5.50	1585.794	0.59
7.686	14.86	5.50	1654.742	0.59
8.218	14.86	5.50	1723.690	0.58
7.421	16.21	6.00	1861.585	0.45
7.951	16.21	6.00	1930.532	0.45
8.482	16.21	6.00	1999.480	0.45
7.421	17.11	6.50	2068.428	0.37
7.796	17.11	6.50	2137.375	0.36
8.218	17.11	6.50	2206.323	0.36
6.892	18.91	7.00	2206.323	0.30
7.279	18.91	7.00	2275.270	0.30
7.686	18.91	7.00	2344.218	0.30

TABLE (AII.2) Continued .....

9.207	18.91	1.00	1034.214	1.89
11.665	18.91	1.00	1103.161	1.99
13.784	18.91	1.00	1172.109	2.01
12.457	18.91	0.50	68.947	150.36
31.393	18.91	0.50	137.895	157.13
51.091	18.91	0.50	206.842	143.44
38.751	0.00	0.00	68.947	486.38